The heparin binding properties of the bone morphogenetic protein antagonist gremlin

Arnold Junior Nkola Tatsinkam

School of Biological Sciences

Royal Holloway, University of London

A thesis submitted for the degree of

Doctor of philosophy

February 2015

Declaration of authorship

I, Arnold Junior Nkola Tatsinkam, hereby declare that this thesis and the work presented in it is entirely my own. Where I have consulted the work of others, this is always clearly stated.

Signed:

Date:

Abstract

Gremlin, a 184 amino acid glycosylated protein, is one of several high-affinity endogenous antagonists of the bone morphogenetic protein (BMP) cytokines including BMPs -2, -4 and -7. Both gremlin and its BMP ligands have been shown to bind tightly to heparan sulfate (HS) polysaccharides present on cell surfaces. However, the role played by HS in the interaction between gremlin and its BMP ligands remains unknown. In this study, the heparin binding site on gremlin was characterised. Since the three-dimensional structure of gremlin remains experimentally unresolved, prediction of its heparin binding site was based on docking calculations using its homology models. Within the primary sequence, the predicted heparin binding site comprises interspersed basic residue clusters of arginines and lysines. Using site-directed mutagenesis, strategic combinatorial substitutions of these basic clusters were made. Six C-Myc-tagged gremlin mutants, MGRs 1 - 6, were cloned and expressed in parallel with a C-Myc-tagged wildtype gremlin protein. All six gremlin-Myc mutants showed markedly reduced heparin binding compared to the wildtype, using heparin affinity chromatography and a heparin-binding ELISA. This verified the predicted mapping of the heparin/HS binding site on gremlin. Ion-exchange chromatography of these gremlin-Myc proteins on sulfopropyl (SP)-Sepharose columns showed comparatively weak binding, thus indicating that the interaction between gremlin and heparin/HS is specific. Using a novel Myc-capture GREM1/BMP-4 double sandwich ELISA, the BMP-4 binding capability of both wildtype gremlin-Myc and mutant MGR5 were demonstrated. Moreover, the addition of either soluble unfractionated heparin or the low molecular weight heparin, tinzaparin, in this ELISA neither markedly promoted nor inhibited the interaction between wildtype gremlin-Myc and BMP-4. Overall, these showed that heparin binding is not essential for BMP-gremlin binding.

In order to study the functional activities of three selected gremlin-Myc mutants alongside wildtype, their capabilities to inhibit BMP-SMAD1/5/8 signalling were investigated in two functional assays established in C2C12 myoblastic cell lines. Firstly, SMAD1/5/8 phosphorylation was responsive to both BMPs -4 and -7, but this assay failed to generate a graded phospho-SMAD1/5/8 dose response on a sufficiently consistent basis to allow comparison of these gremlin-Myc proteins. This was resolved in the second assay, which employed a SMAD1/5/8-specific luciferase reporter construct. In this reporter assay, the functional activities of concentrated wildtype gremlin-Myc, MGR5 and MGR6 were confirmed.

Table of contents

List of figures

List of tables

List of abbreviations

3-D	Three-dimensional
ActR	Activin receptor
ALK	Activin receptor-like kinase
Amp^r	Ampicillin resistance
ANOVA	Analysis of variance
APC	Antigen-presenting cell
APS	Ammonium persulphate
ATCC	American Type Culture Collection
BAMBI	BMP and activin membrane-bound inhibitor
BCA	Bicinchoninic assay
bFGF	basic fibroblast growth factor
bHLH	Basic helix-loop-helix
Bla	Blasticidin
BMP	Bone morphogenetic protein
BMPR	Bone morphogenetic protein receptor
bp	Base pair
BSA	Bovine serum albumin
CAN family	DAN and Cerberus family
CDMP	Cartilage-derived morphogenetic protein
cDNA	Complementary deoxyribonucleic acid
CDS	Coding sequence
CHO	Chinese hamster ovary
CMV	Cytomegalovirus
CO_2	Carbon dioxide
CV2	Crossveinless 2
Cys	Cysteine
DAN	Differential screening-selected gene aberrative in neuroblastoma
dATP	Deoxyadenosine triphosphate
DCTA	1,2-diaminocyclohexane-N.N,N',N'-tetraacetic acid

dCTP	Deoxycytidine triphosphate
dGTP	Deoxyguanosine triphosphate
DMSO	Dimethyl sulfoxide
DN	Diabetic nephropathy
DNA	Deoxyribonucleic acid
DTT	Dithiothreitol
dTTP	Deoxythymidine triphosphate
ECD	Extracellular domain
ECM	Extracellular matrix
EDTA	Ethylenediaminetetraacetic acid
EGFP	Enhanced green fluorescent protein
ELISA	Enzyme-linked immunosorbent assay
EMT	Epithelial-to-mesenchymal transition
EndMT	Endothelial-to-mesenchymal transition
EXT	Exostosin
EXTL	Exostosin-like
FBS	Fetal bovine serum
FGF	Fibroblast growth factor
FGFR	Fibroblast growth factor receptor
GAG	Glycosaminoglycan
GDF	Growth differentiation factor
GDNF	Glial cell derived neurotrophic factor
GlcA	β-D-glucuronic acid
GlcNAc	α-N-acetylglucosamine
GlcNS6S	N-sulpho-N-glucosamine 6-*O*-sulfate
GREM1	gremlin (gremlin-1)
GS domain	Glycine and serine rich domain
HBGF	Heparin-binding growth factor
HME	Hereditary multiple exostoses
HPLC	High performance liquid chromatography
HRP	Horseradish peroxidase
HS	Heparan sulfate

HSQC	Heteronuclear spin quantum convergence
HSV	Herpes simplex virus
I.M.A.G.E.	Integrated Molecular Analysis of Genomes and their Expression
I-SMAD	Inhibitory SMAD
ID genes	*Inhibitor of differentiation* genes
IdoA	L-iduronic acid
IdoA2S	2-*O*-sulfated L-iduronic acid
IFNγ	Interferon gamma
Ig	Immunoglobulin
IL	Interleukin
IP	Immunoprecipitation
Kan	Kanamycin
kb	Kilobase
K_d	Disociation constant
kDa	KiloDalton
LB	Luria-Bertani
luc$^+$ gene	*Luciferase* gene
MAD	Mothers against decapentaplegic
MAE	Murine aortic endothelial
MALDI	Matrix-assisted laser desorption/ionization
MAPK	Mitogen-activated protein kinase
Maxi prep	Large scale DNA purification
MCS	Multiple Cloning Site
MES	2-N-morpholinoethanesulfonic acid
MH1 and 2	Mothers against decapentaplegic homology 1 and 2
Mini prep	Small scale DNA purification
mRNA	Messenger ribonucleic acid
MW	Molecular weight
NA domain	N-acetylated domain
NDST	N-deacetylase/N-sulfotransferase
Neo	Neomycin
NIBSC	National Institute of Biological Standards and Control

NMR	Nuclear magnetic resonance
NOESY	Nuclear Overhauser effect spectroscopy
NS domain	N-sulfated domain
Oc	Osteocalcin
OE PCR	Overlap extension polymerase chain reaction
Oligo	Oligonucleotide
OOE PCR	One-step overlap extension polymerase chain reaction
OP	Osteogenic protein
ORF	Open reading frame
Ori	Origin of replication
p-SMAD	Phospho-SMAD
pA	Polyadenylation
PAGE	Polyacrylamide gel electrophoresis
PAPS	3’-phosphoadenosine 5’-phosphosulfate
PBS	Phosphate buffer saline
PCR	Polymerase chain reaction
PDB	Protein data bank
PP1	Protein phosphatase-1
PPM1A	Metal-ion protein phosphatase-1A
PRDC	Protein related to DAN and Cerberus
QS	Quick-Stick
R-SMAD	Regulatory SMAD
RANTES	Regulated on activation normal T cell expressed and secreted
RE	Restriction endonuclease
RGM	Repulsive guidance molecule
RLU	Relative light unit
RNA	Ribonucleic acid
ROS	Rat osteosarcoma
SAP	Shrimp alkaline phosphatase
SAXS	Small angle X-ray scattering
SBE	SMAD binding element
SDS	Sodium dodecyl sulfate

SEM	Standard error of mean
SeMet	Selenomethionine
SMAD	Signalling mothers against decapentaplegic
SP-Sepharose	Sulfopropyl-Sepharose
SPR	Surface plasmon resonance
ssDNA	Single-stranded deoxyribonucleic acid
SV40	Simian virus 40
T-SMAD	Total-SMAD
TAE	Tris-acetate-ethylenediaminetetraacetic acid
TBS	Tris buffer saline
TEMED	Tetramethylethylene-diamine
TGFβ	Transforming growth factor beta
TGN	Trans-Golgi network
TK	Thymidine kinase
USAG-1	Uterine sensitization-associated gene-1
UTR	Untranslated region
UV	Ultraviolet

Chapter 1: Introduction

1.1 The BMPs: discovery and the subfamily

The BMP subfamily of cytokines consists some of twenty secreted molecules that regulate a wide spectrum of developmental processes during embryonic development and several cellular processes in postnatal and adult animals. Embryogenic processes include dorso-ventral patterning, dorsal neural tube development, skeletogenesis and organogenesis of some major organs such as the eye, lung, liver and kidney (Macias *et al*., 1997; Ducy and Karsenty, 2000; Liu and Niswander, 2005; Little and Mullins, 2006). Therefore, the tight regulation of BMP activity is essential for healthy development.

BMP activity was first discovered by Urist (1965) who demonstrated that in demineralised matrix of bone and dentin, an inductive factor caused *de novo* bone formation at ectopic sites in rats when transplanted intramuscularly. However, cloning and purification of the first BMPs, BMPs -1, -2 and -3, was only achieved over two decades later (Sampath *et al.,* 1987; Wang *et al.,* 1988; Luyten *et al.,* 1989). BMP-1 was identified as a novel regulatory protease whereas BMP-2 and BMP-3 were found to be novel members of the transforming growth factor beta (TGFβ) superfamily (Wozney *et al.,* 1988).

To date, at least 35 members of the TGFβ superfamily have been identified and are subdivided into four main subfamilies namely, activins/inhibins, TGF-βs, BMPs/growth and differentiation factors (GDFs) and the neurotrophic factors such as glial cell derived neurotrophic factors (GDNFs), (Weiskirchen and Meurer, 2013). Their common grouping stems from the high sequence homology they share, indicating evolution from a common ancestral gene (Kingsley, 1994; Rider and Mulloy, 2010). The increasingly divergent biological roles of individual BMP members also led to progressive changes in their naming, from osteogenic proteins (OPs) and cartilage-derived morphogenetic proteins (CDMPs) to BMPs and GDFs, predominantly (Ducy and Karsenty, 2000; Rider and Mulloy, 2010).

Phylogenetic analyses based on the sequence homology of their conserved cystine-knot domain present in their mature forms results in further subgrouping of the BMPs (Kingsley, 1994; Hogan, 1996; Yamashita *et al.,* 1996; Rider and Mulloy, 2010). Most notably, BMP-4 and BMP-7, both of which are used in this study, are allocated to

different subgroups with the former subcategorised with BMP-2 only, and the latter with the BMPs -5, -6 and -8 (Newfeld *et al.*, 1999; Hinck, 2012).

1.2 Synthesis and Processing of BMPs.

BMPs are synthesised as large monomeric pre-pro-polypeptides within the endoplasmic reticulum. Such polypeptide consist of a short N-terminal signal sequence pre-domain linked to a latency associated polypeptide pro-domain that regulates proper folding and in turn is linked to the mature polypeptide region itself (Xiao *et al.*, 2007). This varies in size for each BMP ranging between 400 - 500 amino acids in length (Ali and Brazil, 2014).). The model for synthesis and processing of BMP-4 is shown in Figure 1.1.

To achieve the active mature BMP-4 ligand, sequential post-translational modifications of the pre-pro-polypeptide takes place in the trans-Golgi network (TGN). First, the signal peptide is cleaved off proteolytically at a consensus R-X-K-R site (S1 site, Figure 1.1) releasing the pro-polypeptide domain. In the case of BMP-4, the precursor protein is cleaved at both S1 and S2 sites by the proprotein convertase, furin (Ali and Brazil, 2014). For most BMPs including BMPs -4 and -7, glycosylation of the monomeric pro-polypeptide takes place at a conserved NXS/T site in the mature polypeptide region. Next, proteolytic cleavage of the pro-domain occurs at a consensus R-X-X-R site, which is rendered accessible due to the acidic environment within the post-TGN (S2 site, Figure 1.1). This liberates a stable glycosylated mature monomeric BMP ligand from its pro-domain. Homo-dimerization of this secreted BMP-4 monomers then takes place via a covalent disulfide linkage (Rider and Mulloy, 2010). This then results in the secretion of a stable biologically active dimeric BMP-4 ligand into circulation for BMP receptor activation at distant target tissues (Nelsen and Christian, 2009, Ali and Brazil, 2014). It is worth noting that although this processing is axiomatic for all BMPs, non-covalent dimerization has also been reported, such as for BMP-15 (Nelsen and Christian, 2009).

Dissociation of the pro-domain from the active mature ligand is not always the case. A crystal structure of active BMP-9 revealed that its pro-domain remains non-covalently bound to the mature peptide region resulting in a biologically active BMP-9:pro-region complex (Brown *et al.*, 2005).

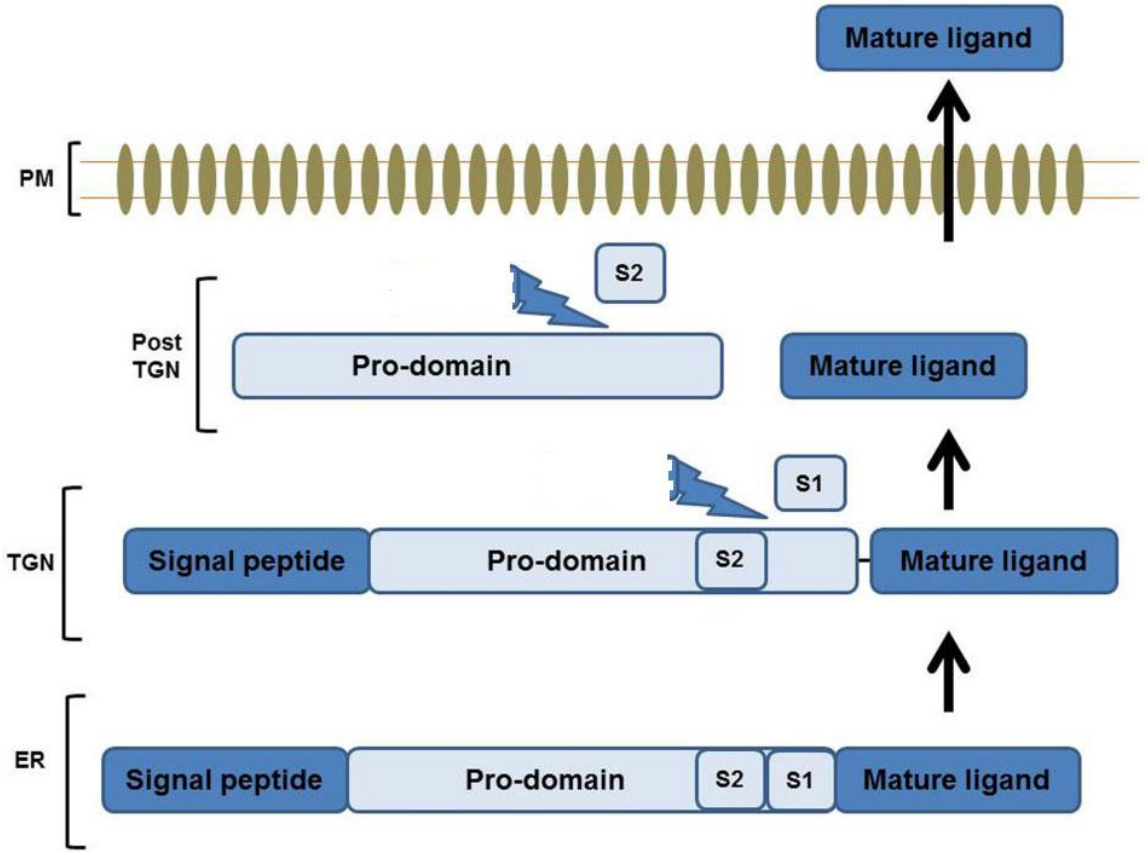

Figure 1.1: BMP-4 synthesis and processing.
The model shown above serves as a general model for synthesis and processing of BMPs. BMPs are synthesised as large pre-pro-mature ligand complexes within the endoplasmic reticulum (ER) and transported to the trans-Golgi network (TGN) for post-translational modifications. Furin cleavage (blue coloured-bolted arrow) at S1 site is thought to occur in the TGN and results in release of a pro-domain-mature ligand complex within the post-TGN. This released complex is further cleaved at the S2 site by furin which then results in the release and secretion of a mature monomeric BMP ligand. Dimerization of this BMP monomer with another BMP monomer yields then a biologically active dimeric ligand. PM = Plasma membrane. Adapted from Ali and Brazil, 2014.

1.3 General structure of BMPs

The structural hallmark of all members of the TGFβ superfamily is the presence of a conserved cysteine-rich ring structure motif, the cystine-knot motif (McDonald and Hendrickson, 1993; Avsian-Kretchmer, 2003). As members of the TGFβ superfamily, all BMPs, with the exception of BMP-1, possess the characteristic TGFβ cystine-knot motif. The crystal structures of a number of BMPs have been resolved to date including that of BMP-7 (Figure 1.2; Greenwald *et al.*, 2003). Although BMP-4 crystallography has not yet been achieved, that of its closest homologue, BMP-2, has (PDB file: 3BMP; Scheufler *et al.*, 1999).

Analyses of the BMP-7 crystal structure revealed that the cystine ring of BMPs comprises eight residues, four of which are cysteines (Cys). These Cys residues form two intrachain disulfide bonds in a pairwise manner; Cys 2 and Cys 5 and between Cys 3 and Cys 6. A third disulfide bond formed between Cys 1 and Cys 4, threads back through the ring giving it its characteristic 3-D knot structure (refer to Figure 1.2A), (Avsian-Kretchmer, 2003). Also present around the cystine-knot motif (not shown in figure), is another cysteine residue (Cys 7) that is directly involved in Cys 7:Cys' 7 covalent dimerization of two BMP-7 monomers. In terms of the overall tertiary structure, analogy to the "palm" of the hand is often made in reference to the cystine-knot motif (Figure 1.2B) (Griffith *et al.,* 1996; Rider and Mulloy, 2010).

Projecting from the cystine-knot motif are two pairs of anti-parallel β-stranded loops, which are analogous to "fingers" (Figure 1.2B). In Figure 1.2A, these are formed between Cys 1 and Cys 2 and between Cys 4 and Cys 5. Also present is a C-terminal loop located opposite the fingers that in most BMPs forms a four-turn α-helix analogous to the "wrist" of the hand (Figure 1.2B). In Figure 1.2A, this "wrist" region would replace the uncoiled loop between Cys 3 and Cys 4 (Avsian-Kretchmer, 2003). The analogy making use of hand features to describe BMP structures is best illustrated using ribbon structure of the BMP-7 monomer as shown in Figure 1.2B.

Dimerization of most BMPs including BMPs -4 and -7, takes place in a head-to-tail orientation via covalent formation of a disulfide bond via the unpaired cysteine residue just outside the cystine-knot motif of each monomer. In this head-to-tail orientation, the wrist region (head) of one monomer is tucked into the concave face of the β-fingers (tail) of the other monomer (Griffith *et al.,* 1996; Rider and Mulloy, 2010). This is illustrated in Figure 1.3.

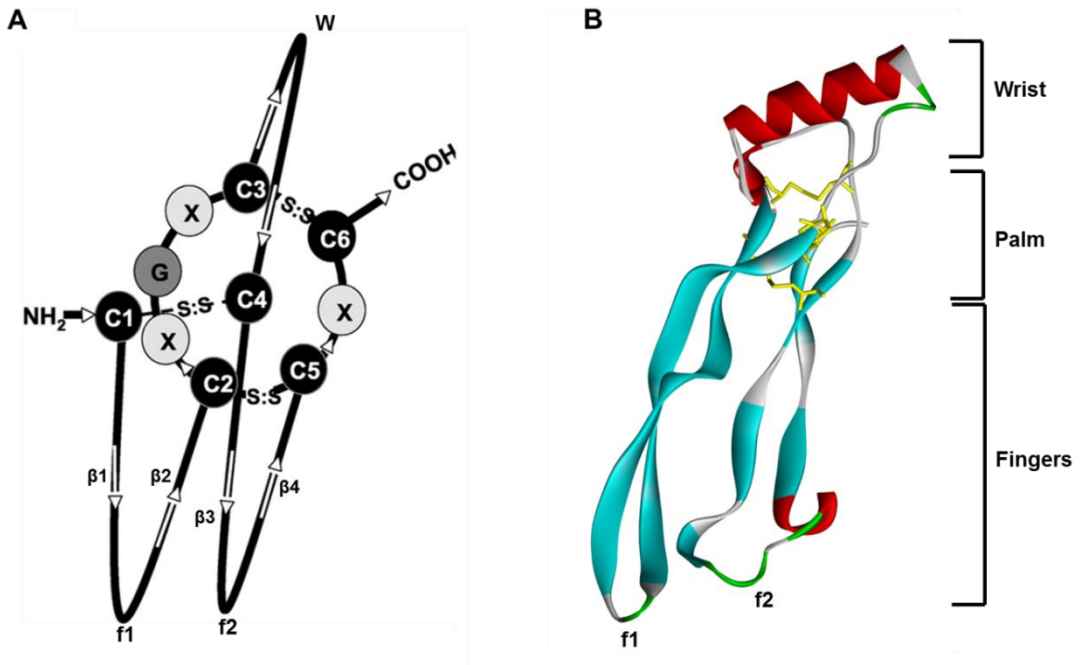

Figure 1.2: Structural features of a BMP-7 monomer.
BMP-7 structure representative of general structural features of most BMP subfamily members A) Cartoon representation of eight-membered cystine ring (palm region) possessing a pair of disulfide bonds formed between C2:C5 and C3:C6. The disulfide bond between C1:C4 passing through the ring, gives it its three-dimensional structure. A pair of anti-parallel β-stranded loops emanate from the cystine ring forming the finger loops, f1(β1 and β2) and f2 (β3 and β4). Opposite the finger region, at the C-terminal end of the cystine ring, is another loop that typically forms a four-turn α-helix forming the wrist (W). The unpaired cysteine residue located outside the cystine ring used for dimerization is not shown. Adapted from Avsian-Kretchmer and Hsueh, 2003. B) Ribbon representation of the crystallographic structure of a BMP-7 monomer highlighting the wrist, palm and finger regions. Disulfide bridges within the cystine ring are coloured in yellow. Adapted from McClarence, 2011. Original source, Griffith *et al.*, 1996. PDB file, 1LXI.

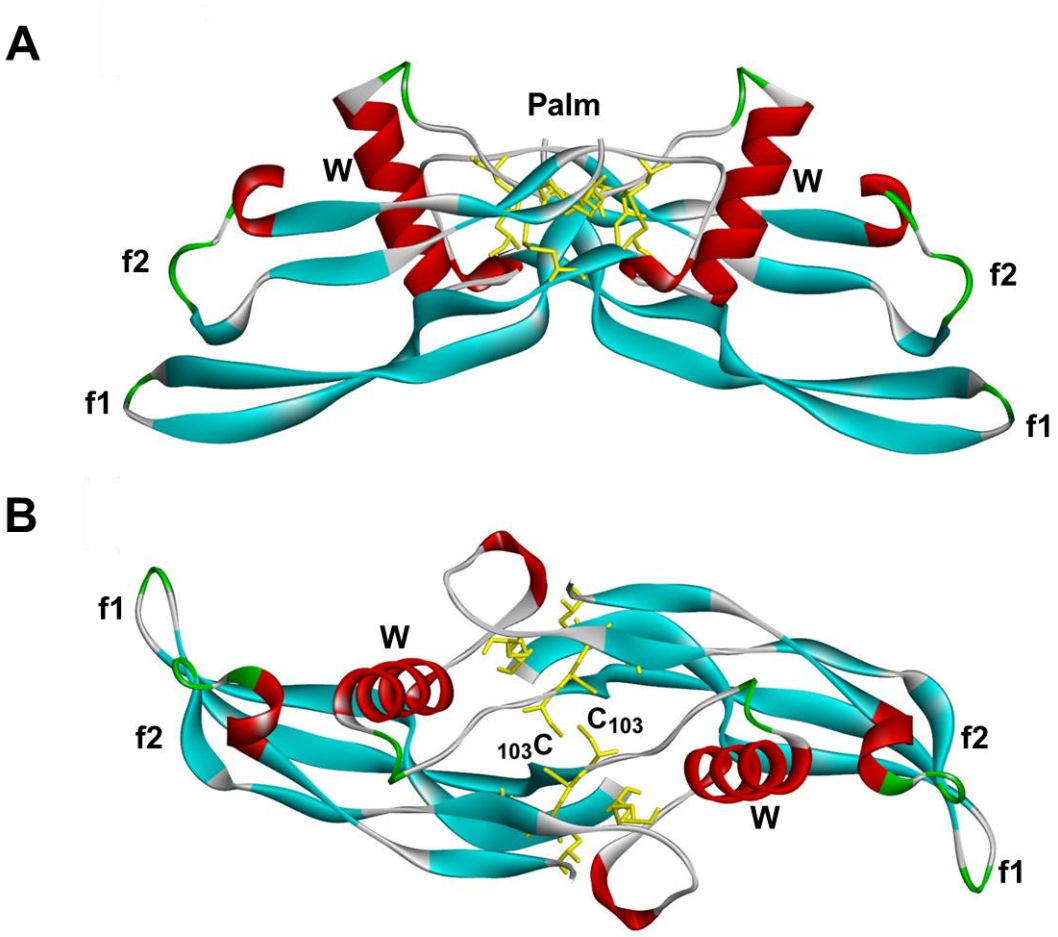

Figure 1.3: High resolution structures of BMP-7 dimers.
Ribbon representations of the three-dimensional crystal structure of a BMP-7 dimer as viewed A) from the front and, B) from above. A covalent disulfide bond is formed between the unpaired cysteine residue (in this case, C103) located outside the cystine ring of each BMP monomer that joins the palm regions of both monomers together. The dimer oriented head-to-tail, has the 4-turn α-helix (coloured in red) in the wrist region (W), (head) of one monomer tucked into the concave surface of the finger region (tail) of the other monomer. The β-finger loops are coloured in turquoise with patches of grey, green and red colours. All α-helices are coloured in red. All disulfide bridges in the palm regions are coloured in yellow. Adapted from McClarence, 2011. Original source: Griffith *et al.*, 1996. PDB file, 1LXI.

1.4 Mechanism of receptor activation by BMPs

Members of the TGFβ superfamily elicit biological effects by binding to type I and type II serine (Ser)/threonine (Thr) receptors on the cell surfaces of target cells (Yamashita *et al.*, 1996; Chen *et al.*, 2004b; Ali and Brazil, 2014). This is illustrated in Figures 1.4 and 1.5. Both types of TGFβ receptors possess an N-terminal extracellular ligand binding domain, a transmembrane region and a C-terminal cytoplasmic Ser/Thr kinase domain (Shi and Massagué, 2003). Also present on cell surfaces are several co-

receptors that structurally resemble the type I/II receptors themselves, but lack the kinase domain. These include the BMP and activin membrane-bound inhibitor (BAMBI) illustrated in Figure 1.5, the membrane-associated receptors of the repulsive guidance molecule (RGM) family of facilitators and enhancers of BMPs-2/-4 signalling and the type III class of receptors (endoglin and betaglycan) that enhance BMP -2/-4/-7/-9 signalling (David *et al.*, 2007; Onichtchouk *et al.*, 1999; Babitt *et al.*, 2006; Camus and Lambert, 2007; McLean and Guglielmo, 2010). In short, these kinase domain-deficient co-receptors regulate BMP signalling by either inhibiting or enhancing assembly of the types I and II receptor complex.

In the human genome, the 12 members that make up the TGFβ receptor family are dedicated entirely to TGFβ signalling, seven of which are type I and the remaining five, type II receptors (Manning *et al.*, 2002). BMP ligands bind to three type I receptors namely: activin-like receptor kinase (ALK)2, ALK3 also called BMP receptor 1A (BMPRIA) and ALK6 or BMPRIB, and to three type II receptors: BMP type II receptor (BMPRII), activin A receptor type II (ActRII) and activin B receptor type II (ActRIIB), (Nohe *et al.*, 2004). BMP ligand binding to a pair of type I receptor ligand binding domains results in the recruitment of a pair of type II receptors required for the full activation of the type I receptors via which a downstream signal transduction is propagated (ten Dijke and Hill, 2004). This order of recruitment of type I to type II receptors is the reverse of that seen with TGFβ-1 (Ali and Brazil, 2014).

A considerable degree in promiscuity of BMP ligands is observed in their interactions with the different types I/II receptor subsets. Nonetheless, preferential high affinity binding of BMP ligands to each receptor type also takes place. For instance, BMPs -2/-4 show preferential high affinity binding to both ALK3 and ALK6, and although BMP-7 can also show bind to ALK3 at low affinity, it shows preferential high affinity binding to both ALK2 and ActRII, instead (Kirsch *et al.*, 2000a; Greenwald *et al.*, 2003; Ali and Brazil, 2014).

The crystal structures of the BMPs -2 and -7 complexed with the ligand binding ectodomains of BMPRIA and ActRII have been resolved by Kirsch *et al.* (2000b) and Greenwald *et al.* (2003), respectively. These have helped elucidate the general mechanism of receptor activation of the BMPs. As shown in Figure 1.4, in the tetrameric assembly complex, a dimeric BMP-7 ligand is complexed to two molecules of ActRII ECDs. A predominantly hydrophobic surface cavity on the convex binding surface of both pair of BMP-7 monomer β-fingers makes direct contact with a similarly

charged concave binding surface on each ActRII ECD (refer to Figure 1.4). Another important observation in this complex is that no direct physical interaction occurs between the individual receptor ECDs which is strongly indicative of downstream signalling activation via a ligand-mediated cooperative mechanism (Greenwald *et al.*, 2003).

It follows that the binding of a BMP ligand to its receptor ECDs, results in conformational changes that occur in the cytoplasmic kinase domains of the pair type I receptors. This then facilitates their phosphorylation and sequential recruitment of pair type II receptors. It is worth noting that, although BMP-7 demonstrates high affinity to ActRII, signalling activation occurs primarily via low affinity binding to a pair of type I receptor ECDs that subsequently results in the recruitment of its high affinity pair of ActRII ECDs (Greenwald *et al.*, 2003). Full activation of type I receptors is achieved by the type II receptor phosphorylation of the unique Gly and Ser rich GSGSGS sequences (GS domain) located immediately N-terminal of the cytoplasmic kinase domains of both type I receptors (Massagué, 1998; Miyazono *et al.*, 2010).

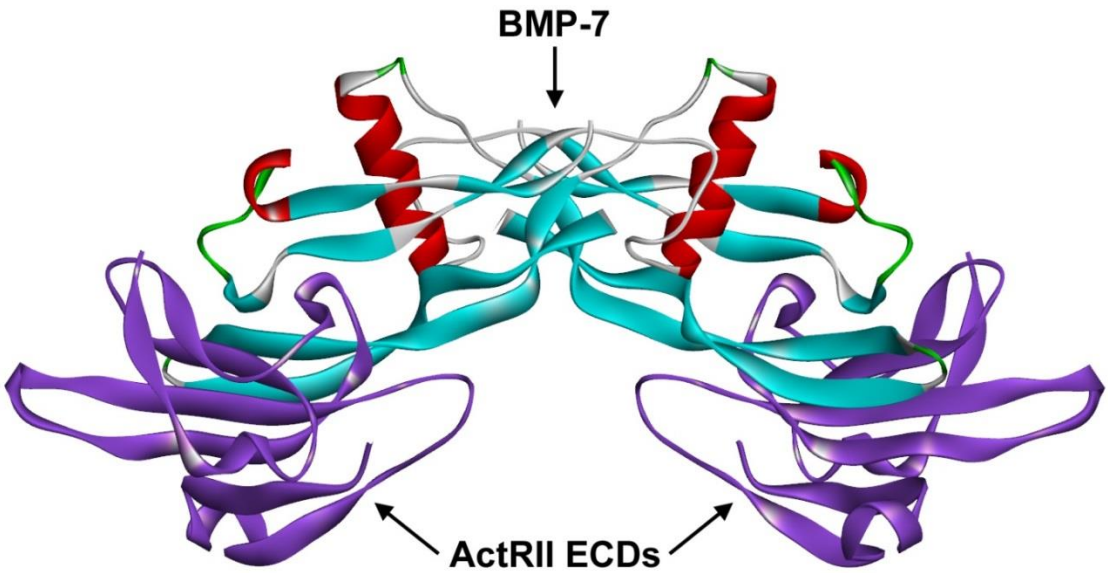

Figure 1.4: A BMP-7 dimer complexed with activin receptor type II ectodomains. Shown is a ribbon representation of the three-dimensional crystal structure of the BMP-7 dimer complexed to two molecules of activin A receptor type II (ActRII) ectodomains (ECDs). The convex binding surface of the pair of β-fingers on each BMP-7 monomer makes direct contact with a concave binding surface on each ActRII molecules. As observed, ActRII ECDs do not make direct contact with each other. The four-turn α-helices in the wrist region of one monomer are tucked as described in the previous figure legend. ActRII ECDs are coloured purple. Adapted from McClarence, 2011. Original source: Greenwald *et al.*, 2003. PDB file, 1LX5.

1.5 BMP-induced downstream signalling via SMAD proteins

Two modes of BMP signalling have been described that are each linked to a different signalling mechanism. In the first mode, the BMP ligand binding to pre-assembled types I and II receptor complexes at cell surfaces results in BMP signalling via canonical SMADs-dependent pathways (Massagué *et al.,* 2005). In the second mode, the BMP-ligand first induces assembly of receptor complexes at cell surfaces. This results in SMADs-independent signalling that induces p38 mitogen-activated protein kinase (MAPK), (Nohe *et al.,* 2002). Herein, focus is placed on the canonical SMADs-dependent signalling pathway as illustrated in Figure 1.5.

SMAD proteins discovered by Derynck *et al.* (1996), are the vertebrate homologues of the *Drosophila melanogaster* mothers against decapentaplegic (MAD), (Sekelsky *et al.,* 1995) and *Caenorhabditis elegans* Sma gene (Riggins *et al.,* 1996). Three classes of SMAD proteins exist based on their activators and functions (Shi and Massagué, 2003; Ali and Brazil, 2014). The first subclass of regulatory SMADs (R-SMADs), SMAD1, SMAD5 and SMAD8 (SMAD1/5/8), responds to BMPR1 activation by BMP ligands. The second subclass of R-SMADs, SMAD2 and SMAD3 (SMAD2/3), respond to TβRI receptor activation by other TGFβ superfamily ligands and inhibit SMAD1/5/8 downstream signalling (Massague *et al.,* 2005; Murakami *et al.,* 2003). Recent findings have, however, demonstrated that there are exceptions in this rigid paradigm of specific ligand type to R-SMADs activation. For instance, endothelial homeostasis has been linked to TGFβ-mediated phosphorylation of SMAD1/5 via BMPR1 in endothelial cells (Chen and Massagué, 1999; Lux *et al.,* 1999, 2013; Guillot *et al.,* 2012). Phosphorylated R-SMADs bind to a common cytoplasmic co-mediator SMAD (Co-SMAD), SMAD4, which forms the second class of SMAD proteins. The inhibitory SMADs (I-SMADs), SMAD6 and SMAD7 down-regulate R-SMAD signalling by binding competitively to SMAD4 and BMPR1 receptors, respectively (Hata *et al.,* 1998; Kavsak *et al.,* 2000).

Phosphorylation of R-SMADs occurs directly via activated type I receptors (Macias-Silva *et al.,* 1996). The MAD homology 2 (MH2) domain conserved in all types of SMADs, serves as the receptor recognition domain. Phosphorylation of R-SMADs via the MH2 domain induces conformational changes that increase their affinity for SMAD4 and also leads to the exposure of a nuclear import region present in this domain (Xu *et al.,* 2000; Shi *et al.,* 2007). The MH1 domain conserved only in R-

SMADs and SMAD-4 antagonises the functions of the MH2 domain and is responsible for SMAD-mediated DNA binding and interaction with certain DNA binding cofactors (Miyazono *et al.,* 2010). The stable R-SMADs:SMAD4 complexes formed accumulate within the nucleus following their nucleocytoplasmic shuttling against released R-SMADs from dissociated complexes within the nucleus (Liu *et al.,* 1997; Hoodless *et al.,* 1999; Watanabe *et al.,* 2000; Shi and Massagué, 2003). Although several models have been proposed, the mechanism of nucleoplasmic shuttling is not yet clearly understood.

Within the nucleus, R-SMADs:SMAD4 complexes induce the assembly of various transcription factors and together, regulate expression of various target genes such as *SMAD6, inhibitor of differentiation (ID)* genes, *BAMBI* and *SMAD*7 (Ali and Brazil, 2014). Regulation of target gene expressions is achieved by binding of the active complexes to the SMAD binding elements (SBEs) motif which constitute of GC rich sequences located upstream and within the promoters of these target genes (Miyazono *et al.,* 2010). Increased binding affinity of an active R-SMAD/SMAD4 complex to the SBE motif is observed with an increase in the size of the SBE motif. Hence, because only one or two SBEs are found within the putative promoters of target genes, it follows that their binding affinity to active R-SMAD:SMAD4 complexes is weak (Shi *et al.,* 1998; Massague *et al.,* 2005). *In vitro,* increased binding affinity of the active complexes to the SBE motif has been achieved by using concatemers with multiple SBE repeats hence driving stronger expression of the *BMP* target gene (Zawel *et al.,* 1998; Zhao *et al.,* 2003 and 2004). These findings have enabled the routine cloning of several SMADs-specific luciferase reporter constructs, which as demonstrated later in this study, are useful tools in functional studies of BMP-induced signalling.

1.6 Regulation of BMP signalling

Modulation of BMP signalling actions is achieved both intracellularly and extracellularly. Multiple levels of modulatory processes are established in these cellular compartments that collectively down-regulate SMAD1/5/8 signalling. Both intra- and extra-cellular regulations of canonical BMP-SMAD1/5/8 signalling are illustrated in Figure 1.5.

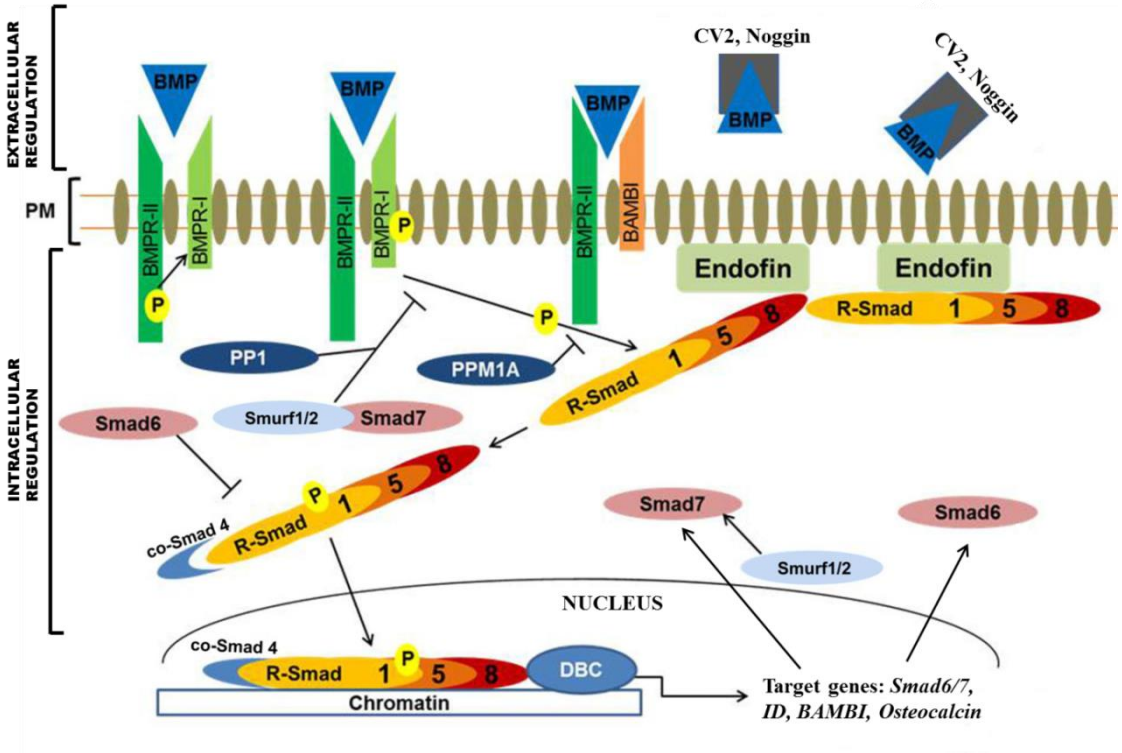

Figure 1.5: Activation and regulation of the canonical BMP-SMAD signalling pathway.

The active dimeric BMP ligands bind directly to and activate both TGFβ type I and II serine/threonine kinase receptors (BMPRs -I and –II, respectively as shown). Following phosphorylation of R-SMADs, SMAD1/5/8, the heteromeric R-SMADs:SMAD4 complex translocates into the nucleus. There, it binds to specific SMAD binding elements (SBEs) within the promoters of its target genes in concert with various DNA binding co-factors (DBC). The signalling cascade is tightly regulated intra- and extra-cellularly. Presence of pseudo-receptors such as BAMBI on the plasma membrane (PM), down-regulate signalling by trapping active BMP ligands extracellularly. Secreted extracellular BMP antagonists such as Noggin and crossveinless 2 (CV2), bind directly to BMP ligands and prevent their subsequent binding to their receptors. Intracellularly, the pathway is inhibited by the I-SMADs, SMADs -6 and -7. SMAD6 prevents complexing of R-SMADs and SMAD4. SMAD7 complexed with Smurf1/2 compete with R-SMADs for BMPR-1-mediated phosphorylation. PP1 (protein phosphatase-1) and PPM1A (metal-ion protein phosphatase-1A) are inhibitory phosphatases. Adapted from Ali and Brazil, 2014.

Introduced in the previous section, the I-SMADs, SMAD6 and SMAD7, inhibit SMAD signalling by binding directly to the phosphorylated R-SMADs or to the activated type I receptors, respectively. Direct binding of SMAD6 to activated R-SMADs prevents the formation of R-SMADs:SMAD4 complexes, thus inhibiting downstream signal transduction (Hata *et al.*, 1998). On the other hand, competitive binding of SMAD7 to the activated pair of type I receptors antagonises R-SMADs activation (Suzuki *et al.*, 2002). The independent cytoplasmic interactions of both I-

SMADs with the E3-ubiquitin ligases, Smurf1 and Smurf2, result in the poly-ubiquitination and subsequent proteasomal degradation of the corresponding signalling component they are complexed with (Murakami *et al.,* 2003; Guglielmo *et al.,* 2003).

In addition, protein phosphatases such as protein phosphatase 1 (PP1) and the metal ion-dependent protein phosphatase (PPM1A) catalyse the dephosphorylation of both phosphorylated TGFβ/BMP receptors and R-SMADs hence dampening downstream signal transductions (Chen *et al.,* 2006; Lin *et al.,* 2006). Furthermore, transcriptional regulation can be achieved by a number of transcriptional processes such as *BMP* promoter methylation and hypermethylation, recruitment of various co-repressors, histone deacetylation and silencing of the messenger RNA (mRNA) transcripts by small interference RNAs (siRNAs), (Wen *et al.,* 2006; Kimura *et al.,* 2008; Walsh *et al.,* 2010 ; Takeda *et al.,* 2004).

As implied in Section 1.4, BMP signalling can be also down-regulated extracellularly by the coreceptor BAMBI. BAMBI is similar in structure to both types I/II receptors, however, it lacks their intracellular kinase domain and, therefore, cannot propagate signal transduction intracellularly. This pseudoreceptor acts by competing negatively for the same BMP ligands as do types I/II receptors thus trapping the ligands themselves and blocking their activities (Onichtchouk *et al.,* 1999). More importantly, extracellular modulation of BMP-SMADs signalling can also be achieved by a subfamily of secreted cytokine molecules, the BMP antagonists (Figure 1.5). These antagonist molecules bind directly to the mature BMP ligands and prevent subsequent activation of the type I receptors, which abolishes direct signal transductions downstream (Walsh *et al.,* 2010; Ali and Brazil, 2014).

To date, a diverse number of BMP antagonists have been discovered in vertebrates that, like the BMPs, play critical roles in early developmental and homeostatic processes in adult organs (Rider and Mulloy, 2010; Walsh *et al.,* 2010). Early clues into the mechanism of BMP ligand-antagonist interactions were drawn from high resolution crystallographic structures of the TGFβ superfamily dimer, Noggin complexed with the BMP-7 dimer (Figure 1.6; Groppe *et al.,* 2002) and the *D. melanogaster* homologue, crossveinless 2 (CV2) complexed with the BMP-2 (Zhang *et al.,* 2008). Both CV2 and Noggin exhibit incredibly similar mechanisms of BMP antagonism despite sharing a remarkably low sequence homology. Both antagonists form head-to-head dimers (wrist-to-wrist dimers) that bind the BMP ligand at the same convex interface of the β-finger epitope pair as was shown earlier in the BMP-7:ActRII

ECDs tetrameric complex (refer to Figure 1.4 and Figure 1.6). This head-to-head orientation of both antagonists is such that the β-finger pairs projecting from opposite directions form a clamp around the ligand thus trapping it. This leads to its sequestration in an inactive complex that is unable to activate both type I and II receptors (Figure 1.6; Groppe *et al.*, 2002).

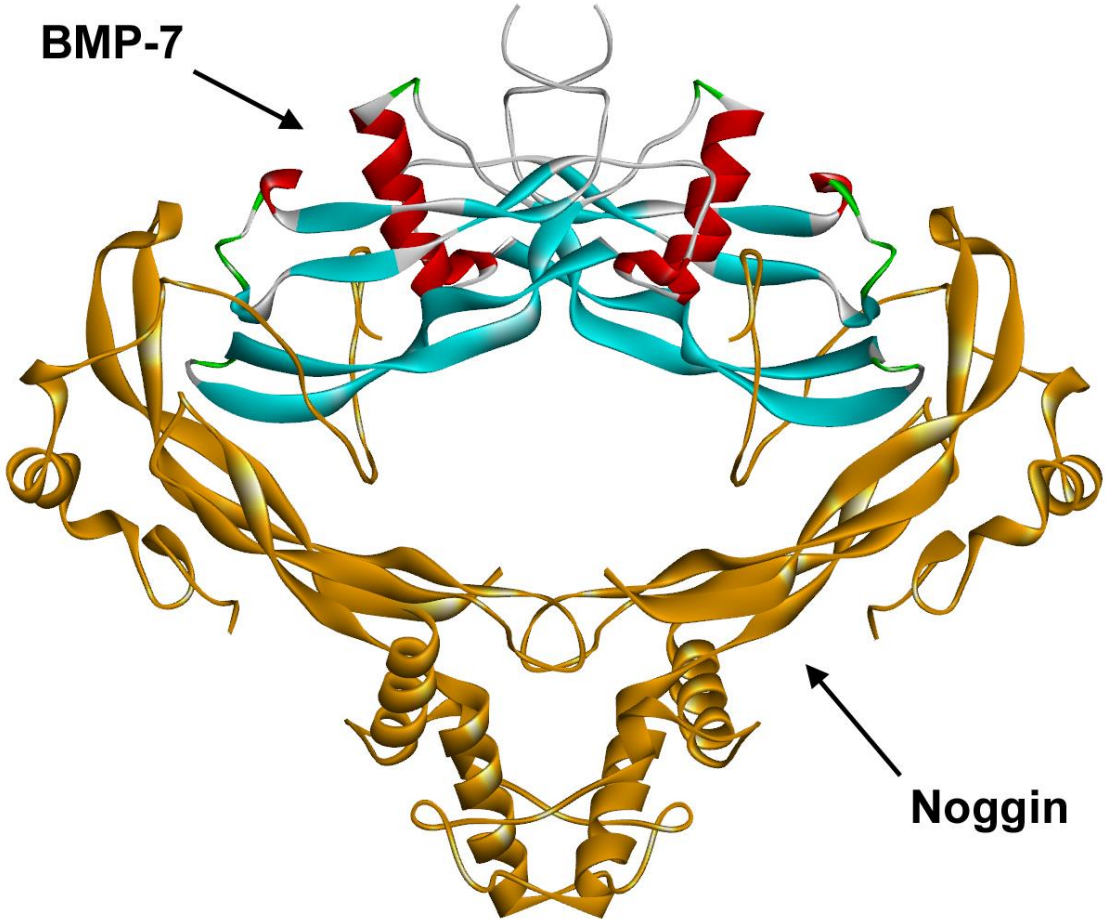

Figure 1.6: The Noggin-BMP-7 complex.
Shown is the ribbon representation of the three-dimensional crystal structure of the BMP antagonist, Noggin (in gold) complexed with BMP-7 as labelled. Unlike the head-to-tail BMP-7 homodimer, Noggin forms a head-to-head 'clamp-shaped' homodimer in which the disulfide bonded cystine-knot motif in the palm region and wrist (W) region on both monomers form a centralised core structure. The wrist region in Noggin is extended and possesses an extra α-helical coil. This arrangement enables its projecting finger loops to form a clamp around the active BMP-7 ligand thereby trapping it. Adapted from McClarence, 2011. Original source: Groppe *et al.*, 2002. PDB file, IM4U.

1.7 Structural features of the CAN family of BMP antagonists

Many BMP antagonists have been identified in both vertebrates and invertebrates (Zimmerman *et al.*, 1996; Hsu *et al.*, 1998; Waterston *et al.*, 2002). Like the BMPs themselves, many BMP antagonists also possess in them the characteristic cystine-knot motif. Therefore, they are regarded as distant members of the TGFβ superfamily that evolved divergently from a common ancestral gene (Avsian-Kretchmer and Hsueh, 2004; Rider and Mulloy, 2010).

Avsian-Kretchmer and Hsueh (2004) categorised all cystine knot-containing BMP antagonists within the human genome using different bioinformatics tools and phylogenetic analyses. This was based on their sequence homology, predicted structures and the sizes of their cystine rings. Three subfamilies were identified which included, the eight-membered ring which included Cerberus and DAN (CAN) subfamily members, nine-membered ring which included twisted gastrulation protein (TSG), and the ten-membered ring which included the chordin and Noggin. The CAN subfamily members were further subcategorised into four subgroups that included, gremlin and protein related to DAN and Cerberus (PRDC) also known as gremlin-2, Cerberus and COCO (dand5), uterine sensitization-associated gene-1 (USAG-1) and sclerostin, and DAN. Their conserved CAN (or DAN) domain is defined with consensus sequence $CX_6QX_6CX_6NX_2CXGXCXSX_3PX_{(8–13)}CX_2CXPX_8XLXCX_{(15–18)}CXX$ which highlights all the six conserved cysteine residues that form the core cystine-knot motif and two extra cysteine residues also conserved (Pearce *et al.*, 1999; Balemans and Van Hul, 2002).

Avsian-Kretchmer and Hsueh (2004) predicted that on the basis of sequence homology, the CAN family members are likely to share close tertiary structural resemblance to the BMPs (Figure 1.7A). In most, they also possess an extra pair of cysteine residues at the tip of the β-fingers that forms an extra intrachain disulfide bond linking both finger tips together (Figure 1.7). This results in a more stable and compact cystine-knot motif in the CAN family members. The first experimental clues into the structural features of CAN family members were obtained from the high resolution NMR structure of sclerostin generated by Veverka *et al.* (2009) (refer to Figure 1.7B). In this structure, the two pairs of β-finger loops are consistent with BMPs except linked at their tip by the extra disulfide bond. The BMP cystine-knot motif is conserved as demonstrated by Veverka *et al.* (2009) using MALDI mass spectroscopic data. The pairing arrangement of six cysteine residues was also consistent with that within the

cystine-knot motif of BMPs (Figure 1.7A). On the other hand, a disorientated loop in sclerostin replaced the four-turn α-helix in the wrist region of BMPs (Figure 1.7B).

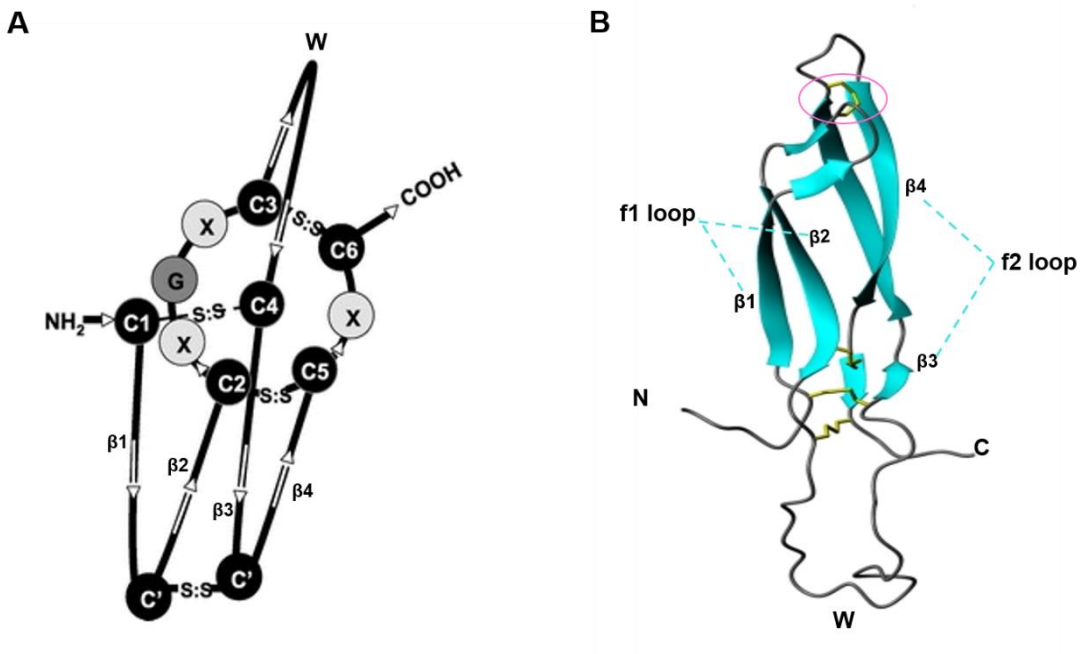

Figure 1.7: High resolution structure of sclerostin.
The structural features of sclerostin shown serve as a general representation of structural features of the CAN family of BMP antagonists. As can be observed, both A) Cartoon representation and, B) Inverted ribbon representations of the three-dimensional NMR structure of sclerostin share close resemblance with the BMPs themselves as described earlier in the legend of Figure 1.2. However, sclerostin, which exists as a monomer, possesses an additional pair of cysteine residues (C': C') that join the tips of the finger loop pair (f1 and f2) by forming a disulfide bridge. This disulfide linkage is highlighted with a pink circle. Moreover, a disordered loop in the wrist region (W) of sclerostin replaces the four-turn α-helix typically present in the wrist regions of BMPs. Both C- and N-terminal chains are also disordered and flexible. The disulfide bridges within the cystine-knot motif and at the fingertip are shown in yellow. Diagrams adapted from Avsian-Kretchmer and Hsueh, 2003 and Veverka *et al.,* 2009, respectively. PDB file, 2K8P.

Previous, homology modeling of CAN family members as conducted by Avsian-Kretchmer and Hsueh, 2004, were based on the X-ray crystallographic structure of the TGFβ superfamily member, human chorionic gonadotropin, which is distantly related to CAN family members. Therefore, by resolving the NMR structure of sclerostin, it was made possible to obtain more accurate predicted models of the CAN family members despite its monomeric structure, which is atypical of most BMP antagonists such as Noggin and CV2. It follows that all sclerostin-based models of CAN family members are monomeric and have also inherited all of its disordered loops

(Rider and Mulloy, 2010). Although, such predictions may not be truly representative of each individual unresolved CAN member, the elucidation of the NMR structure of sclerostin was pivotal. This represented major advance towards our understanding of the general features and properties of CAN family members, themselves.

More recently, the X-ray crystallographic structure of PRDC, a second CAN family member, has been resolved by Nolan *et al.* (2013). As mentioned earlier in this section, PRDC is the closest homologue of gremlin, the focus of this study. Contrary to its sclerostin-based monomeric model, the crystal structure has revealed that PRDC does exist as a dimer. Like the BMPs, PRDC forms a head-to-tail oriented dimer however, whose monomers are non-covalently linked (Figure 1.8B). This dimeric orientation of PRDC is contrary to that of Noggin and CV2, which as mentioned previously in Section 1.6, formed head-to-head oriented covalently-linked dimers (Groppe *et al.,* 2002; Zhang *et al.,* 2008). In a PRDC dimer, the amino acids in the wrist region (head) of one monomer create intimate contact with the fingertips (tail) of the adjacent monomer via van der Waals interactions (Nolan *et al.,* 2013). Extensive hydrogen bonding between the extending β-fingers of each monomer also helps to stabilise the dimer. Interestingly, the odd unpaired cysteine residue (Cys7) located just outside the cystine-knot motif BMPs is also present in PRDC, but here is not utilised for covalent dimerization.

The CAN family members share high sequence homology within the cystine-knot motif, however, significant sequence variations are observed around their terminal ends, which results in variable loop ends conformations (Nolan *et al.,* 2013). While both N- and C-terminal loop ends are highly disordered in sclerostin (refer to Figure 1.7B), an α-helix is formed in the highly flexible N-terminal loop in PRDC that may interact with neighbouring PRDC dimers (Figure 1.8A), (Veverka *et al.,* 2009; Nolan *et al.,* 2013).

Figure 1.8: High resolution structures of the BMP antagonist, PRDC.
The dimeric PRDC crystal structure is both represented as a centralised ribbon diagram and as pale blue and green rotated solution structures (B). The PRDC monomer is represented as either a blue or green ribbon diagram, isolated (A) and overlaid on a dimeric solution structure (B). As observed, the PRDC monomer closely resembles the sclerostin monomer shown in the previous figure possessing disordered and flexible chains at the C-terminal and in the wrist region (W). The N-terminal chain remains fairly disordered and flexible, but possesses a conserved α-helical coil, α1 helix, at its end (A). PRDC forms a head-to-tail dimer (B, central) in a similar oriented manner to BMPs themselves as described previously in the legend of Figure 1.3. In addition to the 'wrists-tucked in fingers' Van der Waals stabilisation, this dimer is also stabilised by extensive hydrogen bonding along the long axis of the interacting anti-parallel finger pair (F1 and F2) of both monomers (Van der Waals and hydrogen bonds are not shown). This then creates extended convex and concave binding surfaces which remain exposed on the outside. Adapted from Nolan *et al.,* 2013. PDB file, 4JPH.

A

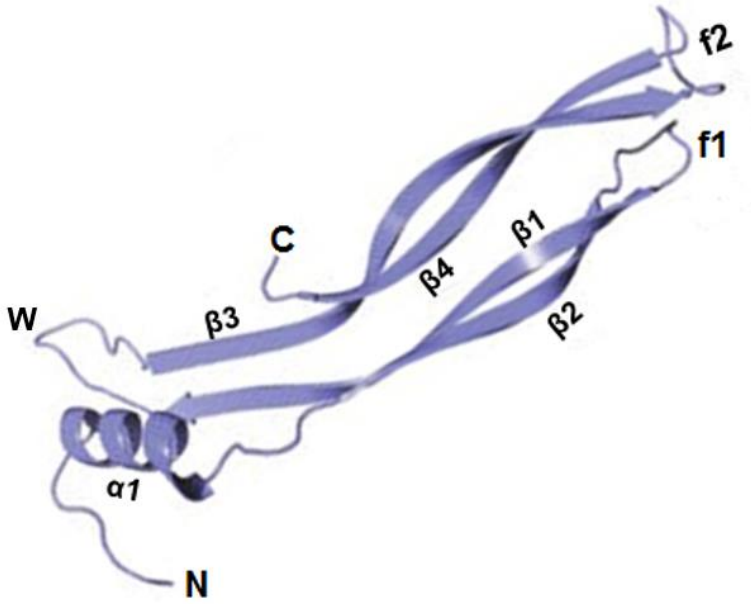
f2
f1
C
β1
β4
β3
β2
W
α1
N

B

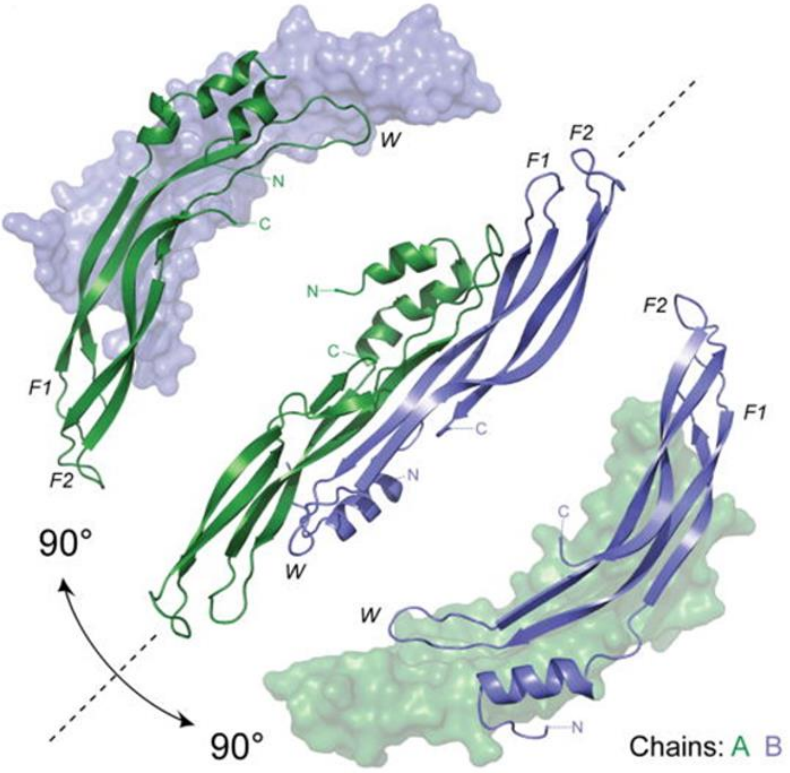
W
N
C
F2
F1
F1
F2
N
C
F2
F1
C
N
W
W
C
N
90°
90°
Chains: A B

Given high sequence homology both within and outside the conserved cysteine residues between gremlin and PRDC, it is plausible that gremlin may also adopt a similar dimeric structure. Thus, the PRDC structure may serve as the better template than sclerostin for homology modeling of the gremlin structure. Unfortunately, the PRDC structure only became available after this current study was underway. Nonetheless, such PRDC-based gremlin model was generated by our collaborator, Professor Barbara Mulloy, Royal Holloway, University of London and has been incorporated into this study. Fortunately, apart from aspects of dimerization and a conformational change in the N-terminal loop, both sclerostin-based and PRDC-based gremlin models are fundamentally consistent.

1.8 Binding sites on sclerostin and PRDC

1.8.1 Amino acid numbering system

A consensus has yet to be agreed on for the numbering of amino acid residues in primary sequences of proteins. Typically, crystallographers assign the number one to the first amino acid residue in the resolved crystal structures which may not necessarily correspond with the first amino acid residue in their full length primary sequences. This gets further confusing when homology modeling is conducted on such high resolution structures. In this thesis, sequence alignments are provided for assistance whenever there is a conflict in numbering assignments. The numbering system adopted matched that of the primary polypeptide sequence of the *Mus musculus* gremlin-1 precursor (NCBI reference sequence: NP_035954.1).

1.8.2 Binding sites on sclerostin

The work by Veverka *et al.* (2009) involved the generation of a high resolution NMR structure of sclerostin, using purified *Escherichia coli* cell-expressed ^{15}N, ^{13}C and ^{1}H-isotopic backbone-labelled sclerostin. For complete sequence-specific resonance assignments, the cross-relaxations were measured between isotopic-labelled nuclei in spatial proximity at varying ^{1}H-^{1}H distance constraints in order to generate multiple nuclear Overhauser effect spectroscopy (NOESY) spectra. These were achieved by generating two-dimensional ^{15}N, ^{1}H- and ^{13}C, ^{1}H-heteronuclear spin quantum convergence (HSQC)-NOESY spectra and the ^{15}N, ^{13}C, ^{1}H- triple resonance spectra. The NOE cross peak assignments generated were automatically combined to produce preliminary structures that were further processed (by multi-cycling annealing under

redundant dihedral angle constraints) in order to generate a small family of converged sclerostin highly precise NMR solution structures. To determine the binding sites on sclerostin, heparin oligosaccharides prepared from its NMR structure (PDB file: 1HPN; Mulloy *et al.,* 1993) were docked onto those converged NMR structures with lowest intermolecular energy. The heparin oligosaccharides included two pentasaccharide chains in the $^{1}C_{4}$ chair and $^{2}S_{0}$ skew-boat conformations, endecasaccharide and dodecasaccharide chains. Surface contact residues were either extracted automatically or monitored by the backbone changes induced in the positions of the ^{15}N, ^{1}H-HSQC amide signals in sclerostin. The heparin binding site predicted using docking calculations was mapped as a linear positively charged patch of largely arginine and lysine residue side chains. This spanned across an entire surface of the long axis of sclerostin encompassing both f2 loop and the disordered loop in the wrist region (refer to Figure 1.7).

Mapping of the heparin binding site achieved by NMR spectral analyses of amide signals in the sclerostin backbone following its binding to a dodecameric heparin fragment, were highly consistent with initial predictions. Subsequently, fresh docking calculations also observed an overlap with the heparin binding site predicted following initial docking of converged sclerostin NMR structures with the two other heparin oligosaccharides. The arginine and lysine contact residue side chains are highlighted in the sequence alignment shown in Figure 1.9. Altogether, this demonstrated that binding of sclerostin to heparin was stabilised mainly via specific electrostatic interactions which are supported by a network of hydrogen bonding between polar groups on heparin and backbone amide groups on sclerostin.

A potential hydrophobic protein binding site was also predicted from these docking calculations. It was located on the concave face of the disordered and flexible loop in the wrist region and f2 loop (refer to Figure 1.7B), on the opposite side to the heparin binding site. It is plausible this protein binding site may overlap with the BMP binding site, which is expected to share a similar charge. The predicted contact amino acid residues in this significantly hydrophobic patch are highlighted in the sequence alignment shown in Figure 1.9.

1.8.3 Binding sites on PRDC

In the studies by Nolan *et al.* (2013), recombinant wildtype PRDC was over-expressed in *E. coli* inclusion bodies that were then extracted, solubilized and components separated using size exclusion chromatography. The wildtype PRDC was

purified by ion-exchange chromatography under denaturing conditions and then subjected to oxidative refolding of its disulfide bonds. The refolded PRDC was further purified using reverse phase high performance liquid chromatography (HPLC), (Kattamuri *et al.,* 2012). Selenomethionine (SeMet)-substituted PRDC was expressed initially in transformed *E. coli* batch cultures grown to saturation in SeMet-labelling auto-inducing media (Studier, 2005). Both wildtype and SeMet-substituted PRDC crystals were grown by hanging-drop vaporising diffusion under mild dehydrating conditions for better defined X-ray diffraction patterns. X-ray crystallography generated a high resolution three-dimensional structure of PRDC which forms a dimer (refer to Figure 1.8).

Lower resolution PRDC structures were generated from the wildtype PRDC crystal using small angle X-ray scattering (SAXS) in order to validate further the high resolution PRDC structure and also to visualise the molecular envelope of the full length PRDC protein. Based on these experimental structures, predictions were made on the BMP binding site of PRDC following docking to NMR structures of various BMP ligands. These predictions were validated experimentally by site-directed mutagenesis of these contact residues followed by surface plasmon resonance (SPR) of the generated PRDC mutants on immobilised BMPs -2 and -4 biosensor chips. In this study, the putative heparin binding site on wildtype PRDC was also predicted by analysis of the distribution of electrostatic charges across its surface envelope.

Binding of the dimeric PRDC protein to BMP ligands was shown using site-directed mutagensis and SPR to be stabilised mainly via hydrophobic interactions with contact residues located mainly on the convex binding surface of its centralised cystine-knot domain. The most critical hydrophobic contact residues formed a partially buried hydrophobic patch and included Trp-72, Tyr-98, Phe-104 and Phe-114. These residues appeared to be strongly conserved across all other CAN family members including gremlin, DAN and COCO. These hydrophobic contact residues have been highlighted in the sequence alignment shown in Figure 1.9.

Strong binding of PRDC to heparin was demonstrated experimentally (K_d 54 nM) by SPR on immobilised heparin biosensor chips. By scanning the electrostatic surface of the PRDC structure, a large electropositive potential was identified in the same convex binding surface of the cystine-knot or DAN domain which partially overlaps with the BMP binding site. A similar charged patch was also identified in the helical region of the disordered N-terminal loop. Based on these observations, Nolan *et*

al. (2013) suggested that binding sites on mainly the f2 loop within the cystine-knot domain and α1 N-terminal helical region contribute to heparin binding which when occupied may allosterically inhibit BMP ligand binding to its BMP binding site (refer to Figure 1.8). In other words, both heparin and BMP binding sites may be physically distinct from one another however, may allosterically regulated each other in the presence of a ligand. The arginine and lysine contact residues within the predicted heparin binding site on PRDC are highlighted in Figure 1.9. Interestingly, a considerable overlap is observed in the contact residues that form the heparin binding site on both sclerostin and PRDC (Figure 1.9). Moreover, it can be seen that gremlin shares similar positively charged residues at these key positions in both PRDC and sclerostin. Moreover, the amino acid residues at the dimer interface of PRDC (F96 – I106) are also conserved in gremlin (F117 – I127) (Figure 1.9).

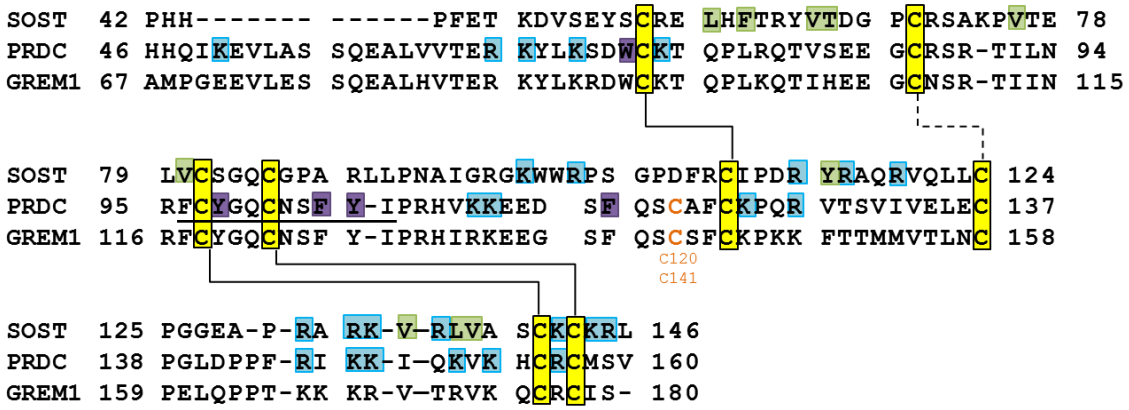

Figure 1.9: Comparison of the BMP and heparin binding sites on sclerostin and PRDC.

The primary sequence alignment shows differently numbered contact residues within mapped binding sites on sclerostin and PRDC compared to gremlin thus providing a conversion platform between them. The putative heparin binding site residues are highlighted in light blue colour. The hydrophobic residues forming the BMP binding site and a potential protein binding site in PRDC and sclerostin are highlighted in purple and light green colours, respectively. The amino acid residues at the dimer interface on PRDC are underlined. The conserved cysteine residues are highlighted in yellow with solid lines connecting cystine ring residues and the broken line, indicating the disulfide bond joining the finger pair at their tip. The unpaired cysteine residue located outside the cystine ring is highlighted in orange colour and is absent in sclerostin. SOST: sclerostin; GREM1: gremlin.

1.9 Heparan sulfate and heparin: glycosaminoglycan subclass

Heparin and heparan sulfate (HS) glycosaminoglycans (GAGs) are chemically related highly acidic unbranched polysaccharides that are covalently linked to HS proteoglycans, such as syndecans and glypicans (Gallagher and Walker, 1985; Esko and Lindahl, 2002). Both GAGs are characterised by alternating disaccharides of uronic acid [D-glucuronic acid (GlcA) or L-iduronic acid (IdoA)]-β1, 4-N-acetylglucosamine (GlcNAc) repeat units (Esko and Selleck, 2002). The numerous post-polymerisation modifications such as N-deacetylation and N-sulfation reactions that occur in the hexoses during nascent GAG chain polymerisation result in diversely patterned sulfated GAG sequences (Lindahl, 1989). Ultimately, these generate heparin and HS chains that share only subtle differences between them. Heparin undergoes more extensive modifications that render it typically more sulfated than heparan sulfate which possesses multiple unmodified regions along its chain length (Gallagher and Walker, 1985; Murphy *et al.,* 2004). Nevertheless, there are yet no agreed structural criteria for distinguishing both apart.

Heparin has long been used therapeutically as an anticoagulant capable of inactivating main agents along the coagulation cascade via direct binding to antithrombin III (Rodén, 1989; Lindahl, 1989). Contrary to confined localisation of heparin in the secretory granules of mast cells, virtually all cells in humans possess the capability to produce HS (Esko and Lindahl, 2001). In spite of these natural differences in their relative abundance, extensive industrial and therapeutic use of heparin over the past years results in heparin being practically more abundant and readily available commercially than HS. This combined with their close structural resemblance has enabled heparin to be used routinely as a model agent in biochemical studies of binding interactions that in physiological context would involve HS.

Both heparin and HS sequences are not encoded directly by gene templates, but rather are created by a cascade of specific enzymes along a shared biosynthetic pathway (Sugahara and Kitagawa, 2002). As such, the fine structure of the GAG chains depends ultimately on the regulated expression and concerted actions of these arrayed biosynthetic enzymes. This takes place principally within the lumen of the Golgi apparatus and involves multiple glycosyltransferases, sulfotransferases, and an epimerase; many of which have been purified and structurally characterised (Brandan and Hirschberg, 1988; Campbell *et al.,* 1994; Kobayashi *et al.,* 1996; McCormick *et al.,* 2000). Concomitantly, concerted action by a series of cytoplasmic enzymes

maintains adequate supply of the nucleotide sugars, UDP-Xyl, UDP-Gal, UDP-GlcA, UDP-GlcNAc and nucleotide sulfate, PAPS into the lumen of the Golgi apparatus via multiple membrane transporters (Hirschberg *et al.*, 1998; Berninsone and Hirschberg, 2000).

1.10 Biosynthesis of unmodified nascent HS and heparin chains

Biosynthesis of all GAG chain types is initiated by the stepwise assembly of a tetrasaccharide linkage sequence, GlcAβ1,3Galβ1,3Galβ1,4Xylβ1-*O*-linked to serine residues within consensus sequences, Ser-Gly/Ala-X-Gly, on core HS proteoglycan polypeptides (Esko and Zhang, 1996; Sugahara and Kitagawa, 2000). Biosynthesis of heparin/HS is illustrated in Figure 1.10. This sequential addition of sugar residues to the Ser residue on the core glycoprotein is catalysed by four glycosyltransferases, xylosyltransferase (XylT), galactosyltransferase I (GalT-I), GalT-II and glucuronyltransferase I (GlcAT-I), in the reverse order respectively (Esko and Lindahl, 2001).

After assembly of the tetrasaccharide linkage, the biosynthetic pathway to heparin/HS chains is triggered by the addition of a fifth α1,4-linked αGlcNAc sugar residue by a key enzyme, α-N-acetylglucosaminyltransferase I (GlcNAcT-I), (Sugahara and Kitagawa, 2000). Thereafter, polymerisation of the heparin or HS chain takes place by alternating additions of GlcAβ1,4- and GlcNAcα1,4-linked residues to form the characteristic backbone repeat sequence of this class of GAGs. This is catalysed by glycosyltransferases of the exostosin (EXT) family of tumor suppressors, EXT1, EXT2 and EXT-like (EXTL), EXTL1 and EXTL3 (refer to Figure 1.10), (McCormick *et al.*, 1998; Lind *et al.*, 1998; Sugahara and Kitagawa, 2000). A third member to the latter family, EXTL2 possesses GlcNAcT-I activity and as such, is involved in chain initiation in the linker region (Kitagawa *et al.*, 1999).

EXT1 and EXT2 proteins are both heparin/HS co-polymerases. Both proteins demonstrate GlcA/GlcNAc transferase activity and form EXT1/EXT2 hetero-oligomeric complexes that then accumulate in the lumen of the Golgi apparatus (McCormick *et al.*, 1999). On the other hand, EXTL1 possesses only GlcNAcT-II activity and as such, adds only GlcNAc residues during heparin/HS chain polymerisation (Kim *et al.*, 2001). EXTL3 however is bi-functional possessing both GlcNAcT-I and GlcNAcT-II activities and therefore can possibly contribute to both heparin/HS chain initiation and polymerisation (Kim *et al.*, 2001).

Figure 1.10: Heparin and heparan sulfate (HS) biosynthesis.
Geometric symbols depicting each sugar residue are defined in the legend. The post-modification reactions catalysed by the various enzymes are abbreviated above and below the sugar residues modified. The NA, NA/NS and NS domains are defined according to the sequential distribution pattern of unmodified N-acetylated and modified sulfated sugar residues. Abbreviations: EXT: exostosin family of tumour suppressors, EXTL: EXT-like family member, GlcNAc: N-acetylglucosamine, GlcA: glucuronic acid, NS: N-sulfation, 2S, 3S, 6S: 2-O-, 3-O-,6-O-sulfations. PAPS: 3'phosphoadenosine 5'-phophosulfate. Adapted from Esko and Lindahl, 2001.

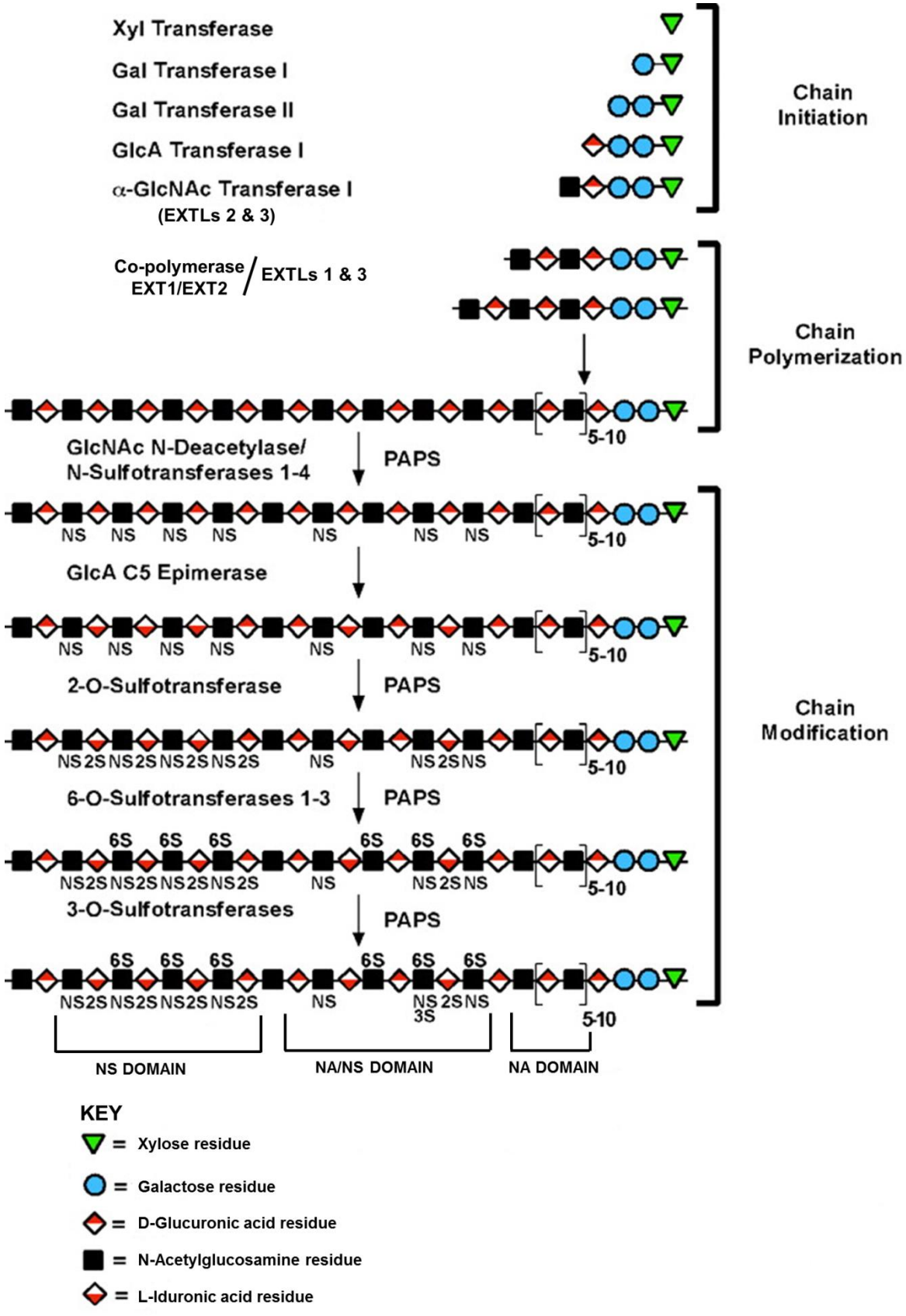
Xyl Transferase
Gal Transferase I
Gal Transferase II
GlcA Transferase I
α-GlcNAc Transferase I
(EXTLs 2 & 3)
Chain Initiation
Co-polymerase EXT1/EXT2 / EXTLs 1 & 3
Chain Polymerization
5-10
GlcNAc N-Deacetylase/ N-Sulfotransferases 1-4
PAPS
NS NS NS NS NS NS NS
5-10
GlcA C5 Epimerase
2-O-Sulfotransferase
PAPS
Chain Modification
NS2S NS2S NS2S NS2S NS NS2S NS
6-O-Sulfotransferases 1-3
6S 6S 6S 6S 6S 6S
3-O-Sulfotransferases
3S
NS DOMAIN
NA/NS DOMAIN
NA DOMAIN
KEY
= Xylose residue
= Galactose residue
= D-Glucuronic acid residue
= N-Acetylglucosamine residue
= L-Iduronic acid residue

1.11 Post-modification incorporations of nascent HS/ heparin chains

As the nascent chain is polymerized, its hexose residues are subjected to a series of post-incorporation modifications that include, GlcNAc N-deacetylation and N-sulfation, C5 epimerization of D-GlcA to L-IdoA residues and variable *O*-sulfations at C2 of IdoA and GlcA, at C6 of GlcNAc and N-sulfoglucosamine (GlcNS) residues, and at C3 of N-glucosamine (GlcN) residues. These modifications are catalysed by the bi-functional N-deacetylase/N-sulfotransferases (NDSTs), uronyl C5-epimerase and 2-*O*-, 6-*O*- and 3-*O*-sulfotransferases, respectively (Aikawa *et al.,* 2000; Esko and Lindahl, 2001). GlcNAc N-deacetylation and N-sulfation by NDSTs is a prerequisite to both epimerization and variable *O*-sulfations (refer to Figure 1.10), (Sugahara and Kitagawa, 2002).

Concerted actions of these enzymes on nascent unmodified heparin/HS chains result in variably sulfated chains that demonstrate strong aspects of sequence organisation and domain patterning. Close examination of the polymeric heparin/HS chain revealed three main domains which include; regions of contiguous N-acetylated disaccharides that form the NA domains, those with contiguous N-trisulfated disaccharides of variable length that form the NS domains and mixed regions with alternating NA/NS domains or variable region (refer to Figure 1.10), (Dietrich *et al.,* 1973; Gallagher, 2001; Murphy *et al.,* 2004; Khan *et al.,* 2013). In heparin and highly sulfated HS, the NS domains are unusually extended and encroach on the NA domains; conversely, in low sulfated HS, larger unmodified NA domains are predominant (Gallagher, 2001).

Considerable variability is exhibited in these accompanying post-incorporation modifications. As a result, heparin/HS chains are highly heterogeneous in their sequences and length. As many as 48 different disaccharides combinations could occur in heparin of which 23 have been identified to date (Esko and Selleck, 2002).

Given that other modifications depend first on actions of NDSTs, it follows that most modified disaccharides tend to cluster in the NS and NA/NS domains. These may then serve as potential docking sites for specific ligands (Lindahl *et al,* 1998). On the other hand, the NA domains have not yet been shown to directly influence protein binding and as such may serve as spacers between NS domains (Mulloy and Forster, 2000). As discussed later in Section 1.13, the specificity in heparin/HS interactions with various proteins rather points to a deeper level of sequence organisation along the chain; the classic example being the binding of heparin to antithrombin III that is

strongly dependent on a specific pentasaccharide sequence on heparin containing a central 3-*O*-sulfated GlcN residue (Bourin and Lindahl, 1993).

1.12 Heparin and HS: Conformations and dynamics

Partial activity of NDSTs and variable N-sulfations in backbone disaccharide repeat units result in highly acidic three-dimensional heparin/HS structures flanked by spatially defined patterns of carboxylate and sulfate substituents (Figure 1.11).

Heparin and its derivatives possess similar rigid glycosidic bond conformations differing mainly in their degree of flexibility due to different internal mobility (Mulloy *et al.,* 1993). Given that all D-glucopyranose monosaccharide residues in GAGs are stable in $^{4}C_{1}$ conformation, it is expected that most epimerised L-hexapyranoses, L-IdoA monosaccharide residues would be stable in the inverted $^{1}C_{4}$ solution conformation (Mulloy and Forster, 2000). As demonstrated in NMR studies and more recently with SAXS, L-IdoA residues are rather unusual in that they can exhibit both $^{1}C_{4}$ chair and $^{2}S_{0}$ skew-boat solution conformations within the heparin oligosaccharide (refer to Figure 1.11) (Khorramian and Stivala, 1986; Sanderson *et al.,* 1987; Ferro *et al.,* 1990; Mulloy *et al.,* 1993; Pavlov *et al.,* 2003). As such, the epimerisation of D-GlcA to L-IdoA residues results in changes to the internal mobility of heparin which alters the equilibrium shifts between its different conformations. The dynamic interchange between these two conformations causes twists in the pyranose ring of IdoA residues that occur without disrupting the glycosidic bonds. It is these twists that provide a small degree of flexibility to the whole polysaccharide chain without necessarily causing it to bend (Hricovini *et al.,* 1997; Mulloy and Forster, 2000). This is an important feature for its specific binding to different protein ligands.

By contrast to heparin and its derivatives, it has been demonstrated that HS forms longer and more bent three-dimensional structures (Khan *et al.* 2013). This was demonstrated using SAXS crystallography on different length HS oligomers possessing only the NA domains. By extensive depolymerisation of HS using heparitinase I, an enzyme that cleaves only within the NS domain, Khan *et al.* (2013) were able to generate a suitable model for unsulfated heparan. NMR spectroscopy on heparan, demonstrated that the NA domains in HS lacked both the rigidity and internal mobility shown by heparin and its derivatives. As such, it can be said that the flexibility and bending along a HS chain which possesses relatively more and larger NA domains is greater than that along a heparin chain with more NS domains instead. Another reason for this observed difference in rigidity between HS and heparin could be that HS is not

as much influenced by the greater repulsion between the regular repeats of acidic groups that occur in the more abundant NS domain of heparin (Khan *et al.*, 2013).

Overall, the greater flexibility of HS chains may account for their binding to a diverse range of protein ligands in all orientations. For example, this may explain HS binding to the platelet factor 4 ligand that possesses multiple heparin binding sites that are not linearly arranged to accessibility by a single extended NS domain on the heparin chain (Stringer and Gallagher, 1997; Stringer *et al.,* 2002). With greater flexibility and bending in an NA domain that separates two NS domains, it is plausible that the same HS chain can still access the differently oriented heparin binding sites on the platelet factor 4 ligand.

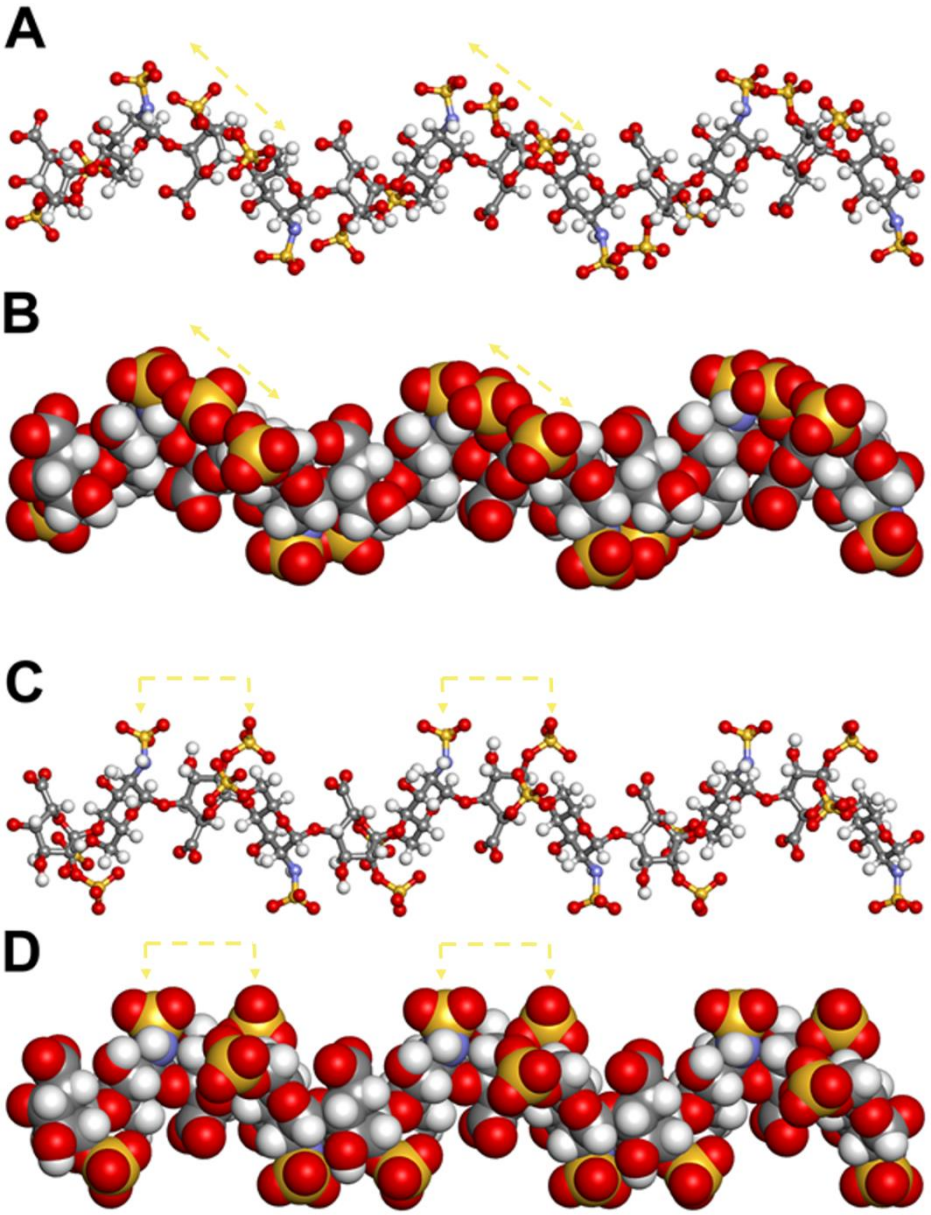

Figure 1.11: Structural conformations of heparin.
Ball and stick (A and C) and space fill (B and D) representations of a high resolution NMR heparin dodecasaccharide structure. Shown are the two conformations adopted by heparin: $^{1}C_{4}$ chair (A and B) and $^{2}S_{0}$ skew-boat (C and D) conformations caused by presence of 2-O-sulfated iduronic residues (IdoA2S) in its backbone disaccharide repeat. In the ball and stick representations, this backbone is visible and represented by repeat patterns of a carbon atom (grey ball) bonded to a single hydrogen, oxygen, nitrogen (white, red and purple balls, respectively) and/or another carbon atom via a single bond (grey stick). The different conformations result in arrangements of side-chain trisulfate groups as indicated by the broken orange double headed arrows. For acidic side-chain groups: a sulfate group (SO_3^-) = one yellow ball (sulfur atom) bonded to three red balls, a carboxylate group (COO^-) = one grey ball bonded to two red balls. Adapted from McClarence, 2011. Original source: Mulloy *et al.*, 1993. PDB file, 1HPN.

1.13 Specificity of binding interactions of HS/heparin to diverse cytokine proteins

The projecting side chain carboxylate and sulfate groups and rigidity of the NS domains of both heparin and HS implies that binding interaction with proteins is mainly coulombic and occurs superficially at their surface interfaces (Esko and Selleck, 2002). For this reason, ionic strength elution using heparin affinity chromatography constitutes a standard method for isolating and characterising heparin binding proteins (Kjellén and Lindahl, 1991). As highly acidic macromolecules, heparin/HS can bind to basic patches on protein surfaces and in this high affinity ionic binding via its NS domain, nonionic interactions such as Van der Waals forces and hydrogen bonding may also contribute significantly. This was demonstrated by Thompson *et al.* (1994) in studies that analysed the heparin binding domain on basic fibroblast growth factor (bFGF) from heparin-bFGF co-crystals. Although the basic lysine and arginine contact residues constituted the majority, they only contributed to 30% of the binding free energy in context of pure electrostatic interactions with sulfated moieties on heparin. This may represent changes to the protein structure, leading to a more rigid protein as it binds to heparin, following the initial electrostatic attraction that brings them together. As such, this reinstated the importance of these interactions beyond charge-specific binding alone.

Interestingly, analyses of both BMPs -2 and -7 crystal structures revealed larger binding cavities located on their convex surfaces opposite the receptor ECD binding sites forming arginine- and lysine-rich positive patches. These were predicted to form their putative heparin/HS binding sites (Griffith *et al.,* 1996; Scheufler, 1999). This suggests that the presence of a defined heparin binding site on proteins may be mandatory for interactions with heparin and HS.

As with the NMR structure of sclerostin and the PRDC crystal structure (refer to Sections 1.8.2 and 1.8.3), predicting the heparin binding site can be achieved using the high resolution structure of heparin in computational docking techniques. These techniques employ a primary sequence-based approach together with some extra geometrical information to predict heparin binding sites of proteins with no experimental three-dimensional structures (Hileman *et al.,* 1998; Bitomsky and Wade, 1999). These have led to the general characterisation of the heparin binding site. Typically, a heparin binding site on a protein, spans a distance about 20 Å (Margalit *et al.,* 1993). This approximates to the distance between trisulfated clusters along one side

of heparin, about 17 Å, that itself matches the periodicity of the right-handed α-helix of heparin in solution formed typically by both $^{1}C_{4}$ chair and $^{2}S_{0}$ skew-boat conformations (Mulloy *et al.,* 1997; Mulloy and Forster, 2000).

Interestingly, to current knowledge, heparin oligosaccharides bound to all growth factors are all derived from multiples of the main trisulfated disaccharide repeat unit in the NS domains (Mulloy and Forster, 2000). This differs from the antithrombin III central pentasaccharide recognition sequence that is unusual in many features. This include presence of a 3-*O*-sulfated glucosamine adjacent to GlcA residue that must be located at the non-reducing end of a fully modified trisulfated disaccharide repeat (Rosenberg and Lam, 1979; Lindahl *et al.,* 1980; Choay *et al.,* 1983).

1.14 Biological roles of HS/heparin interactions with cytokine proteins

HS being found on virtually all cell surfaces and in the extracellular matrix interacts with a litany of extracellular molecules including growth factors, adhesion molecules and cytokines playing important roles in a wide range of physiological and pathophysiological processes in humans (Takada *et al.,* 2003; Esko and Selleck, 2002). As demonstrated by Solomon (1963), biosynthesis of HS is critical during early embryogenic development. Missense or frameshift mutations in either EXT1 or EXT2 resulted in hereditary multiple exostoses (HME), a skeletal disorder characterised by cartilage-capped tumour outgrowths from the growth plate of endochondral bone. The process of normal bone formation requires action of various morphogens and growth factors whose diffusion must be tightly regulated at their sites of action (Karsenty, 2003; Nishimura *et al.,* 2012). As such, unrestricted diffusion in HME, as a result of incorrect biosynthesis of HS, serves today as a natural demonstration of the important role HS may play in localising activities of these key extracellular molecules at their specific target sites.

A similar circumstance in which HS provides a local tissue depot for active circulating cytokines such as the interleukins -2, -4 and -12 and morphogens including several BMPs, has also been reported (Hogan, 1996; Hasan *et al.,* 1999; Mummery and Rider, 2000; McLellan *et al.,* 2006; Zhong *et al.,* 2007). This results in the initiation of immune responses and in the establishing and maintenance of morphogenic concentration gradients across fields of cells that result in body patterning, respectively.

Commonly, the protective and stabilising functions of heparin/HS as shown *in vitro* go hand in hand with its binding interaction with several cytokines and growth factors. A fine example is its binding to the IL-12-induced macrophage and antigen

presenting cell (APC)-secreted cytokine, interferon gamma (IFNγ), which is critical for adaptive cellular immunity. High affinity binding of HS to IFNγ occurs at a C-terminal peptide of IFNγ that otherwise is highly susceptible to proteolytic degradation that decrease in its blood clearance and accumulation at target tissues (Lortat-Jacob, 1994 and 1996). Similar protective role against proteases such as trypsin and plasmin was also previously reported in the binding of heparin to heparin-binding growth factor-I (also known as FGF-1), (Rosengart *et al.,* 1988). Furthermore, heparin/HS-induced localised accumulation of both IFNγ and FGF-1, acidic FGF (aFGF) and the more prominent activated serine protease, thrombin, increases their stability within the extracellular microenvironment; hence increases protection from pH and thermal denaturation (Machovich and Arányi, 1977; Rosengart *et al.,* 1988; Volkin *et al.,* 1993; Lortat-Jacob, 1994).

Heparin has also been demonstrated to act as a catalyst in protein-protein interactions; it may either accelerate the rate of the protein-protein binding reaction or accelerate the rate of recognition of a protein for its binding partner. In the inactivation of thrombin by the serine protease inhibitor antithrombin III, the catalyic function of heparin is observed via the latter role (Gettins *et al.,* 1993; Chuang *et al.,* 2001). Antithrombin III is unique in that the recognition and binding to the sequence-specific pentasaccharide in heparin is required for its full activation (refer to the previous section). Interestingly, high affinity binding to heparin results in a conformational change in antithrombin III that accelerates its inhibition of thrombin via a bridging mechanism. In this mechanism, thrombin binding to a bridging site next to bound antithrombin III, along the same heparin chain, enhances the rate of recognition of antithrombin III for thrombin (Chuang *et al.,* 2001); thus formation of a trimolecular complex of antithrombin III: heparin: thrombin in intimate contact.

The function of heparin/HS as a co-receptor or as a stabiliser of FGF-1-FGF receptor-2 (FGFR-2) signalling complex has been demonstrated, although in recent years has remained much a subject of debate (Harmer, 2006). Two crystallographic models have been proposed to support both cases, the first by Pellegrini *et al.* (2000) and the second by Schlessinger *et al.* (2000), respectively. In the former, a single heparin decasaccharide chain serves as the fundamental organising unit of the 2:2 FGF-1:FGFR-2 tetrameric complex by dimerising two bound FGFs molecules without causing any intermolecular protein-protein contact. This then results in a change in the FGFs that increases their affinity for two FGFR-2 molecules. In the latter, the

Schlessinger-Mohammadi model, two heparin decasaccharide chains are required to form a 2:2:2 FGF:FGFR-2:heparin hexameric complex, instead of the single heparin chain, pentameric complex in the previous Pellegrini model. Here, heparin-mediated binding of FGF-1 to FGFR-2 results in a stable 1:1:1 ternary complex in which highly sulfated sequences at the non-reducing end of heparin make extensive contacts with positively charged binding domains of both proteins. This then results in the recruitment of a second 1:1:1 FGF:FGFR-2:heparin ternary complex via both direct FGFR-2:FGFR-2 and FGF-1:FGFR-2 inter-ternary complex secondary interactions (Schlessinger *et al.,* 2000). At this stage, heparin contributes only indirectly by promoting FGFR-2:FGFR-2 contacts hence, its suggested less fundamental role as a stabiliser (Schlessinger *et al.,* 2000). Worth highlighting, the 6-*O*-sulfate in the heparin decasaccharide seemed to play a pivotal role in both 1:1 FGF-1:FGFR-2 interaction and 2:2 FGFR-2:FGFR-2 interactions. Its desulfation was observed to markedly diminish both interactions thus demonstrating anew an aspect of binding specificity of heparin/HS binding ligands as argued previously (Schlessinger *et al.,* 2000).

The role of heparin/HS in BMP-mediated processes *in vivo* remains unclear although its BMP-mediated *in vitro* effects have been well established in functional studies. Traditionally, cell lines such as the murine C2C12 myoblastic cell line have served routinely as convenient cellular model for functional studies of BMP activity (Damon *et al.,* 1992; Larrain *et al.,* 1998; Jiao *et al.,* 2007; Kuo *et al.,* 2010). Restating, a hallmark of BMPs is their ability to induce *de novo* bone formation *in vivo* by promoting the transdifferentiation of myoblast cells to cartilage-forming chrondroblasts and bone-forming osteoblasts cells (Urist, 1965; Urist and Strates, 1971). In model cell lines such as C2C12 cells, this process is observed as a down-regulation of muscle-type markers and up-regulation of osteoblastic markers such as alkaline phosphatase that are easily quantitated in bioassays. In recent years, more sensitive reporter bioassays have enabled even earlier tracing and quantitation of BMP gene markers when co-expressed alongside a tractable reporter gene such as the firefly *Photinus pyralis luciferase (luc^{+})* gene. As mentioned previously in Section 1.5, this can be achieved by targeting enriched SBE concatemers incorporated within the promoter region of *BMP* target genes. Commonly targeted gene promoters include the *osteocalcin* and *Id1* gene promoters. The former is employed in this study. The latter expresses the inhibitor of DNA binding-1 (Id1) protein, a basic helix-loop-helix (bHLH) transcription factor that lacks a DNA binding domain. Id1 binds with high affinity to bHLH E protein family

members inhibiting their binding to promoter E boxes thus regulating DNA transcription (Zhao *et al.,* 2003; Perk *et al.,* 2005; Korchynskyi and ten Dijke, 2002).

Clear demonstrations of the effect of HS in BMP-mediated activities were seen in work conducted by Irie *et al.* (2003) when assessing its role in BMP-7-induced signalling in rat osteoblastic osteosarcoma 17/2.8 (ROS 17/2.8) cell cultures. They observed that BMP-7-induced SMAD1/5/8 phosphorylation is inhibited following pre-treatment of cells with heparitinase and chlorate, which removes endogenous cell surface HS and inhibit GAG chain sulfation, respectively (Baeuerle and Huttner, 1986; Humphries and Silbert, 1988). This indicates that HS is involved in BMP-7-induced signalling activity. The addition of exogenous soluble unfractionated heparin to both heparitinase- and chlorate-treated cells did not restore BMP-7-induced SMAD1/5/8 phosphorylation. This suggested that endogenous HS anchored to membrane surfaces of cells was essential for BMP-7 signalling.

In contrast, pre-incubation of BMP-7 with other GAGs such as chrondroitin sulfate and keratan sulfate, and de-6-*O*-sulfated and de-N-desulfated/re-acetylated heparins, did not interfere with BMP-7-induced SMAD1/5/8 phosphorylation. This with reversed interpretation, demonstrated the importance of these modified residues in the intact HS chains themselves and served as further supporting evidence for structural organisation and sequence specificity in interactions of HS with cytokine proteins. As such, Irie *et al.* (2003) suggested two possible roles of heparin in BMP-7-induced signalling activity; either 1) as forming a local depot promoting augmentation of BMP-7 concentrations at target sites, or 2) as a co-receptor facilitating binding of BMP-7 to its receptors.

Unlike BMP-7, the effects of heparin/HS in BMPs -2 and -4-induced signalling activities are not so clearly understood owing to the contradictory observations reported to date. For example, in studies conducted in C2C12 cell cultures, Jiao *et al.* (2007) observed that pre-incubation of BMP-2 with intact soluble heparin inhibited signalling activity and that both heparitinase and chlorate treatments of cells potentiated BMP-2 activity. On the other hand, similar studies by Takada *et al.* (2003) and Zhao *et al.* (2006) both observed a potentiation of BMP-2-induced activity following pre-incubation with intact soluble heparin. Also, they observed that heparitinase treatment had no effects. Moreover, Zhao *et al.* (2006) showed that in the presence of intact soluble heparin, BMP-2 degradation was blocked and its half-life increased *in vitro*. When administered with BMP-2 simultaneously into mice *in vivo*, larger amounts of

mineralized bone were induced comparatively. Taken altogether, these various studies are conflicting making it difficult to suggest the role of heparin/HS in activities of BMPs -2 and -4, unlike BMP-7. It seems differences in precise experimental procedure and conditions under which each experiment was conducted may have accounted for these conflicting views. Therefore, more detailed studies on the interactions of HS with these BMPs will be required on individual basis in order to fully understand the role of HS in BMP signalling activities.

1.15 Gremlin and its biological functions

Gremlin also known as gremlin-1, is both a membrane-associated and secreted protein constituting of 184 amino acids. It also possesses the characteristic cystine-knot motif (DAN domain; residues 94 - 184) that is shared by all members of the CAN subfamily of BMP antagonists (Wordinger *et al.,* 2008). The human gremlin gene, *GREM1*, also known as down-regulated by the oncogene mos (*drm*) encoding the gremlin protein, has been mapped to chromosome *15q13-q15* (Topol *et al.,* 2000b). Upon expression, it is subjected to post-translational modifications including N-glycosylation and phosphorylation that may account for the experimental variations in its reported molecular weight that ranges between 20 – 30 kDa (Topol *et al.,* 1997; Topol *et al.,* 2000a; Wordinger *et al.,* 2008).

The *GREM1* gene was originally identified as *drm* by screening an ovary complementary DNA (cDNA) library for activities that induced formation of a secondary axis in *Xenopus laevis* embryos. Gremlin expression was observed mainly in neural crest regions (Hsu *et al.,* 1998). In mouse embryos, gremlin is expressed in the intermediate mesenchyme, Wolffian duct and in mesonephric tubules from E9.5 paralleling BMPs -2 and -4 expression patterns (Vainio and Lin, 2002; Ducy and Karsenty, 2000). As development proceeds, a shift in gremlin expression to the condensing metanephric mesenchyme is observed, now synchronising BMP-7 expression pattern (Nishinakamura and Sakaguchi, 2014). Gremlin homozygous knockout (*GREM1*$^{-/-}$) mice, exhibit conspicuous skeletal phenotype with deficient outgrowth and incorrect digitation events, and elsewhere, show complete failure of kidney development that lead to neonatal lethality (Khokha *et al.,* 2003; Michos *et al.,* 2004).

Gremlin is a BMP antagonist known to regulate extracellularly the activities of BMPs including those of the BMPs -2, -4 and -7. This has been demonstrated both *in vivo* and *in vitro* (Hsu *et al.,* 1998; Sudo *et al.,* 2004; Sun *et al.,* 2006; Zanotti *et al.,*

2008). *In vivo*, *GREM1*$^{-/-}$*:Bmp4*$^{+/-}$ mice exhibit rescued normal kidney phenotype which in this case strongly demonstrates gremlin as a bona fide BMP-4 antagonist (Michos *et al.,* 2007). It is believed that gremlin by binding directly to the active BMP ligands, prevents them from engaging their receptors thus abrogating BMP-induced SMAD1/5/8 signalling.

This accepted paradigm as a common mechanism of BMP antagonism stemmed primarily from crystallographic studies of ligand-antagonist complexes such as the Noggin-BMP-7 and CV2-BMP-2 complexes (refer to Section 1.6). Interestingly, fresh emerging studies on the mode of gremlin action are now revealing this widely accepted paradigm may be overly simplistic. Indeed, Sun *et al.* (2006) reported a novel intracellular regulatory mechanism of BMP-4 activity by gremlin in addition to its axiomatic extracellular regulatory mechanism. In this novel mechanism, gremlin interacts directly with the BMP-4 precursor protein within cells to effectuate more efficient inhibition of BMP-4 activity. It appears however that such an interaction between gremlin and BMP-4 is tissue-specific, as it was detected only in embryonic lung and not embryonic kidney (Sun *et al.,* 2006). Nonetheless, it remains the case that significant deviation from the existing paradigm on BMP antagonist actions may exist that will necessitate further investigations on an individual basis. Furthermore, Alborzinia *et al.* (2013) revealed extracellular binding of gremlin and Noggin to fluorescently-labelled BMP-2 did not prevent the ligand itself from binding to its receptors. Instead, interactions with both gremlin and Noggin altered the fate of BMP signalling by increasing the rate of BMP-2 endocytosis through endosomes for lysosomal degradation. Also, heparitinase treatment of the HeLa cells was also observed to reduce gremlin- and Noggin-induced BMP-2 endocytosis thus suggesting a co-receptor role of HS in modulating endocytosis of activated receptor complexes.

Gremlin also has BMP-independent activity. Stabile *et al.* (2007) demonstrated a novel pro-angiogenic activity for gremlin occurring by its high affinity binding (K_d value 47 ± 15 nM) to vascular endothelial growth factor receptors (VEGFRs) on the surface of endothelial cells (ECs). This stimulates EC intracellular signalling and migration *in vitro* which ultimately lead to potent pro-angiogenic response *in vivo* (Stabile *et al.,* 2007; Mitola *et al.,* 2010; Chiodelli *et al.,* 2011). Chiodelli *et al.* (2011) demonstrated high affinity binding (K_d value 20 nM) between gremlin and heparin to reminisce physiological interactions with endogenous HS on cell surfaces of ECs that localises gremlin within endothelial extracellular matrix. This highlights anew, the

importance of HS in pathophysiological processes. Another BMP-independent activity of gremlin has been reported elsewhere (Chen *et al.,* 2004a). During early embryogenic development, Slit proteins mainly act as midline repellents of axon guidance cues and also act as inhibitors of leucocyte chemotaxis. Gremlin has been shown to bind directly to the Slit proteins 1 and 2 in a BMP-independent manner hence strongly potentiating their inhibitory effects on leucocyte chemotaxis (Chen *et al.,* 2004a). However, this study has not been followed up on.

In terms of disease involvement, gremlin is implicated in various chronic diseases. Increased levels of gremlin expression has been associated with ocular diseases such as diabetic retinopathy (Kane *et al.,* 2005) and glaucoma (Wordinger *et al.,* 2007), human tumours such as cervical and colon cancers (Namkoong *et al.,* 2006; Karagiannis *et al.,* 2014, respectively) and fibrotic disorders in the lung, liver, eye, heart, kidney, and osteoarthritis (Ali and Brazil, 2014). Gremlin expression in these pathological states is triggered by various stimuli such as mechanical stress, activation by TGF-β1, and elevated glucose.

In recent years, particular attention and great interest have been invested in understanding the molecular events underlying chronic fibrotic disorders of the kidney. This interest is sparked in part by observations that in healthy adult kidney, gremlin expression is low, but re-emerges in fibrotic pathological states such diabetic nephropathy (Roxburgh *et al.,* 2009), tubulointerstitial fibrosis reminiscent of early development (Wang *et al.,* 2001; Nakamura and Yanagita, 2012).

Fibrosis is a progressive healing process leading to excessive tissue scarring caused by insults such as hyperglycaemia, hypoxia and ischaemic stimuli. Fibrotic responses typically reflect an increase in the local pool of myofibroblasts that secrete extracellular matrix (ECM) proteins such as collagen-1 and fibronectin (Ali and Brazil, 2014). The main origin of myofibroblasts during fibrosis remains divided in opinion however. Gaining wider interest are the processes of epithelial-to-mesenchymal transition (EMT) and endothelial-to-mesenchymal transitions (EndMT). In these processes insulted differentiated epithelial or endothelial cells adopt mesenchymal phenotypes endowed with motility (Iwano *et al.,* 2002; LeBleu *et al.,* 2013).

In terms of EMT and fibrosis, most interest has surrounded BMP-7, TGFβ-1 and gremlin. In diabetic nephropathy (DN), genetic deficiency in BMP-7 is associated with pro-fibrotic activities involving over-expression of both TGFβ-1 and gremlin (Ali and Brazil, 2014). Conversely, *GREM1*$^{-/+}$ mice are partially protected from DN and *in*

vivo delivery of gremlin siRNA restored BMP-7 levels in DN ameliorating the fibrotic process. These clinical findings revealed gremlin as a potential therapeutic target for the treatment of DN (Roxburgh *et al.,* 2009; Zhang *et al.,* 2010).

An important study conducted by Rodrigues-Diez *et al.* (2014) revealed that gremlin can cause EMT of human renal proximal tubuloepithelial-2 (HK2) cells by early activation of SMAD2/3 signalling pathway. Gremlin is known to act as downstream mediator of TGFβ-1 which itself, activates SMAD2/3 signalling pathways, in turn inhibiting BMP-7-induced SMAD1/5/8 signalling pathways. Intriguingly in this study, gremlin early activation of SMAD2/3 pathways occurred in both a BMP- and TGFβ-1-independent manner. It is suggested that its prolonged incubation with the HK2 cells induced over-expression of TGFβ-1 itself that then sustained the gremlin-mediated signalling activity.

1.16 Prediction of the heparin binding site on gremlin

Gremlin has been shown to bind directly to both the BMPs -2, -4 and -7 (Hsu *et al.,* 1998; Sudo *et al.,* 2004) and with high affinity to heparin/HS GAG chains on cell surfaces (Chiodelli *et al.,* 2011). Likewise, it was also established that BMP ligands, in addition to possessing binding sites for their cell surface receptors, also possess in them distinct binding sites for heparin/HS docking (Griffith *et al.,* 1996; Scheufler, 1999; Greenwald *et al.,* 2003). This suggests that heparin/HS may play important role in the binding interactions of gremlin and its BMP ligands. In kidney fibrosis a significant decrease in levels of BMP-7 expression correlate with gremlin re-expression at high levels; a mechanism that remains to be elucidated (Ali and Brazil, 2014). In this current study, a question is addressed towards potential formation of a trimolecular complex of the BMP ligand and gremlin along the same heparin/HS chain as was seen earlier in the heparin-mediated interaction of antithrombin III and thrombin (refer to Section 1.14).

This current study is aimed at mapping the heparin binding site on gremlin and investigating its role in gremlin-mediated antagonism of BMP signalling activities. With no experimental three-dimensional structure, a gremlin model was predicted by homology based on templates of the high resolution NMR and crystal structures of its closest homologues, sclerostin and PRDC, respectively (Veverka *et al.,* 2009; Nolan *et al.,* 2013). The high resolution structures of both sclerostin and PRDC have been discussed previously in Sections 1.8.2 and 1.8.3, respectively. Our research collaborator, Professor Barbara Mulloy, Royal Holloway, University of London, has generated these predicted models of gremlin and has predicted its putative heparin

binding site using docking calculations with short chain heparin ligands prepared from the parent NMR structure, 1HPN (Mulloy *et al.*, 1993; Forster and Mulloy, 2006).

Rider and Mulloy (2010) have studied the homology modeling of just not gremlin, but of all other CAN family members of BMP antagonists by basing themselves on the NMR template structure of sclerostin, (PDB file: 2K8P). In this current study, site-directed mutagenesis studies were based on predictions made by Rider and Mulloy (2010). As shown earlier in Figure 1.7B, sclerostin possesses disordered terminal tails, which in its NMR structure are undefined. Moreover, sclerostin possesses a variable loop in its wrist region that replaces the four-turn α-helix in BMPs. As a result of these structural variations in sclerostin, only the core sequences within the conserved cysteine residues for all the other CAN members were used in pair-wise alignments with the 2K8P sequences in order to generate the relevant homology models. The alignments were conducted using the Modeler module of InsightII (Accelrys) and models visualised in Discovery Studio 2.5 (Accelrys). In this work, gremlin like sclerostin is modelled as a monomer possessing the characteristic CAN family features as described previously in Section 1.16 (refer to Figure 1.13).

To predict the heparin binding site on the predicted gremlin model and models for other CAN family members, Rider and Mulloy (2010) then conducted a series of docking calculations according to published protocol by Forster and Mulloy (2006). Gremlin was docked with two heparin pentasaccharide ligands in $^{1}C_{4}$ chair and $^{2}S_{0}$ skew-boat conformations with flexibility allowed in only their exocyclic bonds. These oligosaccharides were prepared from the parent NMR structure 1HPN to consist of three GlcNS6S (N-sulpho-N-glucosamine 6-O-sulfate) residues separated by IdoA2S (L-iduronic acid 2-*O*-sulfate) residues. In addition, docking was also made with a heparin endecamer ligand in which both glycosidic and exocyclic bonds were fixed. Using all three oligosaccharides is a useful approach as the pentasaccharide ligands will identify the ‘core’ binding site whereas the endecamer ligand may identify extensions to the heparin binding site on the protein and also provide clues into the preferred orientation of bound heparin. Docking calculations were conducted using Autodock, version 2.4 from which the intermolecular energies of binding and contact co-ordinate sets were extracted for the lowest energy docked complexes.

Based on these docking calculations, USAG-1, COCO, PRDC and gremlin, were all predicted to bind to heparin. They each possessed a marked positively charged patch along their long axes, which is characteristic of heparin binding sites seen so far.

Interestingly, DAN and Cerberus, which are both predicted not to bind to heparin, do not possess these basic patches. Comparison of all surface basic and acidic residues across the surfaces of these predicted models indicated that both DAN and Cerberus possessed fewer basic surfaces overall. This is illustrated in Figure 1.12. As discussed in more detail in Chapter 3, these last two antagonistic proteins were highly relevant in this study for design of site directed mutagenesis studies on the predicted heparin binding site on gremlin. This was done in order to generate several functional gremlin mutant proteins with the correct spacing and orientation of the conserved cysteine residues yet possessing reduced binding to heparin/HS. The sclerostin-based three-dimensional structure of gremlin docked onto a heparin endecamer chain is shown in Figure 1.13, on which the pinpointed arginine and lysine contact residues in the predicted heparin binding site have been highlighted.

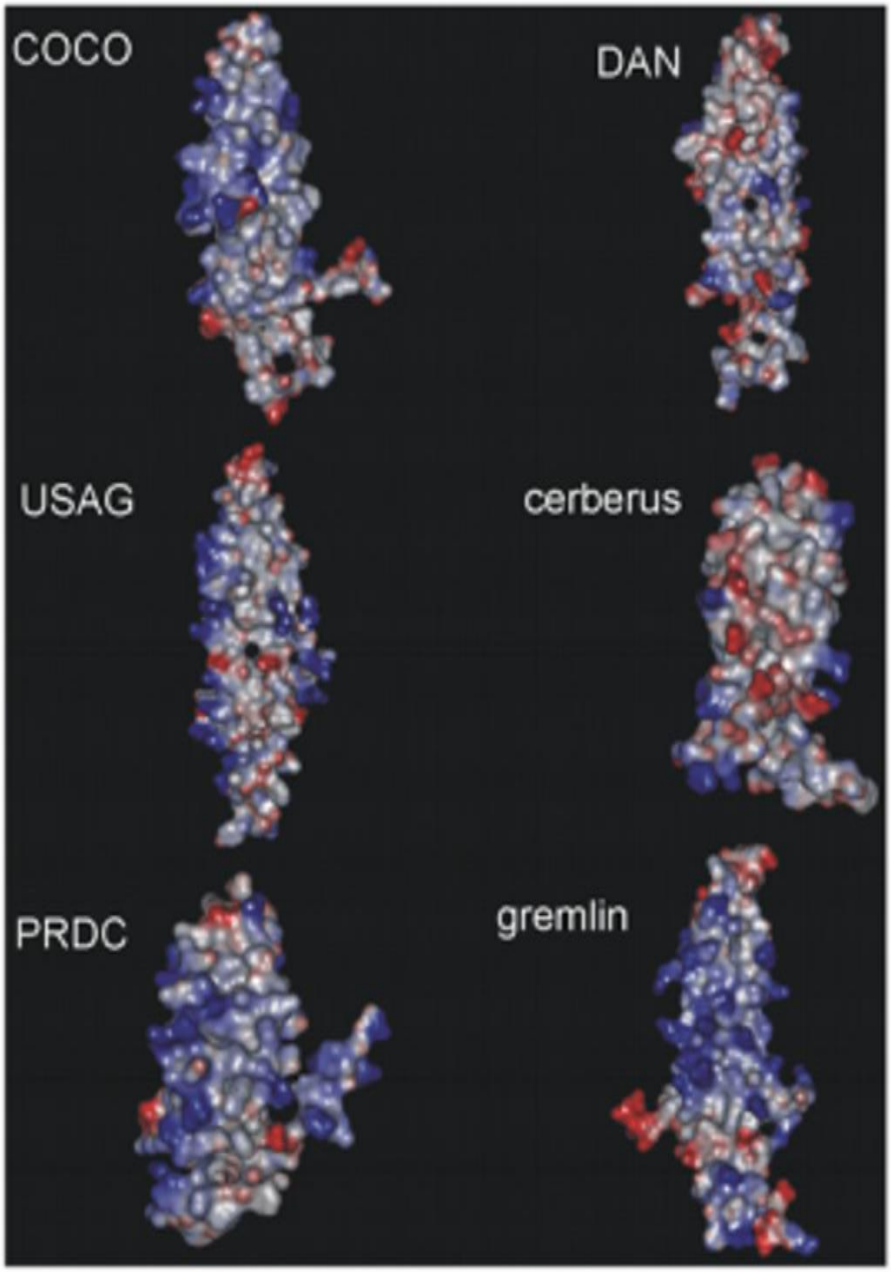

Figure 1.12: Molecular models of CAN family of BMP antagonists based on sclerostin.

Shown are the predicted solution structures of CAN family of BMP antagonists based on the NMR structure of sclerostin (PDB file, 2K8P). Models are displayed in the same orientation as the ribbon diagram shown in Figure 1.7B with fingers pointing upwards. DAN and Cerberus are the only two members within the CAN family that are predicted not to bind to heparin/HS. Comparison of their binding surfaces shows that DAN and Cerberus possess fewer basic surfaces (blue colour) and more hydrophobic patches (red colour) than other members. Figure used with permission from Rider and Mulloy, 2010.

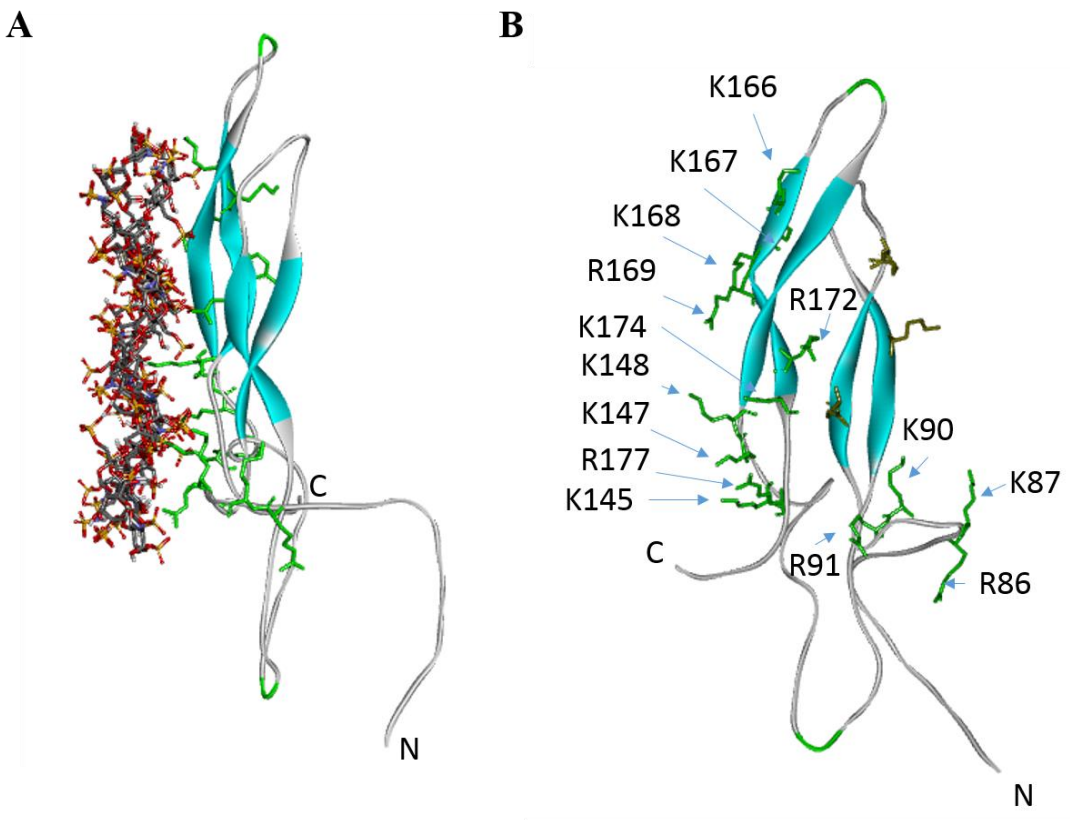

Figure 1.13: Docking of a predicted gremlin model with a heparin oligosaccharide. Shown is a homology model of the wildtype gremlin monomer based on the NMR structure of sclerostin (PDB file: 2K8P) A) docked onto an 11-mer heparin oligosaccharide and B) The docked gremlin monomer without the heparin oligosaccharide rotated through about 90° displaying all potential contact basic arginine (R) and lysine (K) residues that form its heparin binding site. This gremlin model shares similar structural features with sclerostin as described in the legend of Figure 1.7. The amino acid side chains are shown as green sticks. Homology modeling and docking calculations were conducted by our collaborator Professor Barbara Mulloy, Royal Holloway, University of London.

PRDC also called gremlin-2 is a closer homologue of gremlin than is sclerostin. Therefore, recent resolution of its crystal structure by Nolan *et al.* (2013) which revealed its existence as a dimer rather stimulated the need for fresh homology modeling based on the PRDC template, 4JPH. This would allow direct analysis to be made into the degree of overlap between the coordinate set of contact residues within both predicted heparin binding sites.

This homology modeling was kindly conducted by our collaborator, Professor Barbara Mulloy, Royal Holloway, University of London. Apart from the homology modeling itself that was conducted on the SWISS-MODEL server, docking calculations were conducted similarly, as described previously in this section when using sclerostin.

This new homology modeling server has the advantage of predicting whether a structure oligomerizes.

Previously in Section 1.7, PRDC was described to form a head-to-tail oriented dimer consisting of two monomers that share the same structural features as sclerostin except for the flexible helical N-terminal tail (refer Figure 1.8). The gremlin model based on PRDC shared identical structural features with PRDC itself (Figure 1.14). Moreover, docking calculations extracted contact residues within its predicted heparin binding site were identical to those previously pinpointed on the sclerostin-based gremlin structure. Of note, both the experimentally determined BMP binding site and the amino acid residues at the dimer interface in PRDC are both conserved in this predicted gremlin dimer, and are also highlighted in Figure 1.14.

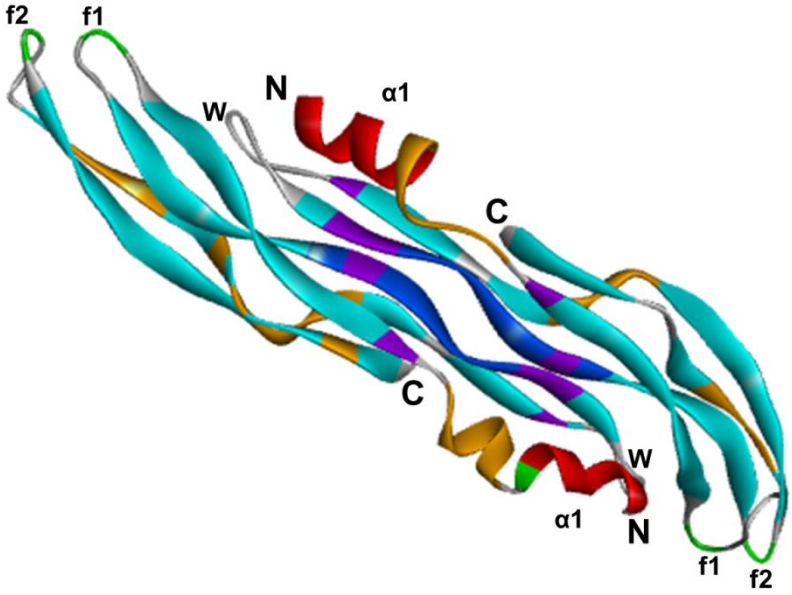

Figure 1.14: Homology model of gremlin based on PRDC.
Gremlin forms a dimer when modelled by homology based on the crystal structure of the PRDC dimer sharing the same features described previously in the legend of Figure 1.8. The dimer interface is coloured in blue. Purple coloured patches represent amino acid residues that form the predicted BMP binding site on gremlin according to experimental mapping on PRDC (Nolan *et al.*, 2013). The heparin binding sites are coloured in orange. All α-helices are coloured in red, β-strands are coloured in cyan and all turns are coloured in green.

1.17 Use of homology modeling and docking calculations in structural predictions

Using docking calculations, the heparin binding sites on generated gremlin models have been predicted. It is important however to emphasise that these predictions, serve only as hypothesis generation tools. Therefore, validation of such predictions will require full experimental verification as aimed in this current study.

The need of experimental verification relates directly to the underlying limitations of these predictive tools themselves. Homology modeling is based on the reasonable assumption that two homologous proteins will share very similar structures and, therefore, shows large bias towards the template structure. It cannot predict conformational changes in the new structure and also, cannot find new binding sites in the new structure that are not present in the template structure itself. Also, heparin and HS chains are highly heterogeneous in their sequence pattern which renders use of specific heparin oligomers in docking calculations limiting. Moreover, although the docking program, Autodock, version 2.4, allows for flexibility in the heparin ligand, it uses rigid protein approximation in order to speed up the calculation. Therefore, it cannot model proteins that require conformational changes in order to achieve a fit with the ligand. Not even rotation in amino acid side chains on the protein is allowed.

1.18 Hypotheses

The initial hypothesis in this study states that the heparin/HS binding site on gremlin is constituted mainly of positively charged clusters of arginine and lysine residues.

The second hypothesis states that the heparin/HS binding site on gremlin is physically distinct and independently regulated from its BMP binding site, also present.

The third hypothesis states that heparin potentiates gremlin binding interaction with its BMP ligands.

The fourth hypothesis states that HS binding will have a significant effect on BMP antagonist activity *in vitro*.

1.19 Aims

To test these hypotheses, the following experimental aims will be achieved:-

1.19.1 Aim 1: To clone and express C-Myc-tagged wildtype and mutant gremlin proteins

The initial aim of this study will be to test experimentally the predictions made by docking calculations on the heparin binding site in gremlin. Using site-directed mutagenesis, the predicted contact basic clusters will be targeted and substituted strategically by both neutral and acidic clusters as discussed in Chapter 3. The hope is to clone and express several functional gremlin mutants possessing reduced binding to heparin/HS.

Commercially purified wildtype gremlin recombinant protein is supplied tagged only with a polyhistidine (His) tag comprising ten histidine residues that each carries on them a partial positive charge. Given that the binding interaction between the basic clusters on gremlin and the sulfate groups on heparin/HS chains is believed to be largely ionic, a potential caveat is introduced if basing this study on the His-tagged gremlin protein alone. It is possible that such polybasic structure of His-tag could serve or contribute artefactually to heparin/HS binding (Lacy and Sanderson, 2002; Alfano *et al.,* 2007). Thus, wildtype gremlin protein will be cloned and expressed, with a substitute C-terminal Myc sequence possessing only one strongly positively charged lysine residue, EQKLISEEDL. The gremlin mutants generated will also incorporate the same C-Myc tag.

The expression of both wildtype gremlin-Myc and mutant proteins will be achieved transiently in Chinese Hamster Ovary-S (CHO-S) mammalian cell cultures. Given that gremlin is mainly a secreted protein, this study will examine its expression in harvested CHO-S cell culture supernatants mainly.

1.19.2 Aim 2: To detect gremlin-Myc expression and assess the heparin binding properties of wildtype gremlin-Myc

In order to compare the level of wildtype gremlin-Myc expression to those of its mutants in crude CHO-S culture supernatants, a Myc-capture gremlin ELISA will be used. The expression of a gremlin protein of the correct molecular weight will be confirmed by Western blotting using a polyclonal gremlin primary antibody.

In order to demonstrate that expressed wildtype gremlin-Myc in crude CHO-S culture supernatant does indeed maintain similar heparin binding properties to purified

gremlin-His protein, the heparin-binding ELISA will be used. In this ELISA, heparin coupled at its reducing end with bovine serum albumin (BSA), heparin-BSA, is used as capture layer for gremlin alongside mock-BSA (Najjam *et al.,* 1997). The aim here will be to competitively inhibit binding of both Myc- and His-tagged gremlin proteins with soluble unfractionated heparin. The EC_{50} values extrapolated from both inhibition curves generated will be compared for similarities in their heparin binding properties.

1.19.3 Aim 3: To assess the heparin binding capabilities of gremlin-Myc mutants compared to the wildtype

The heparin binding capabilities of the gremlin-Myc mutants compared to wildtype will be assessed using both the heparin-binding ELISA and heparin affinity chromatography. Both methods will be based on the principle that at constant pH, altering the ionic strength alone of the applied buffer solution will disrupt the ionic bonds formed between interacting molecules. The change in ionic strength will reflect the strength of the ionic interactions themselves. In both methods, NaCl prepared at increasing concentrations will be used to vary the ionic strength of the buffer solution at pH, 7.5. Therefore, NaCl salt concentrations will serve as a surrogate measure of binding affinity between gremlin-Myc and heparin. In the heparin-binding ELISA, the heparin-BSA capture layer will be incubated with different crude gremlin-Myc CHO-S culture supernatants prepared at increasing NaCl concentrations. In heparin affinity chromatography, the bound gremlin-Myc proteins will be eluted from packed HiTrap heparin-Sepharose and AF-heparin HC650M bead columns using a step NaCl gradient.

1.19.4 Aim 4: To indicate that binding of gremlin to heparin occurs via specific ionic interactions and to purify expressed gremlin-Myc proteins

Having assessed the heparin binding capabilities of the gremlin-Myc mutants against wildtype, we will seek to shed some light into the nature of their ionic interactions; that is whether heparin binding is more specific than binding to a simple cationic exchanger sulfopropyl (SP)-Sepharose matrix. As a highly acidic polysaccharide, heparin has the capability to bind any positive point charge on other molecules. However, as elaborated previously in Sections 1.13, the contact amino acid residues on heparin-binding cytokines such as gremlin, constitute mainly of clusters of positively charged arginines and lysines whose spacing is likely to be defined. These experiments will test whether binding of gremlin to acidic sulfate and carboxylate side-

chain groups on the heparin/HS chains is stronger than binding to sulfopropyl groups on the cationic exchange Sepharose matrix.

Moreover, attempts will also be made at partially purifying the expressed gremlin-Myc proteins from their crude CHO-S culture supernatants. This will be achieved by scaling up the SP-Sepharose ion-exchange chromatography.

1.19.5 Aim 5: To investigate BMP binding capabilities in wildtype gremlin-Myc and its mutants and assess the effect of heparin on these capabilities

Most studies of TGFβ signalling have demonstrated that strong hydrophobic interactions promote affinity between ligand:antagonist and ligand:receptor functional pairs (Groppe *et al.,* 2002; Thompson *et al.,* 2005; Veverka *et al.,* 2009; Nolan *et al.,* 2013). On the other hand, strong ionic interactions promote affinity between any cytokine and heparin/HS ligands (Ruppert *et al.,* 1996; Scheufler, 1999; Veverka *et al.,* 2009; Nolan *et al.,* 2013). This rather implies that both BMP and heparin binding sites on the same cytokine molecule can be distinguished as clusters of either hydrophobic or positively charged residues, respectively.

Gremlin is one of several antagonists BMPs. Such affinity towards its BMP ligands strongly highlights presence of a specific BMP binding epitope on gremlin. By resolving the crystal structure of PRDC, Nolan *et al.* (2013) mapped its BMP binding site and showed this was distinct from its predicted heparin binding site. In this case however, both BMP and heparin binding sites are located in close proximity to each other such that ligand binding to one results in competitive inhibition of other. The existence of physically distinct BMP and heparin binding sites as observed on PRDC is in agreement with the second hypothesis of this current study on gremlin (Refer to Section 1.18). However, it proposes otherwise in competitive binding of their ligands.

Therefore, an aim of this study will be to first demonstrate that the cloned wildtype gremlin-Myc and its mutants have maintained their natural BMP binding capabilities and also check if they are correctly folded. First, this will be achieved by immunoprecipitation of purified BMP-4 protein on gremlin-Myc-bead complexes followed by Western blotting. Alternatively, the same aim will be achieved by a novel ELISA approach that will generate BMP-4 immunoreactivity only, the Myc-capture GREM1/BMP4 double sandwich ELISA. Moreover, this ELISA will also enable investigations into the effect of heparin on the binding interaction between gremlin-Myc and BMP-4. This in a way, will mimic the approach of surface plasmon resonance

(SPR) used by Nolan *et al.* (2013) for similar studies on the effect of heparin in PRDC interaction with BMP-2 on immobilised BMP-2 sensor chips. In the ELISA, gremlin-Myc will be immobilised on a 9E10 Myc antibody capture layer in wells of a 96-well ELISA plate, instead.

1.19.6 Aim 6: To assess whether expressed gremlin-Myc proteins are functionally active and investigate the role of HS in gremlin interaction with BMPs

In order to assess whether expressed wildtype gremlin-Myc alongside its selected low-heparin binding mutants are functionally active, two functional assays will be established in C2C12 myoblastic cell cultures. Both functional assays will assess the capability of gremlin to inhibit BMP-SMAD1/5/8 signalling in the cells following pre-incubations with BMPs -4 and/or -7 purified proteins. Also, effort will be made at concentrating the expressed gremlin-Myc proteins from their crude CHO-S culture supernatants, beforehand.

First, in the SMAD1/5/8 phosphorylation assay, both BMPs -4 and -7 dose response curves will be established, as a semi-quantitative measure of induced SMAD1/5/8 levels of phosphorylation. From the responsive ranges of these curves, a fixed dose will be chosen and inhibited using purified gremlin-His protein and/or the concentrated gremlin-Myc proteins.

Alternatively, functional activity of expressed gremlin-Myc proteins will be assessed using a luciferase-secreted reporter construct in a similar manner described by Sudo *et al.* (2004). In this quantitative assay, a BMP-2/4/7-specific reporter DNA construct is transiently transfected into P19 embryonal carcinoma cell cultures. Luciferase enzymatic activity is measured as a direct correlation of transcriptional activation of a BMP-SMAD1/5/8 downstream target promoter gene. Similarly to the SMAD1/5/8 phosphorylation assay, BMPs -4 and/or -7 dose response curves will be established prior to inhibition of a chosen responsive dose of BMPs -4/-7 with the concentrated gremlin-Myc proteins.

In both functional assays, experiments assessing functional activities of gremlin-Myc proteins will also serve as an investigation into the role of HS in their interaction with BMPs. These next experiments are made interesting by comparing side-by-side wildtype gremlin-Myc against its low-heparin/HS binding mutants. Given that both wildtype gremlin-Myc and its BMP ligands can bind to HS, use of gremlin mutants possessing reduced binding for HS, provides a powerful tool in this

investigation. This will provide a way of investigating the direct role HS plays in gremlin activities. Additional investigations into the role of HS will be carried out on heparitinase and chlorate treated-C2C12 cells prior to addition of both BMP and gremlin-Myc proteins. Heparitinase treatment will deplete HS on cell surfaces entirely whereas chlorate treatment will inhibit sulfation in general. Therefore, these experiments seek to investigate whether HS is indispensable to the functional activities of both BMP and wildtype gremlin-Myc proteins and seek to comment on the specific nature of this interaction, respectively.

CHAPTER 2: Materials and methods

2.1 DNA digestion reactions with restriction endonuclease enzymes

The restriction endonuclease enzymes, NotI and XhoI, and their accompanying preparation buffers were purchased either from Promega Corporation, USA or Fermentas International Inc, Canada. A typical double digestion reaction consisted of the following components:

DNA plasmid	1-2 µg
10x restriction enzyme buffer	2.0 µl
(10x Bovine Serum Albumin	0.2 µl if required)
NotI enzyme	1.0 µl
XhoI enzyme	1.0 µl
Ultrapure distilled water (Sigma-Aldrich, USA)	made up to 20 µl final volume

The reaction mixtures were mixed and incubated at 37 °C for 2 - 3 h.

2.2 Agarose gel electrophoresis

Agarose gel electrophoresis experiments were conducted in a similar manner described by Sambrook *et al.* (1989), replacing ethidium bromide as fluorescent dye with the less toxic WebGreen DNA dye (Web Scientific, UK). The samples were run on 1% (w/v) agarose gel prepared by dissolving molecular grade agarose (Bioline, UK) in Tris-acetate-EDTA (TAE) buffer [40 mM Tris-acetate, 1 mM ethylenediaminetetraacetic acid (EDTA)]. The mixture was microwave heated to help dissolve the agarose. WebGreen DNA dye (1 µl) was added into the cooling agarose solution, which was then poured into a horizontal gel casting tray with inserted well combs. The agarose gel was left to set at room temperature. Once set, the gel was placed in an electrophoresis tank (Bio-Rad, USA) containing enough TAE buffer to cover the gel to a depth of about 1 - 1.5 mm. In analytical gel runs, a maximum of 300 ng DNA sample was prepared in 6x DNA loading dye (Bioline, UK) and ultrapure water to 10 µl final volumes. In preparative gel runs, the DNA amount was increased 5-fold and prepared only in 6x DNA loading dye to 20 - 30 µl final volumes.

Prepared DNA samples were loaded into the buffer-filled wells of the gel alongside 5µl Hyperladder I DNA molecular weight marker (Bioline, UK). The gel was then subjected to electrophoresis at 110 V until suitable migration of the leading visible bands was achieved. Separated DNA bands were visualised and photographed using a U:Genius 3 basic UV gel imaging system with camera and UV transilluminator (Syngene, UK).

2.3 DNA extraction and purification from agarose gels

Migrated DNA bands on agarose gels were visualised on a Dark Reader blue light transilluminator platform (Clare Chemical Research, USA). Each DNA gel slice was carefully excised to no more than 400 mg in weight using a sterile scalpel (Swann-Morton, UK). The embedded DNA was then extracted and purified using the QIAquick Gel Extraction Kit (Qiagen, UK), according to the supplier's protocol. As recommended, silica membrane-bound purified DNA fragments were eluted into sterile 1.5 ml microcentrifuge tubes from the QIAquick spin columns by applying 30 µl elution buffer (10 mM Tris-HCl, pH 8.5), standing at room temperature for 1 min, and then centrifuging at 17900 x g for 1 min.

2.4 DNA quantitation

The concentrations of DNA fragments, extracted and purified, were estimated using the NanoDrop 1000 spectrophotometer and accompanying software, version 3.5.2 (Thermo Scientific, UK). Blanking of the instrument was done using the QIAquick elution buffer. Per DNA sample, the average of three independent readings was taken. An independent reading is defined as a fresh measurement after a full close-restart cycle of the software program which requires blanking of the instrument.

2.5 GREM1 cDNA clone

A 1639 bp complementary DNA (cDNA) I.M.A.G.E clone containing the complete coding sequence of wildtype *M. musculus gremlin* or *gremlin-1* gene (*GREM1*), (Unigene ID: MM.166318, GenBank accession number: NM_011824), was purchased as a stab culture of *E. coli* colony from Source BioScience Lifesciences (Nottingham, UK). A streak plate was prepared on an ampicillin-selective Luria-Bertani (LB) agar plate (refer to Section 2.10). The purified GREM1 cDNA was obtained by Mini prep (refer to Section 2.13.1) of an isolated single colony. This served as a DNA template for PCR cloning of the wildtype GREM1 DNA insert described next.

2.6 Polymerase Chain Reaction (PCR) using Taq and Pfu DNA polymerases

All PCR amplifications were carried out routinely using both Taq and Pfu polymerases together in the same reaction for high fidelity amplifications. Both DNA polymerases were supplied by Promega, USA. The Taq polymerase was present in the supplied ready-to-use GoTaq green master mix 2x solution (Promega, USA) used routinely. In this master mix solution, the Taq polymerase was supplied in 2x Green GoTaq reaction buffer (pH 8.5), 400 µM dATP, 400 µM dGTP, 400 µM dCTP, 400 µM dTTP and 3 mM $MgCl_2$. Supplementation of the green master mix 2x solution with Pfu polymerase was done during assembly of the PCR reaction mix.

Pfu DNA polymerase is from *Pyrococcus furiosus DSM3638* (Fiala and Stetter, 1986) and offers high fidelity amplification by possessing a proofreading 3' to 5' exonuclease activity that the Taq polymerase lacks (Cline *et al.,* 1996). Taq DNA polymerase is from *Thermus aquaticus* (Chien *et al.,* 1976).

In a typical PCR reaction mixture, the following components were assembled in 0.5 ml thin-walled sterile PCR tubes placed on ice:

GoTaq green master mix 2x solution	25 µl
Appropriately diluted DNA template	1 µl
10 µM sense primer	1 µl
(10 µM second sense primer if necessary	1 µl)
10 µM anti-sense primer	1 µl
(10 µM second anti-sense primer if necessary	1 µl)
Sterile water	Make up to 49 µl final volume
Pfu DNA polymerase	1 µl

The number of pairs of non-complementary and complementary PCR primers used per PCR reaction mixture varied depending on the underlying PCR cloning strategy adopted. In the standard PCR and overlap extension (OE) PCR (Figure 3.5), only a pair of non-complementary PCR primers was used per reaction mix. In the one-step OE (OOE) PCR (Figure 3.6), at least one pair of non-complementary PCR primers together with a complementary pair of PCR primers were both used in the same reaction mix.

The full sequences of PCR primers are listed in Tables 3.3 - 3.5. The annotations used in these tables are consistent with those in Figures 3.5 and 3.6.

The above listed components were mixed thoroughly and PCR was carried out in a G-Storm GS482248 well multi-block thermal cycler using the following parameters:

Initial denaturation:	95 °C 2 min	
Denaturation:	95 °C 40 s	31 cycles
Annealing:	60 °C 60 s	
Polymerase extension:	72 °C 2 min	
Final extension:	72 °C 10 min	

For gradient PCR, several PCR reaction mixtures were set up in the same thermal cycler, and an annealing temperature gradient was set up ranging between 60 – 72 °C. All other parameters were kept constant. PCR products were stored at -20 °C. PCR products were purified using the QIAquick PCR purification kit (Qiagen, USA) following the manufacturer's protocol. The silica membrane-bound purified DNA inserts were eluted into sterile 1.5 ml microcentrifuge tubes as described previously in Section 2.3.

2.7 Processing of PCR products

Following PCR purification of the full-length GREM1 DNA inserts, restriction digestion, agarose gel electrophoresis, agarose gel extractions and NanoDrop measurements were performed sequentially as described previously (refer to Sections 2.1 – 2.6, respectively). DNA sequencing as described in Section 2.14, in the case of the full-length GREM1 DNA insert, was conducted using the same pairs of outer non-complementary PCR primers used for its cloning.

2.8 DNA ligation reactions

DNA ligation reactions were carried out using the Quick Stick (QS) ligase kit (Bioline, UK) according to the supplier's protocol. For most ligation reactions, the molar ratio of vector DNA to insert DNA was maintained at 1:3 unless stated otherwise. Also, the recommended maximum limit of 100 ng total DNA per reaction was followed. Reactions were assembled in sterile 1.5 ml microcentrifuge tubes at room temperature with the following components:

GREM1 insert DNA	70 ng
+/-TSAP- treated pCMV-Tag5A vector DNA	30 ng
Sterile water	Adjust volume to 14 µl
QS ligase	1 µl
4x QS ligase buffer	5 µl

Reactions were incubated at room temperature for 15 min and 1 - 10 ng ligation products were transformed into competent *E. coli* cells. In negative control reactions, only the empty +/-TSAP-treated vector was added.

2.9 Mammalian expression vectors

2.9.1 pCMV-Tag5A expression vector (Figure 3.8)

The pCMV-Tag5 expression vector (Agilent Technologies, USA) was supplied with three shifted reading frames of its multiple cloning site (MCS) relative to the C-terminal Myc sequence. These, designated as 5A, 5B and 5C, allowed flexible adaptations of the vector to different cloning strategies. In the MCS frame 5A (GenBank accession number: AF076312), the MCS is directly in frame with the C-terminal Myc sequence. Both frames 5B (GenBank accession number: AF076777) and 5C (GenBank accession number: AF076778) are out of frame with the C-terminal Myc sequence caused by the insertion of one and two alanine leading base nucleotides, respectively, between MCS frame 5A and the C-terminal Myc sequence. In this study, only the pCMV-Tag5 vector with in frame 5A, hereafter called pCMV-Tag5A vector, was compatible with our chosen cloning strategy. This made use of only NotI and XhoI RE enzymes for subcloning of GREM1 inserts directly into the MCS of the vector such that it remained in frame with C-terminal Myc sequence. Vector digestion was carried out as described previously in Section 2.1.

Typically, restriction digestion of the pCMV-Tag5A expression vector was followed by treatment with thermosensitive shrimp alkaline phosphatase (TSAP), purchased with its accompanying preparation buffers from Promega, USA. To 20µl pCMV-Tag5A double digest mixture, 1 µl TSAP and 1 µl multi-core 10X buffer were added and incubated at 37 °C for 10 - 15 min. After incubation, the TSAP was heat inactivated at 65 °C for 15 min. This was followed by agarose gel electrophoresis, agarose gel extraction and NanoDrop measurements as previously described in Sections 2.2, 2.3 and 2.4, respectively.

2.9.2 pEGFP-C1 expression vector

Because of the fluorescent property of EGFP protein, EGFP expression was used as an indirect means to monitor the levels of expression of gremlin-Myc proteins during the transfection process itself. Subsequently, because of a lack of reports into the specific binding of EGFP to BMPs, heparin/HS and gremlin, the EGFP culture supernatants became routinely employed as negative control supernatants in all immunoassays.

The plasmid map, of the pEGFP-C1 expression vector shows several shared features with the pCMV-Tag5A expression vector map (refer to previous section) which are discussed in Chapter 3, Section 3.6.1. Notably, the former also possessed a CMV promoter driving strong expression of the downstream *EGFP* gene and other genes within its MCS at its C-terminal end (Figure 3.12). Other shared features included the SV40 ori and F1 ori also inversely oriented, the SV40 promoter and both SV40 and HSV TK polyadenylation signals.

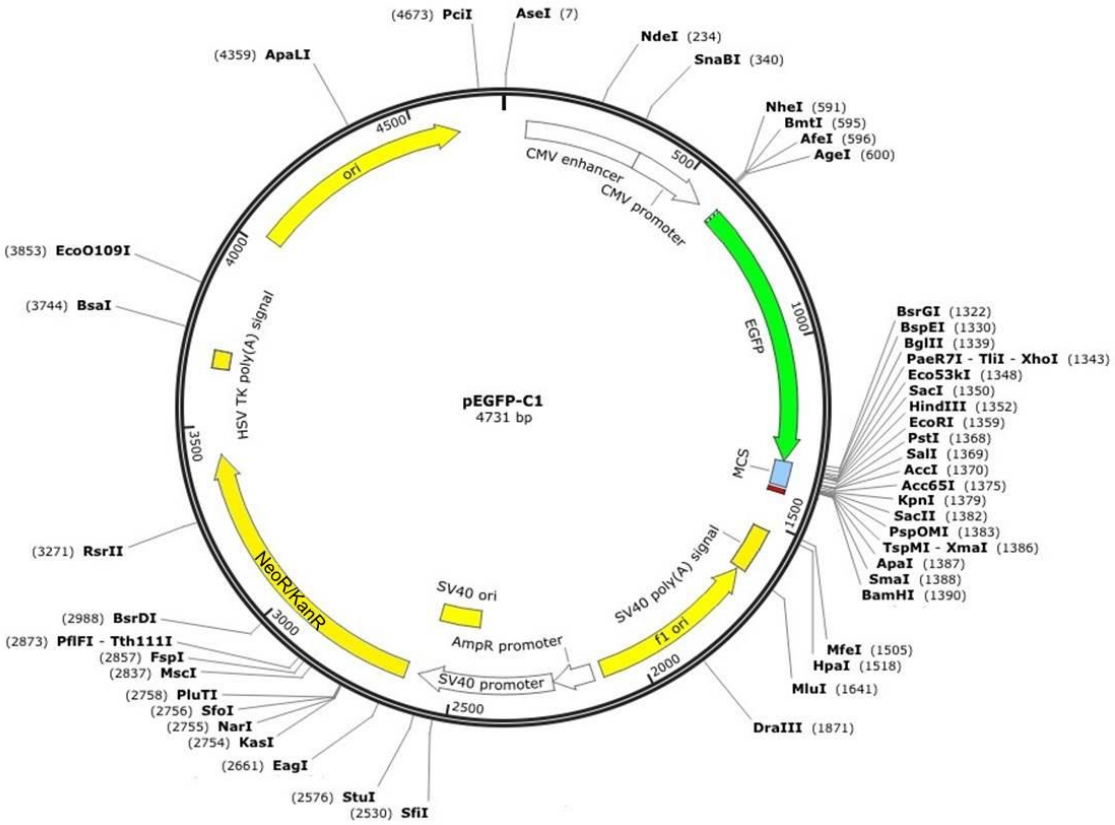

Figure 2.1: Plasmid map of the pEGFP-C1 expression vector construct.
The CMV enhancer-promoter drives expression of the *EGFP* gene and genes within the MCS (light blue colour). A stop codon (red colour) at the C-terminal end of the MCS terminates both expressions. Coloured in yellow: origin of replication (ori), f1 ori, SV40 ori, neomycin resistance/kanamycin resistance (NeoR/KanR) gene, herpes simplex virus (HSV) TK and SV40 polyadenylation [poly(A)] signals. Arrows indicate direction of transcription by promoters. Restriction sites are indicated on the outside of the plasmid circle. Refer to legend of Figure 3.8 for abbreviation listing. Adapted from Clontech Laboratories, Inc, USA.

2.9.3 pGL3-basic expression vector

Subcloning of a SMAD1/5/8-specific DNA insert, 12XSBE-Oc insert DNA, into the MCS of the pGL3-basic expression vector (Promega Corporation, USA), was carried out by Zhao *et al.* (2003). More details on the 12XSBE-Oc-Luc^{+}-pGL3 reporter construct are provided later in Section 2.30.1. This was a kind donation from Dr Zhao Ming, University of Texas Health Science Center, Texas.

The pGL3-basic expression vector (4818 bp in size) on itself lacks eukaryotic promoter and enhancer sequences required to drive expression of its incorporated *Photinus pyralis* firefly luciferase gene (*luc*$^{+}$). This provides maximum flexibility for cloning properly inserted and oriented putative regulatory sequences into its MCS as

such. The plasmid map of this expression vector as provided by the manufacturer is as shown below:

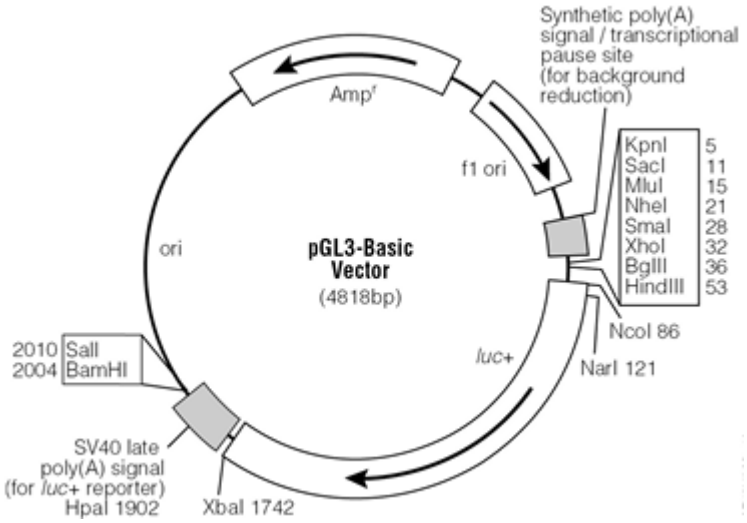

Figure 2.2: pGL3-basic expression vector map.
Functional promoter can be inserted upstream of the firefly luciferase gene (*luc*+) in the multiple cloning site (MCS). Potential enhancer elements can also be inserted upstream of the promoter in front of the *luc*+ gene or in the BamHI-SalI restriction sites downstream the *luc*+ gene. In addition, the vector possesses both an f1 and *E. coli* origin of replication (ori), a gene that confers ampicillin resistance (Amp^r) and two polyadenylation (polyA) signals upstream and downstream the MCS and *luc*+ gene respectively. The polyA signals are grey shaded. The arrows indicate the direction of transcription and the numbering represent the respective regions of restriction sites along the vector circle map.

2.10 Bacterial growth media

- Luria-Bertani Broth (LB) medium (Sigma-Aldrich, USA): 10 g/L tryptone, 5 g/L yeast extract, 5 g/L NaCl, prepared in deionised water and autoclaved at 121 °C for 20 min.

- Miller's LB Agar medium (Merck KGaA, Germany): 15 g/L Agar, 10 g/L tryptone, 5 g/L yeast extract, 10 g/L NaCl, prepared in deionised water and autoclaved at 121 °C for 20 min.

Both growth media were made selective by adding either kanamycin or ampicillin antibiotics to a final concentration of 10 µg/ml or 50 µg/ml, respectively, according to the specific antibiotic resistance gene incorporated in plasmids of the growing competent *E. coli* bacterial cells.

2.11 Preparation of bacterial glycerol stocks

Glycerol stocks were prepared for long term storage of sequence-verified positive integrative transformants. A 1:1 dilution of the bacterial starter culture (refer to Section 2.13) was made in 30% (v/v) sterile glycerol also prepared in selective LB medium. Glycerol stock aliquots were frozen immediately in liquid nitrogen and then transferred to -80 °C.

2.12 Transformation of competent *E. coli* bacterial cells

For transformations, the DH5α and Top10 *E. coli* strains were used. DH5α competent cells purchased from Invitrogen Life Technologies (California, USA) were used routinely. Top10 competent cells were a kind donation by the George Dickson's laboratory, Royal Holloway, University of London and were used only when transformations into DH5α competent cells were unsuccessful. Top10 competent cells had originally been purchased from the same supplier above.

Transformations of 1 - 10 ng ligation products into 100 µl aliquots of DH5α competent cells were carried out as outlined in the manufacturer's protocol. Treated competent cells were plated on selective LB agar plates at low and high volumes of 20 µl and 150 µl, respectively. Plates were incubated overnight at 37 °C. Next day, plates with bacterial colonies were parafilm-sealed and stored at 4 °C. Transformations into Top10 competent cells were also conducted in a similar manner as that described above except that only 50 µl aliquots of competent cells were used instead.

For streak plate preparations, single bacterial colonies were picked and streaked onto new plates of selective LB agar or compartmentally onto the same plate. Streaked plates were then incubated overnight at 37 °C before sealing with parafilm and storing at 4 °C.

2.13 DNA purification

2.13.1 Small scale purification of DNA (Mini prep)

Mini prep of DNA was carried out using the QIAprep Spin Mini prep kit (Qiagen, USA) following the manufacturer's protocol. Sterile selective LB medium (5 ml) was inoculated with a picked single bacterial colony and then incubated at 37 °C for 16 h with vigorous shaking at 225 rpm (orbital incubator, S150, Stuart, UK), under sufficiently aerated conditions.

This formed the bacterial starter culture and was carried out using a sterile 15 ml centrifuge tube (Orange Scientific, Belgium). Mini prep was then conducted as guided by the manufacturer's protocol. The silica membrane-bound purified DNA was eluted into a sterile 1.5 ml Eppendorf tube by applying 30 µl elution buffer into QIAquick spin column and then centrifuging at 17900 x g for 1 min.

2.13.2 Large scale purification of plasmid DNA (Maxi prep)

Typically, the positive integrative transformants to be processed by Maxi prep, were picked either from an LB agar growth plate or from its frozen glycerol stock. In the latter case, frozen glycerol stocks at -80 °C were partially thawed in ice and a sterile inoculation loop was dipped into the thawing glycerol stock and then dropped into 5 ml selective LB medium for preparation of its starter culture (refer to previous section).

Maxi prep of plasmid DNA was conducted routinely prior to sequencing, mammalian transfections and functional studies all of which required highly purified plasmid DNA material. Maxi prep of DNA was carried out using the Qiagen endofree plasmid maxi kit (Qiagen, USA) following the manufacturer's protocol. Initially a selective starter culture was prepared as described in the previous section. Fresh selective LB medium (100 ml) in a sterile 500 ml conical flask was inoculated with 100 µl starter culture and then incubated under the same conditions stated in the previous section. The procedure hereafter was carried out as outlined in the manufacturer's protocol. The eluted purified DNA was air-dried for 10 - 20 min, resuspended in 150 - 300 µl elution buffer (10 mM Tris-HCL, 1 mM EDTA; pH 8) and then transferred into a sterile 1.5 ml microcentrifuge tube.

2.14 Plasmid DNA sequencing

The same pair of sequencing primers was used for sequencing all Maxi prep purified DNA plasmids. Their oligonucleotide sequences are listed in Table 2.1. The only exception occurred during sequencing of purified GREM1 inserts following PCR amplification. In this case, the sequencing primers constituted the same pair of non-complementary outer primers used for the PCR amplification process itself. These are provided in Tables 3.3 – 3.5.

Table 2.1: GREM1-Myc plasmid construct sequencing primer oligonucleotides.

Sequencing primer direction	Sequencing primer oligonucleotides (5' – 3')
Sense	CTA GCG ATT ACG CCA AGC TC
Antisense	TAT AGG GCG AAT TGG GTA CAC

The primers were designed to complement 60 - 100 base pairs upstream of the NotI restriction site and the Myc sequence/stop codon at the N- and C-terminal encoding regions of the GREM1 insert-in-vector, respectively, using the ApE plasmid editor software, version 1.17 supplied by Invitrogen, UK. Sequencing was conducted commercially by The Sequencing Service at the University of Dundee, Scotland (College of Life Sciences; http://www.dnaseq.co.uk). As required, 30 µl sequencing primers at 3.2 pmol/µl and 30 µl DNA containing 600 ng were prepared for each sequencing reaction and then submitted. Results were decrypted using Chromas Lite software, version 2.0, in order to access and export relevant FASTA files for further analyses. The Transeq tool was used on these FASTA files for translations of base nucleotide sequences to polypeptide sequences. ClustalW2 was used for multiple polypeptide sequence alignments. Both tools are accessible from the European Bioinformatics Institute (EBI) website, http://www.ebi.ac.uk.

2.15 Confirmation of positive integrative transformants

Mini preps followed by NotI and XhoI double restriction digestions and agarose gel electrophoresis were carried out to preliminary screen for positive integrative transformants, post-transformations into *E. coli* cells. These were expected to possess both restriction sites. These were carried out as described previously in Sections 2.13.1, 2.1 and 2.2, respectively. Maxi preps of selected colonies were then carried out using the same starter cultures generated initially during their mini preps. Sequencing of Maxi prep purified DNA plasmids was carried out next as the confirmatory screening test.

2.16 Gremlin-Myc expression in mammalian cell cultures

2.16.1 Chinese Hamster Ovary S-strain (CHO-S) cell cultures

CHO-S cells are a stable aneuploid cell line established from the ovary of an adult Chinese hamster (Puck *et al.,* 1958). Frozen vials of CHO-S cells were generously donated by Christine Ball, National Institute of Biological Standards and Control (NIBSC). Each frozen vial contained 1 ml aliquot of 1 x 10^7 CHO-S cells prepared in 90% (v/v) Freestyle CHO expression medium (Invitrogen, USA) and 10% (v/v) dimethyl sulfoxide (DMSO), (Sigma-Aldrich, USA).

Maintenance, sub-culturing and transfections of CHO-S cells were carried out in accordance with the protocols outlined in the *Freestyle MAX CHO Expression System* manual (version C, publication part number: 25-0920) provided by Invitrogen Life Technologies from whom the cells were purchased initially. All reagents used unless specified otherwise, were also purchased from this company.

2.16.2 CHO-S cells: sub-culture

For the establishment of CHO-S cells, liquid nitrogen frozen vials of CHO-S cells were thawed in a 37 °C water bath and transferred quickly into 125 ml sterile polycarbonate Erlenmeyer flasks (Corning Incorporated, USA) each containing 30 ml pre-warmed CHO expression medium supplemented with 8 mM L-Glutamine (Gibco Life Technologies, USA). The cells were then incubated in humidified atmosphere at 37 °C in 8% CO_2 with shaking at 135 rpm (microtitre plate shaker, Stuart, UK). After 48 h, cells were prepared for counting by preparing 2.5:1 a sample of cell suspension with 1% (w/v) nigrosine (VWR international, USA) in deionised water. The prepared cell suspension was then counted using a Fuchs-Rosenthal hemocytometer (Hausser Scientific, UK) on a BH-2 model light microscope (Olympus, UK). The cells were then sub-cultured into new flasks by seeding at 0.2 - 0.3 x 10^6 cells/ml in pre-warmed L-glutamine-supplemented CHO expression medium to 30 ml total volume and then incubating under the same conditions stated above. A minimum of 5 passages at interval of 24 - 48 h, were conducted routinely prior to transfections at cell density of 1 x 10^6 cells/ml.

2.16.3 CHO-S cells: transient transfections, harvests and microscopy

Initially, transfections were carried out using cloned wildtype and mutants GREM1-pCMV-Tag5A constructs alongside a pEGFP-C1 construct, a kind donation from Dr. Philip Chen, Royal Holloway, University of London (Figure 2.1). The latter transfection served as a means to monitor the levels of protein expression by the CHO-S cells themselves. Prior to transfections, this previously sequence-verified construct was transformed into DH5α competent cells, grown on ampicillin-selective LB agar plates and a picked single bacterial colony was Maxi prep purified, as described in Sections 2.12 and 2.13.2, respectively.

Before transfection, 24 h before, sub-cultured CHO-S cells were seeded at 0.6 x 10^6 cells/ml and incubated as specified previously. On the day of transfection, the cells were seeded at 1.0 x 10^6 cells/ml instead. The following preparations were then made in separate sterile 1.5 ml microcentrifuge tubes:

Maxi prep DNA plasmid	37.5 µg
OptiPro SFM medium	562.5 µl
Freestyle MAX transfection reagent	37.5 µl
OptiPro SFM medium	562.5 µl

The separate preparations were then mixed together and stood at room temperature for 10 min and no longer than 20 min for the formation of DNA-lipid complexes. The mix was then added dropwise into the sub-cultured cell suspension whilst gently swirling the flasks. Transfected cells were incubated for 48 h in humidified atmosphere at 37 °C in 8% CO_2 with shaking at 135 rpm (microtitre plate shaker, Stuart, UK). Harvesting of CHO-S cell culture supernatants was carried out 48 h post-transfections by centrifuging the cell suspensions at 245 x g for 10 min. When appropriate, protease inhibitor cocktail (P8340, Sigma-Aldrich, USA) was added at a 1:55 dilution ratio into the cell culture supernatants. Aliquots of treated cell culture supernatants were then stored at -20 °C.

2.17 Commercially purified recombinant proteins

The purified recombinant proteins of His-tagged recombinant murine gremlin (gremlin-His), human BMP-4 and human BMP-7 were purchased from R&D Systems, USA. These were reconstituted as recommended.

2.18 Concentration of crude gremlin-Myc CHO-S culture supernatants

Where required, concentration of expressed gremlin-Myc proteins in their crude CHO-S culture supernatants was achieved using Amicon Ultra-15 centrifugal filter units with 10 kDa cut off (Merck Millipore Ltd, Germany). Crude CHO-S culture supernatants (15 ml) were loaded into the filter units and centrifuged at 4 °C for 60 min at 4000 x g. A 20-fold concentration of gremlin-Myc proteins was achieved. For optimal recovery, the concentrated samples were dispensed into sterile 1.5 ml microcentrifuge tubes immediately after centrifugation, as recommended by the manufacturer. For optimal gremlin-Myc activity, the concentrated samples were used on the same day of preparation avoiding any freeze-thaw cycles.

2.19 Sandwich enzyme-linked immunosorbent assay (ELISA)

2.19.1 Sandwich ELISA general procedure

Microtiter plates (96-well, Nunc, Denmark) were coated with 100 µl/well of capture antibody prepared at 2 - 4 µg/ml. Plates were then incubated overnight at 4 °C on a gently rotating platform after which wells were washed thrice in PBS. Wells were blocked by adding 200 µl/well of PBS containing 0.5% (w/v) BSA blocker (PBS-0.5% (w/v) BSA) solution and incubated at room temperature for 1 h with gentle shaking. After incubation, the well washes were repeated with PBS-0.05% (w/v) BSA solution, instead. Both primary antibody and conjugated enzymes were prepared in this buffer. Next, 100 µl/well experimental samples were loaded into the wells and incubated at room temperature for 90 min with gently shaking after which, washes were repeated in PBS-0.05% (w/v) BSA solution. Biotinylated primary or detection antibody (100 µl/well) prepared at 0.8 µg/ml was added into washed wells and incubated, as described for experimental samples. After incubation, the wells were washed thrice in PBS-0.05% (v/v) Tween20 (Molecular Sigma Biology, UK) solution. Next, 100 µl/well alkaline phosphatase-streptavidin conjugated enzyme prepared 1:1000 was added into the wells and incubated at room temperature for 30 min with gentle shaking. Wells were then washed thrice in PBS-0.05% (v/v) Tween20 and then twice in PBS alone. After washing, 100 µl/well substrate tablet solution of para (p)-nitrophenylphosphate tablets (Sigma, UK) dissolved in deionised water (5 ml per tablet pair) was added into the wells. It followed that the plate was then incubated in a non-illuminated 37 °C shaker incubator (Denley Wellwarm1, UK) until a yellow colour, not so intense, was apparent in experimental wells. The absorbance readings at 405 nm wavelengths were then

measured using an Emax plate spectrophotometer (Molecular Devices, California, USA) on the Softmax Pro software, version 3.0. The blanks in all these experiments constituted of wells which had only been blocked, washed identically and substrate solution added.

2.19.2 Heparin-binding ELISA

Coating was done overnight at 4 °C with 100 µl of 5 -10 ng/well heparin-BSA and treated-BSA complexes prepared in 50 mM Tris-HCl containing 12.7 mM EDTA buffer, pH 7.4. Both were synthesised as described in Section 2.20. The experiment hereafter was conducted as described in the previous section except that PBS-5% (w/v) BSA was used as blocker solution and PBS-0.5% (w/v) BSA solution used as wash and antibody incubation buffer instead.

2.19.3 Myc-capture gremlin ELISA

This sandwich ELISA targets the C-Myc tag on both expressed wildtype and gremlin proteins. An anti-Myc 9E10 antibody (Abcam, UK) prepared 1:500 in 50 mM Tris-HCl containing 12.7 mM EDTA buffer, pH 7.4, is used as coating antibody. Everything else was carried out as described in Section 2.19.1.

2.19.4 Myc-capture GREM1/BMP-4 double sandwich ELISA

The Myc-capture GREM1/BMP-4 double sandwich ELISA was conducted on crude wildtype and selected mutant gremlin-Myc cell culture supernatants to assess their BMP-4 binding capabilities. This ELISA was a development of the Myc-capture gremlin ELISA described in the previous section in which both gremlin bound to BMP-4 were sandwiched by the Myc antibody-capture layer and the detecting primary antibody, indeed. In this double sandwich ELISA, BMP-4 added was incubated overnight at 4 °C prior to detecting with a monoclonal biotinylated BMP-4 detecting primary antibody (R&D Systems, USA) prepared at 4 µg/ml as described in Section 2.19.1.

2.20 Synthesis of heparin-BSA conjugate

A reducing-end coupled heparin-BSA complex was synthesised as described by Najjam and co-workers (1997). Porcine intestinal mucosa heparin (grade 1-A) and BSA (99% pure grade) were both purchased from Sigma-Aldrich, UK. Heparin, 1.5 g, dissolved in 1 ml deionised water was dialysed against three changes of 1.5 L of 1 M NaCl and then two further changes of the same volume in deionised water using cellulose dialysis tubing, 23 mm x 15 mm, (Sigma-Aldrich, UK). Changes were made at 2 h

intervals except the last change in deionised water which was carried out overnight at 4 °C. The dialysed material was then freeze-dried for 48 – 72 h using a freeze-dryer (Lyovac GT 2, Lebold-Heraeus, Germany). Freeze-dried heparin (680 mg) and 34 mg BSA were dissolved in 5 ml 0.2 M potassium phosphate buffer, pH 8, after which 25 mg sodium cyanoborohydride (Sigma-Aldrich, UK) was added, cautiously. The reaction mixture was then incubated in a 37 °C water bath for 48 h. Using gel filtration, the reducing-end coupled heparin-BSA conjugate was separated from free heparin and BSA in the mixture. Sepharose CL 4B beads with a bead diameter of 45 - 165 µm (Pharmacia Biotech, UK), were packed slowly to a column height of 84 cm over 24 - 48 h, in a 1 x 100 cm column (Pharmacia Biotech, UK). Once packed, the column was then washed with 3 – 5 bed volumes of 0.25 M ammonium bicarbonate, pH 8. The flow rate was also adjusted to 9 ml/h during the washes. Gel filtration was conducted throughout at 4 °C. Coupling mixture, 5 ml, was loaded onto the column and the first 84 fractions, 1.5 ml in volume, were collected with the first 20 ml eluate discarded. The protein contents in the remaining fractions were estimated using the bicinchoninic assay (BCA) reagent kit (Pierce, Europe) in 96 well microtiter plates following the manufacturer's protocol. Standards, 0 - 15 ng amounts of BSA per 20 µl prepared in 0.25 M ammonium bicarbonate buffer, pH 8 were included. Absorbance readings at 595 nm were measured using the same plate reader described in Section 2.19.1.

From the protein content profile, leading peak fractions in which the heparin-BSA conjugate was expected to elute, were analysed on non-reducing 10% polyacrylamide gels. Separate gels were then stained for heparin with 0.08% (w/v) Azure A and for BSA with 0.25% (w/v) Coomassie blue R250, respectively. Both stains were purchased from Sigma-Aldrich, USA. Protocols for these GAG and protein staining methods were as published previously by Rider (1997) and Laemli (1970), respectively. Fractions containing the heparin-BSA conjugate as indicated by the presence of the excluded complex together with low amount of free BSA and moderate amounts of free heparin, were pooled and freeze-dried for 48 h. This was then resuspended in 50 mM Tris-HCl containing 12.7 mM EDTA buffer, pH 7.4 and its protein content was measured against a BSA standard curve in the same buffer as shown in Figure 2.3. The stock solution was then reconstituted in this same buffer at 75 ng/µl. Aliquots were then stored at -20 °C. A mock-BSA conjugate was previously prepared in our laboratory, in which free BSA had been processed using the same method described above. This served as a negative control in sandwich ELISA immunoassays.

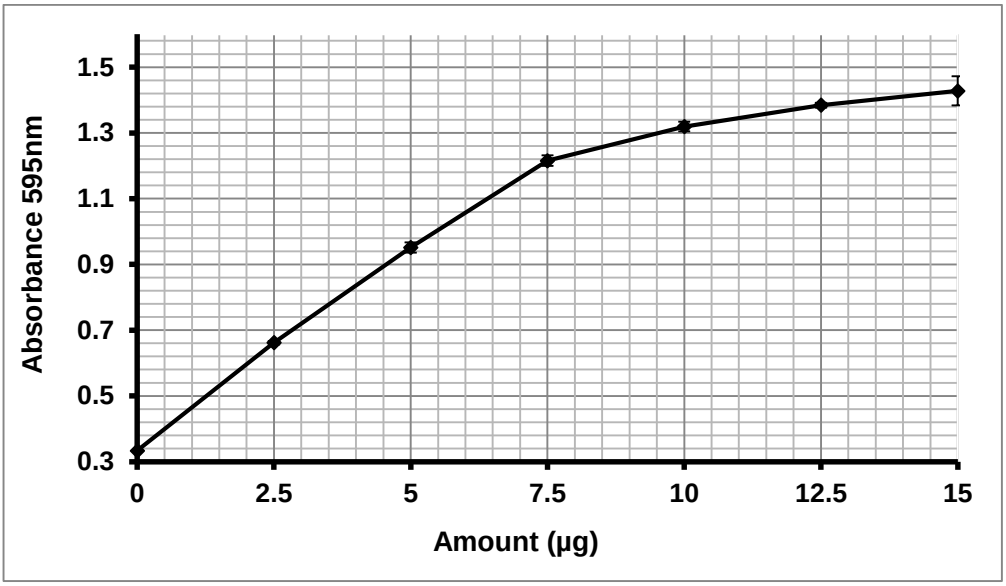

Figure 2.3: BSA standard curve.
BSA amounts were prepared in 0.25 M ammonium bicarbonate buffer, pH 8 or in 50 mM Tris-HCl/12.7 mM EDTA buffer, pH 7.4 to determine the protein content of gel filtration eluates and for the reconstitution of purified heparin-BSA complex, respectively. This was achieved using the bicinchoninic assay (BCA) reagent kit. Each point on the curve represents the average of triplicate absorbance readings at 595 nm and error bars represent the SEM.

2.21 Heparin affinity chromatography

Heparin affinity chromatography of expressed gremlin-Myc culture supernatants was carried out at an analytical scale. AF-heparin beads, 200 µl, (HC650M, Tosoh Bioscience, Japan) were equilibrated as recommended by the manufacturer in two changes of 1 ml PBS-1M NaCl at room temperature for 10 min and then once in 1 ml PBS at room temperature for 20 - 30 min. Equilibrated beads were then loaded into a 0 - 20 µl bevelled filter tip (Starlab Ltd, UK) and a 1 ml syringe barrel (Becton Dickinson S.A., Spain) was tightly connected to serve as a reservoir. The loading volume of crude gremlin-Myc culture supernatants ranged between 1 – 2 ml depending on the levels of gremlin-Myc immunoreactivity each possessed. All applied crude culture supernatants were prepared 1:1 in PBS-0.2% (w/v) BSA. The run was conducted at a flow rate of 12 - 14 ml/h using a pump (Minipuls3, Gilson, UK) and 1 ml eluates were manually collected in 1.5 ml microcentrifuge tubes. After loading, the column was washed with a minimum of 5 ml PBS-0.2% (w/v) BSA. This was followed by a step NaCl elution gradient ranging from 0.2 – 1.0 M NaCl buffers in PBS. Immediately after the run, 125 µl sample from each eluate was diluted in 25 ml deionised water for conductivity measurements. Conductivity readings were measured using a conductivity meter (model HI9813-5, Hanna Instruments, Romania). The standard curve shown in Figure 2.4

generated by similar dilution of known NaCl in PBS buffers, was used to calculate the corresponding NaCl concentrations of the eluates. The gradient fractions were dialysed against two changes in 0.5 – 1 L PBS; the first overnight at 4 °C and the second for 1 h at 4 °C, using dialysis tubing cellulose membrane with 10 mm average flat width (Sigma-Aldrich, UK). After dialysis, the dialysed samples were squeezed into 1.5 ml microcentrifuge tubes and immunoassay of all fraction samples was conducted using the Myc-capture gremlin ELISA as described in the Section 2.19.3.

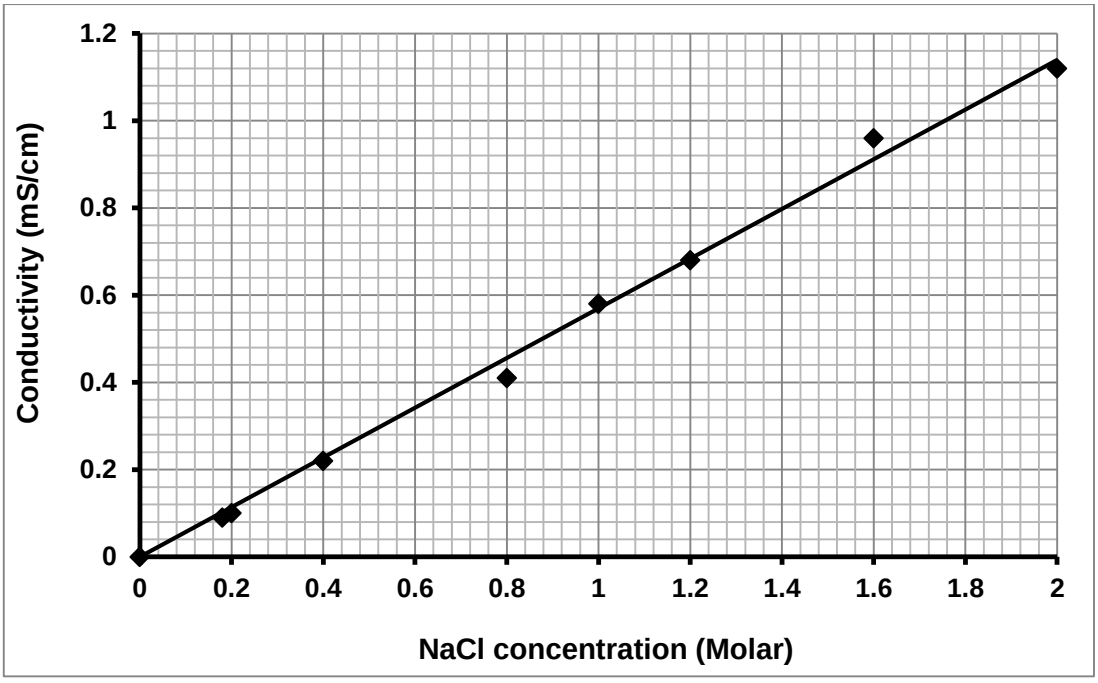

Figure 2.4: Conductivity standard curve.
The standard curve shows the conductivity at shown NaCl concentrations after diluting 1/200. The line equation is given as y = 0.5697x; where, y is the conductivity value measured and x is the NaCl concentration to be determined. 0.18 M NaCl indicates PBS molarity. 0 M NaCl indicates molarity of deionised water.

2.22 Ion-exchange chromatography

Ion-exchange chromatography of expressed gremlin-Myc culture supernatants was conducted as described by Stabile *et al.* (2007) on sulfopropyl (SP)-Sepharose bead columns (Sigma-Aldrich, USA) carrying the side chain $-CH_2CH_2CH_2SO_3^-$. The same experimental set-up as described for heparin affinity chromatography was also employed in these experiments. In a typical experiment, 400 µl SP-Sepharose beads were equilibrated in two changes of 1 ml 50 mM MES (Sigma-Aldrich, USA) solution prepared in deionised water buffered to pH 6.5 with 1M NaOH solution (50 mM MES-NaOH buffer, pH 6.5). The beads were equilibrated at room temperature for 10 min each. An additional equilibration step was carried out for the same length of time in 1 ml 50

mM MES-NaOH buffer, pH 7.5 which also served as wash buffer for the column and as elution buffer when prepared with NaCl.

2.23 SDS-polyacrylamide gel electrophoresis (SDS-PAGE)

Gel electrophoresis was conducted on 15% (w/v) polyacrylamide gels using a similar method described by Laemli (1970). This was performed using the Bio-Rad Mini-Protean III mini-gel system (Bio-Rad, USA). Resolving gels (15% w/v) consisted of 1.7 ml deionised water, 3.75 ml bis-acrylamide (30% (w/v)), 1.9 ml resolving buffer 1.5 M (1.88 M Tris-base, pH 8.8), 75 µl sodium dodecyl sulphate (SDS; 10% (w/v)), 75 µl ammonium persulphate (APS; 10% (w/v)) and 3 µl N,N,N,N-tetramethylethylene-diamine (TEMED). The stacking gel consisted of 1.45 ml deionised water, 475 µl bis-acrylamide (30% (w/v)), 625 µl stacking buffer 0.5 M (0.625 M Tris-base, pH 6.8), 15.75µl APS 10% (w/v) and 3.75µl TEMED. All chemicals were purchased from Sigma-Aldrich, UK. Where appropriate, experimental samples were prepared under reducing and non-reducing conditions in 2x SDS sample buffer with/without 2-mercapto-ethanol, respectively. The 2x SDS sample buffer was prepared by diluting in deionised water, a 5x SDS sample buffer stock constituting, 0.8 ml glycerol (100% v/v), 1.6 ml SDS (10% w/v), 1 ml stacking buffer pH 6.8, 4 ml deionised water, 0.2 ml bromophenol blue (5% w/v) with/without 0.4 ml 2-mercapto-ethanol. Samples were denatured by boiling for 5 min. The polymerised gel was placed in an electrophoresis tank accordingly and then submerged in running buffer, pH 8.3 containing, 0.025 M Tris-base, 0.19 M glycine and 10 ml SDS (10% w/v). Samples (15 - 20 µl) were then loaded into gel wells alongside 5 µl SeeBlue Plus2 pre-stained standard (Invitrogen, UK). Gel electrophoresis was conducted at 200 V until suitable migration of bands down the gel.

2.24 Silver staining of polyacrylamide gels

Silver staining was conducted following ion-exchange chromatography of expressed wildtype gremlin-Myc (refer to Section 2.22) and SDS-polyacrylamide gel electrophoresis of fraction eluates as described in the previous section. This was carried out using the ProteoSilver silver stain kit (Sigma-Aldrich, USA) following the manufacturer's protocol. An image of the gel was obtained using an hp scanjet 8200 scanner.

2.25 Western blotting and development of blots

Western blotting was conducted according to the method of Sambrook and co-workers (1989). A polyacrylamide gel sandwich constituting two sponges (Bio-Rad, USA), two Whatman papers (Whatman, UK), a polyacrylamide gel and a nitrocellulose membrane (pore size: 0.45µm; Amersham BioSciences, UK) was assembled. Electroblotting was conducted using the Bio-Rad Mini Trans-Blot system (Bio-Rad, UK) with the Bio-Rad Mini-Protean III gel tank alongside an ice pack. The blotting buffer pH 7.9 (0.025 M Tris-base, 0.19 M glycine, 1 ml SDS (10% w/v) and 200 ml methanol (20% (v/v)) was ran at 100 V. After 1 h blotting, the membrane was washed for 10 min in Tris buffered saline (TBS), pH 7.6 (0.02 M Tris-base and 1.37 M NaCl) and then blocked for 1 h in TBS-5% (w/v) dried skimmed milk powder (Marvel, UK), which had been centrifuged at 4472 x g for 10 min using a 50 ml centrifuge tube (Orange Scientific, Belgium) and the supernatant decanted into another sterile 50 ml centrifuge tube. Both primary and secondary antibodies were prepared in blocking solution to the required concentration. The membrane was incubated overnight at 4 °C with the primary antibody after which it was washed twice in TBS-0.05% (v/v) Tween20 and once in TBS over 15 min at room temperature with gentle shaking. The same sequence of washes was repeated after incubation of the membrane with the HRP-conjugated secondary antibody at room temperature for 1 h. The membrane was then incubated with the substrate, SuperSignal West Pico chemiluminescent substrate (Pierce, UK) following the supplier's protocol. The blot was exposed immediately to a Kodak biomax film (Kodak, UK) for 1 min in a darkroom. The exposed film was developed using an automatic film processor (Photon Imaging System, UK).

2.26 Gremlin-Myc immunoprecipitation (IP)

IP experiments of expressed wildtype gremlin-Myc and its mutants in crude CHO-S cell culture supernatants were carried out using rabbit polyclonal anti-C-Myc agarose affinity beads (Sigma-Aldrich, USA). Equilibration the beads and IP experiments were conducted as in the supplier's protocol. Typically, 50 - 150 µl agarose anti-C-Myc beads were equilibrated in two changes of PBS-1M NaCl, pH 7.4 for 10 min each, at room temperature under gentle rotation in 2 ml Eppendorf tubes. Between each equilibration step, the beads were centrifuged at 68 x g for 60 s and stood at room temperature for 2 – 3 min before discarding the supernatant. Next, 1 - 2 ml gremlin-Myc culture supernatant was loaded onto the equilibrated beads and incubated overnight at 4

°C with gentle rotation. In the case of crude MGR3 culture supernatant, a prolonged bead binding step was performed over 48 h at 4 °C with gentle rotation. The gremlin-Myc-bead complexes were then centrifuged at 68 x g for 60 s and the resulting supernatant collected and prepared in reducing 5x SDS sample buffer for Western blotting. Pelleted bead complexes were then washed five times in 1 ml PBS and when appropriate with 1 ml PBS-0.05% (v/v) Tween20, for 5 min each at room temperature with gentle rotation followed by a spin as specified above. Reducing SDS sample buffer 2x (50 µl), (refer to Section 2.23) was then added to the pelleted bead complexes, which were stood at room temperature for 1 – 2 min and then boiled for 1 min to elute bound gremlin-Myc from the bead complexes. The boiled bead complexes were centrifuged as specified above and supernatants collected for Western blotting (refer to previous section). Western Blotting was performed using 0.4 – 0.8 µg/ml goat polyclonal gremlin primary antibody and 1:2500 diluted HRP-conjugated rabbit polyclonal anti-goat IgG secondary antibody.

2.27 IP of BMP-4 on gremlin-Myc-bead complexes

Anti-Myc beads were loaded with gremlin-Myc, as described in the previous section. The bead complexes were then incubated overnight with 500 ng BMP-4 prepared in 1 ml PBS-0.1% (w/v) BSA. After bead binding, the IP experiment was conducted as described in the previous section after the initial bead binding step. Centrifugation and boiling of beads were also conducted as specified in the previous section.

2.28 Murine C2C12 myoblastic cells: supply and maintenance

A frozen vial of murine C2C12 myoblastic cells, strain C3H, was kindly provided by Dr. John Beechamp, Royal Holloway, University of London. The cells had been originally purchased from the American Type Culture Collection (ATCC), USA at low passage number. All reagents used for their maintenance unless stated otherwise were purchased from Gibco Life Technologies, USA.

For growth, differentiation and freezing of C2C12 cells, different medium was prepared as follows:

- DMEM-10%FBS growth medium: Dulbecco's Modified Eagle Medium (DMEM; modified with high glucose, GlutaMAX-I, sodium pyruvate and phenol red) containing sterile 10% (v/v) fetal bovine serum (FBS).

- DMEM-5% horse serum differentiation medium: DMEM containing 5% (v/v) sterile horse serum.

- Freezing medium: 0.5 - 1 ml aliquots of C2C12 cell suspension at cell density 1.0 x 10^6 cells/ml containing 10% (v/v) dimethyl sulfoxide (DMSO; Sigma-Aldrich, USA).

Stocks of 100% FBS and horse serum were heat inactivated at 56 °C for 30 min and then filtered-sterilised. Aliquots were stored at -20 °C. C2C12 cell suspensions prepared in freezing medium were aliquoted into 1.8 ml cryo-vials (Nunc, Denmark). These were then frozen overnight to -80 °C at a freezing rate of -1 °C/min by inserting them into an extruded polystyrene block. Next day, the frozen vials were transferred into liquid nitrogen for long term storage.

To sub-culture the cells, a liquid nitrogen frozen vial of C2C12 cells was thawed in a 37 °C water bath and then transferred to a 50 ml centrifuge tube (Corning Incorporation, USA) containing 10 ml pre-warmed growth medium. The cell suspension was centrifuged at 250 x g for 5 min and the cell pellet was resuspended in 15 ml fresh pre-warmed growth medium. This was then plated into a tissue culture flask with 75 square cm surface area (T75; Corning incorporation, USA). The flask was cultured in humidified atmosphere at 37 °C and 5% CO_2 for 2 - 3 days until cells were 70% confluent. The cells were then passaged by discarding the spent growth medium and washing the adherent cell layer twice in sterile PBS. Cells were then trypsinized by applying 800 µl trypsin [prepared by a 1:10 dilution of its 10X stock solution (Gibco Life Technologies, USA) in sterile PBS] and standing at room temperature for 3 – 5 min until rounding of cells was apparent under the microscope. Pre-warmed growth medium (10 ml) was then added to quench the trypsinization process. The cell suspension was transferred into a 50 ml sterile centrifuge tube and centrifuged at 250 x g for 5 min. The cell pellet was resuspended in 5 - 10 ml pre-warmed growth medium and a cell count was performed by diluting a sample of cell suspension 2.5:1 in 1% (w/v) nigrosin stain prepared in deionised water. After counting, cells were split and plated into new T75 flasks at 6 - 8 x 10^4 cells/ml. All sterile tissue culture plasticware was purchased from Corning Incorporation, USA.

2.29 BMP-SMAD1/5/8 phosphorylation assay in C2C12 cell cultures

In this functional assay, both BMPs -4 and -7 were expected to induce SMAD1/5/8 phosphorylation in C2C12 myoblastic cells (Kuo *et al.*, 2010). In these assays, the cells were plated into wells of a 12 well tissue culture plate at 0.2 x 10^6 cells/ml cell density in pre-warmed differentiation medium (refer to previous section). The plate was cultured

overnight in humidified atmosphere at 37 °C and 5% (v/v) CO_2 after which, the adhered cell layers were treated with varying amounts of BMPs -4 and -7. When appropriate, both BMPs -4 and -7 were pre-incubated with different amounts of purified gremlin-His at room temperature for 45 – 60 min with gentle rotation. Expressed gremlin-Myc proteins in crude culture supernatants were not used in this assay. Both BMPs with/without gremlin-His, were prepared at each required amount in pre-warmed differentiation medium to a total volume of 0.5 ml. For treatment, the spent medium, 0.5 ml, was replaced with the freshly prepared BMP and/or gremlin-His samples. Treated cells were then incubated in humidified atmosphere at 37 °C and 5% (v/v) CO_2 for 45 min, after which wells were washed twice in sterile PBS. Cell lysis and detachment from well surfaces were achieved by adding 200 µl boiling reducing 2x SDS sample buffer into each well and then scraping the well surfaces with sterile cell scrapers (Corning Incorporation, USA). The lysates were immediately boiled for 5 min, centrifuged at 12816 x g for 1 min and the supernatants collected for Western blotting. Polyacrylamide gel electrophoresis and Western blotting were then conducted as described previously in Sections 2.23 and 2.25, respectively except that TBS-5% (w/v) BSA was used as blocker and antibody preparation buffer. Typically, when probing the same nitrocellulose membrane, phospho-SMAD1/5/8 immuno-detection was conducted first before stripping and re-probing for total SMAD1/5/8 immuno-detection. Both primary antibodies used in this functional assay are listed below and were detected using the same 1:2500 diluted HRP-conjugated goat polyclonal anti-rabbit IgG secondary antibody (Dako, Denmark).

- Phospho-SMAD1(Ser463/465)/SMAD5(Ser463/465)/SMAD8(Ser426/Ser428)) rabbit polyclonal antibody (p-SMAD1/5/8 primary antibody, Cell Signaling Technology, USA; working dilution 1:1000).

- SMAD 1/5/8 N-18 (raised against peptide mapping at the N-terminus of human SMAD 1) goat polyclonal antibody (SMAD1/5/8 primary antibody, Santa Cruz Biotechnology Incorporation, USA; working dilution 1:500).

2.30 Luciferase reporter assay in C2C12 cell cultures

2.30.1 Preparation of the 12XSBE-Oc-Luc$^+$-pGL3 construct

The SMAD1/5/8-specific signalling reporter construct, 12XSBE-Oc-Luc$^+$-pGL3 (refer to Figure 2.2 for the backbone map) was provided by Dr. Zhao Ming, University of Texas Health Science Center, Texas, USA. The insert had been subcloned into the pGL3 expression vector constituted of 12 copies of SMAD1 binding element (12XSBE)

in front of an osteocalcin (Oc) basal promoter that was also cloned in front of the *P. pyralis* firefly luciferase gene (*luc*$^{+}$). These specific modifications would enable cellular expression of the luciferase enzyme as a direct response to BMP-SMAD1/5/8 signalling (Zhao *et al.*, 2003; Sudo *et al.*, 2004).

This sequence-verified reporter construct was supplied as a spotting on a marked filter paper. This was extracted by soaking the trimmed filter paper in 100 µl elution buffer (recipe in Section 2.13.2) in a sterile 1.5 ml Eppendorf tube and stood at room temperature for 20 min. Its DNA concentration was then quantitated by NanoDrop measurement (refer to Section 2.4). DNA construct (4.8 ng) was then transformed into 100 µl DH5α competent cells and bacterial colonies were grown on ampicillin-selective LB agar plates as described previously in Section 2.12. This was followed by Maxi prep purification during which glycerol stocks of the starter culture were also prepared accordingly (refer to Sections 2.11 and 2.13.2). The air-dried purified reporter construct was resuspended in 300 µl of the same elution buffer above, and stored at -20 °C.

2.30.2 Transient transfections of C2C12 cells

Transient transfections of the 12XSBE-Oc-Luc^{+}-pGL3 reporter construct into sub-cultured C2C12 cells used either Lipofectamine 2000 or Fugene transfection reagents both purchased from Invitrogen Life Technologies, USA and Promega Corporation, USA, respectively. The Opti-MEM medium used by both transfection protocols was purchased from the former supplier. Transfections were carried out according to the manufacturer's protocol. To achieve the same transfection efficiency per plate well, cells were transfected in a single tissue culture flask after which they were split into wells of a 24-well tissue culture plate for separate treatments (refer to Section 2.28).

2.30.2.1 Lipofectamine 2000 transfection method

Initially, sub-cultured C2C12 cells were plated into in a T25 tissue culture flask at 2 x 10^5 cells/ml containing 5 ml pre-warmed growth medium (refer to Section 2.28) and incubated overnight in humidified atmosphere at 37 °C and 5% (v/v) CO_2. When above 90% confluency, the cells were washed once in sterile PBS and fresh pre-warmed growth medium replenished. The transfection reagent and reporter DNA construct were prepared separately as follows:

Lipofectamine 2000 transfection reagent	28 µl
Pre-warmed Opti-MEM medium	250 µl
12XSBE-Oc-Luc^{+}-pGL3 construct	6 µg
Pre-warmed Opti-MEM medium	250 µl

Both preparations were mixed together and incubated at room temperature for 10 min for the formation of DNA-lipid complexes. After incubation, the DNA-lipid preparation was added to cells in the T25 flask with fresh growth medium. Cells were then incubated overnight in the conditions described above after which, the transfected cells were passaged as in Section 2.28. Cells were plated into wells of a 24-well tissue culture plate at 0.7 – 2.0 x 10^5 cells/well for overnight incubation.

2.30.2.2 Fugene 6 transfection protocol

Transient transfections using the Fugene 6 transfection reagent were carried out with few changes to the Lipofectamine 2000 transfection method described in the previous section. Firstly, transfections were conducted when cells were 70% confluent. Secondly, the lipid-DNA complexes were prepared as follows:

Pre-warmed Opti-MEM medium	450 µl
Fugene 6 transfection reagent	18 µl

These were incubated prior to use at room temperature for 5 min

12XSBE-Oc-Luc^{+}-pGL3 construct	9 µg
(Added to the above preparation)	

Incubate at room temperature for 20 min as above

After incubations, the DNA-lipid preparations were added to the 70% confluent cells in a T25 flask each containing 5 ml fresh growth medium. The cells were then incubated for 4 h in humidified atmosphere at 37 °C and 5% (v/v) CO_2 prior to passaging and splitting into wells of 24-well tissue culture plates at 0.7 – 2 x 10^5 cells/well. The cells were adhered to the well surfaces during incubation for 16 h.

2.30.3 BMP-4 and gremlin treatments of C2C12 cell cultures

C2C12 cells transiently transfected in 24-well tissue culture plates were washed once in sterile PBS. Varying concentrations of BMP-4 in 0.5 ml fresh pre-warmed growth medium were loaded into the wells. In inhibition experiments with gremlin, the

same final volume was maintained and a fixed concentration of BMP-4 was used. This was then pre-incubated with either varying volumes of concentrated gremlin-Myc preparations or varying concentrations of purified gremlin-His. Pre-incubations of BMP-4 and gremlin were carried out at room temperature for 45 – 60 min with gentle rotation after which the samples were applied to the wells. The treated cells were then incubated for 24 h in humidified atmosphere at 37 °C and 5% (v/v) CO_2.

2.30.4 Measurement of luciferase activity

After BMP-4/gremlin treatments described in the previous section, the treated C2C12 cells were washed twice in sterile PBS. Cells were then lysed by adding 0.2 ml/well cell culture lysis reagent, CCLR (25 mM Tris-phosphate (pH 7.8), 2 mM dithiothreitol (DTT); 2 mM 1,2-diaminocyclohexane-N,N,N´,N´-tetraacetic acid (DCTA), 10% (v/v) glycerol, 1% (v/v) Triton X-100) prepared in deionised water from its 5x stock solution. This was provided with the Luciferase Assay System purchased from Promega Corporation, USA. The plate wells were then scraped and cell lysates were transferred into 1.5 ml sterile microcentrifuge tubes and centrifuged at 12816 x g for 30 s. Supernatants of cell lysates were then collected into sterile 1.5 ml microcentrifuge tubes and luciferase activity was measured immediately after.

The expressed *P. pyralis* firefly luciferase enzyme that is present in cell lysates catalyses the oxidation of luciferin to oxyluciferin ion through a single electron transition using ATP•Mg^{2+} cation and molecular oxygen as co-substrates. In this transfer of chemical energy, photons of light are emitted as oxyluciferin produced in the excited state returns to the ground state (Kricka, 1988). In the conventional luciferase assay, the intensity of light emitted decreases rapidly over a few seconds. However by incorporating coenzyme A (CoA), the kinetics are significantly improved allowing greater enzymatic turnover that results ultimately in sustained light intensity that is nearly constant for at least 1 min (Fraga *et al.*, 2005).

Measurement of secreted luciferase activity was carried out in a 96 well plate (Nunc Incorporation, Denmark) by adding 100 µl/well of luciferase assay reagent luciferin substrate (Promega Corporation, USA) to 30 µl cell lysate supernatants. The plate was read immediately in a GloMax 96 microplate luminometer (Promega Corporation, USA). Readings were made over an integration time of 10 s with 2 s delay in order to obtain readings from a flat portion of the signal curve.

Initially, the linear range of light detection for the luminometer was determined as advised by the manufacturer by plotting a standard curve of relative light unit (RLU)

against known doses of purified luciferase enzyme. This QuantiLum recombinant firefly luciferase enzyme was also purchased from Promega Corporation, USA and was prepared in CCLR lysis buffer supplemented with 1 mg/ml BSA. The standard curve obtained was as shown in Figure 2.5.

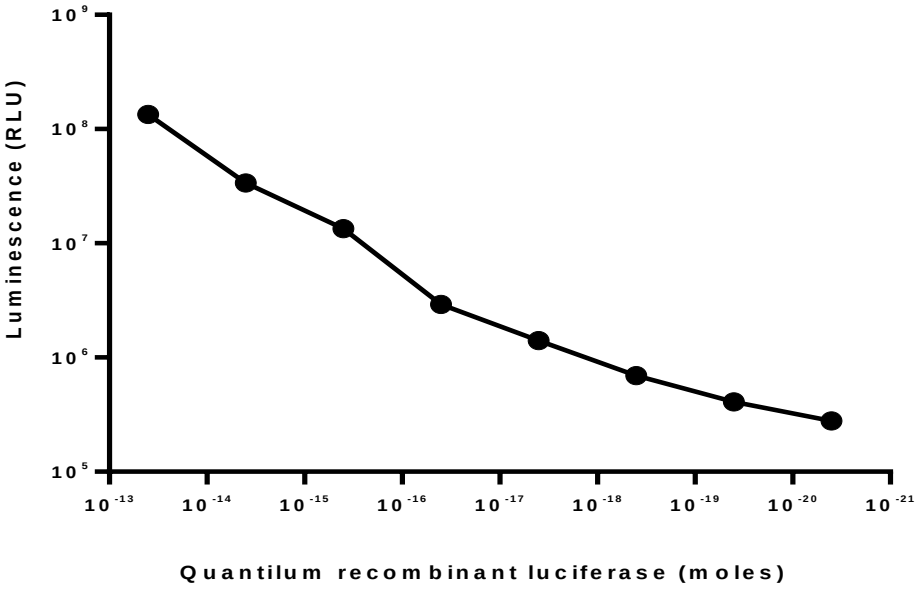

Figure 2.5: Standardizing the Luciferase Assay System.
Varying amounts of the standard purified enzyme, firefly Quantilum recombinant luciferase were prepared in cell culture lysis reagent supplemented with 1 mg/ml BSA. 30 µl samples were added into wells of a 96 well plate followed by 100 µl/well of luciferin substrate. GloMax 96 microplate luminometer set to 10 s integration time with 2 s delay before and between two read cycles. The first of each paired measurement has been plotted.

Chapter 3: Cloning of wildtype and mutant GREM1-Myc constructs

3.1 Introduction

Earlier in this thesis, the prediction of the heparin binding site on gremlin and other CAN family members was discussed extensively (refer to Chapter 1). Briefly, at the beginning of this study, only the high resolution NMR structure of sclerostin had been resolved experimentally by Veverka *et al.* (2009). In this sclerostin structure, a distinct heparin/HS binding site was identified experimentally which raised interest into the heparin/HS binding properties of other CAN family members. Based on this sclerostin structure, Rider and Mulloy (2010) were able to generate predicted homology models for other CAN family members including gremlin. In docking calculations with short chain heparin oligosaccharides, they were then able to map a predicted heparin binding site on some of these CAN family members; except for DAN and Cerberus which were predicted not to bind to heparin/HS. Unfortunately, without accompanying supportive experimental evidence, these predictions are uncertain.

This current study of gremlin would serve as an experimental verification of the predictions made by Rider and Mulloy (2010). Present within the primary sequence of gremlin are three interspersed basic clusters constituting largely of arginine and lysine residues, which they predicted formed its putative heparin binding site. Using strategic site-directed mutagenesis, work in this chapter will seek to clone and express various C-Myc-tagged mutant gremlin proteins incorporating specific substitutions within these basic clusters. Equally, a C-Myc-tagged wildtype gremlin protein will be cloned and expressed as a more suitable alternative to the only commercially available His-tagged gremlin protein. The potential risk of the polyhistidine tag acting as an artefactual heparin binding site in gremlin mutants was considered. The goal of this site-directed mutagenesis was to express gremlin-Myc mutants with reduced heparin/HS binding capabilities. The BMP antagonist activities of such mutants could then be assessed so as to investigate the importance of heparin/HS in gremlin activity. An outline of the specific objectives met in this chapter is as follows;

- To design suitable mutants of gremlin within the predicted contact basic clusters in wildtype gremlin.

- To clone both wildtype and mutant GREM1 inserts incorporating all targeted substitutions.

- To subclone all GREM1 inserts into a suitable C-Myc tagging expression vector hence generate targeted sequence-verified GREM1-Myc constructs.

- To transfect the sequence-verified GREM-Myc constructs into CHO-S cells.

3.2 Cloning of the wildtype GREM1 insert

The initiation of translation involves a scanning mechanism by which small 40 S ribosomal subunits bind initially at or near the 5' terminus of an mRNA, migrating linearly and stopping when the first AUG codon is reached. At this point, 60 S ribosomal subunits are recruited and peptide bond formation is initiated. Studies by Kozak and Shatkin (1978) and Kozak (1980) provided the first experimental evidence in support of this hypothesis. This mechanism is relevant as it brings into perspective the possible regulatory effects 5'-noncoding sequences may exert on translation. Kozak (1984) showed that the sequence context influences the ability of the AUG codon to be recognised as initiator codon by eukaryotic ribosomes. By introducing point mutations around the translation start site of a clone preproinsulin gene (Kozak, 1984) and by compiling the 5'-noncoding sequences from 699 vertebrate mRNAs (Kozak, 1987), an optimal sequence for the initiation of translaton was revealed. This was termed as the Kozak consensus sequence forming the recognition sequence *GCCRCCAUGG*, where a purine base, *R*, at -3 is particularly highly conserved amongst vertebrates (refer to Figure 3.1), (Kozak, 1984 & 1987). The purines at -3 and +4 positions were shown to have dominant effects as substituting any or both with a pyrimidine base resulted in translational inefficiency and dramatic reduction in translation-dependent protein expression (refer to Figure 3.1), (Kozak, 1986 & 2002). Moreover, translation proceeds efficiently as long as both of these purines conform thus restating their essential nature (Kozak, 2002). Thus, the Kozak consensus sequence will promote a high yield of translation-dependent protein expression.

In most cloning studies that aim to achieve an optimal yield of a specific eukaryotic protein, it is now common practice that its genomic sequence in the translational start site is made to conform to the Kozak motif. This can be done by conforming either entirely or in part at least at the -3 and +4 positions. Given that the aim of this current study was to obtain high yields of several C-Myc-tagged gremlin proteins in mammalian cell cultures, an assessment of the genomic sequence in the translational start site of the murine clone of *GREM1* gene was performed.

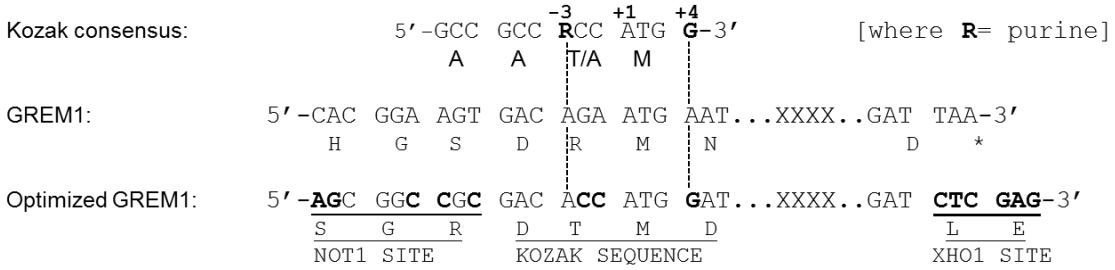

Figure 3.1: Base substitutions incorporated into the 5'- and 3'-ends of all cloned murine GREM1 inserts cloned.

At the 5' end, a NotI restriction endonuclease (RE) site was introduced followed by a sequence optimized at the -2, -1 and +4 positions to resemble the Kozak consensus sequence. At the 3' end, the introduced XhoI RE site replaced the putative stop codon (asterisk). Introduced bases within GREM1 sequence are emboldened and at RE sites, are underlined. Alignment of base nucleotides at -3 and +4 positions of the Kozak consensus sequence are indicated by the vertical broken lines. Respective polypeptide residues (abbreviated) are shown below each codon. XXXX represents the coding sequence of the *GREM1* gene.

As shown in Figure 3.1, the genomic sequence around the ATG start codon of the murine *GREM1* clone conforms largely to the Kozak consensus sequence at most notably, the -3 position. In a significant base change at +4, an adenine residue was replaced by a guanine residue that introduced a negatively charged aspartic amino acid residue (D) into the coding sequence (CDS) of the *GREM1* gene in place of the polar asparagine residue (N). However, this single polypeptide substitution took place within the signal peptide of gremlin predicted to be formed by the first 22-24 coded polypeptide residues (Topol *et al.,* 2000a; Katoh and Katoh, 2004). Given that cleavage of the signal peptide occurs in the Golgi apparatus during post-translational modifications, it implies that this single base substitution in not present in the mature gremlin protein (Hsu *et al.,* 1998*;* Topol *et al.,* 2000a). On another hand, despite having a less dominant effect on initiation of translation, both purine bases at the -1 and -2 positions were substituted by the pyrimidine base, cytosine in order to achieve in greater conformation to the Kozak consensus sequence. The single base nucleotide mismatch observed at the -5 position was left unchanged as this GCC codon was shown to matter least in the initiation of translation (Kozak, 2002).

Also as shown in Figure 3.1, the NotI and XhoI RE sites were introduced at both ends of all GREM1 inserts enabling sticky end ligation into the multiple cloning site (MCS) of the expression vector also possessing both RE sites. This feature was also

exploited as a diagnostic marker of successful transformation prior to selecting plasmid clones for sequencing. The N-terminally located NotI site (GCGGCCGC) was introduced directly upstream and in frame with the optimised Kozak sequence in the 5' untranslated region (UTR) whilst the C-terminally located XhoI site (CTCGAG) substituted the putative TAA stop codon normally found at the end of the GREM1 open reading frame (ORF).

Cloning of the GREM1 insert was expected to generate a band fragment, 560 bp in size, after purification and trimming by NotI/XhoI double digestion. Experimentally, a band fragment of this size was obtained as illustrated in Figure 3.2A. Topol and co-workers (1997) identified the *GREM1* gene as *drm*, down-regulated in v-mos-transformed cells possessing a 552 bp (184 amino acids) ORF and that was located on chromosome 15q13 - q154. This finding on *drm*, now synonymous to *GREM1*, was also confirmed elsewhere (Hsu *et al.*, 1998; McMahon *et al.*, 2000; Topol *et al.*, 2000b). Given that the published GREM1 gene size incorporated neither extended Kozak sequences in the 5'-UTR nor NotI/XhoI RE sequences, the increase in size to 560 bp was expected in this study.

A gradient PCR was required initially in order to determine an optimal annealing temperature to serve the general purpose of cloning. As shown in Figure 3.2B (upper panel), a strong amplification of the GREM1 insert (~ 0.6 kb) was observed between 60 – 68 °C annealing temperature. As a result, an optimal annealing temperature of 60 °C was chosen for all subsequent types of PCR reactions employed in this study. Non-specific bands at 4 and 6 kb were detected in all experimental PCR reactions that were too large to be primer dimers. This most likely indicated use of a high concentration of the DNA template. The results also demonstrated weak detection of GREM1 inserts in the negative control reactions, in which no DNA template had been added (Figure 3.2B, bottom panel). This was most likely due to contamination of the control PCR samples. When a standard PCR reaction was conducted in which the DNA template was diluted 1000 fold and more negative control reactions were included in parallel as indicated in Figure 3.3, no non-specific bands and contaminations were observed in the experimental and negative control tracks.

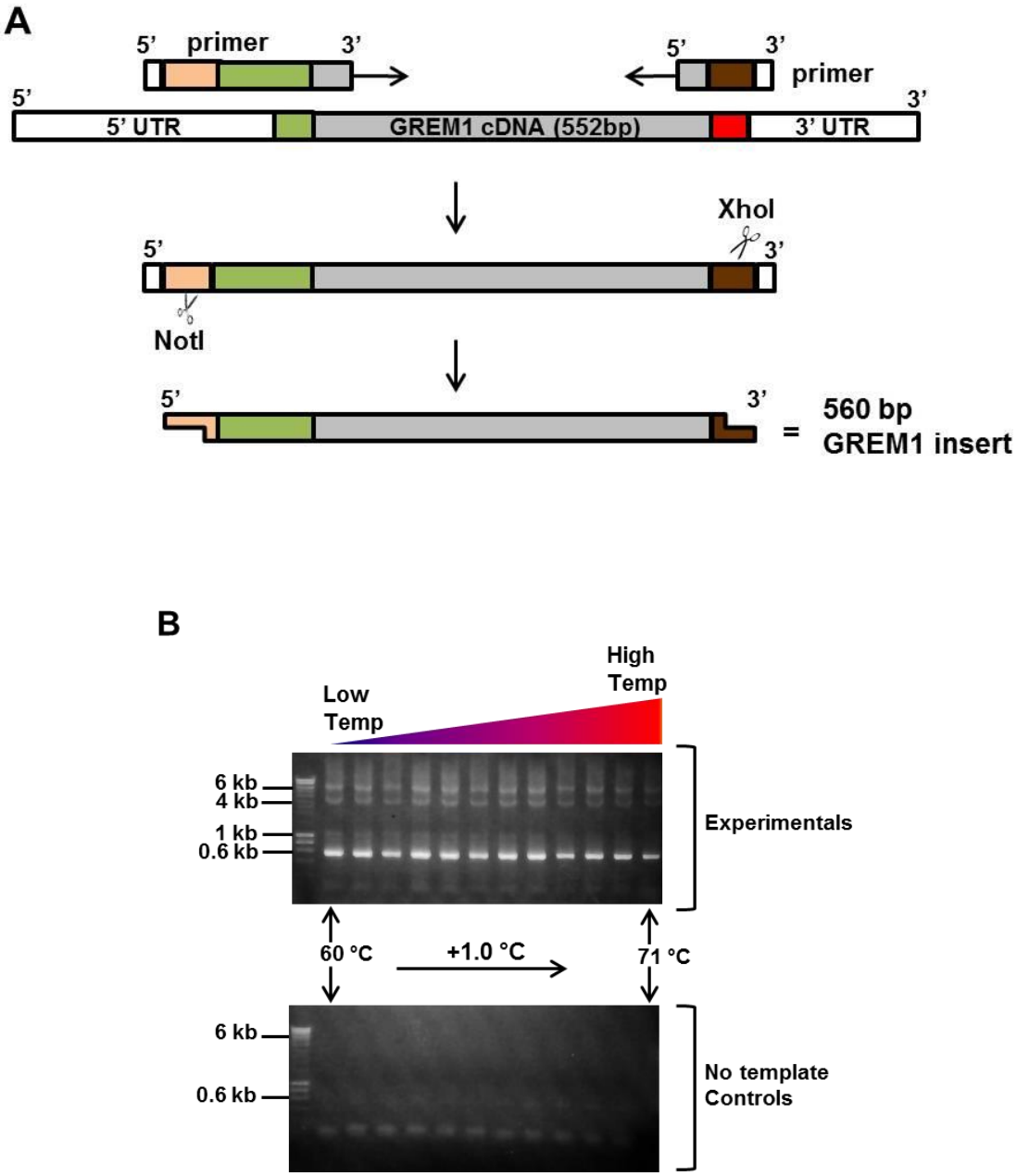

Figure 3.2: Cloning of the wildtype GREM1 insert.

A) Schematic representation of the cloning and RE double digestion of the wildtype GREM1 insert (560 bp in size). Orange colour: NotI RE site, green colour: optimal Kozak sequence, XhoI RE site: brown colour, grey colour: unmodified coding sequences. B) Gradient PCR cloning of the wildtype GREM1 insert at increasing annealing temperatures (Temp). The insert is shown as ~0.6 kb bands in the top panel. The respective negative control reactions are shown in the bottom panel in which no GREM1 I.M.A.G.E. cDNA template (1.6 µg/µl) is added. Non-specific bands are also observed in both gels.

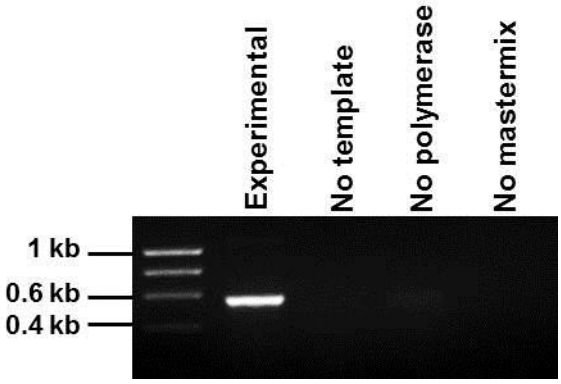

Figure 3.3: Standard PCR amplification of the wildtype GREM1 insert.
Detection of a GREM1 insert, ~0.6 kb, by standard PCR amplification using 1.6 ng/µl (1000 fold diluted). Several negative control reactions are included as indicated.

3.3 Design of site-directed mutagenesis within the GREM1 insert

In addition to constructing a C-Myc-tagged wildtype GREM1 construct, this study also aimed at constructing several C-Myc-tagged mutant GREM1 constructs possessing targeted substitutions in the predicted putative heparin/HS binding site of the wildtype. The heparin binding site on a homology model of gremlin based on the experimental structure of sclerostin was predicted as detailed in Chapter 1, Section 1.16. In gremlin, the alignment of basic surface patches that formed its heparin binding site were present within its primary sequence as three interspersed basic clusters that constituted largely of arginine and lysine residues. The full primary polypeptide sequence of the gremlin precursor highlighting these basic clusters is shown in Figure 3.4A. In this study, these basic clusters were termed basic clusters I, II and III as also indicated in Figure 3.4A. Basic cluster III forms the largest basic cluster and together with cluster II, are located on the third β-stranded finger loop of gremlin (refer Figures 1.13 and 3.4B). According to Rider and Mulloy (2010), these two formed the main site of interaction for heparin/HS binding. Cluster I is located just outside the first β-stranded loop closest to the wrist region (refer to Figures 1.13 and 3.4B).

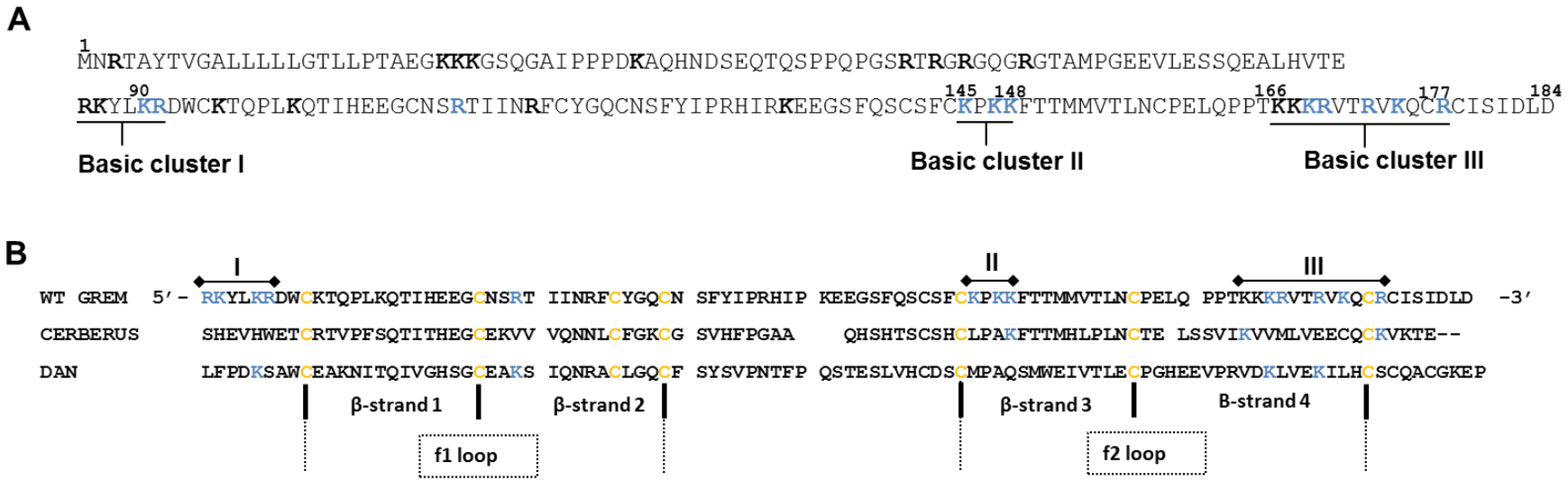

Figure 3.4: Predicted basic clusters in the precursor wildtype GREM1 primary sequence.
A) Basic clusters predicted to form the putative heparin binding site on gremlin. Highlighted in blue colour are the contact arginine and lysine residues. Highlighted in black and emboldened are the non-contact arginine and lysine basic residues B) Primary sequence alignment of wildtype (WT) GREM1 against predicted non-heparin binding homologues, Cerberus and DAN. Conserved cysteine residues are highlighted in yellow colour. f1 and f2 loops denote β-finger loops.

Based on their collective docking calculations, Rider and Mulloy (2010), predicted heparin/HS binding for all CAN family members except DAN and Cerberus. As mentioned previously in Chapter 1, Section 1.16, both CAN members were observed to possess far fewer surface basic residues compared to their heparin binding homologues (refer to Figure 1.12). Another difference between heparin-binding CAN members and the non-heparin-binding DAN and Cerberus, was apparent after a primary sequence alignment of homologous regions possessing basic cluster residues. Remarkably, such an alignment made against the precursor gremlin primary sequence revealed that both DAN and Cerberus lacked the three basic clusters identified earlier (Figure 3.4B).

Observations that both DAN and Cerberus lacked the basic contact clusters in gremlin were highly relevant for this current study. This enabled strategic substitutions to be made within the contact basic clusters in gremlin. Alanine-scanning mutagenesis is a typical strategy used to identify key residues for protein function, by systematic alanine substitution of predicted functional residues (Morrison and Weiss, 2001). Alanine residues are often deemed suitable as they are non-bulky and nonpolar however, because of their small side chain sizes, their use in tandem can result in loss of size conservation in the resulting mutant protein (Morrison and Weiss, 2001). Such loss of size conservation may ultimately alter the tertiary structure of the protein hence damaging it. Moreover, substituting these basic residues on the surface of the protein with fairly hydrophobic alanine residues may in itself alter the orientation of tertiary structure. Therefore, in order to retain the cysteine partners within the wildtype gremlin-Myc and its mutants in appropriate orientations and spacing so that the correct disulfide bridges are formed, size conservation was important. As such, the identification of largely neutral clusters in both DAN and Cerberus homologous to the basic contact clusters in gremlin was highly relevant as this could be used preferably with lesser risk in misfolding and loss of size conservation (refer to Figure 3.4B). Table 3.1 summarizes the designed changes made to the wildtype GREM1 ORF at its contact basic clusters in order to generate its different mutagenic inserts.

Basic clusters	Gremlin nucleotide sequences		Gremlin polypeptide sequences		Reference source of changes (refer to Figure 3.4)
	Wildtype sequence	Nucleotide mutations	Wildtype sequence	Amino acid mutations	
I	AAGCGA	**C**A**TT**G**G**	RKYLKR	HW	Cerberus, upstream of strand 1
II	AAGCCCAAGAAG	**AT**GCCC**GC**G**C**AG	KPKK	MPAQ	DAN, strand 3
IIIa	AAGAAGAAAAGG	AGG**CTT**AA**CGTG**	KKKR	KLNV	KL = HindIII restriction site N = Minimal base change V= Cerberus, IKV, strand 4
		A**TT**AAA**GT**G		KIKV	Cerberus, strand 4
IIIb	CGCGTGAAG CAGTGCCGT	C**T**CGTG**G**AG CAGTGCC**T**T	RVKQCR	LVEQCL	L & E = Cerberus, LVEXXQCX, strand 4 L = Minimal base change

Table 3.1: Summary of design of site-directed mutagenesis of gremlin.
Designed base nucleotides incorporated within the basic clusters (I – III) are emboldened and underlined in red colour. The targeted amino acid residues in these basic clusters are highlighted in blue colour. The substitutions were designed to resemble homologous sequences in DAN and Cerberus.

As a general rule, a strategy of minimising the number of base nucleotide changes was always chosen in order to achieve efficient mutagenesis. As shown in Table 3.1, some or all polypeptide sequences of basic clusters I and II, KR (90 – 91) and KPKK (145 – 148), would be replaced with their homologous sequences, HW and MPAQ, on Cerberus and DAN, respectively (Table 3.1).

Basic cluster III was subdivided further into clusters IIIa (KKKR, 166 - 169) and IIIb (RVKQCR, 172 – 177), (Table 3.1). It followed that two different substitutions were designed in the former. In the first, residues 167 – 169 of cluster IIIa would be substituted with the homologous polypeptide sequence, IKV, from Cerberus generating the cluster KIKV. The basic residue (K-168) would be left unchanged given that it is not amongst the predicted basic contact residues in gremlin (refer to Figure 3.4). In a second design, the same substituting homologous sequence from Cerberus was modified to LNV, to yield the sequence KLNV, instead. In this sequence, both KL residues would introduce a HindIII restriction site with recognition sequence AAG CTT (refer to Table 3.1) that together with both Not1 and Xho1 RE sites, will serve as diagnostic markers to provide an early indication of successful mutagenesis. In this case, K-168 residue was substituted despite the above observation. Its substitution with a neutral asparagine residue (N) was selected, as this is a polar residue with a neutral side chain whose incorporation would require the least number of base nucleotide substitution within this basic cluster (refer to Table 3.1).

The designed polypeptide sequence, LVEQCL, would substitute for the basic cluster IIIb polypeptide sequence, RVKQCR (172 – 177). This was made to resemble the homologous polypeptide sequence, LVEECQCK and LVEKILHCS, in Cerberus and DAN, respectively (refer to Figure 3.4B and Table 3.1). The substitution of R-177 with a nonpolar leucine residue possessing a neutral side chain, was again for reasons of minimal base nucleotide substitution (refer to Table 3.1).

3.4 PCR-based methods used for site-directed mutagenesis

In order to clone specific GREM1 mutant inserts possessing basic contact residue substitutions, different PCR cloning methods were employed. A brief description of these PCR cloning methods will be provided.

In standard PCR, the ability of oligodeoxyribonucleotide (oligo) primers to bind tightly onto their complementary sequences on the target gene allows mismatch nucleotides to be incorporated into the cloned DNA fragment. It is this ability which

enabled the incorporation of both terminal NotI and XhoI RE sites together with optimized Kozak sequence within the GREM1 nucleotide sequence, as illustrated earlier in Figure 3.2A. However, a major drawback of standard PCR itself is that oligo primers longer than 110 nucleotides are difficult to produce (Wosnick *et al.,* 1987). These result in standard PCR being able to introduce mismatch nucleotides at the initial sites complementary between the target gene and the pair of oligo primers. Internal changes to target gene beyond these sites are not possible in a single reaction. Given that several designed substitutions in the gremlin basic clusters were internally located, alternative PCR-based methods were required. In this study, both overlap extension (OE) PCR and one-step OE (OOE) PCR, were employed, which both enable internal mutations to be incorporated anywhere along the length of the target gene (Higuchi *et al.,* 1988; Ho *et al.,* 1989; Ke and Madison, 1997, Urban *et al.,* 1997).

As illustrated in Figure 3.5, OE PCR requires several rounds of PCR to generate intermediate DNA fragments that have ends overlapping each other. These are generated using one or several pairs of complementary mutagenic internal oligo primers together with standard PCR pair of non-complementary outer oligo primers. In a subsequent "fusion" reaction, the overlapping intermediate DNA fragments, are mixed at equimolar ratios and standard PCR conducted using only the outer oligo primers. As a result, the full target insert is generated.

On the other hand, in a OOE PCR reaction, as illustrated in Figure 3.6, all appropriate pairs of complementary internal mutagenic and standard PCR outer oligo primers are added together. Both OOE PCR and OE PCR proceed via the same mechanism, although the former does not require the physical processing and purification of intermediate DNA fragments generated. As a result, OOE PCR is a more rapid and less laborious alternative to OE PCR. In the published protocol by Urban and co-workers (1997), reduced concentrations of internal mutagenic primers were used that ensured they were fully consumed during the early cycles. Thus, only the newly formed template and outer oligo primers were left behind during the late cycles for further extension of the full length target gene (refer to Figure 3.6). In this current study however, the concentrations of both outer and internal oligo primers were kept the same.

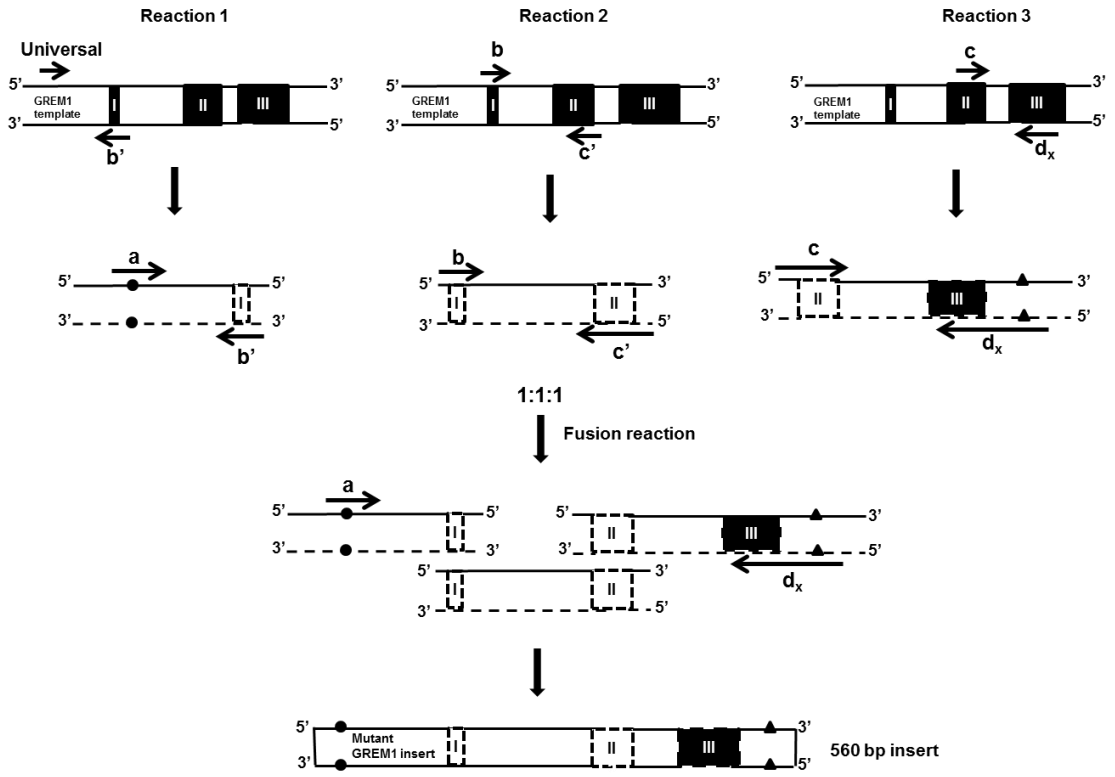

Figure 3.5: Schematic diagram of the overlap extension PCR (OE PCR) method of site-directed mutagenesis.

In the method illustrated, three intermediate DNA fragments were amplified from a wildtype GREM1 template and combined in a 'fusion' reaction to generate a mutagenized GREM1 insert. For amplification reactions (reactions 1 – 3) three standard PCR reactions were carried out independently, using as shown a combination of non-complementary pair of outer oligo primers (Universal/a and d_x) and two non-complementary pairs of internal mutagenic primers (b and c; their respective reverse oligo primers c' and d') that introduced base mutations within the basic clusters I and II on the template. In the fusion reaction, the purified intermediate fragments were mixed 1:1:1 in a final standard PCR reaction that used only the outer primers. The leading (5' – 3' direction) and lagging (3' – 5' direction) strands are highlighted as solid and broken lines, respectively.

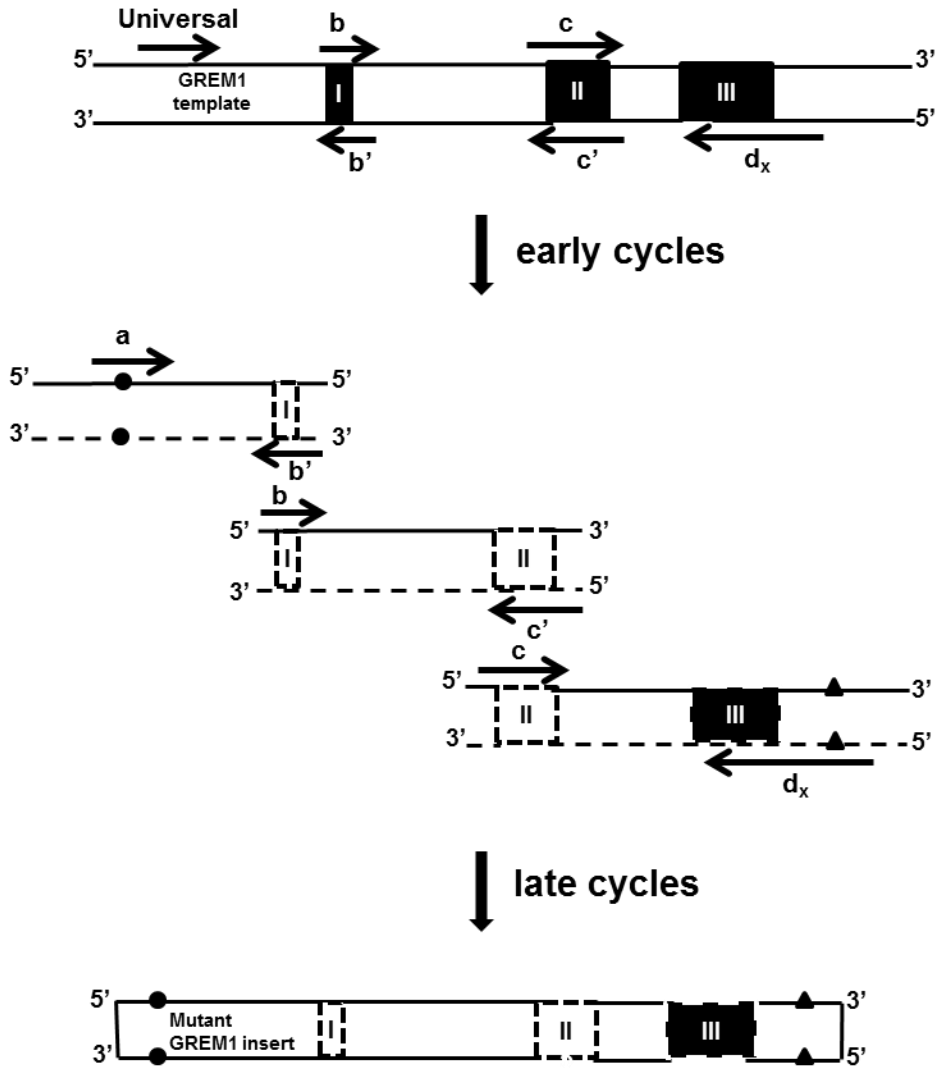

Figure 3.6: Schematic diagram of the one-step overlap extension PCR (OOE PCR). This method essentially involves a single standard PCR reaction in which two or more complementary pairs of internal mutagenic primers (b and c and their respective reverse primers b' and c') are used together with a non-complementary pair of outer oligo primers (universal/a and d_x) to clone a mutant GREM1 insert. Symbols and annotations are described in the legend of the previous figure.

3.5 Application of PCR-based methods in cloning of mutant GREM1 inserts

In addition to the wildtype GREM1 insert, a total of seven different mutant GREM1 constructs were cloned by applying the different PCR-based methods described in the previous section. These included: mutant gremlin (MGR)1, MGR2, MGR1+2, MGR3, MGR4, MGR4 and MGR6, all numbered in the order they were expressed except for MGR1+2. These names were also applied to their respective expressed proteins. The MGR1+2 insert was not successfully expressed in this study but incorporated both MGRs 1 and 2 mutations. As shown in Table 3.2, only both MGRs1 and 2 inserts possessed

individual mutations of basic clusters II and III, respectively. The remaining inserts each possessed combined mutations of either basic clusters I or III together with the basic cluster II mutations.

Mutant GREM1 inserts cloned	Basic cluster mutated
MGR1	II
MGR2	III
MGR1+2	II + III
MGR3	II + IIIa
MGR4	II + IIIa
MGR5	II + IIIb
MGR6	I + II

Table 3.2: List of all GREM1 mutant inserts cloned.
The table provides a list of all mutant GREM1 inserts cloned together with the respective targeted contact basic cluster they were each made to possess.

During cloning of GREM1 inserts, the same universal forward oligo primer was always employed (Figures 3.5 and 3.6). This incorporated, at all their 5' termini, both NotI RE site in frame with the optimized Kozak sequence (refer to Figures 3.1 and 3.2A). The outer reverse oligo primer that could be made either non-mutagenic or mutagenic, always incorporated a XhoI RE site at the C-terminal ends of the GREM1 inserts (refer to Figures 3.1 and 3.2A). The application of standard PCR, OE and OOE PCR methods in cloning GREM1 inserts are summarised in Tables 3.3 – 3.5 respectively.

By standard PCR, the wildtype, MGRs 2 – 5 and MGR1+2 inserts were generated using the universal forward oligo primer paired with either a non-mutagenic (d_1) or mutagenic ($d_{2\text{-}5}$) reverse oligo primers (Table 3.3). The mutant inserts, MGRs 1+2, 5 and 6 were generated by OE PCR and in addition, MGRs 1, 1+2 and 6 were generated by OOE PCR. In both of these methods, one or two pairs of complementary mutagenic internal oligo primers, annotated *b* and *c* (refer to Tables 3.4 and 3.5, Figures 3.5 and

3.6), were used together with a pair of complementary outer oligo primers listed in Table 3.3.

By both standard and OOE PCR methods, a wildtype or mutant GREM1 insert, 560 bp in size, was typically generated as shown previously in Figure 3.2. On the other hand, the DNA intermediates generated when cloning the MGRs 1+2, 5 and 6 inserts by OE PCR method, were as shown in Figure 3.7. These were generated prior to the final fusion reaction that yielded the full mutant inserts, ~0.6 kb in size.

Note that all bands produced correspond in size to their anticipated lengths. In cloning of the MGR1+2 insert, two intermediate GREM1 DNA fragments, ~ 440 bp and ~ 120 bp, were generated using a sequence-verified wildtype GREM1-Myc construct as template (Figure 3.7A).The larger DNA was generated using the outer forward universal oligo primer and a reverse mutagenic oligo primer, *c',* which mutagenized the basic cluster II (refer to Figure 3.5 and Table 3.4). The ~ 120 bp DNA fragment was generated possessing mutations in basic cluster III by the non-complementary pair of mutagenic oligo primers, *c* and d_2 (refer to Table 3.4). The same result was also achieved during similar cloning of the MGR5 insert (Figure 3.7A). In this case, the same combination of oligo primers was also utilised except that the d_5 reverse mutagenic outer oligo primer was used instead of the d_2 reverse oligo primer (refer to Table 3.4).

In cloning the MGR6 insert, three intermediate DNA fragments were generated of approximate sizes 280 bp, 160 bp and 120 bp as shown in Figure 3.7B. Using the same template as above, the fragments were generated using three non-complementary pairs of oligo primers that included the universal forward and *b'* , *b* and *c',* and, *c* and d_1, respectively. The internal oligo primers used here were mutagenic which resulted in the combined mutagenesis of both basic clusters I and II only (refer to Figure 3.5 and Table 3.4). When using a sequence-verified MGR1 DNA plasmid as template instead, already possessing in it targeted mutations to basic cluster II, two intermediate DNA fragments of equal size, 280 bp, were generated (Figure 3.7C). This required use of one less non-complementary pair of oligo primers that included, the universal forward with *b'* and *b* with d_1. These mutagenized the basic cluster I only in both intermediates.

Primers		Primer sequences [Corresponding polypeptide sequence] All in 5' – 3' direction	Template used with primers	GREM1 inserts cloned
Universal (Forward)		AT AGCGGCCGCGACACCATGGATCGCA CCGCATACACTGTGGGAGCGTTGCTT [SGRDTMDRTAYTVGALL]	All listed below	All
d_x (Reverse)	d_1	GTAGTCGACCTCGAGATCCAAGTCGATGGATAT [ISIDLDLEVDY]	GREM1 cDNA	WT
	d_2	TTTCTGCTCGAGATCCAAGTCGATGGATATGCAAAGGCA CTGCTCCACGAGTGTGACCACGTTAAGCTTGGTGGGTGG C [PPTKLNVVTLVEQCLCISIDLDLEQK]	wtGREM1myc MGR1-Myc	MGR2 MGR1+2
	d_3	TTTCTGCTCGAGATCCAAGTCGATGGATATGCAACGGCA CTGCTTCACGCGTGTGACCACGTTAAGCTTGGTGGGTGG C [PPTKLNVVTRVKQCRCISIDLDLEQK]	MGR1-Myc	MGR3
	d_4	TTTCTGCTCGAGATCCAAGTCGATGGATATGCAACGGCA CTGCTTCACGCGTGTGACCACTTTAATCTTGGTGGGTGG C [PPTKIKVVTRVKQCRCISIDLDLEQK]		MGR4
	d_5	TTTCTGCTCGAGATCCAAGTCGATGGATATGCA AAGGCACTGCTCCACGAGTGTGACCCTTTTCTT [KKRVTLVEQCLCISIDLDLEQK]		MGR5

Table 3.3: List of primers and GREM1 mutant inserts cloned by standard PCR method. Provided are the sequences of oligo primers used for site-directed mutagenesis by standard PCR method. The templates used in this method are also provided. The NotI, HindIII and XhoI RE sites and optimal Kozak sequence are highlighted in purple, brown, blue and green colours, respectively. The polypeptide sequences of the base nucleotide sequences provided are enclosed in brackets. The substituted wildtype basic clusters are underlined in the polypeptide sequences. Optimal template concentrations for wildtype GREM1-Myc (wtGREM1myc) and GREM1 I.M.A.G.E. cDNA templates = 1.6ng/µl, MGR1-Myc template = 380ng/µl and 10µM working concentration for all primers.

Primers		Primer sequences [Corresponding polypeptide sequence] All in 5' – 3' direction	Templates used with primers	GREM1 inserts cloned
Universal (Forward)		AT AGCGGCCGCGACACCATGGATCGC ACCGCATACACTGTGGGAGCGTTGCTT [SGRDTMDRTAYTVGALL]	All listed below	All
b (Forward)		ACAGAGCGCAAGTATCTGCAT TGGGATTGGTGCAAAACTCAG [TERKYLHWDWCKTQ]	wtGREM1myc MGR1-Myc	MGR6
c (Forward)		TCTTGCTCCTTCTGCATGCCC GCG**C**AGTTCACCACCATGATG [SCSFCMPAQFTTMM]	wtGREM1myc	MGR1+2 MGR5 MGR6
d_x (Reverse)	d_1	GTAGTCGACCTCGAGATCCAAGTCGATGGATAT [ISIDLDLEVDY]	wtGREM1myc MGR1-Myc	MGR6
	d_2	TTTCTGCTCGAGATCCAAGTCGATGGATATGCAAAGGCA CTGCTCCACGAGTGTGACCACGTTAAGCTTGGTGGGTGGC [PPTKLNVVTLVEQCLCISIDLDLEQK]	wtGREM1myc	MGR1+2
	d_5	TTTCTGCTCGAGATCCAAGTCGATGGATATGCA AAGGCACTGCTCCACGAGTGTGACCCTTTTCTT [KKRVTLVEQCLCISIDLDLEQK]		MGR5

Table 3.4: List of primers and GREM1 mutant inserts cloned by OE PCR-based method. Provided are the sequences of oligo primers used for site-directed mutagenesis by OE PCR method. The templates that enabled application of this method are also provided. Refer to the legend of the previous table for highlights, template and oligo primer concentrations.

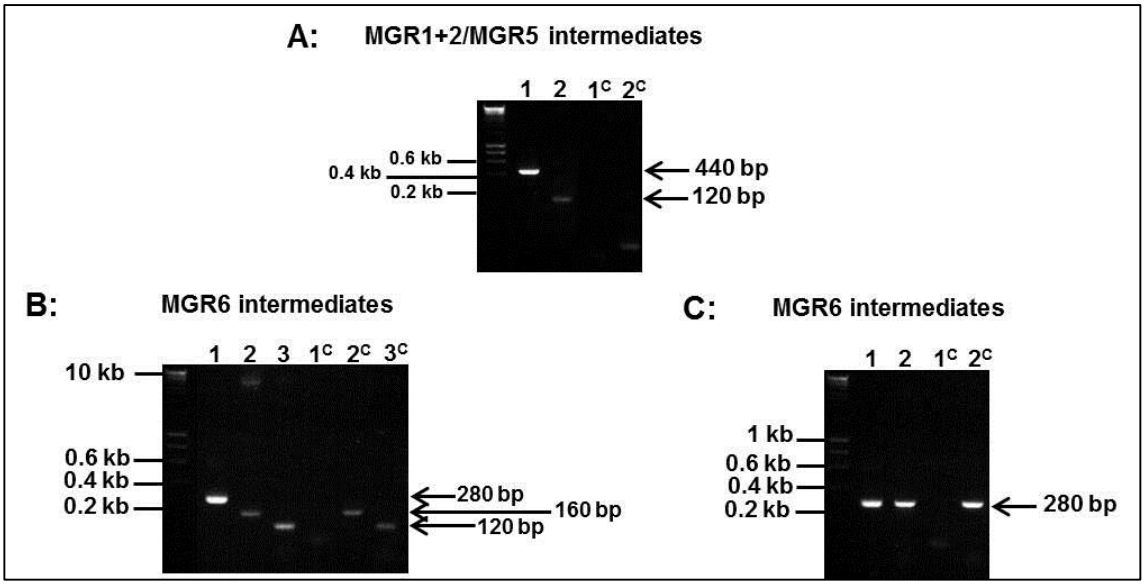

Figure 3.7: Intermediate DNA fragments of GREM1 mutant inserts generated using OE PCR.

A) Cloning of MGR1+2 and MGR5 mutant inserts using the wildtype GREM1 DNA plasmid as template. In both cases, two intermediate DNA fragments, 440 bp and 120 bp in size were generated in experimental lanes (Lanes 1 and 2). B) MGR6 cloning using the wildtype GREM1 DNA plasmid as template generated three intermediate DNA fragments, 280 bp, 160 bp and 120 bp, in the experimental lanes (Lanes 1, 2 and 3). C) MGR6 cloning using the MGR1-Myc DNA plasmid as template generated two intermediate DNA fragments of equal size, 280 bp in experimental lanes (Lanes 1 and 2). All control reactions (Lanes 1^c, 2^c and 3^c) did not have the templates added to them, and some contamination is observed. Note that the indicated band sizes represented the expected theoretical intermediate sizes.

Primers		Primer sequences [Corresponding polypeptide sequence] All in 5' – 3' direction	Template used with primer	GREM1 insert cloned
Universal (Forward)		AT AGCGGCCGCGACACCATGGATCGC ACCGCATACACTGTGGGAGCGTTGCTT [SGRDTMDRTAYTVGALL]	All listed below	All listed below
b (Forward)		ACAGAGCGCAAGTATCTGCAT TGGGATTGGTGCAAAACTCAG [TERKYLHWDWCKTQ]	MGR1-Myc	MGR6
c (Forward)		TCTTGCTCCTTCTGCATGCCC GCGCAGTTCACCACCATGATG [SCSFCMPAQFTTMM]	wtGREM1myc MGR2-Myc	MGR1 MGR1+2
d_x (reverse)	d_1	GTAGTCGACCTCGAGATCCAAGTCGATGGATAT [ISIDLDLEVDY]	wtGREM1myc MGR1-Myc	MGR1 MGR6
	d_2	TTTCTGCTCGAGATCCAAGTCGATGGATATGCAAAGGCA CTGCTCCACGAGTGTGACCACGTTAAGCTTGGTGGGTGGC [PPTKLNVVTLVEQCLCISIDLDLEQK]	MGR2-Myc	MGR1+2

Table 3.5: List of primers and GREM1 mutant inserts cloned by OOE PCR method.
Provided are the sequences of oligo primers used for site-directed mutagenesis by OOE PCR method. The templates that enabled application of this method are also provided. Colour highlights and both template and oligo primer concentrations are provided in the legend of Table 3.3. MGR2-Myc template working concentrations = 3.8 µg/µl.

3.6 Subcloning the GREM1 inserts into the pCMV-Tag5A expression vector

3.6.1 The pCMV-Tag5A expression vector

The next stage of the cloning process involved subcloning previously constructed wildtype and its mutant GREM1 inserts into a pCMV-Tag5A mammalian expression vector via sticky-end ligation at the NotI and XhoI RE cleavage sites they all incorporate (Figure 3.8). This subcloning strategy ensured that MCS of the expression vector remained in frame with its C-Myc sequence and stop codon (refer to Figure 3.8). As such, this would enable C-terminal tagging of all subcloned GREM1 inserts with a Myc sequence. The three different MCS frames of this expression vector were described previously in Chapter 2, Section 2.9.1. In addition to possessing an adaptable MCS, this expression vector also possessed essential features as shown in Figure 3.8.

A cytomegalovirus (CMV) immediate-early enhancer containing promoter, pCMV promoter, found directly upstream of the MCS, drives strong expression of the subcloned GREM1 gene in CHO-S expression systems (Stinski and Isomura, 2008). A Simian virus 40 (SV40) early promoter controls expression of both *neomycin* and *kanamycin resistance* genes that in this study, conferred kanamycin resistance to all positive integrative transformants (Gazdar *et al.*, 2002; Liu *et al.*, 2013). Another promoter, the blasticidin promoter, directly upstream the SV40 promoter, drives strong expression of *blasticidin deaminase* gene that confers resistance to blasticidin. Blasticidin is a nucleoside antibiotic which inhibits protein synthesis in both prokaryotes and eukaryotes (Kimura *et al.*, 1994; Mamoun *et al.*, 1999; Goyard and Beverley, 2000). Although this feature was not exploited in this study, this promoter would have offered another screening option post-transfection for the isolation of positive integrative transfectants in blasticidin selective medium.

The expression vector also carried two origins of replication (ori), pUC ori and f1 ori, at which sites replication was initiated during the transformation of DH5α and TOP10 competent cells. The pUC ori enables high copy number replication of GREM1-Myc single-stranded DNA (ssDNA) constructs while the f1 ori acts similarly however in the reverse orientation to the pUC ori. Given that both ssDNA constructs are complementary, it meant that only double-stranded GREM1-Myc constructs were always generated for eukaryotic expression systems (Dotto and Horiuchi, 1981; Dotto *et al.*, 1981; Dente *et al.*, 1983).

Two polyadenylation (pA) signals, SV40 pA and the Herpes simplex virus thymidine kinase (TK) pA, were also present in the expression vector. These both trigger the termination of transcription by RNA polymerase II resulting in cleavage of the GREM1 pre-mRNA (Huang and Workman, 2013; MacDonald and McMahon, 2010).

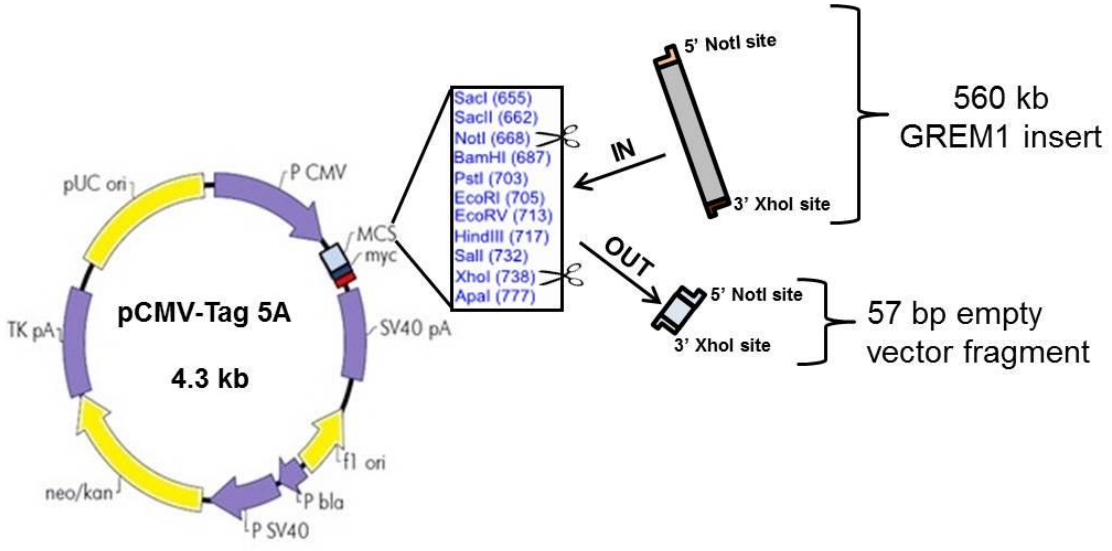

Figure 3.8: Plasmid map of the pCMV-Tag5A expression vector.
The pCMV-Tag5A vector possesses a multiple cloning site (MCS, light blue colour) which is in frame with a Myc sequence (dark blue colour) that in turn is in frame with a stop codon at its C-terminal end (red colour). Subcloning of GREM1 inserts into the MCS (light blue colour) occurs at their mutual NotI and XhoI RE cleavage sites. Other features of the vector include; P CMV: cytomegalovirus promoter, SV40 pA: Simian virus 40 polyadenylation signal, f1 ori: f1 origin, P bla: blasticidin promoter, P SV40: SV40 promoter, neo/kan: neomycin/kanamycin resistance gene, TK pA: thymidine kinase pA, pUC ori: pUC origin of replication. Coloured arrows indicate direction of transcription.

3.6.2 Preparing the pCMV-Tag5A expression vector

Alkaline phosphatases are non-specific phosphomonoesterases that catalyse the hydrolysis of a wide variety of phosphate monoesters and small organic molecules such as DNA and RNA (Nilsen *et al.*, 2001; de Backer *et al.*, 2002). By dephosphorylating the ends of an empty linearized expression vector prior to ligation, vector-vector re-ligation would be prevented. This stated benefit of SAP treatment however has remained questionable mainly due to the non-specificity of the enzyme itself. As such, at the initial phase of this current study, the empty expression vector was linearized by NotI and XhoI double digestion and then treated with/without thermolabile shrimp alkaline phosphatase (SAP) in parallel.

As shown in Figure 3.9, the SAP-treated vector migrated only slightly further down the gel with approximately the same size, between 4 - 5 kb, as the untreated vector. Given that SAP treatments had no marked adverse effects on both transformations and transient transfections, the SAP-treated vector was used hereafter.

Figure 3.9: Thermolabile SAP treatment of the pCMV-Tag5A expression vector. Bands of approximately the same size and intensity were detected following -/+ SAP treatment of an empty pCMV-Tag5A vector after its double digestion with NotI/XhoI RE enzymes.

3.7 Screening of bacterial transformants

3.7.1 Preliminary screening by restriction endonuclease digestion

To recapitulate, all GREM1 inserts possessed end-to-end NotI and XhoI RE cleavage sites and in addition, three inserts, MGRs 1+2, 2 and 3, also possessed a HindIII RE site within their basic cluster IIIa (refer to Sections 3.2 and 3.3). Together, these RE cleavage sites provided a rapid diagnostic tool for the preliminary screening of positive integrative transformants prior to sequencing.

As shown in Figure 3.10A, NotI and XhoI double digestions in positive integrative transformants, reproducibly showed two bands, ~ 4 kb and ~ 0.6 kb, corresponding to the approximate sizes of the expression vector (4.3 kb) and all GREM1 inserts (0.56 kb), respectively. In single digestions using either NotI or XhoI enzymes, a single band of ~ 5 kb is seen. In the uncut DNA plasmid, two bands are consistently seen of variable sizes. These diagnostic features were characteristic for all positive integrative transformants and indicated that a DNA fragment with the approximate size of the GREM1 insert had been subcloned successfully within MCS of the pCMV-Tag5A expression vector. It also indicated that no random mutations had occurred at both targeted RE sites. Only sequencing could reveal conclusive evidence of successful cloning.

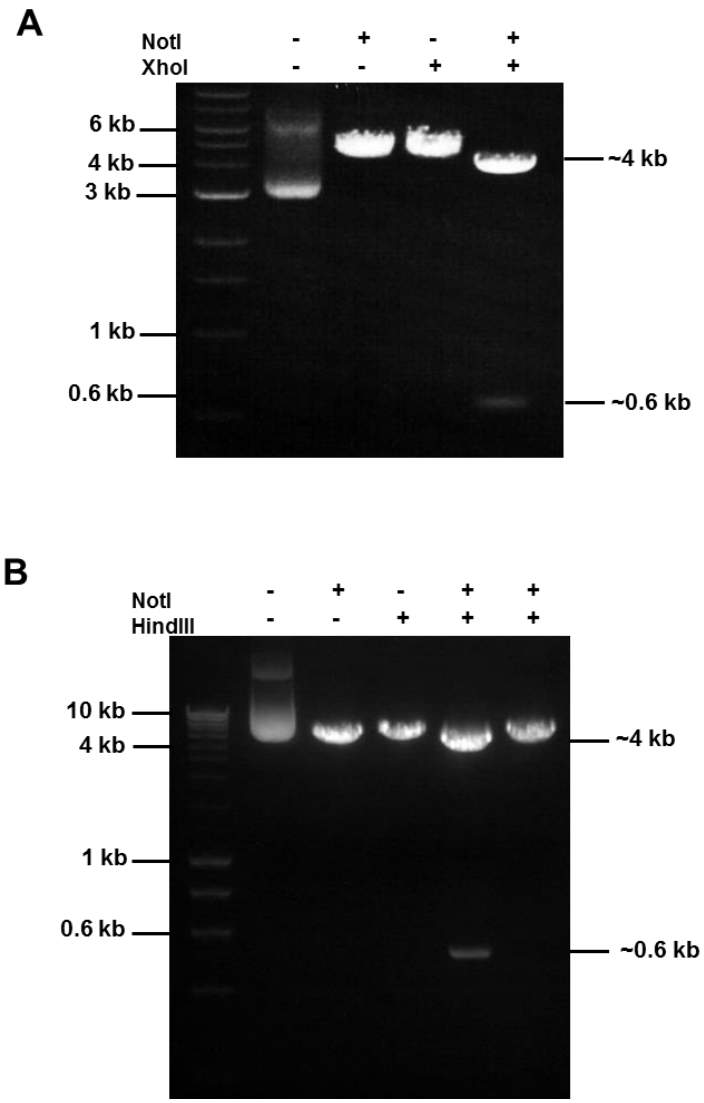

Figure 3.10: Preliminary screening by restriction endonuclease (RE) digestion. Purified DNA construct from positive integrative transformants were both single and double digested with A) NotI and XhoI RE enzymes. This diagnostic test was applicable to all GREM1 constructs (B) NotI and HindIII RE enzymes. This test was only applicable to MGR2 (shown) and MGR3 constructs both incorporating HindIII RE sites at the C-terminal end of their GREM1 inserts close to the XhoI RE site.

In positive integrative transformants expected to possess the additional HindIII RE site, similar results to those described using NotI/XhoI RE, were obtained after NotI/HindIII double digestions (Figure 3.10B). This was not surprising as the HindIII site was located close to the XhoI site at the C-terminal end of the GREM1 insert. Nonetheless, this alternative NotI/HindIII diagnostic approach was more informative as it indicated successful incorporation of the HindIII site within of basic cluster IIIa of these GREM1 mutant inserts. As shown in Figure 3.10B, this alternative screening approach was made even more informative when conducted alongside a similar double

digestion of the wildtype GREM1-Myc plasmid that lacks a HindIII cleavage site. Of the three candidate GREM1 inserts only the MGR1+2 constructs consistently failed to demonstrate two bands typical of such double digestion as mentioned above. Therefore only the MGRs 2 and 3-Myc constructs were sequenced (refer to Figure 3.11).

As it carried the largest number of mutations, it was always expected that the MGR1+2 construct would be the most difficult to clone gremlin mutant. Despite using different PCR cloning strategies, altering the ligation ratios, and the amounts of ligated DNA transformed into both DH5α and TOP10 competent cells, the same outcome was consistently obtained. Consequently, cloning of the MGR1+2-Myc construct was aborted and the other six out of seven mutant GREM1-Myc constructs were sequenced.

3.7.2 Sequencing of GREM1-Myc constructs

As shown in Figure 3.11, sequence analyses was performed on six out of seven GREM1-Myc mutant constructs after preliminary screening mentioned in the previous section. Part of the wildtype GREM1-Myc sequence is also included. As revealed, all designed substitutions within wildtype basic clusters I – III were successfully completed in the MGRs 1 – 6 mutant GREM1-Myc constructs (refer to Sections 3.3 and Figure 3.11). In MGR1, substitution of 3/3 contact basic residues within basic cluster II was achieved. In MGR2, substitution of 5/5 contact basic residues including one non-contact lysine residue was achieved within basic cluster III. MGRs 3 - 5 all carried the same substitutions in the MGR1 substitution combined with partial substitutions of basic cluster III (refer to Figure 3.11). In combination, MGR3 possessed the same substitutions as those within the basic cluster IIIa of MGR2 whereas MGR4 possessed 1 out of 2 (1/2) substitutions of the same basic cluster including one substitutions of a non-contact lysine residue. Furthermore, MGR5 in addition to MGR1 substitutions, possessed the same 3/3 substitutions of contact basic residues within the basic cluster IIIb. On the other hand, MGR6 possessed combined MGR1 substitutions together with 2/2 substitutions of contact basic residues in basic cluster I (refer to Figure 3.11).

Moreover, all incorporated RE sites and optimized Kozak sequence were also verified (not highlighted in Figure 3.11). More importantly, the C-terminal Myc sequence followed by the stop codon were correctly incorporated in both wildtype and mutant GREM1 constructs. This confirmed that only C-Myc-tagged gremlin proteins would be expressed in CHO-S mammalian expressing cells upon translation of these GREM1-Myc constructs.

Listed in Table 3.6 are the total yields of these GREM1-Myc constructs as obtained after extraction from positive integrative transformants and Maxi prep purification. Also provided are the underlying PCR-based methods that were used initially for the cloning of their GREM1 inserts. Altogether, these results demonstrate that using different PCR-based methods to that of wildtype GREM1-Myc construct did not affected the total yields of its mutant constructs. No direct analyses were made in this study comparing their efficiencies.

Figure 3.11: Sequence alignment of all GREM1-Myc constructs.

The polypeptide sequence alignment highlights the changes to the basic clusters in wildtype (WT) GREM1 as confirmed by sequencing. Basic contact residues: blue colour highlight, confirmed substitutions introduced: red colour highlight, conserved cysteine residues: yellow colour highlight, C-Myc sequence: purple colour highlight, asterisk: stop codon.

Purified DNA plasmid	Total yield (µg)	PCR-based method applied
WT GREM1-Myc	510	Standard PCR
MGR1	1140	OOE PCR
MGR2	1140	Standard PCR
MGR3	930	Standard PCR
MGR4	930	Standard PCR
MGR5	780	OE PCR
MGR6	870	OE PCR

.

Table 3.6: Effects of using different PCR-based strategies on the DNA yields of all GREM1-Myc constructs.

DNA yields as obtained after extraction and Maxi prep purification of both wildtype and mutant GREM1-Myc constructs from a single positive integrative transformant for each. Quantitation was achieved by Nanodrop measurement.

3.8 Discussion

All aims set at the start of these cloning studies were achieved as described in this chapter. Initially, a C-Myc-tagged wildtype GREM1-Myc construct was cloned as an alternative to the commercially purified His-tagged wildtype gremlin. This was achieved primarily by subcloning the wildtype GREM1 insert into the MCS of the pCMV-Tag5A expression vector which was then transformed in competent DH5α *E. coli* cells. Following its sequence verification, the Maxi prep purified wildtype GREM1-Myc construct was then transiently transfected in the CHO-S eukaryotic cell line. The expressed wildtype gremlin-Myc protein was then harvested in crude cell culture supernatants for immunoassay (next chapter).

The wildtype GREM1 insert was cloned from an I.M.A.G.E. clone of murine gremlin using standard PCR. Like all mutant GREM1 inserts cloned, it possessed a NotI RE cleavage site in frame with an optimized Kozak sequence at its N-terminal end and a XhoI RE cleavage site at the C-terminal end which replaced the putative stop codon. By substituting this putative stop codon by this mutual XhoI RE site, C-terminal tagging of the GREM1 insert with the Myc sequence in the expression vector was made possible. A typical GREM1 insert, migrated on 1% (w/v) agarose gels as a PCR band fragment, approximately 0.6 kb in size. Both RE cleavage sites were introduced to facilitate subcloning of the GREM1 insert into the MCS of the pCMV-Tag5A expression vector that also possess them. The optimized Kozak sequence that substituted genomic sequences around the translation start codon has been shown to increase strongly, translation efficiency, thus enabling optimal yield in terms of eukaryotic levels of protein expression (Kozak, 1984 & 1987). Given that these findings have been extensively verified in several studies, no further direct investigations into the Kozak consensus were made in this current study.

By conforming to the Kozak consensus sequence, a single amino acid substitution was made at the N-terminal region of all GREM1 inserts immediately after the methionine start amino acid residue. This was caused by a single base nucleotide change in the GREM1 genomic sequence so as to conform to the +4 position of the Kozak consensus sequence. Findings by Kozak in 1986 and 2002 showed that the purine bases at the -3 and +4 positions within the Kozak consensus sequence have the most dominant effect in promoting proper initiation of translation. It was observed that only a guanine base at the +4 position carried this dominant effect on the initiation of translation unlike the -3 position where either purine bases were suitable candidates. By conforming to

these findings, the adenine base found at the +4 position in the genomic sequence of the *GREM1* gene was substituted by a guanine base. This in turn caused a single amino acid substitution of an asparagine residue (N) to an aspartate residue (D) immediately after the methionine translation start amino acid residue. Fortunately, this polypeptide substitution occurred in the predicted signal peptide region which encompasses the first 22 - 24 polypeptide residues in polypeptide sequence of gremlin precursor protein (Katoh and Katoh, 2004; Topol *et al.,* 2000a). Cleavage of the signal peptide is reported to occur during post-translational modifications in the Golgi apparatus (Hsu *et al.,* 1998*;* Topol *et al.,* 2000a). Therefore, it was highly unlikely that this single polypeptide substitution would cause change to the tertiary structure of mature wildtype and mutant gremlin proteins.

Having successfully cloned the wildtype GREM1-Myc construct, the next aim achieved was generating mutant GREM1-Myc constructs possessing specific mutations within the three predicted basic clusters that form the heparin binding site on the wildtype. These mutants would serve as an experimental verification to the predictions made by Rider and Mulloy (2010) on the heparin binding site on homology models of CAN family members. These homology models were based on the high resolution NMR structure of sclerostin resolved by Veverka *et al.* (2009). Within the gremlin primary sequence, three basic clusters annotated as basic clusters I – III, were identified and constituted largely of arginine and lysine contact residues. In this study, the experimental verification of these predictions were achieved using site-directed mutagenesis. Here, both basic contact and non-contact residues within the basic clusters in gremlin were strategically substituted with mostly, polar and nonpolar residues from homologous regions of DAN and Cerberus. This was designed based on the predictions made by Rider and Mulloy (2010), that DAN and Cerberus would not bind to heparin. By adopting such strategic approach to site-directed mutagenesis, the hope was to express several mutant gremlin-Myc proteins possessing reduced binding for heparin/HS yet still conserved in size compared to the wildtype. Also, this approach increased the likelihood that the gremlin-Myc mutants would remain functionally active as judged by their ability to inhibit BMP signalling activities, *in vitro*.

In this study, seven GREM1 inserts, MGRs 1+2, 1 – 6, were cloned and six out of seven sequence-verified GREM1-Myc constructs, MGRs 1 – 6, were successfully obtained for expression in CHO-S cell culture. MGR1 and MGR2, both carried individual substitutions of basic clusters II and III, respectively. The remaining

constructs were hybrid constructs of MGR1 possessing its substitutions itself combined with substitutions of basic cluster IIIa (MGRs 3 and 4), IIIb (MGR5) and I (MGR6). The incorporation of MGR1 substitutions in all these mutant GREM1-Myc constructs was based on results obtained at earlier MGRs 1 and 2 cloning cycles, expressions and assessment of their heparin binding capabilities. These results are discussed in the next chapter.

In this next round of hybrid mutant constructions, the substitutions within the basic cluster III were carried out in part; either in combination with basic clusters IIIa or IIIb. These were designed as it was expected that cloning of the MGR1+2-Myc construct possessing both full basic cluster substitutions would be difficult.

Oligonucleotide-based site-directed mutagenesis involved use of three different PCR-based methods that included, standard, overlap extension (OE) and one-step overlap extension (OOE) PCRs (Mullis *et al.,* 1986; Higuchi *et al.,* 1988; Urban *et al.,* 1997). In this current work, the diverse alternative cloning routes that these PCR-based methods provided, achieved the same GREM1 inserts. OE and OOE PCRs were both effective in tackling difficult to clone inserts such as MGR1+2 and MGR6. MGR6 was a difficult to clone insert, because both targeted contact residues in basic clusters I and II were internal and also far apart from each other. Their complementary sites could not be reached by the short-length outer mutagenic oligo primers. In this work, sufficient DNA yields of purified GREM1-Myc mutant constructs were obtained irrespective of the underlying PCR-based methods used at initial stages of the process. This indicated that all three methods are effective. It is important to stress that this work did not seek to directly compare between these PCR-based methods. As such, no investigation was made into their efficiencies.

In this study, no direct comparison was made into transformation and transfection efficiency between SAP-treated and -untreated empty pCMV-Tag5A expression vector. However, it is possible to at least comment on its apparent effects in these processes. No marked difference in the number of single colony transformants was apparent in parallel transformations of DH5α cells with both wildtype GREM1- pCMV-Tag5A$^{+/-SAP}$ constructs. Moreover, no marked difference in gremlin-Myc immunoreactivity was detected in crude CHO-S culture supernatants using Myc-capture gremlin ELISAs following parallel transfections with the above constructs (as will be discussed in Chapter 4). Therefore, this study takes a neutral standpoint on the beneficial use of SAP in molecular cloning.

Chapter 4: Mapping of the heparin binding site on wildtype gremlin-Myc

4.1 Introduction

In the previous chapter, the cloning of six C-Myc-tagged mutant gremlin constructs, MGRs 1 – 6, alongside the C-Myc-tagged wildtype was discussed. Both MGRs 1 and 2 incorporated individual basic residue substitutions of basic clusters II and III, respectively. MGRs 3 – 6 were hybrid mutants of MGR1, all incorporating the MGR1 substitutions combined with partial substitutions of either basic clusters I or III. The expression of these gremlin-Myc proteins in CHO-S cells and their analysis will be discussed in this chapter. The aim was to generate functional gremlin-Myc mutants which possessed significantly reduced heparin binding activity.

The hypothesis tested herein is that postulating the existence of a specific heparin binding site on gremlin which consists largely of arginine and lysine residues. An outline of the specific objectives met in this chapter is listed as follows:

- To confirm expression of gremlin-Myc proteins in crude CHO-S cell culture supernatants.
- To compare the heparin binding capabilities of expressed gremlin-Myc against purified gremlin-His.
- To assess the heparin binding capabilities of expressed gremlin-Myc mutants against that of wildtype gremlin-Myc.
- To identify gremlin-Myc mutants with weakest heparin binding affinity for use alongside the wildtype in functional studies next.
- To investigate whether binding of all expressed gremlin-Myc proteins to heparin is specific.

4.2 Gremlin detection in crude gremlin-Myc culture supernatants

Initially detection of gremlin-Myc immunoreactivity in the expressed CHO-S cell culture supernatants was attempted using a Myc-capture gremlin ELISA (refer to Section 2.19.3). In this immunoassay, expressed gremlin proteins are captured via their C-terminal Myc tag on the surfaces of the wells of a 96-well plate coated with the 9E10 Myc capture antibody. A polyclonal biotinylated gremlin detecting antibody and streptavidin-conjugated alkaline phosphatase enzyme complete the sandwich. As such

this immunoassay confirms the co-expression of both gremlin and the C-Myc epitopes within the same protein.

In results as shown in Figure 4.1, gremlin-Myc immunoreactivity was detected at varying levels amongst the different crude gremlin-Myc culture supernatants. Wildtype gremlin-Myc and MGRs 4 – 6 displayed the highest gremlin-Myc immunoreactivities, with the gremlin-Myc immunoreactivity in MGR1 also high. Both MGRs 2 and 3 demonstrated very weak gremlin-Myc immunoreactivities although these were significantly higher than the background immunoreactivity generated by the EGFP crude culture supernatant. These very weak gremlin-Myc immunoreactivities of both MGRs 2 and 3 may have reflected underlying damage to their gremlin epitopes during their cloning, thus, though they might have been expressed at high levels, being misfolded rendered their gremlin epitopes inaccessible to the gremlin antibody. Another possible explanation could have been that both these mutant GREM1-Myc constructs are not particularly well expressed by the CHO-S cells themselves.

In Figure 4.2, the semi-quantitative nature of the Myc-capture gremlin ELISA was displayed using crude wildtype and MGRs 3, 5 and 6 culture supernatants. By comparing the slopes, both crude wildtype and MGR5 culture supernatants demonstrated the highest and approximately equal gremlin-Myc immunoreactivities. Compared to these, gremlin-Myc immunoreactivities generated in crude MGRs 3 and 6 were approximately several tens of fold lower and half fold lower, respectively (refer to Figure 4.2). These results partly correlated with those shown in Figure 4.1 in that both wildtype and MGR5 exhibited highest gremlin-Myc immunoreactivity followed by MGR6 and then MGR3. The marked difference in gremlin-Myc immunoreactivities between MGR6 and both wildtype and MGR5 was not so apparent due to saturation and flattening of the absorbance readings between 2 – 2.5 units (refer to Figure 4.1). This had been done in order to enable detection of gremlin-Myc immunoreactivity in crude MGRs 2 and 3 culture supernatants as all were immunoassayed on the same 96-well plate.

Given that the aim of this study was to compare the heparin-binding properties of the gremlin-Myc mutants to that of the wildtype, and later to compare their functional activity, it was essential to equalise their gremlin-Myc immunoreactivities beforehand. As shown in Figure 4.3, this was achieved by a dilution of their crude culture supernatants, on a trial and error basis, using the Myc-capture gremlin ELISA.

Equalisations were made against the least immunoreactive culture supernatant of either MGR2 or MGR3.

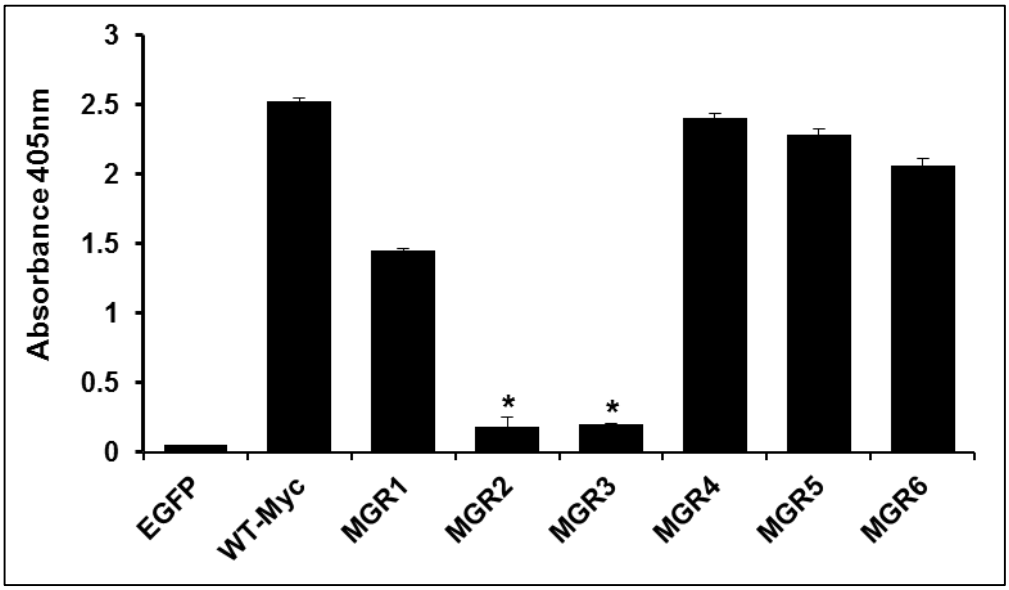

Figure 4.1: Myc-capture gremlin ELISA of crude gremlin-Myc CHO-S culture supernatants.

Gremlin-Myc immunoreactivity was detected in the crude CHO-S cell culture supernatants of expressed gremlin-Myc proteins and EGFP protein, serving as a negative control. The latter served as a negative control generating the background immunoreactivity in the assay. 100 µl/well crude supernatants were captured using 2 µg/ml 9E10 anti-Myc capture antibody and detected using a polyclonal biotinylated murine gremlin antibody at 0.8 µg/ml. Error bars represent SEM of quadruplicate absorbance readings (n=4). One-way ANOVA followed by Bonferroni post hoc test were carried out. Statistical difference compared to the mean background immunoreactivity (EGFP results); * represents $P < 0.05$.

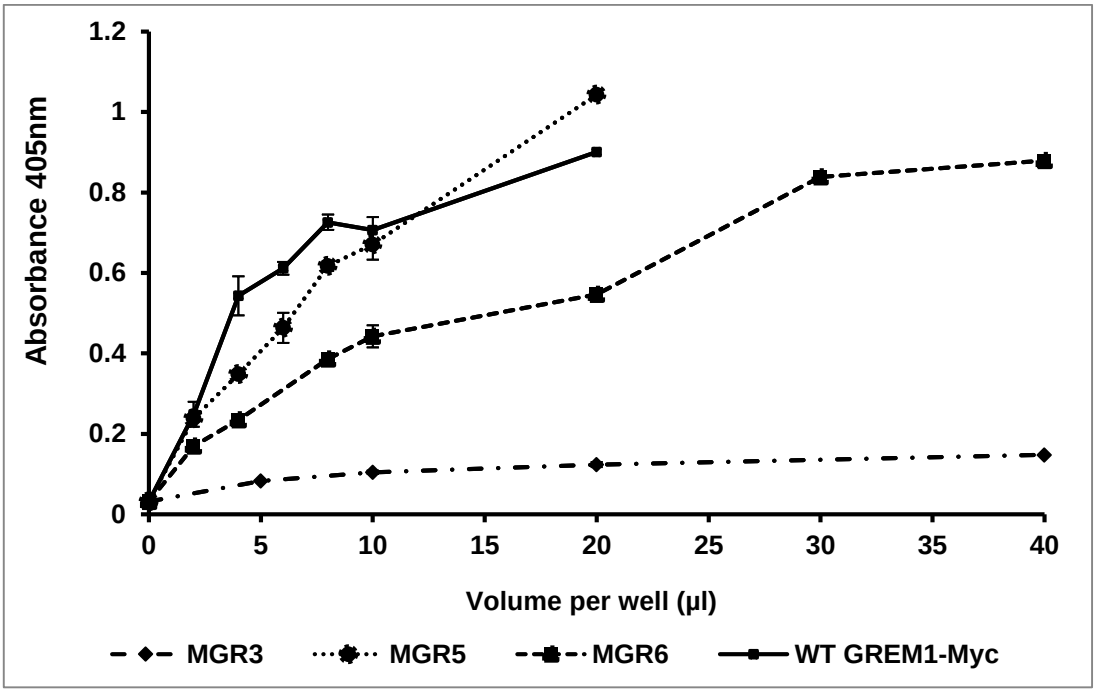

Figure 4.2: Dose response curves of expressed gremlin-Myc proteins.
The dose response curves of expressed gremlin-Myc proteins in crude CHO-S culture supernatants were generated using the Myc-capture gremlin ELISA as described in the legend of the previous figure. The indicated volumes of crude supernatants were made to 100µl with PBS-0.05% (w/v) BSA buffer prior to loading into each well. Error bars represent SEM of quadruplicate absorbance readings (n=4). WT: wildtype gremlin-Myc.

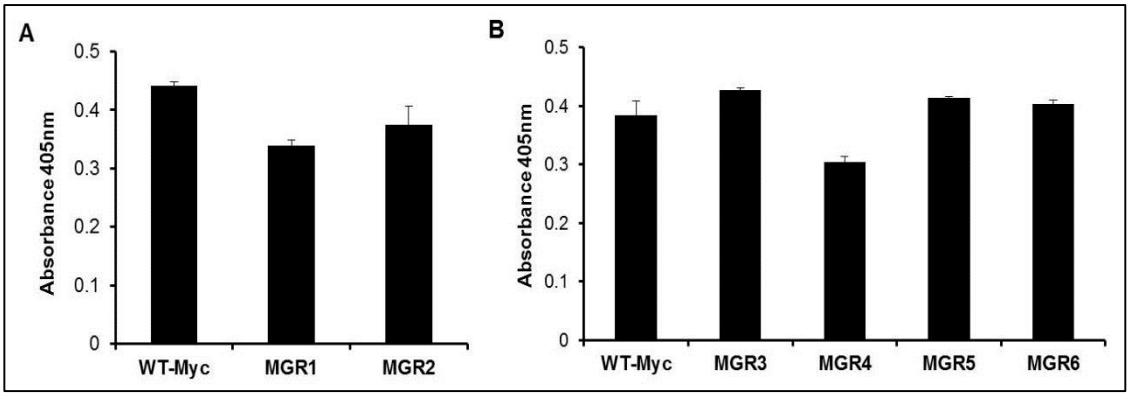

Figure 4.3: Equalising gremlin-Myc immunoreactivity using the Myc-capture gremlin ELISA.
The gremlin-Myc immunoreactivity in the crude gremlin-Myc culture supernatants were equalised by trial-and-error on a dilution basis in PBS buffer. Equalisations were made against low gremlin-Myc expressing culture supernatants MGR2 (A) and MGR3 (B). Dilutions ratios in panel A: 1/100 WT-Myc (wildtype gremlin-Myc), 1/80 MGR1, 1/2 MGR2, and in panel B: 1/40 WT-Myc, 1/2 MGR3, 1/30 MGR4, 1/50 MGR5, 1/15 MGR6. The assay was conducted using 100 µl/well diluted samples as described in the legend of Figure 4.1. Error bars represent SEM of quadruplicate absorbance readings (n=4).

Gremlin detection in most of the crude culture supernatants was also achieved by Western blotting using a polyclonal murine gremlin antibody. As shown in Figure 4.4, both Myc- and His-tagged wildtype gremlin bands shared a similar molecular weight (MW) of 25 kDa that was in line with published findings (Maciel *et al.*, 2008; Sudo *et al.*, 2004; Topol *et al.*, 2000a). The purified His-tagged wildtype gremlin protein showed two bands which differed from the expressed crude wildtype gremlin which consistently showed a single band (left panel, Figure 4.4). This may indicate that both gremlin proteins may be of different isoforms, possibly of different glycosylated forms. Strong gremlin detection was achieved for MGRs 1, 4, 5 and 6, but only faintly for MGR3. No gremlin detection was achieved for MGR2 (left panel, Figure 4.4). The gremlin-Myc proteins shown in separate panels in Figure 4.4 were expressed in different batches of crude culture supernatants both containing protease inhibitors. In the left panel, wildtype gremlin detection was weak whereas in the right panel, strong detection was achieved. It was not possible to reproduce the latter result in repeat experiments with the same batch of crude wildtype gremlin-Myc culture supernatant. Instead, in these repeat experiments, weak wildtype gremlin detection in crude culture supernatants was more consistent. As expected, no gremlin detection was achieved in the crude EGFP culture supernatants used as negative control thus establishing that the 25 kDa band is confined to crude supernatants of cultures where gremlin is anticipated (refer to Figure 4.4).

Unexpectedly, a band, 50 kDa in size, was also detected in all crude culture supernatants including the EGFP negative control (Figure 4.4). Western blot detection of this 50 kDa band was consistently achieved when using the goat polyclonal gremlin primary antibody only. Immunoblots of the same culture supernatants using only the HRP-conjugated anti-goat IgG secondary antibody in absence of the gremlin primary antibody failed to detect this 50 kDa band. This eliminated the possibility of antibody heavy chain cross-reactivity as the cause. Instead, this unknown 50 kDa protein seemed to demonstrate specific binding towards the same goat polyclonal gremlin antibody also employed in the Myc-capture gremlin ELISA. The fact that the EGFP-induced immunoreactivity in the Myc-capture ELISA was significantly lower than the gremlin-Myc-induced immunoreactivities indicated that this 50 kDa band present in all crude culture supernatants does not interfere with gremlin binding to the Myc antibody (refer to Figures 4.1). Nevertheless, it became important to verify this observation in separate tests and also investigate whether this unknown protein could bind to heparin.

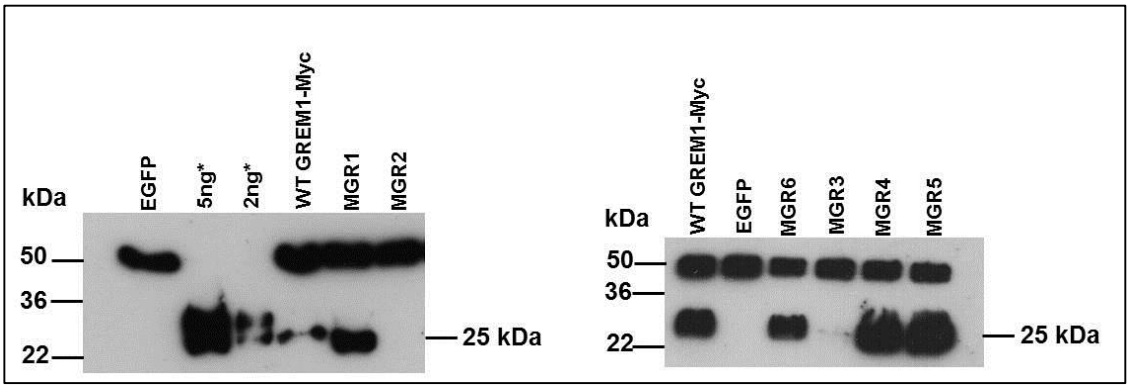

Figure 4.4: Western blot detection of gremlin in crude CHO-S culture supernatants.

Gremlin detection shown at 25 kDa was achieved using a polyclonal murine gremlin primary antibody at 0.8 µg/ml. EGFP culture supernatant served as negative control. A 50 kDa non-specific band was detected in all culture supernatants including the negative control. Asterisks denote positive controls of purified His-tagged gremlin protein.

4.3 Investigating the Myc and heparin binding properties of the 50 kDa protein

The source of the 50 kDa protein was investigated in fresh growth medium of CHO expression medium supplemented with L-glutamine, in conditioned medium from untransfected CHO-S cells and in both crude EGFP and wildtype culture supernatants. This was achieved by Western blotting as described in the previous section. As shown in Figure 4.5A, strong 50 kDa protein was only detected in culture media which had been exposed to the CHO-S cells. These included both crude EGFP and wildtype gremlin-Myc culture supernatants and conditioned medium from untransfected cells. Its detection in the latter was a significant finding as it demonstrated that the 50 kDa protein was constitutively secreted by the CHO-S cells and cannot be a product of the transfection. Detection of this unknown protein was not achieved in the fresh CHO expression medium prior to exposure to the cells. Although fresh CHO expression medium is supplied commercially as a serum-free and protein-free medium, it was important to eliminate this as a potential source of the 50 kDa protein. In these results, weak gremlin detection was achieved in crude wildtype gremlin-Myc culture supernatant thus supporting observations made in the previous section.

Next, the Myc and heparin binding properties of the 50 kDa protein were investigated using immunoprecipitation (IP) experiments of the crude wildtype gremlin-Myc culture supernatant on anti-Myc agarose and AF heparin HC650M beads, respectively. Western blotting of boiled bead supernatants using the goat polyclonal

gremlin primary antibody was then carried out next. As shown in Figure 4.5B, the 50 kDa band was not detected in the boiled bead supernatant (Track 2) following IP on anti-Myc beads. Only strong detection of gremlin at 25 kDa and weaker detection of a non-specific band at 60 kDa, were detected in this track. In this experiment, detection of the 50 kDa band was achieved only in the crude culture supernatant as expected and in the supernatant collected immediately after the bead binding step (Track 1, Figure 4.5B). Altogether, this demonstrated that the 50 kDa protein does not bind to the anti-Myc beads and most probably the 9E10 anti-Myc capture antibody used in ELISA.

The same results were also achieved following incubation with the heparin beads as shown in Figure 4.5C. Here, much stronger gremlin detection was achieved in the boiled bead supernatants (Track 2). Stronger detection of both 50 kDa and 60 kDa bands were achieved only after longer exposure of the film. Again, detection of the 50 kDa band was achieved only in the initial crude culture supernatant and in the supernatant collected immediately after the bead binding step (Track 1, Figure 4.5C). These results therefore established that the 50 kDa protein does not bind to heparin beads whereas the 25 kDa gremlin protein does therefore, the 50 kDa protein is an endogenous protein secreted by the CHO-S cells themselves and recognised by the goat polyclonal primary antibody. On another hand, the fact that the 60 kDa band was detected in boiled bead supernatants from both IP experiments, made it more likely that this band was non-specific.

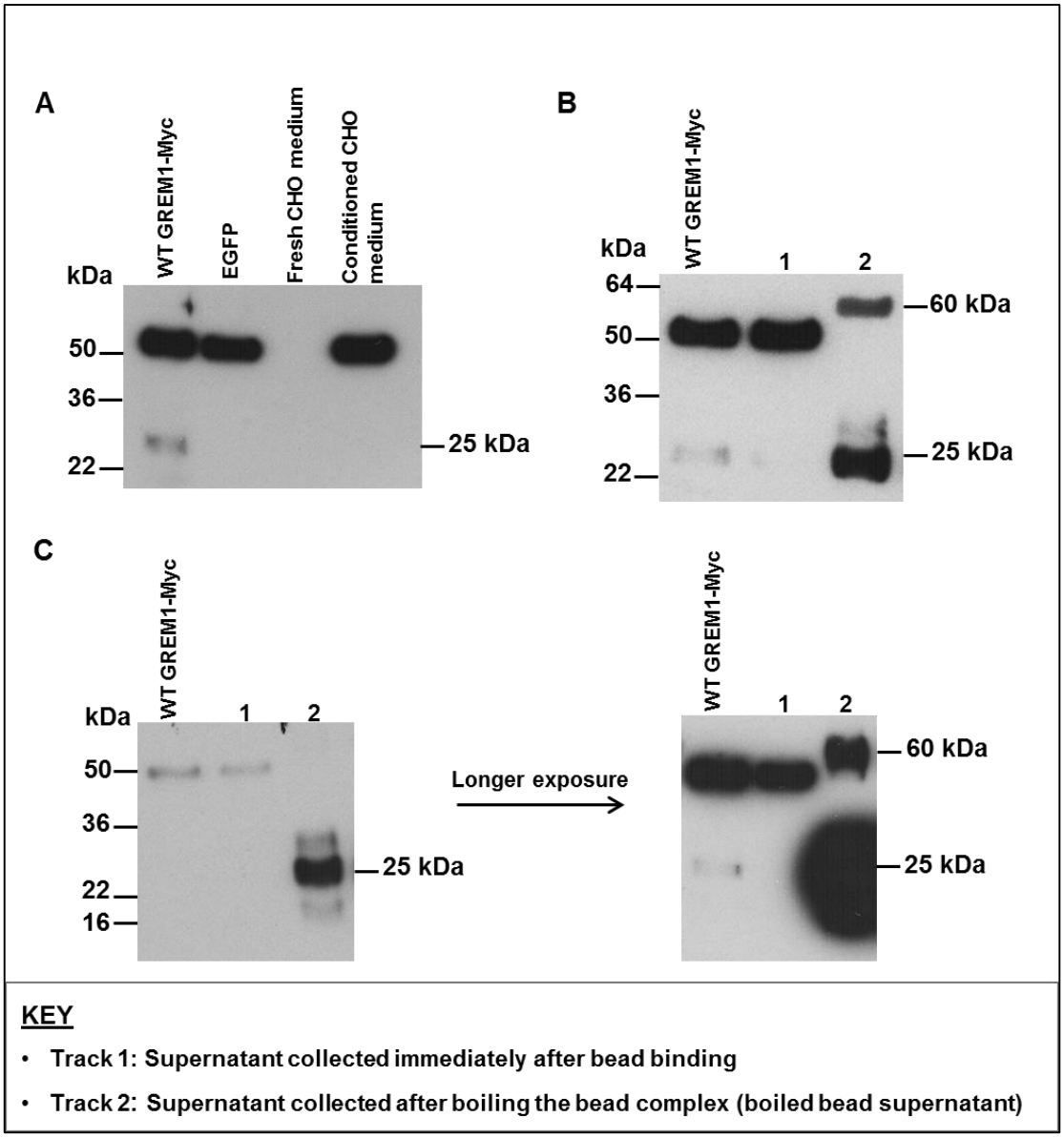

Figure 4.5: Investigating the source, Myc and heparin binding of the unknown 50 kDa protein detected in CHO-S culture supernatants.

A) Western blotting of fresh CHO growth medium and supernatants of CHO-S cell suspensions from untransfected (conditioned CHO medium) and both WT GREM1-Myc- and EGFP-transfected cells. Immunoprecipitation of wildtype (WT) GREM1-Myc crude culture supernatant on: B) rabbit polyclonal agarose anti-Myc beads and C) AF heparin HC650M beads. Gremlin was detected at 25 kDa as described in the legend of Figure 4.4.

4.4 Partial purification of wildtype gremlin-Myc

Partial purification of wildtype gremlin-Myc protein in its crude culture supernatant was achieved using ion-exchange chromatography on an SP-Sepharose column. Both pass-through and dialysed peak fractions were then analysed by silver staining on a 15% polyacrylamide gel. To investigate the long term stability of the partially-purified wildtype gremlin-Myc together with that of the 50 kDa protein,

Western blotting was carried out on the same samples which had been stored for over two weeks at -20 °C.

The wildtype gremlin-Myc elution profile on SP-Sepharose is shown in Figure 4.6A. In these analyses, the peak wildtype gremlin-Myc immunoreactivity eluted at ~ 0.45 M NaCl although gremlin-Myc immunoreactivity was distributed across three surrounding fractions (fractions at 19, 21 and 22 ml elution volumes, Figure 4.6A) that eluted at ~ 0.35, ~ 0.6 and ~ 0.65 M NaCl, respectively. The low gremlin-Myc immunoreactivity observed in the first immunoassayed fraction (fraction at 10 ml elution volume, Figure 4.6A) represented that in a 10 ml pooled pass-through fraction (refer to Figure 4.6A).

Results shown in Figure 4.6B were obtained by silver staining of the collected pooled pass-through fraction, fractions surrounding the main peak fraction alongside a sample of the crude wildtype gremlin-Myc culture supernatant. Stronger detection and a higher number of protein bands were detected in the crude wildtype gremlin-Myc culture supernatant (Track 9, Figure 4.6B) compared to any other fraction sample. This demonstrated that the collected peak fractions (Tracks 3 – 8, Figure 4.6B) including the pooled pass-through fraction (Track 2, Figure 4.6B) were at least more purified than the crude wildtype gremlin-Myc culture supernatant. It was difficult to identify the 25 kDa gremlin protein band in both the crude culture supernatant itself and in the peak fractions. In peak fractions, there were several bands present in the 25 kDa region as shown in Tracks 4 and 5 but none in Tracks 6 and 7 (refer to Figure 4.6B). The crude wildtype gremlin-Myc culture supernatant also displays several bands in this MW region. Nevertheless, the silver staining clearly indicates that large amounts of interacting proteins present in the crude culture supernatants can be removed.

Interestingly, a fairly strong band in the 50 kDa region was detected in only the pooled pass-through fractions and the crude culture supernatant itself (Tracks 2 and 9, Figure 4.6B, respectively). This was a significant finding as it indicated that the unknown 50 kDa protein characterised in the previous section, does not bind to the SP-Sepharose column, thus eluting in the pass-through fraction. This was confirmed by Western blotting detection of a 50 kDa band in the same pooled-peak fraction which had been stored at -20 °C for over two weeks as shown in Track 2, Figure 4.6C.

When the peak fractions were stored for over two weeks at -20 °C and immunoassayed under similar conditions, gremlin detection was only achieved in one out of four peak fractions (Track 6, Figure 4.6D). Intriguingly, gremlin detection was

not achieved in the peak fraction (Track 5, Figure 4.6D) which had possessed the peak gremlin-Myc immunoreactivity in the elution profile shown in Figure 4.6A. These results indicate that partially purified wildtype gremlin-Myc protein is not stable on storage. In addition to the damaging effect of freezing and thawing on this partially purified protein, it is also likely that loss of its activity over storage may be caused by it binding non-specifically to the walls of the tubes in the absence of carrier protein.

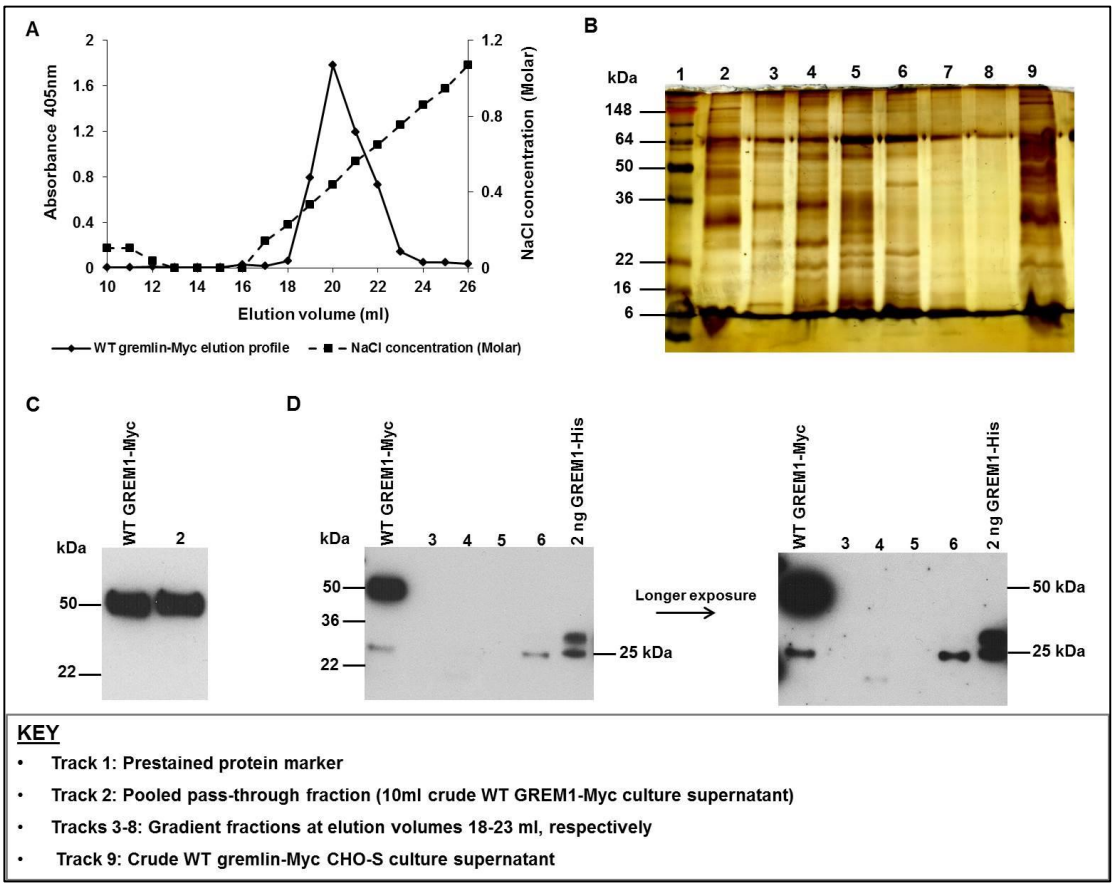

Figure 4.6: Partial purification of wildtype gremlin-Myc using SP-Sepharose and its stability.

A) Wildtype (WT) gremlin-Myc elution profile generated by Myc-capture gremlin ELISA of fraction samples collected following ion-exchange chromatography on an SP-Sepharose column. Dotted points along the WT gremlin-Myc elution profile represent mean of quadruplicate absorbance readings. The dots were larger than the error bars of SEM. B) Silver staining of a 15% (w/v) polyacrylamide gel. Western blot detection of the 50 kDa unknown protein (C) and WT gremlin-Myc protein (D), in fraction samples collected from the same SP-Sepharose column above and crude WT gremlin-Myc CHO-S culture supernatant which had been stored over two weeks at –20 °C. Purified WT gremlin-His protein used as positive control.

4.5 Synthesis of the heparin-BSA conjugate

As described in detail in Chapter 2, Section 2.20, a synthesised heparin-BSA conjugate was used as coating layer in a heparin-binding ELISA as described by Najjam *et al.* (1997). The separation of the heparin-BSA conjugate from uncoupled heparin and BSA involved use of gel filtration on a Sepharose CL 4B column. The protein elution profile shown in Figure 4.7 was obtained by determining the protein content in the eluate fractions. The fully conjugated heparin-BSA complex having the largest size was expected to lead the front end of the elution peak comprising fractions 3 to approximately fraction 17 (Figure 4.7). The major protein content peak fractions, 18 – 45, were expected to contain a relatively higher proportion of unconjugated BSA, partially conjugated heparin-BSA and probably also unconjugated heparin.

Shown in Figure 4.8 are the results obtained after Azure A and Coomassie blue R250 staining of peak fraction samples ranging from fractions 6 – 45. These stained for heparin (upper panels, Figure 4.8) and BSA (lower panels, Figure 4.8), respectively. With Azure A staining, the heparin-BSA complex, which was excluded from the gels due to its large size was detected in peak fractions 6 – 42 whereas with Coomassie staining, this was only detected in peak fractions 9 – 39 (upper and lower panels respectively, Figure 4.8). In these peak fractions containing the excluded heparin-BSA complex, free heparin was not detected in peak fraction 6 whereas low to moderate amounts were detected in peak fractions 9 – 15. Moreover, high amounts of unconjugated heparin were detected in fractions 18 – 42 (upper panels, Figure 4.8). On the other hand, unconjugated BSA was not detected in peak fractions 6 – 12 and was only present in very low and relatively higher amounts in fractions 15 – 18 and remaining peak fractions excepts fractions 36 and 42, respectively (lower panel, Figure 4.8).

For efficient coating of 96-well plates during the heparin-binding ELISA, it was important that only a very low amount of unconjugated BSA was present alongside the heparin-BSA complex in the pooled peak fraction sample. This was because a large amount of unconjugated BSA might occupy protein binding sites in the wells instead of the conjugate. On the contrary, a large amount of unconjugated heparin in the same pooled peak fraction sample would be less problematic, as this binds poorly and could be washed out easily from the wells. On this basis, only peak fractions 7 – 15 which possessed in them very low amounts of unconjugated BSA and moderately high amount of unconjugated heparin were pooled together. This pooled peak fraction

sample was then freeze-dried and reconstituted as described previously in Chapter 2, Section 2.20. Of note, a mock-treated BSA conjugate used in this study had been synthesised previously in our laboratory by a similar procedure for heparin-BSA synthesis.

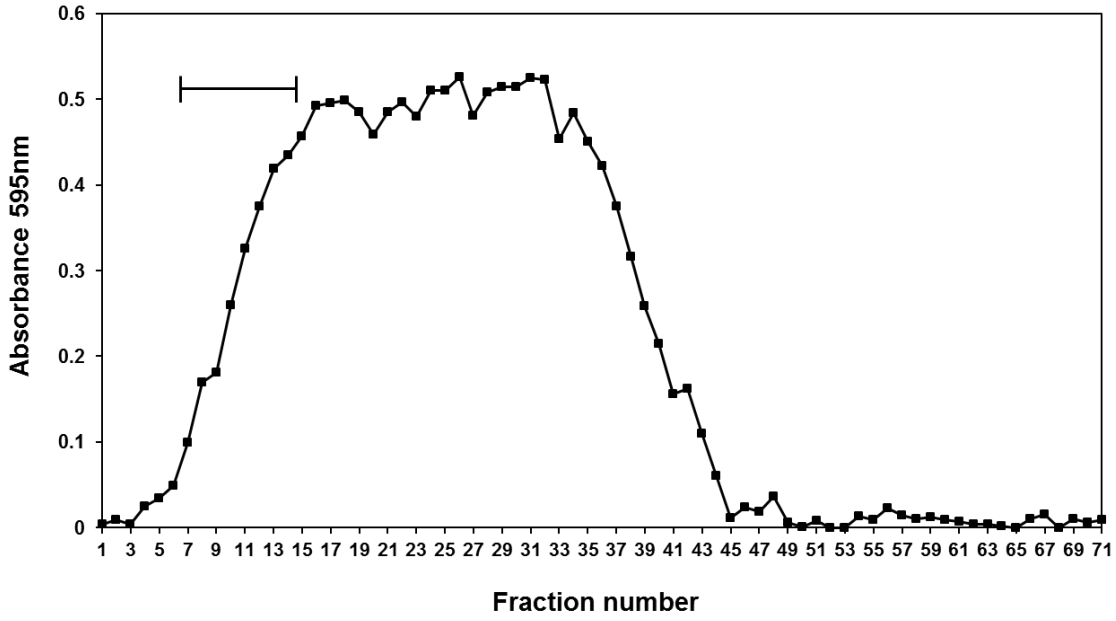

Figure 4.7: Gel filtration profile of heparin and BSA conjugates.
Size exclusion gel filtration on a Sepharose CL 4B column was carried out to separate synthesised heparin-BSA conjugates from uncoupled purified free heparin and BSA. The elution profile was generated by measuring the protein content in eluted fraction samples. The fraction designated as‘1’ starts half-way into the void volume. Horizontal bar indicates the pooled fractions from which the heparin-BSA conjugate was reconstituted.

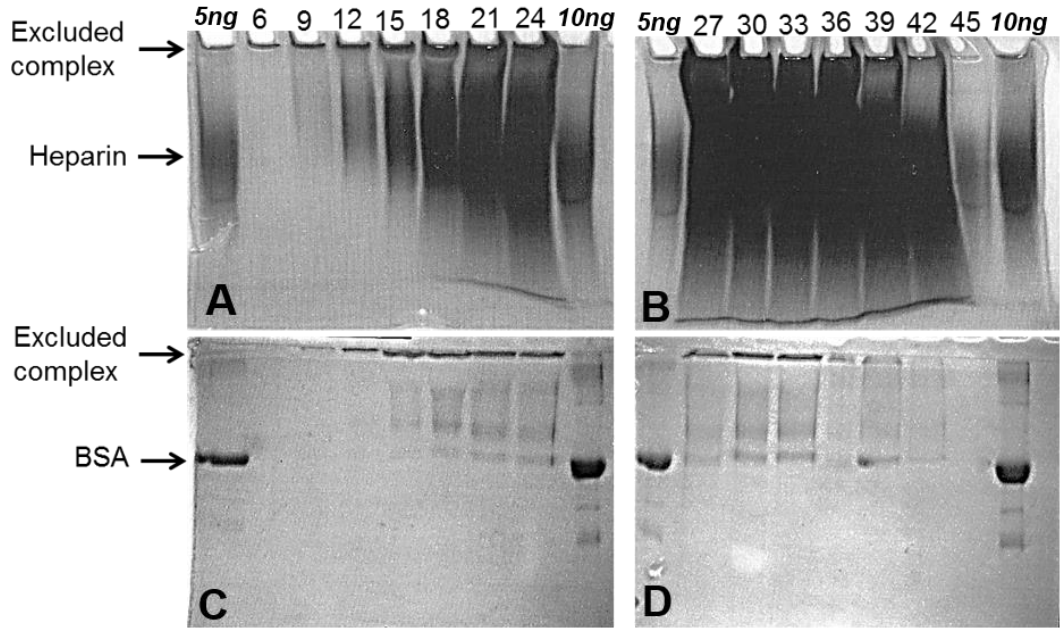

Figure 4.8: Detection of conjugated heparin-BSA complexes.
Fraction numbers are those of eluate fractions provided in Figure 4.7. These peak fractions were stained on non-reducing 10% (w/v) polyacrylamide gels with 0.08% (w/v) Azure A and 0.25% (w/v) Coomassie blue R250 for both free, partially and fully conjugated heparin (panels A and B) and BSA (panels C and D), respectively. Fully conjugated heparin-BSA is annotated as excluded complex. Known amounts of purified free heparin and BSA were included as positive controls (5 ng and 10 ng).

4.6 Assessing the heparin binding capability of expressed His- and Myc-tagged wildtype gremlin proteins using the heparin-binding ELISA

Initially, the heparin-binding ELISA was used in order to investigate whether the wildtype gremlin-Myc protein expressed in this study shared similar heparin binding capability to the purified His-tagged gremlin protein.

As shown in the Figure 4.9, when captured on a heparin-BSA layer, both purified His-tagged gremlin and the crude wildtype gremlin-Myc culture supernatant generated gremlin-Myc immunoreactivities which increased in a dose-dependent manner (solid curves, panels A and B, Figure 4.9). These immunoreactivities were significantly higher than those generated on mock-treated BSA capture layer (broken curves, panels A and B, Figure 4.9). Next, the inhibition curves of both gremlin proteins were compared. This involved the pre-incubations of a fixed dose of gremlin-His (2.5 ng) and fixed volume of crude gremlin-Myc culture supernatant (50 µl) with increasing concentrations of soluble unfractionated heparin prior to addition to the wells. As shown in Figure 4.9, both gremlin proteins displayed similar inhibition curves with the same IC_{50} value of approximately 10 µg/ml (solid curves, panels C and D,

Figure 4.9). In all these experiments, the specific binding of both gremlin proteins to heparin was demonstrated by comparative detection of markedly weaker gremlin-Myc immunoreactivities hence flattened curves from wells coated with mock-BSA (broken curves, Figure 4.9). Since this binding to the conjugate is displaceable with soluble unfractionated heparin, the binding is confirmed to depend on the heparin chains within the conjugate. This also demonstrated that the synthesis of heparin-BSA described in the previous section was successful. Collectively, these results demonstrated that both the wildtype gremlin-Myc protein expressed in this study and purified His-tagged gremlin bind to heparin with the same affinity.

Chiodelli and co-workers (2011) demonstrated high affinity binding of purified His-tagged wildtype gremlin to heparin on immobilised SPR bionsensor chips. A K_d value of 20 nM was provided for this interaction (Chiodelli *et al.*, 2011). As such, considering that both His- and Myc-tagged wildtype gremlin proteins displayed similar heparin binding affinities in the heparin-binding ELISA, it assumes that the expressed wildtype gremlin-Myc protein also shares the same published K_d value. More importantly, these results demonstrate for the first time that the binding of gremlin to heparin is independent of the His tag which might have been artificially causing binding.

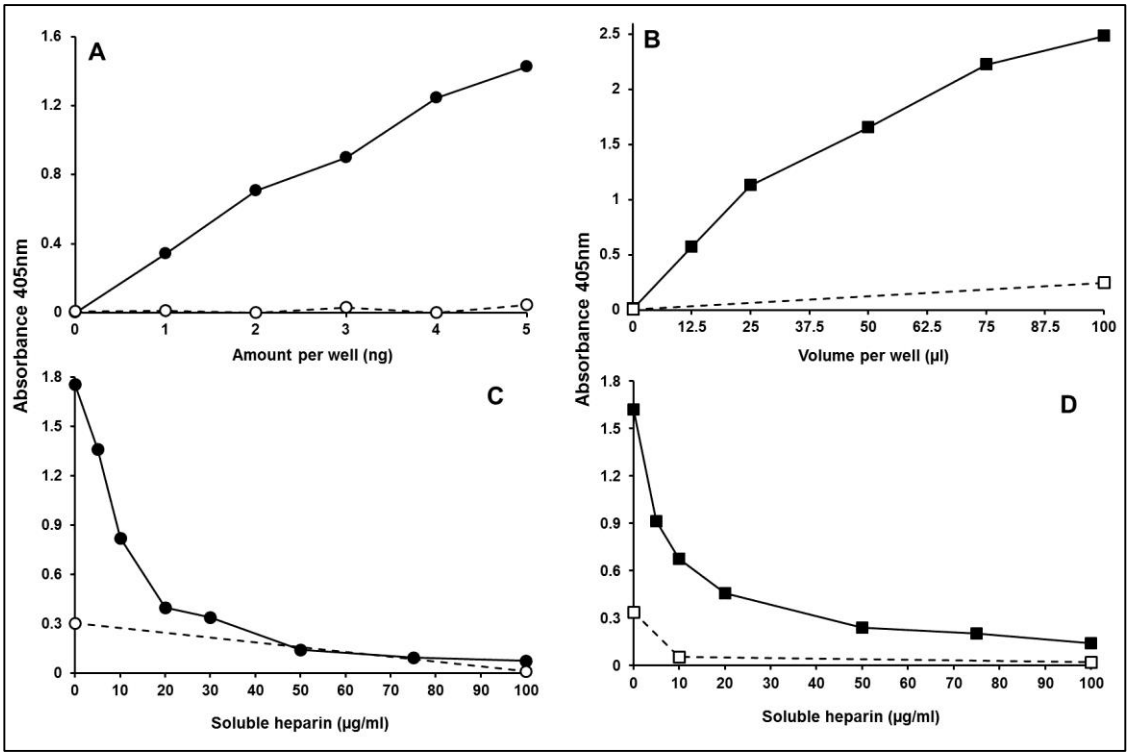

Figure 4.9: The heparin binding properties of expressed gremlin-Myc and purified gremlin-His wildtype proteins.

A and B) Dose response curves generated using the heparin-binding ELISA. C and D) Heparin-binding ELISA at fixed dose (2.5 ng/well) gremlin-His and fixed volume (50 µl/well) gremlin-Myc pre-incubated with increasing concentrations of soluble unfractionated heparin. The solid curves with filled symbols and broken curves with open symbols represent gremlin-Myc (A and C) and gremlin-His (B and D) immunoreactivities in wells captured with 10 ng heparin-BSA and 10 ng mock-treated BSA per well, respectively. All samples were prepared to a final volume of 100µl in PBS-0.05%(w/v)BSA prior to loading into wells. Gremlin detection achieved using the polyclonal biotinylated murine gremlin antibody at 0.8 µg/ml. Dots on curves are representative of quadruplicate absorbance readings (n=4). The symbols sizes were larger than error bars of SEM.

4.7 Assessing the heparin binding activity of expressed wildtype and mutant gremlin-Myc proteins using the heparin-binding ELISA

Having demonstrated that expressed crude wildtype gremlin-Myc shared similar heparin binding affinity as its His-tagged counterpart, its heparin binding affinity was then compared to those of its expressed crude mutants using the heparin-binding ELISA. As covered in the previous chapter, the gremlin-Myc mutants, MGRs 1 – 6, possessed specific mutations that would results in them possessing potentially reduced heparin binding capabilities compared to the wildtype. As earlier introduced in Chapter 1, Section 1.13, the binding interaction of most cytokine proteins with heparin/HS are believed to be largely coulombic and superficial (Esko and Selleck, 2002). Varying the

ionic strength at a constant pH, which disrupts ionic interactions, is a common method employed to measure surrogately the binding affinity between two ionically interacting proteins. In the heparin-binding ELISA, this was achieved by varying the NaCl concentration in PBS buffer in which the crude gremlin-Myc culture supernatants were prepared prior to loading into the heparin-BSA complex-coated plate wells.

First, before conducting the above experiments, it was essential to investigate whether the binding interaction of the heparin-BSA capture layer to the well surfaces was not in itself susceptible to changes in ionic strength.

As shown in Figure 4.10, high levels of wildtype gremlin-Myc immunoreactivity was generated in heparin-BSA coated wells which had been washed after overnight incubation with PBS containing either 0.7 or 1 M NaCl immediately followed with PBS alone (blue columns). These matched the level of wildtype gremlin-Myc immunoreactivity generated in similarly coated wells washed with PBS alone (0.18 M NaCl) which served as positive control (black column above red column, Figure 4.10). As expected in the negative control of wells coated with mock-BSA capture layer and washed with PBS alone, significantly lower gremlin-Myc immunoreactivity was generated compared to that in the positive control (red column, Figure 4.10). As such, these results demonstrated that washing the heparin-BSA capture layer at high NaCl salt concentrations of up to 1 M, had negligible effect on its binding to the well surfaces hence on the immunoassay itself. On the other hand, when crude wildtype gremlin-Myc culture supernatants which had been prepared at either 0.7 M or 1 M NaCl at first were added into heparin-BSA coated wells which had been washed in PBS alone, the high gremlin-Myc immunoreactivity that was generated in the positive control above was significantly reduced (black columns below blue columns, Figure 4.10). This strongly demonstrated that wildtype gremlin-Myc binding to heparin is inhibited at high ionic strength thus suggesting that their binding interaction is mainly coulombic.

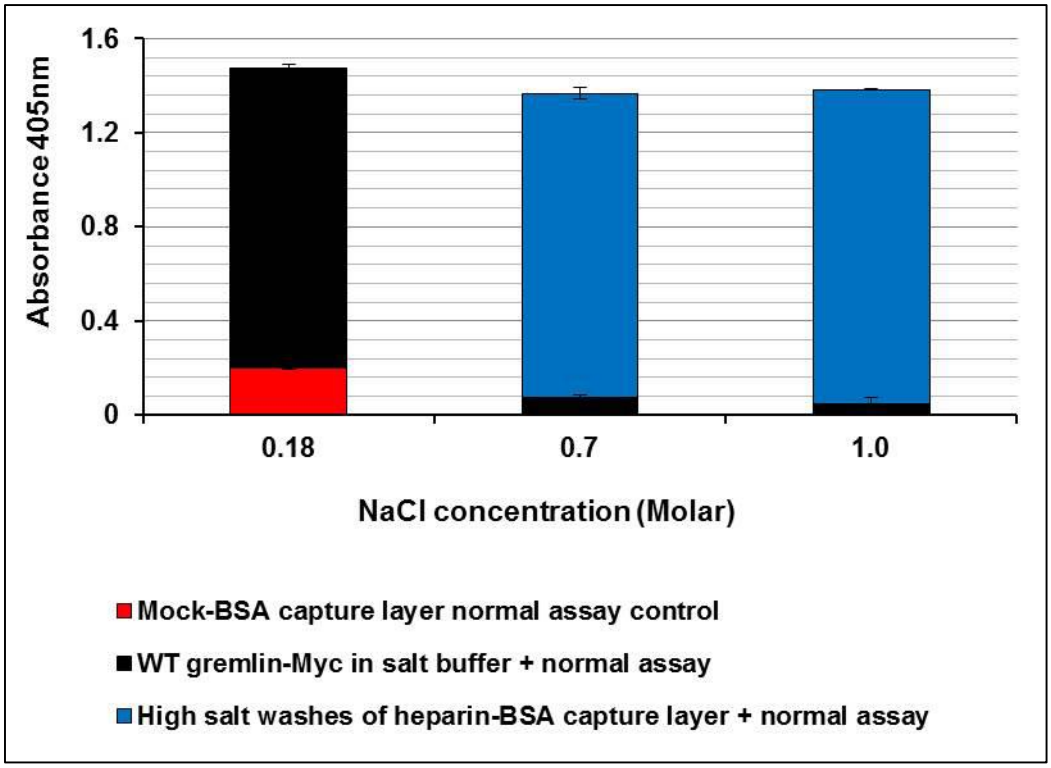

Figure 4.10: Effect of high NaCl concentrations on the heparin-BSA capture layer. Heparin-binding ELISA of crude wildtype gremlin-Myc culture supernatant capturing on 5 ng/well heparin- and mock-treated BSA using the same detection antibody as stated in the legend of Figure 4.9. The blue columns at 0.7 and 1 M NaCl represent gremlin-Myc immunoreactivities generated by washing directly heparin-BSA coated wells, several times with PBS-0.7 M NaCl and PBS-1 M NaCl buffers followed by PBS washes (0.18 M NaCl) prior to blocking and loading of the crude gremlin-Myc culture supernatant. The black columns below the blue columns represent gremlin-Myc immunoreactivity generated by heparin-BSA coated wells washed in PBS alone and blocked before loading 100 µl/well gremlin-Myc samples of the wildtype prepared at 0.7 and 1 M NaCl. The black and red columns at 0.18 M NaCl represent gremlin-Myc immunoreactivities generated by wells coated with heparin-BSA and mock-treated BSA, respectively, in which 100 µl/well crude gremlin-Myc culture supernatant was added (normal assay). Error bars represent SEM of quadruplicate absorbance readings.

Having established that the heparin-binding ELISA is suitable for use at high NaCl concentrations, the heparin binding affinities of the gremlin-Myc mutants could then be compared to that of the wildtype. The mutant gremlin-Myc culture supernatants were investigated alongside the wildtype, which served as the positive control, by preparing them at increasing NaCl concentrations ranging from 0.18 – 1 M. The preparations were then incubated in heparin-BSA-coated wells which had been washed and blocked at PBS concentration (0.18 M NaCl). The crude gremlin-Myc culture supernatants with equalised gremlin-Myc immunoreactivities were applied as described previously using the Myc-capture gremlin ELISA (refer to Section 4.2).

As shown in Figure 4.11, a shift in all mutant gremlin-Myc inhibition curves (broken curves) to the left of the wildtype gremlin-Myc inhibition curve (solid curves) was observed. By comparing the average IC_{50} values over at least four repeat experiments, the order of relative binding affinity of gremlin-Myc proteins to heparin on the heparin-BSA complex, from strongest to weakest, was obtained as follows:
[WT GREM1-Myc] > [MGR2] = [MGR3] = [MGR6]> [MGR1] = [MGR4]> [MGR5]

By all demonstrating lower IC_{50} values to that of wildtype, the gremlin-Myc mutants demonstrated weaker ionic binding to heparin. However, significant binding of both wildtype and mutant gremlin-Myc proteins to the heparin-BSA capture layer was observed at physiological NaCl concentration of 0.18 M.

For most parts, this binding order of heparin affinity derived using the heparin-binding ELISA was not as anticipated. For example, MGRs 3 and 6 demonstrated stronger ionic binding to heparin than MGR1 as shown in the binding order. Both MGRs 3 and 6 were hybrid mutants which incorporated the MGR1 substitutions of basic cluster II combined with partial substitutions in basic clusters III and I, respectively (refer to Chapter 3, Section 3.5). As such, it was expected that, these MGR1 hybrid mutants together with MGRs 4 and 5, would possess weaker ionic binding to heparin than MGR1, at least. In these inhibition ELISAs, use of diluted gremlin-Myc immunoreactivities may have affected the shape of the inhibition curves which in turn may have affected the average IC_{50} values, as such. Given the relevance of this work, it was therefore essential to verify these findings using another method that could circumvent the need for dilution.

Figure 4.11: NaCl inhibition curves of wildtype versus mutant gremlin-Myc proteins generated using the heparin-binding ELISA.

The expressed gremlin-Myc proteins at stated NaCl concentrations were prepared by diluting their crude culture supernatants in PBS buffers with high NaCl concentrations as required but maintaining the same pH 7.4. Dilution ratios were adjusted for each crude gremlin-Myc culture supernatant so as to equalise their gremlin-Myc immunoreactivities throughout. 100µl/well prepared samples were captured on 5 ng/well heparin-BSA and detected using the polyclonal biotinylated murine gremlin primary antibody at 0.8 µg/ml. After gremlin incubation, the NaCl concentration was returned to isotonic (0.18 M NaCl) by washing in PBS prior to loading the primary antibody. The gremlin-Myc immunoreactivities were normalised against those generated at 0.18 M NaCl. Each point on curves represent the average of quadruplicate absorbance readings (n=4). 100% represents the mean absorbance value at 0.18 M NaCl divided by itself and multiplied by 100, for each gremlin protein. Symbols were larger than error bars of SEM. Results are representative of four repeat experiments.

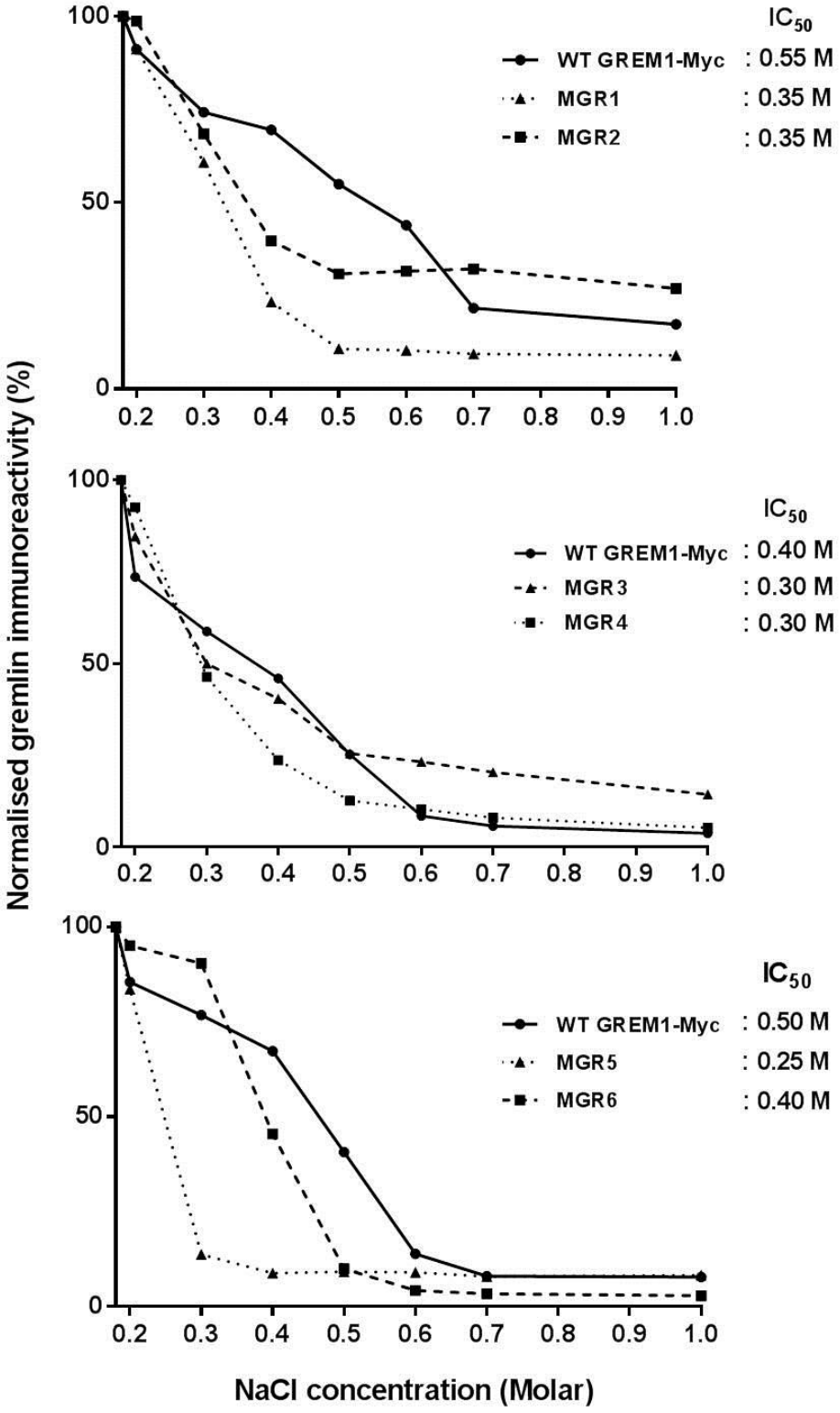
Normalised gremlin immunoreactivity (%)
100
50
0
0.2
0.3
0.4
0.5
0.6
0.7
0.8
0.9
1.0
IC50
WT GREM1-Myc : 0.55 M
MGR1 : 0.35 M
MGR2 : 0.35 M
IC50
WT GREM1-Myc : 0.40 M
MGR3 : 0.30 M
MGR4 : 0.30 M
IC50
WT GREM1-Myc : 0.50 M
MGR5 : 0.25 M
MGR6 : 0.40 M
NaCl concentration (Molar)

4.8 Heparin affinity chromatography

4.8.1 Assessment of the Myc-capture gremlin ELISA for heparin affinity chromatographic analyses

Heparin affinity chromatography (refer to Chapter 2, Section 2.21) was employed next, in order to verify the previous findings of the reduced heparin affinity of the mutants. Heparin affinity chromatography is the most widely used method to study affinity of the ionic basis of protein binding to polysaccharides. This method also eliminates the need to equalise the gremlin-Myc immunoreactivities by dilution of the gremlin-Myc culture supernatants prior to being compared.

Eluate fractions collected during heparin affinity chromatography will be immunoassayed using the Myc-capture gremlin ELISA. Therefore, it was important to test whether this ELISA would be affected by the elevated NaCl concentrations anticipated in the key eluate fractions. This would establish whether the use of high NaCl-containing eluates in the Myc-capture gremlin ELISA was appropriate. Of note, in this control experiment, coated wells incubated with wildtype gremlin-Myc samples prepared at elevated NaCl concentrations were returned to physiological conditions by washing in PBS buffer prior to loading with the biotinylated gremlin primary antibody. As shown in Figure 4.12, a progressive increase in levels of wildtype gremlin-Myc immunoreactivity was observed between 0.11 – 0.2 NaCl which peaked at 0.2 M NaCl. This was then followed by a progressive decrease in immunoreactivity between 0.2 – 0.6 M NaCl. These findings demonstrated that NaCl concentrations > 0.2 M NaCl interfere with Myc capture of wildtype gremlin-Myc in this ELISA. Peak gremlin-Myc immunoreactivity was demonstrated only around physiological NaCl concentration. Given that the binding interaction between the Myc antibody to the Myc epitope on gremlin is not expected to be largely coulombic, a reduction in immunoreactivity may be caused by the antibody adopting a less favourable conformation at high ionic strength. Altogether, this experiment demonstrated that reducing the NaCl concentration in gradient fractions down to 0.18 – 0.2 M NaCl was required after heparin affinity chromatographic runs before ELISA could be reliably performed.

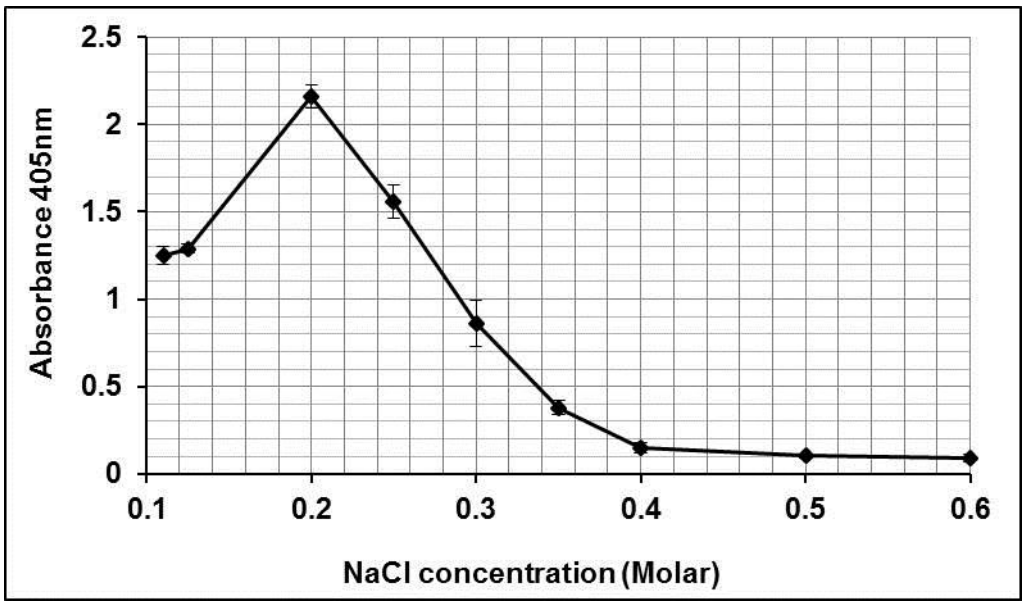

Figure 4.12: Effects of varying the ionic strength on the Myc-capture gremlin ELISA.

Myc-capture gremlin ELISA of wildtype gremlin-Myc culture supernatant; refer to legend of Figure 4.1 for detection antibody used. The gremlin-Myc samples applied (100 µl/well) were prepared at the NaCl concentrations indicated by diluting in the crude gremlin-Myc culture supernatant in the appropriate NaCl in PBS stock solution. Each point on the curve represents the average of quadruplicate absorbance readings (n=4). Error bars represent SEM.

Dialysis presented itself as a useful method for reducing the NaCl concentration in the gradient fractions without associated loss of gremlin-Myc immunoreactivity. In a further control experiment, possible loss of wildtype gremlin-Myc immunoreactivity following dialysis of the crude culture supernatant was investigated. Results, not shown, revealed only negligible loss in gremlin-Myc immunoreactivity following dialysis of the wildtype culture supernatant. Dialysis was, therefore, used preferably over dilution as standard method of reducing the NaCl concentration in gradient fractions after heparin binding chromatography.

4.8.2 Heparin affinity chromatography of wildtype gremlin-Myc protein

Heparin affinity chromatography was conducted using the crude wildtype gremlin-Myc culture supernatant, with/without the presence of protease inhibitors, in order to define its elution profile. At first, this was conducted on either the HiTrap heparin-Sepharose column or the AF heparin HC650M column. The important difference between them is that the former makes use of a larger bed volume compared to the latter performed at much smaller scale. In the HiTrap heparin-Sepharose column,

heparin from porcine intestinal mucosa is coupled to carboxylate groups of Sepharose on agarose matrix whereas in AF heparin HC650M beads, heparin of same origin, is coupled to non-functionalized bead resins instead. The specific coupling mechanisms used are not disclosed by the manufacturers.

As shown in Figures 4.13A and 4.14A, single elution peak profiles with corresponding peak wildtype gremlin-Myc immunoreactivity eluting at 0.7 M and 0.8 M NaCl, respectively were generated on both heparin columns. These were consistently generated from aliquots of the wildtype culture supernatant with no protease inhibitors that had been passed through only 2 – 3 freeze-thaw cycles and stored frozen only for about 1 - 2 weeks. Beyond these conditions, after more prolonged storage or multiple freeze-thaw cycles, double elution peak profiles were generated on both heparin columns instead, as showed in Figures 4.13B and 4.14B. On the HiTrap heparin-Sepharose column, the first and second wildtype gremlin-Myc elution peaks were observed at 0.55 M NaCl and 1 M NaCl (Figure 4.13B) and on the AF heparin HC650M column, these were observed between 0.2 – 0.4 M NaCl and between 0.6 – 0.8 M NaCl (Figure 4.14B).

As demonstrated in Figure 4.14C, when the peak fractions in Figure 4.14B were pooled and re-run separately on AF heparin, each pooled peak fraction generated a single peak elution profile. In both single elution profiles, the individual wildtype gremlin-Myc elution peaks were consistent with those on the parent elution profile shown previously in Figure 4.14B. These findings suggested that at first the CHO-S cells secrete a single unstable wildtype gremlin-Myc protein which after long-term storage with multiple freeze-thaw cycles in the absence of protease inhibitors, segregates into two forms both immunoreactive. Such segregation could occur mostly via proteolytic degradation by endogenous proteases or by aggregation. These explanations were tested by the use of protease inhibitors.

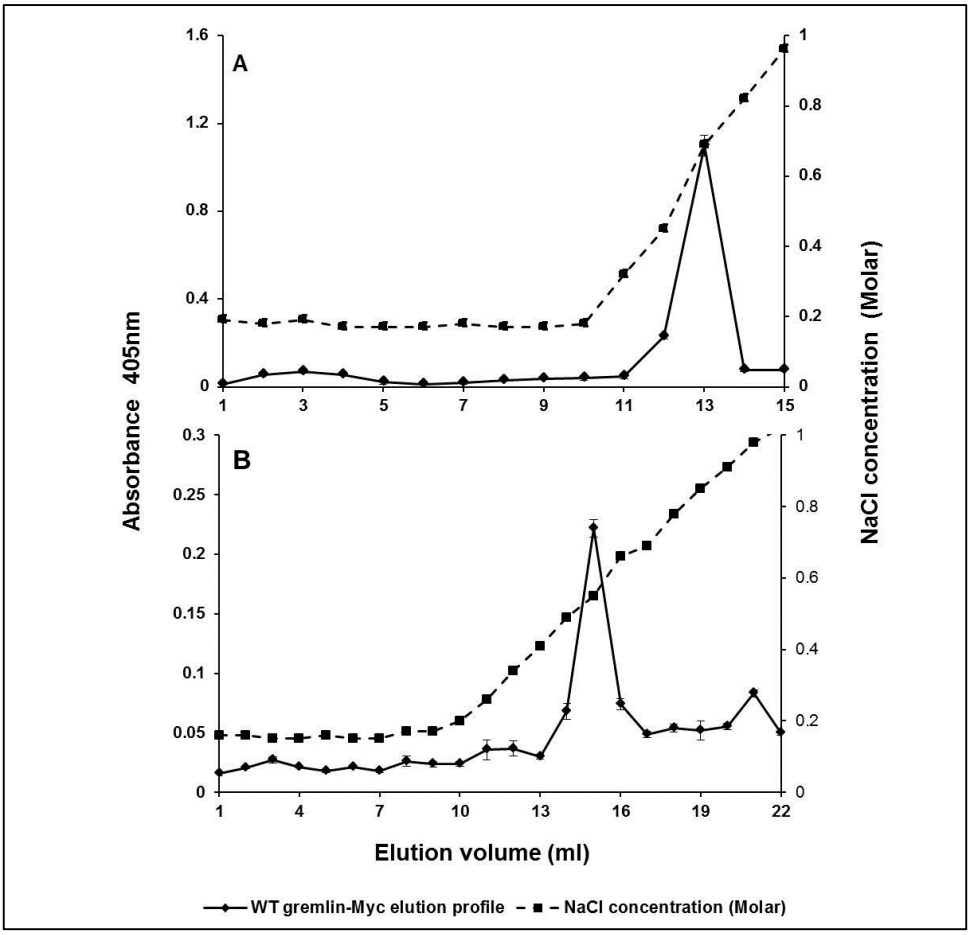

Figure 4.13: Wildtype gremlin-Myc elution profiles generated using HiTrap heparin-Sepharose columns.

Heparin affinity chromatography on HiTrap heparin-Sepharose columns was conducted using crude wildtype gremlin-Myc culture supernatant samples from the same batch freeze-thawed and/or stored: A) 2 - 3 cycles and/or stored frozen only for about 1 – 2 weeks and B) over 3 cycles and/or prolonged storage. Eluted fraction samples (100 µl/well) were assayed using the Myc-capture gremlin ELISA; refer to legend of Figure 4.1 for detection antibody used. Pass-through fractions (1-4), wash fractions (5-9) and gradient fractions (10-22) dialysed prior to assay. Each point on the curve represents the average of quadruplicate absorbance readings (n=4). Error bars represent SEM. NaCl concentrations were measured from conductivities of eluates.

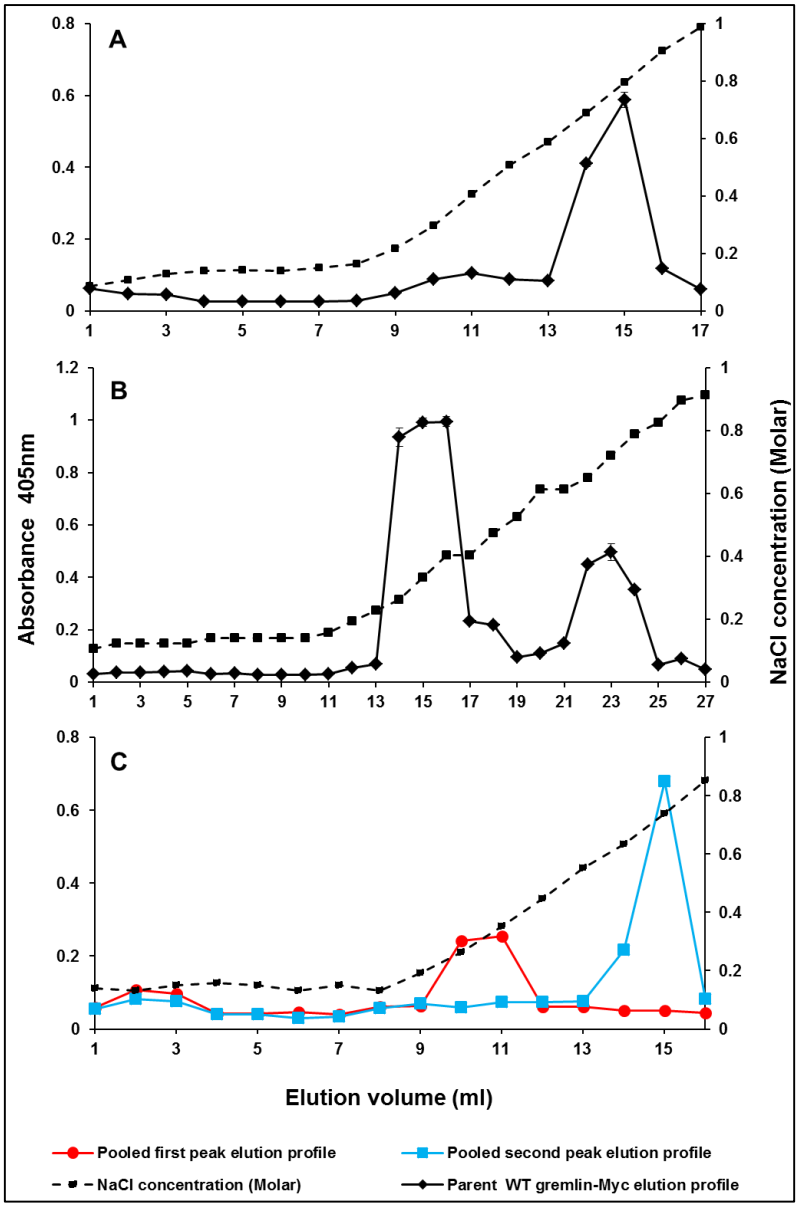

Figure 4.14: Wildtype gremlin-Myc elution profiles generated using AF heparin HC650M bead columns.

Heparin affinity chromatography on packed AF heparin HC650M bead columns was conducted using of crude wildtype gremlin-Myc culture supernatant samples from the same batch freeze-thawed and/or stored: A) 2 - 3 cycles and/or stored frozen only for about 1 – 2 weeks and B) over 3 cycles and/or prolonged storage. The peak fractions in panel B, were pooled separately and run each on a separate AF heparin HC650M column, which generated two elution profiles (C). The separate elution profiles in panel C were highlighted in red and light blue colours. Eluted fraction samples (100 µl/well) were assayed using the Myc-capture gremlin ELISA and all gradient fractions were dialysed to 0.18M NaCl in PBS buffer prior to assay; refer to the legend of Figure 4.1 for detection antibody used. Each point on the curve represents the average of quadruplicate absorbance readings (n=4). Error bars represent SEM. Pass-through fractions (Panel A: 1 - 3; Panel B:1 - 4; Panel C: 1 - 2), wash fractions (Panel A: 4 - 8, Panel B: 5 - 9; Panel C: 3 - 7) and gradient fractions (Panel A: 9 - 17; Panel B: 10 - 27; Panel C: 8 - 16). NaCl concentrations were measured from conductivities of eluates.

When the similar experiments were repeated this time using the crude wildtype culture supernatant containing protease inhibitors the results as shown in Figure 4.15 were obtained. Consistent with previous observations, a single elution peak profile with peak gremlin-Myc elution at ~ 0.8 M NaCl, was produced using 1 – 2 weeks old frozen aliquots of the wildtype supernatant which had been freeze-thawed 2 – 3 times (Figure 4.15A). Interestingly, in the presence of protease inhibitors, the same single peak elution profile was generated despite using frozen aliquots which had been exposed to conditions beyond those stated above (Figure 4.15B). However, it was observed that wildtype gremlin-Myc immunoreactivity in these peak gradient fractions was markedly lower than that normally generated in the fresher aliquot samples in Figure 4.15A. The reduced wildtype gremlin-Myc immunoreactivity was also accompanied by a decrease in the peak wildtype gremlin-Myc elution from ~ 0.8 M NaCl to ~ 0.6 M NaCl (refer to Figures 4.15 A and B, respectively). It is possible the harsh conditions would have adversely affected the structural integrity of the wildtype gremlin-Myc protein and its Myc epitope or caused its aggregation. Altogether, these results indicated that the transition from a single to double peak wildtype gremlin-Myc elution profile as was observed earlier can be prevented by the addition of protease inhibitors to this crude wildtype culture supernatant immediately after its harvesting. This suggested that by inhibiting the activities of endogenous proteases secreted by the CHO-S cells themselves, progressive proteolytic degradation of wildtype gremlin-Myc was inhibited. It is for this reason that protease inhibitors were also added to all mutant gremlin-Myc culture supernatants in this study.

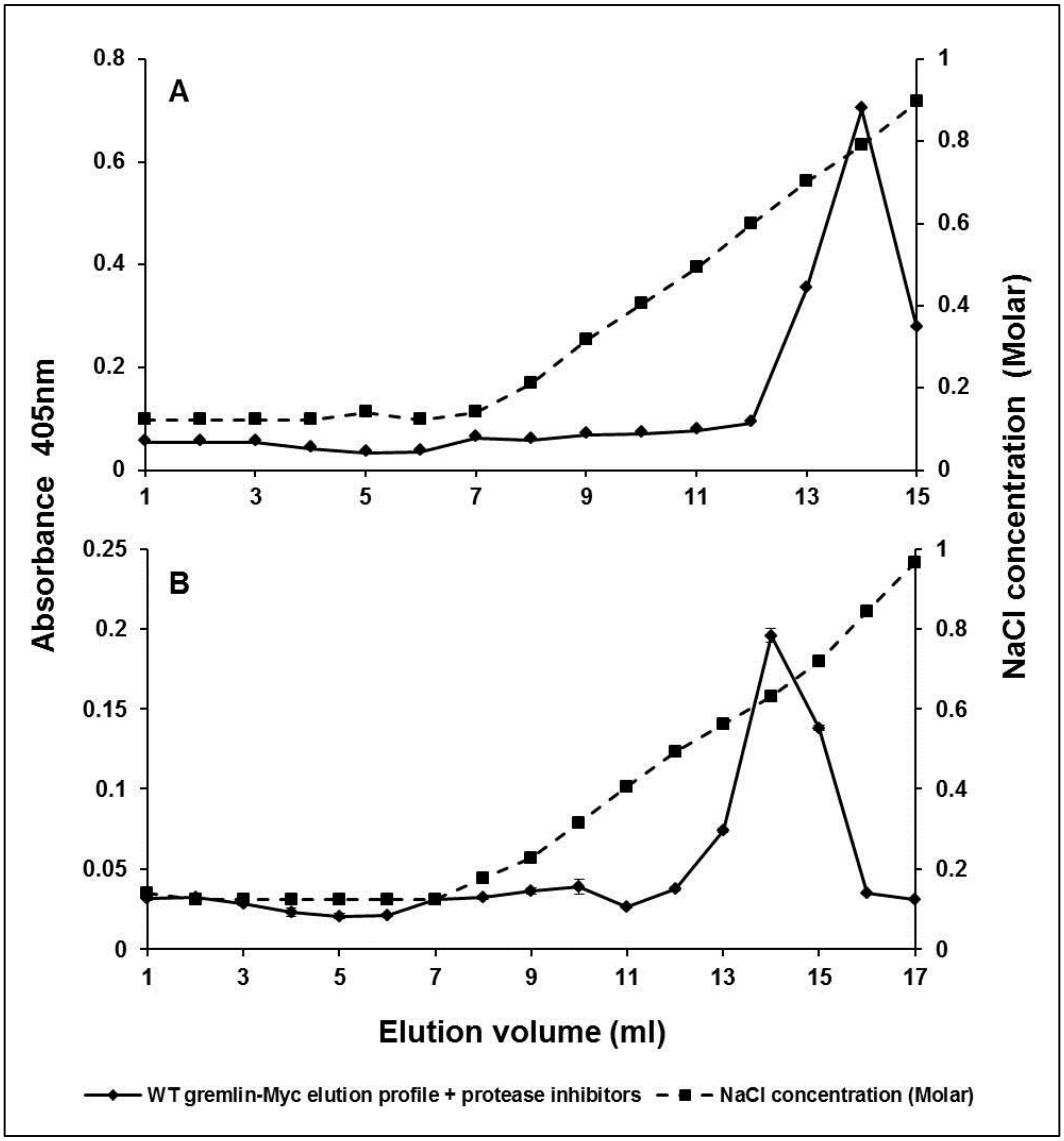

Figure 4.15: Determining the true elution profile of expressed wildtype gremlin-Myc protein.

Heparin affinity chromatography on AF heparin HC650M bead columns was conducted using crude wildtype gremlin-Myc culture supernatant samples from a batch to which protease inhibitor cocktail had been added immediately after its harvesting. Shown are elution profiles of samples freeze-thawed through A) a single cycle and B) multiple cycles. Eluted fraction samples (100 µl/well) were assayed using the Myc-capture gremlin ELISA; refer to legend of Figure 4.1 for detection antibody used. Each point on the curve represents the average of quadruplicate absorbance readings (n=4). Error bars represent SEM. Pass-through fractions (Panels A and B: 1 - 2), wash fractions (Panel A: 3 - 6, Panel B: 3 - 7) and gradient fractions (Panel A: 7 - 15; Panel B: 8 - 17). NaCl concentrations were measured from conductivities of eluates.

4.8.3 The heparin affinity chromatography of mutant gremlin-Myc proteins

The elution of profiles of MGRs 1 – 6 were compared against that of the wildtype in order to verify the previous findings obtained using the heparin-binding ELISA (refer to Section 4.7).

All mutant gremlin-Myc elution peaks shifted left from that of the wildtype gremlin-Myc elution peak at 0.8 M NaCl (Figure 4.16). These shifts have also been summarised in Table 4.1. This demonstrated that reduced binding to heparin had been achieved by targeted site-directed mutagenesis of the three basic clusters predicted to form the putative heparin/HS binding site on wildtype gremlin. By comparing the average elution peaks over three repeat experiments, the order of relative binding affinity of the gremlin-Myc proteins to heparin, from strongest to weakest, was as follows:

Wildtype GREM1-Myc > MGR1 > MGR2 = MGR4 = MGR5 ≈ MGR6 > MGR3

This binding order of the mutant gremlin-Myc proteins differs markedly from that observed using the heparin-binding ELISA (refer to Section 4.7). Here, MGR1 had the highest average elution peak amongst the mutants eluting at 0.5 M NaCl whereas MGR3 had the lowest average elution peak eluting at 0.33 M NaCl (Figure 4.16). MGRs 2, 4, 5 and 6 shared similar elution peak on average, eluting between 0.40 – 0.42 M NaCl (Figure 4.16). Unlike the heparin-binding ELISA, these findings were more consistent with the predicted contact basic residue subsititutions incorporated in each gremlin-Myc mutant. All MGR1 hybrid mutants, MGRs 3 – 6, which possessed the MGR1 substitutions of basic cluster II combined with partial substitutions in either basic cluster I or III, showed weaker binding affinities to heparin compared to that of the parent MGR1 mutant alone (also refer to Chapter 3, Section 3.5). On this note, selection of candidate gremlin-Myc mutants possesing the lowest heparin binding affinity for work in the next phase of this study, was made based on this heparin affinity chromatographic data. Therefore, MGRs 3, 5 and 6 were selected for further analyses later. By demonstrating experimentally that all gremlin-Myc mutants possessed reduced heparin binding capabilities, mapping predictions made by Rider and Mulloy (2010) using a sclerostin-based homology model of gremlin, were verified. Therefore, mapping of the heparin binding site on gremlin has been successfully achieved in this study.

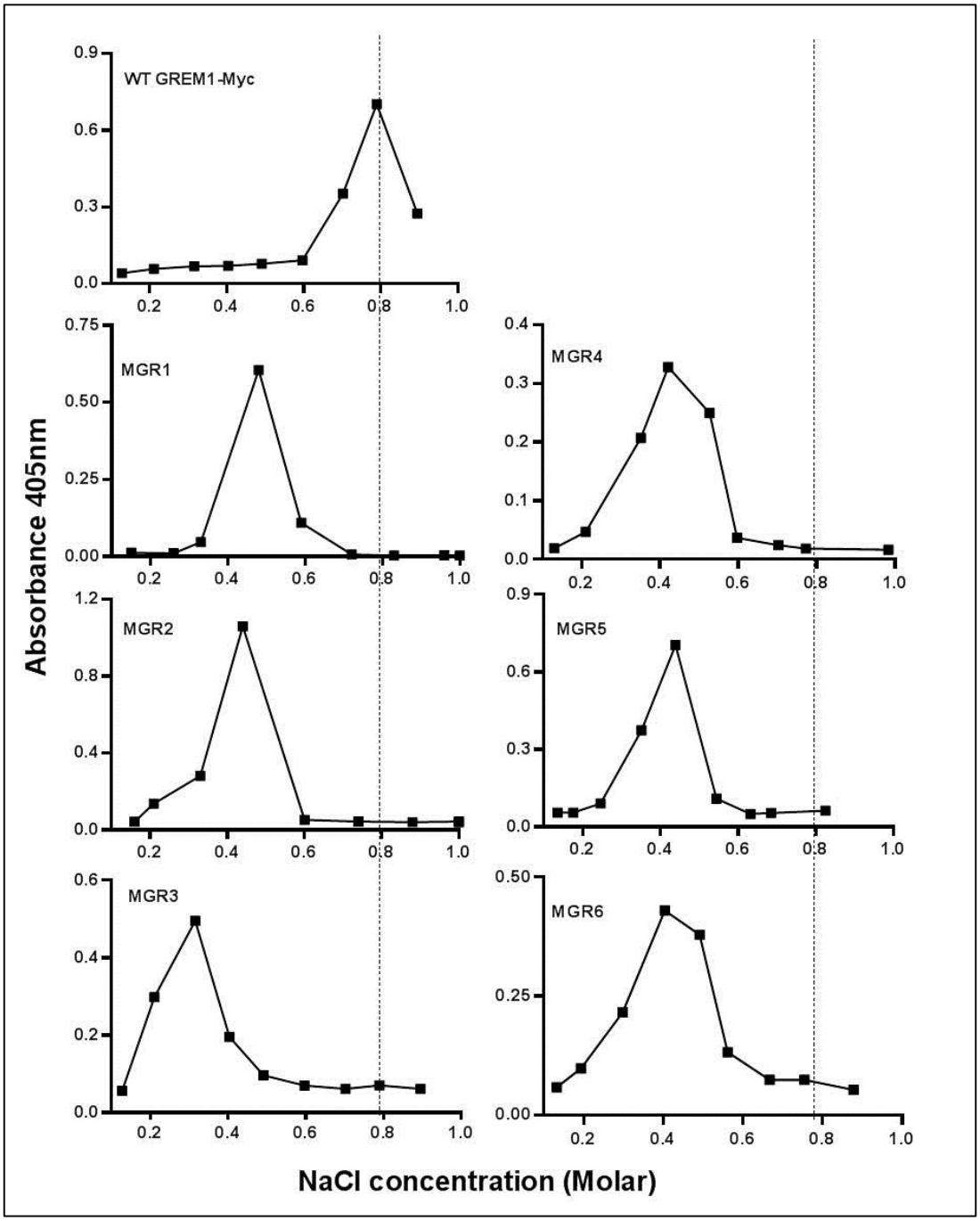

Figure 4.16: Heparin affinity chromatography of mutant gremlin-Myc proteins versus wildtype.

The gremlin-Myc elution profiles shown were generated on packed AF heparin HC650M bead columns by applying crude culture supernatants of wildtype and mutant gremlin-Myc proteins containing protease inhibitors followed by assay of eluates (peak fractions dialysed) using the Myc-capture gremlin ELISA. Refer to legend of Figure 4.1 for detection antibody used for ELISA. The first filled square on all the elution profiles represents the mean of quadruplicate absorbance readings of all pass-through and wash fractions. Vertical broken lines indicate the elution peak of wildtype gremlin-Myc protein.

4.9 SP-Sepharose ion-exchange chromatography of gremlin-Myc proteins

Next, ion-exchange chromatography of the expressed gremlin-Myc proteins was carried out on SP-Sepharose columns possessing $-CH_2CH_2CH_2SO_3^-$ side chains. This was done to investigate whether binding of gremlin-Myc proteins to heparin involved a specificity beyond simple coulombic interactions. This was conducted in a similar manner to heparin affinity chromatography described previously using the bevelled tip columns (refer to Chapter 2, Section 2.22).

As shown in Figure 4.17, wildtype gremlin-Myc eluted at 0.43 M NaCl on average compared to 0.8 M NaCl average peak elution from the AF heparin HC650M column observed in the previous section. On the SP-Sepharose column, both mutant gremlin-Myc elution peaks also shifted to the left of that of the wildtype as seen previously in their heparin affinity chromatography. However, these shifts were much more subtle than those observed using heparin columns (refer to Table 4.1). On basis of their average peak elutions over two repeat experiments, the order of relative binding affinity to SP-Sepharose, from strongest to weakest, was as follows:

$$WT \approx MGR1 \approx MGR4 > MGR2 \approx MGR5 \approx MGR6 > MGR3$$

On SP-Sepharose columns, both MGRs 1 and 4 shared similar average elution peaks with the wildtype eluting at 0.40 – 0.43 M NaCl. MGRs 2, 5 and 6 shared similar average elution peaks, all eluting at 0.33 M NaCl. MGR3 showed the weakest binding to the column eluting at 0.21 M NaCl on average. As can be seen, both the wildtype and mutant gremlin-Myc proteins eluted at lower NaCl concentrations from SP-Sepharose columns compared to their elution from the AF heparin HC650M column. Altogether, the weaker binding of these gremlin-Myc proteins to SP-Sepharose columns strongly indicated that their binding to heparin is more specific. Together, findings using both chromatographic methods demonstrate that the substituted positively charged arginine and lysine residues within predicted basic clusters contribute essentially to the putative heparin binding site on wildtype gremlin.

Gremlin-Myc mutant	Wildtype to mutant shift for heparin affinity (M)	Wildtype to mutant shift for ion exchange (M)
MGR1	0.38	0
MGR2	0.39	0.12
MGR3	0.48	0.22
MGR4	0.39	0.02
MGR5	0.39	0.14
MGR6	0.40	0.10

Table 4.1: Elution NaCl molarity shifts for heparin and ion-exchange chromatography.

The NaCl molarities shown represent the difference in average elution peaks of mutant gremlin-Myc proteins from that of the wildtype as determined from their elution profiles generated after heparin and ion-exchange chromatography on AF heparin and SP-Sepharose columns, respectively.

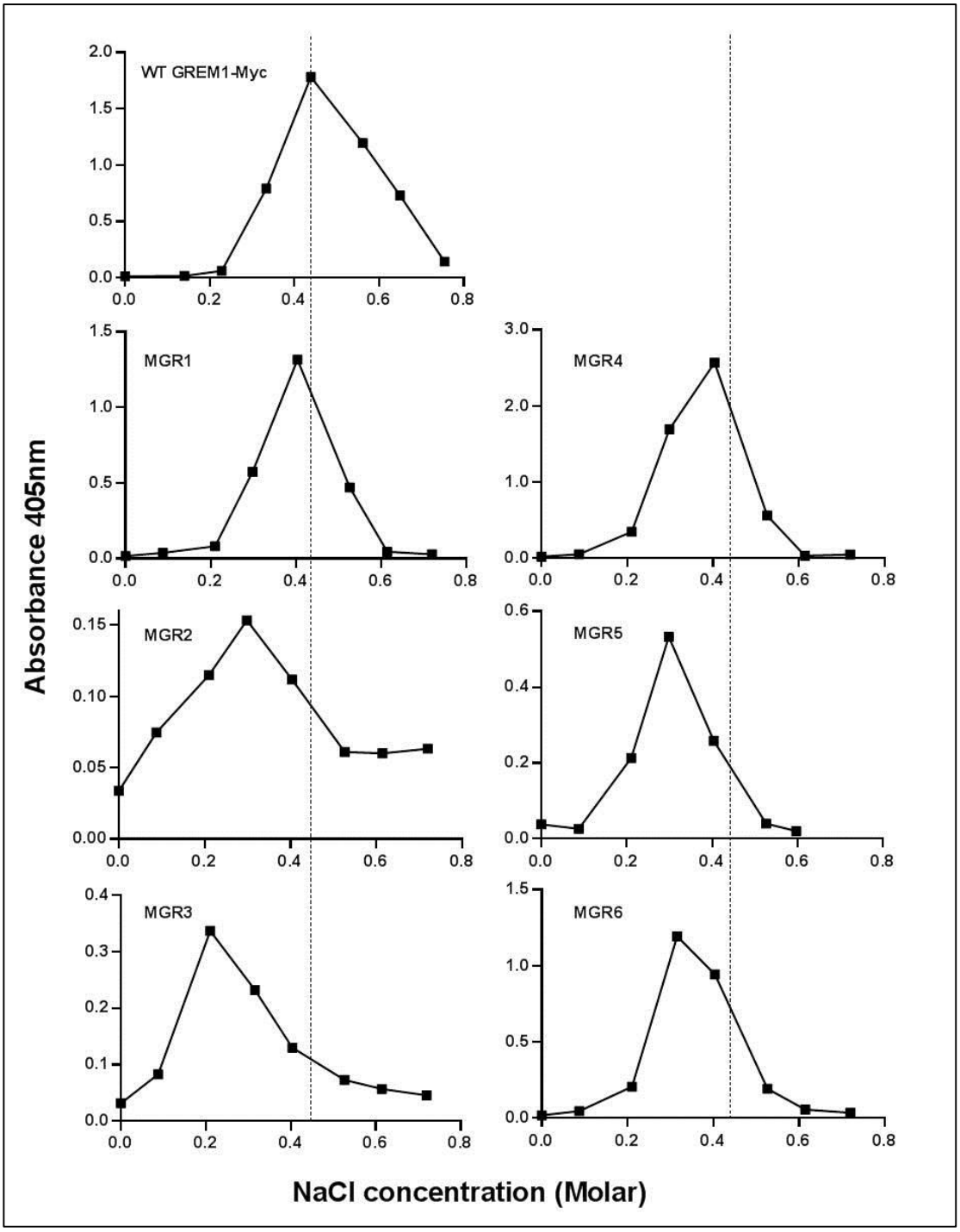

Figure 4.17: SP-Sepharose ion-exchange chromatography of mutant gremlin-Myc proteins versus wildtype.

The gremlin-Myc elution profiles shown were generated on SP-Sepharose columns by applying crude culture supernatants of wildtype gremlin-Myc and its mutant containing protease inhibitors followed by assay of eluates using the Myc-capture gremlin ELISA. Refer to the legend of Figure 4.16 for more details.

4.10 Discussion

Overall, the studies in this chapter aimed at assessing the heparin binding activities of wildtype and mutant gremlin-Myc proteins that were cloned and expressed in the previous chapter using site-directed mutagenesis. Given that such site-directed mutagenesis was based on heparin binding site mapping predictions made by Rider and Mulloy (2010), this study would also serve as an experimental verification of their predictions. All the specific objectives outlined in the introduction of this chapter were met in the study.

Gremlin-Myc detection in all expressed crude gremlin-Myc CHO-S cell culture supernatants was achieved using the Myc-capture gremlin ELISA in which their C-Myc epitope was targeted by using a 9E10 Myc capture antibody. In these crude culture supernatants, varying levels of gremlin-Myc immunoreactivity were observed; most notably, both MGRs 2 and 3 crude culture supernatants possessed the least gremlin-Myc immunoreactivities of all. By this immunoassay, it was possible to deduce conclusively that the gremlin-Myc immunoreactivities generated, was a product of the action of a single protein possessing both gremlin and the Myc epitopes. Using wildtype, MGRs 3, 5 and 6, the gremlin-Myc proteins, assessed further in the next chapter, increase in gremlin-Myc immunoreactivity correlated with increase in loading volumes of their crude culture supernatants. The wildtype and MGR5-induced slopes of gremlin-immunoreactivity were steepest and more or less equivalent, whereas that of MGR6 was about half as steep, thus indicating lower gremlin-Myc immunoreactivity of MGR6 compared to both the wildtype and MGR5. The correlation was less apparent for MGR3, as it possessed the least gremlin-Myc immunoreactivity. Altogether, this demonstrated the semi-quantitative nature of the Myc-capture gremlin ELISA which together with Western blotting, were used to estimate the yields of these gremlin-Myc proteins as discussed further in the next chapter.

The gremlin immunoreactive band, 25 kDa in size, was detected in the crude gremlin-Myc culture supernatants by Western blotting using the same non-biotinylated gremlin detection antibody used in the Myc-capture gremlin ELISA. On one occasion, strong detection was achieved for MGRs 1, 4, 5 and 6 whereas only weak detection was achieved for MGR3 and no detection at all for MGR2. Both weak and strong detection of wildtype gremlin-Myc was achieved using two different batches of its crude culture supernatants. In repeat experiments, weak detections of the wildtype, MGRs 3 and 6 were more consistent even with the presence of protease inhibitors in their crude

culture supernatants during harvesting. On some attempts, MGR5 detection was also weak. According to the Myc-capture gremlin ELISA, weak detection of both MGRs 2 and 3 was also the case, thus it may be concluded that their crude culture supernatants possessed the lowest gremlin-Myc immunoreactivities. It is possible that a major gremlin epitope could have been damaged during their constructions, or that the CHO-S cells themselves could not overexpress both constructs particularly well. On the other hand, weak detections of wildtype and other highly expressed gremlin-Myc mutants may have indicated progressive loss in their activity over prolonged storage and/or repeated freeze-thaw cycles. Nonetheless, detection of a 25 kDa band that matched the size of the purified gremlin-His protein, demonstrated that mutant gremlin proteins with conserved sizes to the wildtype has been successfully cloned and expressed. This observed MW of gremlin was observed previously by Topol *et al.* (2000a) and Sudo *et al.* (2004) in its glycosylated form. Findings in this current study that the commercially purified gremlin-His was consistently detected as two bands, in contrast to the single wildtype gremlin-Myc band, all in the 25 kDa region, indicates gremlin proteins of different isoforms, most likely of different glycosylated forms.

Gremlin detection in all crude culture supernatants including that of the EGFP negative control was accompanied by the detection of a 50 kDa band of an unknown protein. This seemed to bind specifically to the polyclonal gremlin detection antibody used, as use of the secondary antibody alone failed to detect it. It was identified that this unknown protein is an endogenous product of the CHO-S cells themselves, as it was absent in fresh CHO growth medium not exposed to the cells and present in CHO conditioned medium from both transfected and untransfected cells. It was also investigated whether this unknown 50 kDa protein could bind specifically to either Myc antibody or to heparin. IP experiments of crude wildtype gremlin supernatant on either polyclonal anti-Myc agarose beads or AF heparin HC650M beads demonstrated that this unknown protein does not bind to either the Myc antibodies or heparin beads and, therefore, does not interfere with this study. It is important to note that such artefact secretion by mammalian cells is not atypical. Topol *et al. (*2000a) also observed a 50 kDa band in Western blotting detection of gremlin overexpressed in COS-7 mammalian cells in spite of using a polyclonal gremlin detection antibody from rabbit instead of goat origins. In this current study, partial purification of wildtype gremlin-Myc from its crude culture supernatant containing other endogenous proteins, including the 50 kDa protein, was achieved by ion-exchange chromatography on an SP-

Sepharose column. This assessment was based on silver staining and Western blotting of the pass-through and peak gradient fractions alongside the crude wildtype. In the former, partial purification was indicated by the relatively lower amounts of proteins in these fraction eluates compared to those in the crude wildtype gremlin-Myc sample. In the latter, the 50 kDa protein was detected only in the pooled pass-through fraction eluate in which gremlin protein was absent. This, together with dialysed wildtype gremlin-Myc peak fractions had been stored frozen over two weeks prior to immunoassay using Western blotting. In most peak fraction eluates, including the major peak eluate, the gremlin immunoreactive band was not detected. This suggested that in the absence of a protein carrier, partially purified wildtype gremlin-Myc protein is unstable relative to the 50 kDa protein.

Next, a heparin-BSA conjugate complex was prepared in this study as described previously by Najjam *et al.* (1997) for use as capture layer in the heparin-binding ELISA. Using the ELISA, it was observed that both Myc- and His-tagged wildtype gremlin proteins shared the same heparin binding properties. This was demonstrated by both sharing similar dose response curves and soluble unfractionated heparin inhibition curves. In the latter, both proteins exhibited the same IC_{50} value of 10 µg/ml. Chiodelli *et al.* (2011) using SPR experiments demonstrated strong binding of His-tagged wildtype gremlin to immobilised heparin on biosensor chips quoting a K_d value of 20 nM. Given that both Myc- and His-tagged gremlin proteins shared similar IC_{50} values, it would be fair to conclude that Myc-tagged gremlin, expressed in this study, would also bind to heparin with similar affinity. This was also an interesting finding as it demonstrated for the first time that neither Myc nor His tags interfere with heparin binding of wildtype gremlin. This however does not challenge the earlier raised concern on the use of this long (10X) polybasic His tag in binding studies with heparin. Findings by Lacy and Sanderson (2002) demonstrated that presence of a 6XHis tag on the recombinant Sp17 protein, expressed on acrosome-reacted sperm, dramatically increased binding of the protein to HS on cell surfaces of myeloma ARP-1 cells by about 7-fold compared to a 2-fold increase in that of the untagged protein. Moreover, a marked increase in 6XHis-Sp17-induced HS-mediated ARP-1 cell-cell adhesion was observed relative to that induced by the untagged Sp17 protein. The significant decreases in cell surface-bound Sp17 and Sp17-induced cell aggregation in heparitinase-treated ARP-1 cells demonstrate that these are HS-mediated effects. In a different study by Alfano *et al.* (2007), heparin binding of recombinant soluble His-

tagged GDNF family receptor α 1 (GFRα1)-Fc but not of Sf9-expressed FLAG-tagged-GFRα1 was demonstrated using the heparin-binding ELISA. Because binding of both GFRα1 and Fc to heparin are unlikely, it is possible that the polybasic His tag sequence may have introduced an artefactual heparin-binding site.

Next, reduced binding to heparin was demonstrated in all gremlin-Myc mutants, MGRs 1 – 6, using both the heparin-binding ELISA and heparin affinity chromatography. In the former, all their inhibition curves were displaced below that of the wildtype hence their lower IC_{50} values. In the latter, marked shifts in their elution peaks left to that of the wildtype hence their lower major peak-eluting NaCl molarity, were observed. Although marked reduction in heparin binding was exhibited by the gremlin-Myc mutants, complete depletion of their heparin binding was not achieved. This was as shown by their capabilities to bind both heparin-BSA and the AF heparin HC650M column at 0.18 M NaCl and pH of 7.4. This rather indicated that complete depletion of heparin binding of wildtype gremlin may require the total combined substitutions of all its predicted contact basic clusters I – III. This thinking is supported by findings that most gremlin-Myc mutants possessing combined substitutions of basic clusters demonstrated more reduced binding to heparin than mutants with substitutions of a single basic cluster. For example, on the AF heparin column, MGR1 hybrid mutants, MGRs 3 – 6, all demonstrated lower elution peaks than that of MGR1 itself. These hybrid mutants all incorporated the MGR1 substitutions of basic cluster II combined with partial substitutions of either basic cluster I or III (refer to Chapter 3, Section 3.5). Nonetheless, the aim of cloning and expressing gremlin-Myc mutants possessing reduced binding to heparin was achieved in this study. Also, given that site-directed mutagenesis was based on mapping predictions made by Rider and Mulloy (2010), these findings also served as an experimental validation to their findings. Ultimately, mapping of the putative heparin/HS binding site of wildtype gremlin was achieved in this study.

Given that all six gremlin-Myc mutants expressed in this study demonstrated reduced binding to heparin, it was, therefore, important to select a few that possessed the weakest binding affinity to heparin. These candidate gremlin-Myc mutants could then be used alongside the wildtype when assessing further its functional activity as will be covered in the next chapter. In this study, this was made difficult, as the inhibition heparin-binding ELISA and heparin affinity chromatography gave different order of their relative binding affinities. As discussed earlier, it is believed that one

cause might be the large dilutions of the crude gremlin-Myc culture supernatants effectuated in order to equalise their gremlin-Myc immunoreactivities prior to being compared on the inhibition heparin-binding ELISA. Such large dilutions of gremlin-Myc immunoreactivity may have changed the shape of their inhibition curves thus also altering their IC_{50} values. The heparin affinity chromatography circumvented the need of dilutions prior to using the crude culture supernatants and also enabled high loading to be made onto the heparin column for lowly expressed mutants such as MGRs 2 and 3. Moreover, the order of heparin binding affinity obtained in this method was more consistent with the incorporated substitutions in each gremlin-Myc. Using the heparin-binding ELISA, binding of gremlin-Myc to the heparin-BSA capture layer was demonstrated to be inhibited by increase in ionic strength, which demonstrated that their binding interaction is mainly coulombic. Therefore, it was expected that the degree of gremlin-Myc mutants binding to heparin would correlate with the number of contact arginine and lysine residues which were substituted during site-directed mutagenesis. As was exemplified above, the findings by heparin affinity chromatography that all MGR1 hybrid mutants, MGRs 3 – 6, possessed lower affinity to heparin than MGR1 itself, was consistent with their incorporated substitutions. On this basis, MGRs 3, 5 and 6 were selected as those gremlin-Myc mutants possessing the least binding to heparin.

Lastly, all gremlin-Myc mutants including the wildtype demonstrated weaker binding to SP-Sepharose columns, which served as a simple cationic exchanger in ion-exchange chromatography. Although the same shift patterns in elution peaks as those observed using heparin affinity chromatography were also observed in these experiments, these were comparatively much more subtle. As such, these findings strongly suggest that binding of gremlin to heparin is more specific than binding to SP-Sepharose matrices. Together, these verified the hypothesis that gremlin harbours a specific heparin binding site which constitutes largely of arginine and lysine residues.

CHAPTER 5: Investigating the BMP antagonist activity of wildtype gremlin-Myc against its mutants

5.1 Introduction

In the previous chapter, experimental evidence was produced in favour of a proposed specific heparin binding site on gremlin. It was also demonstrated that gremlin binds to heparin mainly via ionic interactions. Therefore, this leads to the further hypothesis that gremlin binding to heparin/HS occurs at a specific binding site on gremlin that is physically distinct and independent of its BMP binding site. This raises the important question on whether the low heparin binding gremlin-Myc mutants retain BMP binding.

To fully verify this new hypothesis, the BMP binding capabilities of wildtype gremlin-Myc alongside the three lowest heparin-binding mutants, MGRs 3, 5 and 6, will be studied. These will be investigated using both immunoprecipitation experiments and a novel Myc-capture GREM1/BMP-4 double sandwich ELISA. This will also be tested in functional assays established in C2C12 myoblastic cell cultures that in addition, will determine whether or not these expressed gremlin-Myc proteins, are functionally active. This will be indicated by their activities in antagonising BMP signalling. In the case of the mutants this will be interesting given their reduced affinity to heparin. In this chapter a further hypothesis that heparin potentiates gremlin binding interaction with its BMP ligands will also be tested using the double sandwich ELISA.

An outline of the specific objectives to be met in this chapter is as follows;

- To assess the BMPs -4/-7 binding capabilities of expressed wildtype gremlin-Myc and its mutant proteins by establishing suitable immunoassays.

- To investigate the effect of heparin on gremlin-Myc interaction with BMPs -4/-7 in immunoassay.

- To establish reliable cellular assays in C2C12 myoblastic cell cultures in order to assess the functional activity of expressed wildtype gremlin-Myc and its mutants.

5.2 Assessing the BMP-4 binding capability of wildtype gremlin-Myc and its mutants by immunoprecipitation (IP)

5.2.1 IP of gremlin-Myc proteins on anti-C-Myc agarose beads

In order to assess biochemically whether the mutagenized Myc-tagged gremlin proteins maintain their natural abilities to bind directly to their BMP ligands, a series of co-IP experiments were carried out. Initially, IP experiments were conducted on rabbit polyclonal anti-C-Myc beads using only the crude culture supernatants of wildtype gremlin-Myc and its low heparin-binding mutants, MGRs 3, 5 and 6. This was done in order to achieve satisfactory loading and recovery of each of these gremlin-Myc proteins from the beads. Results are as shown Figure 5.1.

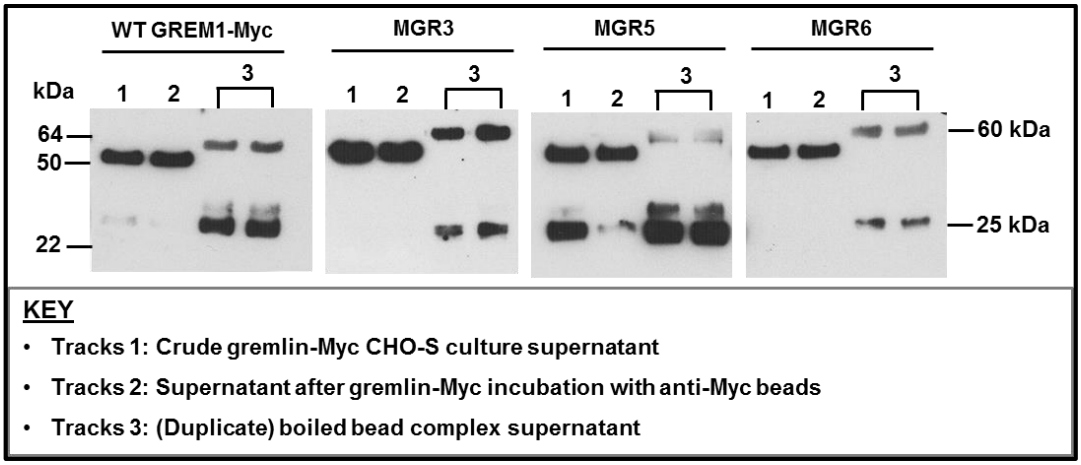

Figure 5.1: Immunoprecipitation (IP) of expressed gremlin-Myc proteins.
IP experiments were conducted using optimized loadings of crude CHO-S culture supernatants of WT gremlin-Myc (1 ml) and its low heparin binding mutants, MGR3 (2ml), MGR5 (1 ml) and MGR6 (1.5ml) on polyclonal rabbit anti-C-Myc agarose beads (50 – 100 µl). Gremlin detection as a 25 kDa band was achieved by Western blotting using a polyclonal gremlin detection antibody. Non-specific bands were also observed at 50 and 60 kDa.

By loading the anti-C-Myc beads with different volumes of crude gremlin-Myc culture supernatants, satisfactory recovery of each expressed gremlin-Myc protein was achieved (Figure 5.1). The satisfactory loading volumes of crude gremlin-Myc culture supernatants required in this work, correlated directly with the levels of gremlin-Myc immunoreactivity detected earlier using the Myc-capture gremlin ELISA (refer to Figure 4.2, Chapter 4). Wildtype and MGR5 crude culture supernatants (1 ml) possessed the highest gremlin-Myc immunoreactivity and therefore the least loading

volumes of 1 ml. Crude MGR6 culture supernatant possessed the next highest gremlin-Myc immunoreactivity hence the second least loading volume of 1.5 ml. Crude MGR3 culture supernatant possessed the least gremlin-Myc immunoreactivity requiring the highest loading volume of 2 ml. In addition, a prolonged incubation period of 48 h of this last culture supernatant with the anti-C-Myc beads was required compared to only 24 h for all others. As shown in Figure 5.1 (Tracks 1), detection of the 25 kDa gremlin band in each crude supernatant was attempted prior to loading onto the beads. Strong gremlin detection was achieved for MGR5 only, weak detection for the wildtype and no detection for both MGR3 and MGR6. Previously, strong detection was achieved for all except MGR3 (refer Figure 4.4, Chapter 4). The reason for these different outcomes was not investigated further, as a gremlin band was detected for all these gremlin-Myc proteins in their boiled bead supernatants (Figure 5.1, Track 3) which was absent or only weakly detected in supernatants collected immediately after bead binding (Figure 5.1, Tracks 2). This indicated successful binding and recovery of gremlin-Myc proteins from anti-C-Myc beads thus confirming that they indeed possess a Myc tag.

In these results, a 50 kDa band was detected in both crude gremlin-Myc culture supernatants and in supernatants collected immediately after bead binding (Figure 5.1, Tracks 1 and 2, respectively). This was not detected in all boiled bead supernatants (Figure 5.1, Tracks 3). These were in line with previous observations which had previously found and assessed this non-specific band as being incapable of binding to both anti-C-Myc and AF heparin HC650M beads (refer to Figure 4.5, Chapter 4).

Also, another non-specific band, 60 kDa, was consistently detected in all boiled bead supernatants (Figure 5.1, Tracks 3). Initially, this was thought to be heavy chain cross-reactivity between escaped fragments of the rabbit polyclonal anti-Myc beads and the rabbit anti-goat HRP-conjugated secondary antibody. However, boiling uncomplexed beads alone and probing only with this secondary antibody did not detect the 60 kDa band. A similar result was observed when the boiled supernatant of gremlin-Myc-bound bead complex was probed using only this secondary antibody. As such, the source of this non-specific band is not clearly understood.

5.2.2 IP of purified BMP-4 on gremlin-Myc-bead complexes

Next, IP experiments were conducted in which purified BMP-4 was loaded onto the gremlin-Myc-bead complex under conditions stated in the previous section. In these experiments, BMP-4 recovery in boiled bead supernatants was assessed using Western

blotting by probing blots of the same samples with both polyclonal BMP-4 and gremlin primary antibodies. The aim of these experiments was to determine the optimal conditions for BMP-4 binding onto the bead complex using wildtype gremlin-Myc first, prior to the testing of its mutants. In this work, 10 ng purified BMP-4 prepared in PBS-1% (w/v) BSA was incubated with the wildtype gremlin-Myc-bead complex under two different conditions; for 2 h at room temperature and for 16 h at 4 °C.

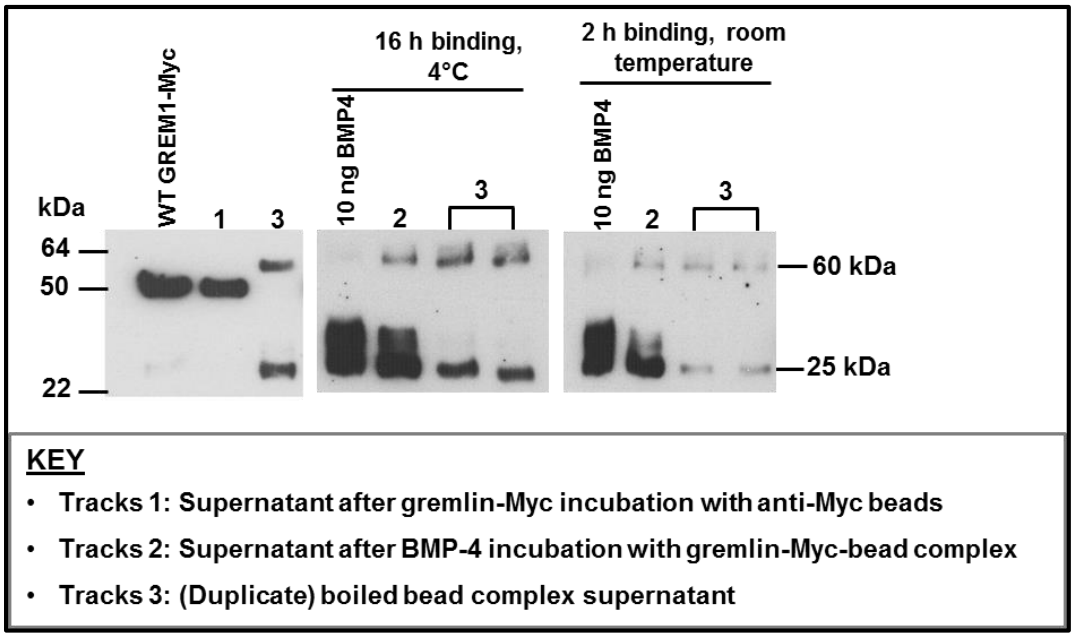

Figure 5.2: IP experiment of BMP-4 on wildtype gremlin-Myc-bead complex. 500ng/ml BMP-4 (10 ng/20µl loaded on gel) was immunoprecipitated on wildtype gremlin-Myc-bead bound complex formed as described in the previous figure legend. Gremlin detection (left panel) and BMP-4 detection (middle and right panels), both at 25 kDa, were achieved by Western blotting using polyclonal gremlin and BMP-4 detection antibodies, respectively. Non-specific bands detected at 50 and 60 kDa are detected across the gels.

As shown in Figure 5.2, optimal BMP-4 binding to the wildtype gremlin-Myc-bead complex occurred on prolonged incubation of 16 h at 4 °C compared to a shorter incubation of 2 h at room temperature. Together, both conditions, demonstrated the BMP-4 binding capability of expressed wildtype gremlin-Myc. As shown, a BMP-4 band, at the anticipated molecular weight of 25 kDa was detected in the initial preparation prior to bead binding, and also in boiled bead supernatants (Figure 5.2, Tracks 3, middle and right panels). The same band of weaker band intensity compared to the initial BMP-4 detection was observed in supernatants collected immediately after

bead binding (Figure 5.2, Tracks 2). This represented the excess unbound BMP-4 after bead binding. In the same boiled bead supernatant, a gremlin band of the correct molecular weight was also detected (Figure 5.2, Track 3, left panel). This demonstrated effective loading of beads prior to further immunoprecipitating with BMP-4 in both experiments. In this gel, a very faint gremlin band was detected in the crude wildtype gremlin-Myc culture supernatant (Figure 5.2, Track 2) which was not visible in the supernatant collected after gremlin-Myc bead binding. Stronger detection of BMP-4 bands in boiled bead supernatants collected after 16 h BMP-4 bead binding at 4 °C compared to those detected at 2 h at room temperature, confirmed optimal conditions for maximum loading of BMP-4 onto gremlin-Myc-bound beads (refer to Figure 5.2, Tracks 3, middle and right panels).

As was found and discussed in the previous section, a 60 kDa non-specific band was detected in all boiled supernatants in spite using two different probing antibodies (Figure 5.2, Tracks 3). In this case, the band was even detected in the supernatant collected after the BMP-4-gremlin bead binding step when probing with the polyclonal BMP-4 primary antibody (Figure 5.2, Tracks 2, middle and right panels). This confirmed that this band was not specific to gremlin detection using the polyclonal gremlin antibody as is the case with the 50 kDa non-specific band. As expected, the 50 kDa non-specific band was detected in the crude wildtype gremlin-Myc supernatant and only in the supernatant collected after the gremlin bead binding step as it does not bind to anti-C-Myc beads (Figure 5.2, labelled track and Track 1, respectively, left panel).

Under the same conditions, similar investigations were carried out using the low heparin-binding gremlin-Myc mutants. Results are as shown in Figure 5.3.

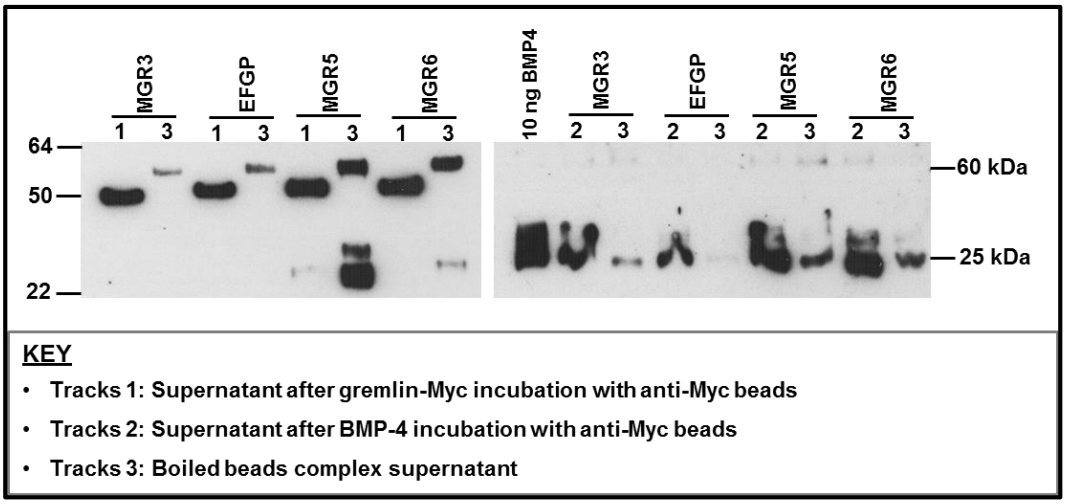

Figure 5.3: IP of BMP-4 on mutant gremlin-Myc-bead complexes.
This experiment was conducted in a similar manner to that described in the legend of Figure 5.2. The gremlin-Myc-bead-bound complexes were prepared with loading volumes stated in the legend of Figure 5.1. Gremlin detection (left panel) and BMP-4 detection (right panel), are both shown at 25 kDa. The non-specific bands at 50 and 60 kDa are also detected.

The results shown in the left and right panels of Figure 5.3 represented blots probed with polyclonal gremlin and BMP-4 primary antibodies, respectively. Samples were collected following loading of 10 ng BMP-4 onto bead complexes of MGRs 3, 5 and -6 mutants including EGFP as the negative control. Strong detection of a BMP-4 band, 25 kDa in size, in the boiled bead supernatants of both MGR5 and MGR6 but weaker in that of MGR3 indicated the BMP-4 binding activities of these gremlin mutants (Figure 5.3, Tracks 3, right panel). This was further supported by only very faint detection of a BMP-4 band in the boiled bead supernatant of the EGFP serving as a negative control (Figure 5.3, Track 3, right panel).

Strong, weak and no gremlin detection in the boiled bead supernatants of MGRs 5, 6 and 3, the same in which BMP-4 detection was achieved, were also observed, respectively (Figure 5.3, left panel, Tracks 3). This was consistent in all repeat experiments and it is not clearly understood why loading of BMP-4 caused weaker gremlin detection in boiled bead supernatants compared to those detected initially in their IP alone (refer Figure 5.1, Tracks 3). A likely explanation could have been gradual loss of gremlin-Myc-bound beads themselves during the extensive wash cycles they were subjected to. Nonetheless, gremlin detection in the boiled bead supernatants of both MGRs 5 and 6, respectively, supported their possession of strong BMP-4 binding activity. MGR3, whose gremlin band could not be detected in the same boiled bead

supernatant in which weak BMP-4 detection was observed, seemed less likely to possess BMP-4 binding capability.

As expected, the BMP-4 bands in all supernatants collected immediately after BMP-4 bead binding were less intense than those loaded initially onto the bead complex (Figure 5.3, right panel, Tracks 2 and labelled track, respectively). This represents the use of excess BMP-4 under these conditions. Again, both 50 and 60 kDa non-specific weak and strong bands were observed in all supernatants collected immediately after BMP-4 bead binding and in all boiled bead supernatants (Figure 5.3, Tracks 2 and 3, respectively).

Successive attempts to reproduce these results were not entirely successful due to the detection of a relatively strong BMP-4 band in the boiled bead supernatant of the EGFP that served as negative control (Results not shown). The likely explanation is due to the 'sticky' nature of BMP-4 itself hence its non-specific binding to the agarose matrix most likely. This occurred despite its preparation in 2%(w/v) BSA-containing buffer and carrying out multiple wash cycles after each bead binding process (results not shown). As such, this limited the observation of specific interactions of BMP-4 with these gremlin-Myc-bead complexes. As a result, the establishment of another protein binding assay was required in order to reliably assess the BMP-4 binding capabilities of both wildtype gremlin and its low heparin-binding mutants.

5.3 Assessing the BMP-4 binding capability of wildtype gremlin-Myc and its mutants by ELISA

5.3.1 Establishment of a novel Myc-capture GREM1/BMP-4 double sandwich ELISA

Following failure to demonstrate consistent BMP-4 binding using anti-Myc beads, a novel Myc-capture GREM1/BMP-4 double sandwich ELISA was established. This immunoassay is an adaptation to the pre-established Myc-capture gremlin ELISA (refer to Chapter 2, Sections 2.19.3 and 2.19.4). It measures the binding of purified BMP-4 to Myc-captured gremlin, thus forming a double antigen sandwich layer. The introduction of a BMP-4 binding step required a change upstream to the detection system, replacing the polyclonal biotinylated gremlin detection antibody with a monoclonal biotinylated BMP-4 detection antibody.

Initially, the functionality of this novel immunoassay was tested using crude culture supernatants of expressed EGFP and WT gremlin-Myc proteins. In the assay, 100

µl/well crude culture supernatants were first loaded into coated wells after which wells were washed. In a stepwise manner, 75 ng/well purified BMP-4, prepared in PBS-0.5% (w/v) BSA buffer, was then loaded prior to its detection upstream. In order to develop a sensitive assay, two different Myc capture antibody concentrations at 2 and 4 µg/ml, were tested.

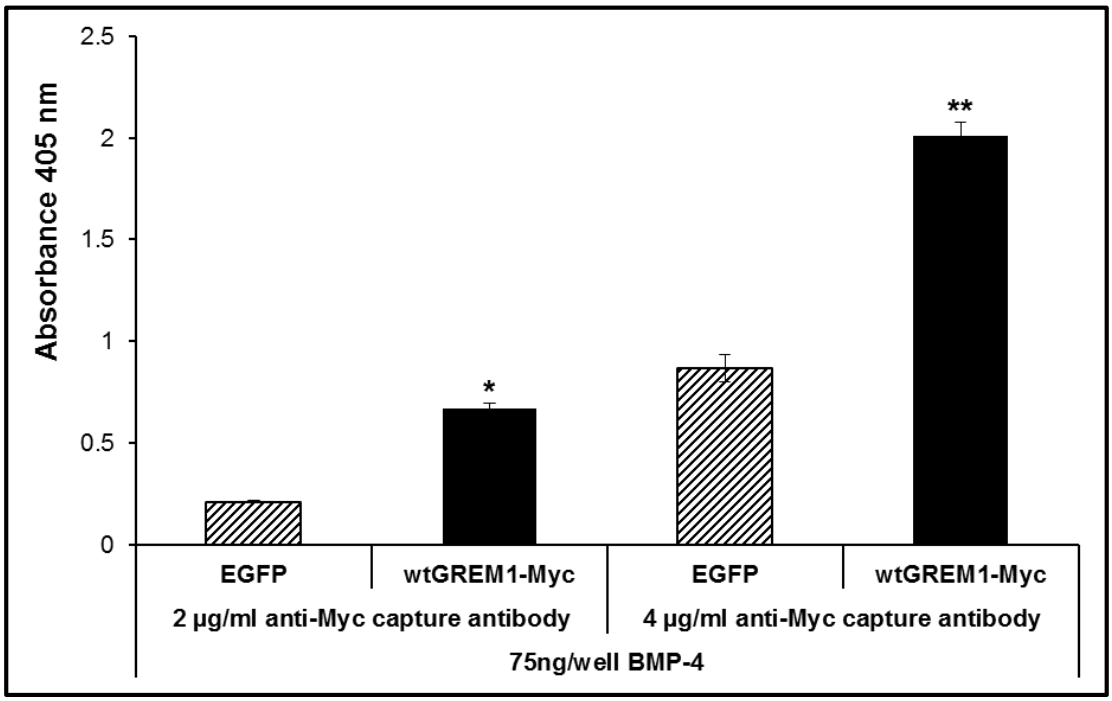

Figure 5.4: Effect of the Myc capture antibody loading in the Myc-capture GREM1/BMP-4 double sandwich ELISA.

Wells coated with 2 and 4 µg/ml 9E10 Myc capture antibody were incubated with 100 µl/well wildtype gremlin-Myc (wtGREM1-Myc) in crude CHO-S culture supernatant (Black columns). Wells loaded instead with 100 µl crude EGFP CHO-S culture supernatant generated the background immunoreactivity (Shaded columns). 75 ng commercially purified BMP-4 was then added. For detection, a biotinylated monoclonal BMP-4 antibody at 2 µg/ml was added to wells. Error bars represent SEM of quadruplicate absorbance readings (n=4). 2-tailed paired-samples T-test conducted comparing EGFP versus wtGREM1-Myc within each paired group. * and ** represent $p < 0.01$ and $p < 0.001$, respectively.

From the results shown in Figure 5.4, the wildtype gremlin-Myc bound BMP-4 immunoreactivity (Figure 5.4, black columns) was significantly higher than that induced by EGFP (Figure 5.4, shaded columns) within each paired group captured at both 2 and 4 µg/ml capture antibody. The EGFP-induced BMP-4 immunoreactivity constituted the background immunoreactivity in this ELISA, as it did not contain any gremlin protein except perhaps that expressed endogenously by the CHO-S cells

themselves which would not be captured on the Myc capture layer being untagged. Moreover, a comparison between both group pairs showed that wildtype gremlin-Myc-induced BMP-4 immunoreactivity at 4 µg/ml capture antibody was significantly higher than the same induced immunoreactivity at half its concentration. Despite observing a corresponding increase in background immunoreactivity, the higher Myc capture antibody concentration was chosen for all subsequent experiments using this ELISA.

5.3.2 Assessing the BMP-4 binding capabilities of expressed gremlin-Myc proteins using the Myc-capture GREM1/BMP-4 double sandwich ELISA

Next, the BMP-4 binding capabilities of the gremlin-Myc mutants, MGRs 3, 5 and 6, were assessed using the established Myc-capture gremlin/BMP-4 double sandwich ELISA. In order to further improve its cost effectiveness, the effect of reducing the dose of BMP-4 in this immunoassay was investigated using both wildtype gremlin-Myc and its low heparin mutants.

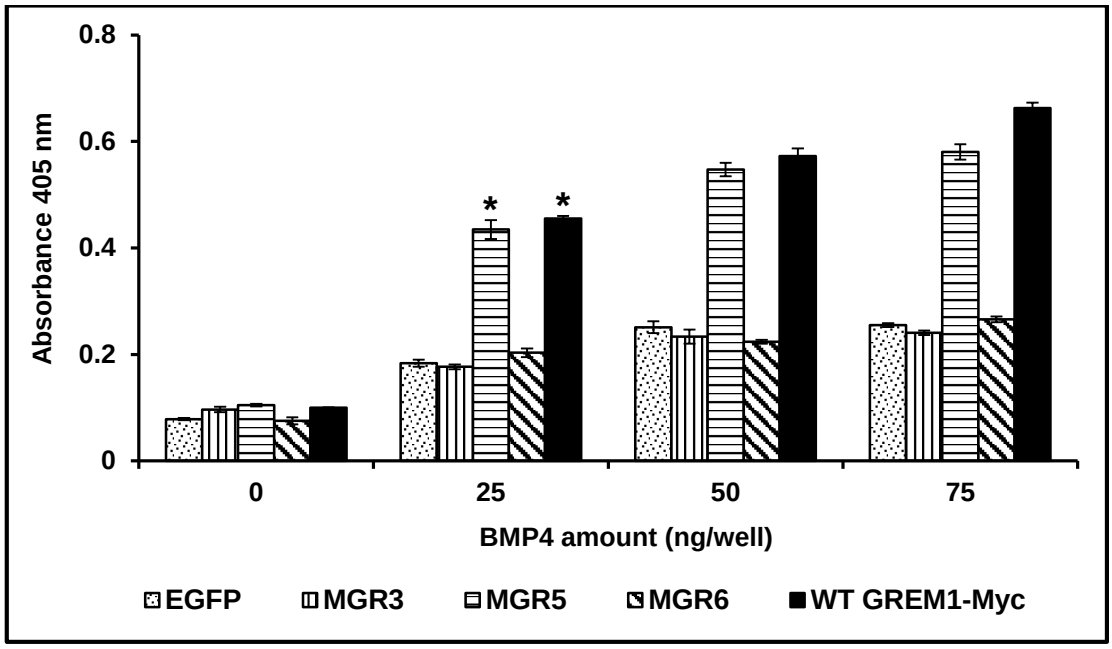

Figure 5.5: Effects of BMP-4 loading in the Myc-capture GREM1/BMP-4 double sandwich ELISA.

Wells coated with 4 µg/ml 9E10 Myc capture antibody were incubated with 100 µl/well crude CHO-S culture supernatants containing either wildtype gremlin-Myc (WT GREM1-Myc) or the mutants, MGRs 3, 5 and 6 or EGFP. Increasing amounts of BMP-4 per well prepared in PBS-0.05% (w/v) BSA were then loaded. Detection was carried out as described in the previous figure legend. Error bars represent SEM of quadruplicate absorbance readings (n=4). Kruskal-Wallis non-parametric one-way ANOVA followed by Bonferroni post hoc test were applied only within the group assayed at lowest BMP-4 amount in comparison to EGFP background immunoreactivity. * represents $p < 0.001$.

Overall, the results shown in Figure 5.5, demonstrated BMP-4 binding capability of both wildtype gremlin-Myc and MGR5. This was demonstrated by their significantly higher induced BMP-4 immunoreactivities compared to those generated by EGFP and MGRs 3 and 6 within each BMP-4 dose group tested (Figure 5.5, projecting black and shaded columns, respectively). Although a progressive dose-dependent increase in wildtype- and MGR5-induced BMP-4 immunoreactivities was observed, there was also a dose-dependent increase in EGFP background immunoreactivity. Thus, the signal-to-background ratio remained fairly constant even with a three-fold increase in BMP-4 amount from 25 ng to 75 ng. As a result, the dose of BMP-4 applied was maintained at 25 ng in all other subsequent experiments that used this ELISA.

In contrast to the wildtype and MGR5, both MGR3- and MGR6-induced BMP-4 immunoreactivities remained similar to corresponding EGFP background immunoreactivities within each dose group (Figure 5.5). This may have reflected their genuine incapability of BMP-4 binding as a direct effect of their incorporated mutations. Alternatively, a trivial explanation is that their levels of expression in their respective crude supernatants may have fallen below the limit of detection of the double sandwich ELISA itself; a limit set perhaps above the levels of MGR6 immunoreactivity in crude culture supernatants despite its strong expression.

5.3.3 Effects of soluble heparin on wildtype gremlin-Myc binding interaction with BMP-4 in ELISA

Recently, the high resolution three-dimensional crystal structure of PRDC, a close homologue of gremlin, has been elucidated by Nolan *et al.* (2013). Their analyses revealed a considerable regional overlap of both its BMP and heparin binding sites on the convex binding surface of the cystine-knot domain on the PRDC dimer. This by no means suggests that both binding sites are identical and, therefore, these should be thought of as being physically distinct. However, their regional proximity on the cystine-knot binding domain means that there is a considerable degree of allosteric competition between both sites in the presence of a binding ligand as argued by Nolan *et al.* (2013). This was confirmed in SPR measurements, when they showed that binding of PRDC to immobilised BMP-2 was inhibited by the addition of unfractionated heparin, ~25 kDa, and tinzaparin. Tinzaparin is a low molecular weight heparin, 5.5 – 7 kDa (Chiodelli *et al.*, 2011). This inhibition occurred in an increasing dose-dependent manner within a tested range of 0.003 – 3 μM. This rather implies that

both heparin and BMP binding sites on PRDC are not fully independent from one another.

In this current study, the Myc-capture GREM1/BMP-4 double sandwich ELISA was used to verify whether expressed wildtype gremlin-Myc behaved similarly to PRDC. In this case, Myc-captured wildtype gremlin-Myc was exposed to increasing concentrations of 0 – 20 µM unfractionated heparin prior to the loading of 25 ng/well BMP-4. In the experimental design, it was foreseen that the use of unfractionated heparin itself might confound the experiment, as it was envisaged that a single extended unfractionated heparin chain could provide several gremlin binding sites. This alone could potentially increase BMP-4 immunoreactivity resulting in multiple cross-linked gremlin-BMP-4 complexes. Therefore in order to minimise such risk, a similar approach to that used by Nolan *et al.* (2013) was applied to this work.

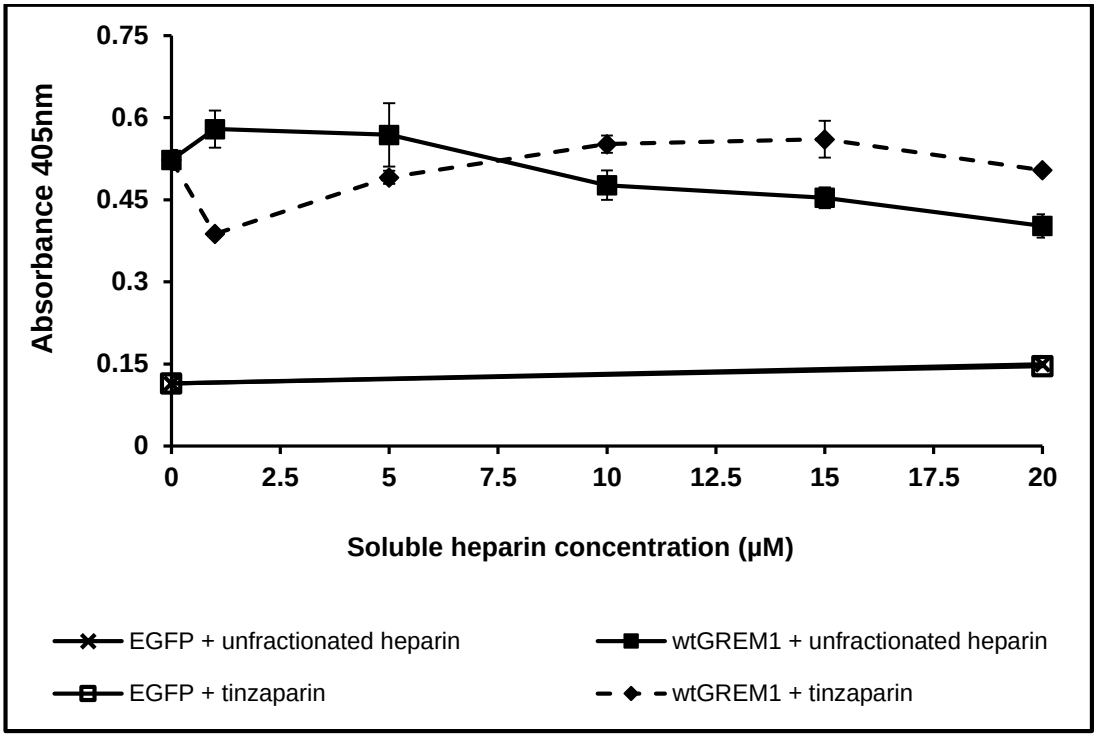

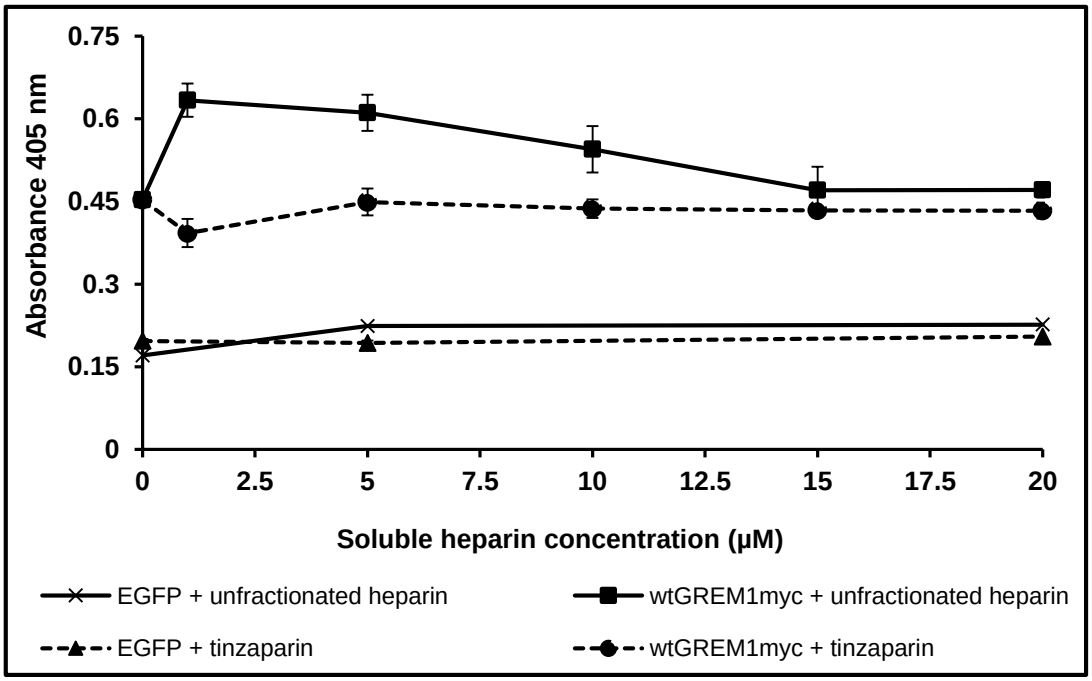

Figure 5.6: Effects of soluble unfractionated heparin and tinzaparin on the binding interaction between wildtype gremlin-Myc and BMP-4.

Top and bottom panels: two sets of results from two independent repeat experiments. The Myc-capture GREM1/BMP-4 double sandwich ELISA was conducted as described in the previous figure legend by coating wells with 4 µg/ml 9E10 Myc capture antibody and loading 100 µl/well crude wildtype gremlin-Myc (wtGREM1myc) or EGFP culture supernatant. Next varying concentrations of the heparins were added to respective wells and incubated for 45 min at room temperature prior to loading with 25 ng/well BMP-4. Error bars represent SEM of quadruplicate absorbance readings (n=4).

In the results as shown Figure 5.6, the wildtype gremlin-Myc-induced BMP-4 immunoreactivity remained fairly constant across the entire concentration range of intact heparin (Figure 5.6, upper solid lines) and tinzaparin (Figure 5.6, upper broken lines). The marked increase in wildtype gremlin-Myc-induced BMP-4 immunoreactivity at 1 µM intact heparin was consistent over two independent repeat experiments (Figure 5.6, upper solid lines). This increase in BMP-4 immunoreactivity together with those observed at 5 and 10 µM (Figure 5.6, bottom panel, upper solid line) may indicate multiply cross-linked gremlin-BMP-4 complexes along an intact heparin chain, as suggested earlier. This was further supported by the constant levels of wildtype gremlin-Myc-induced BMP-4 immunoreactivity across the same concentration range of tinzaparin (Figure 5.6, upper broken line). Throughout this experiment, the wildtype gremlin-Myc-induced BMP-4 immunoreactivities were significantly higher than EGFP background immunoreactivities across the entire concentration range of both heparins (Figure 5.6, lower solid and/or broken lines).

Unlike the binding competition observed by Nolan *et al.* (2013) between BMP-2 and heparin on PRDC, addition of intact heparin and tinzaparin neither inhibited nor promoted gremlin-Myc interactions with BMP-4. As such, these results verified a hypothesis made in this study for the existence of physically distinct heparin/HS and BMP binding sites on gremlin which are independent of one another. In other words, these binding sites are located at different regions on gremlin and do not compete with each other upon binding to their ligands.

5.4 SMAD1/5/8 phosphorylation assay in C2C12 cell cultures

5.4.1. BMPs -4 and -7-induced SMAD1/5/8 phosphorylation

C2C12 myoblastic cell cultures have been widely used for the establishment of functional cellular bio-assays to assess BMP activity (Mulloy and Rider, 2010). Addition of bone-inducing BMPs results in the intracellular phosphorylation of R-SMADs proteins, SMAD1/5/8 and SMAD2/3, that in complex with co-SMAD, SMAD-4, translocate into the nucleus causing transcriptional up-regulation of osteoblastic target gene markers such as alkaline phosphatase (Ali and Brazil, 2014). The end result is the BMP-induced transformation of C2C12 myoblastic muscle-type phenotype into an osteogenic phenotype (Urist, 1965; Higgins *et al.*, 1970).

These intracellular molecular and signalling events, therefore, have led to three widely established methods of quantitating BMP activity: 1) measuring levels of expression of an osteogenic marker, such as alkaline phosphatase (Katagiri *et al.*, 1994; Topol *et al.*, 2000a). 2) Establishing a BMP-specific-luciferase secreted reporter gene assay *in vitro* (Zhao *et al.*, 2003; Sudo *et al.*, 2004; Alborzinia *et al.*, 2013). 3) Measuring the SMAD1/5/8 phosphorylation that occurs early along the canonical signalling pathway (Kuo *et al.*, 2010). In this latter assay, the stimulus-response lag time period is significantly shortened to only 45 – 60 min post-BMP treatment compared to 16 – 24 h post-BMP treatment in the other two methods. As such, the SMAD1/5/8 phosphorylation assay provides more flexible platform to investigate several cellular processes. In this current study, we aimed at adapting this method further by investigating the effect gremlin on BMP-dependent levels of phospho (p)-SMAD1/5/8 activity.

In our initial approach, the responsiveness of the assay to both BMPs -4 and -7, following stimulation of C2C12 myoblastic cells for 45 min at 37 °C, was assessed by generating BMP dose response curves. The results obtained demonstrated that the assay was consistently responsive to both BMPs -4 and -7, as shown by the stronger detection of the 64 kDa p-SMAD1/5/8 protein bands in their presence (Figures 5.7A and 5.8A, top panels, respectively). However, both dose response curves, as determined by densitometry, failed to produce graded response in levels of p-SMAD1/5/8 activity with increasing amounts of the BMPs (Figures 5.7B and 5.8B, solid line curves). In this experiment, and all other subsequent experiments in this functional assay, a loading control was included that involved parallel detection of nonphosphorylated or total (T)-SMAD1/5/8 activity levels in the same experimental samples from which the p-SMAD1/5/8 activity levels were detected. In both cases, strong detection of T-SMAD1/5/8 protein, 64 kDa, was also observed in the same experimental samples (Figure 5.7A and 5.8A, bottom panels). The levels of T-SMAD1/5/8 activity seemed to fluctuate somewhat over the range of BMPs -4/-7 doses, but nonetheless remained fairly constant (Figures 5.7B and 5.8B, broken line curves).

Analysis of the BMP-4 dose response curve showed a sharp increase in levels of p-SMAD1/5/8 activity from 0 - 10 ng BMP-4 which flattened between 10 – 40 ng BMP-4 (Figure 5.7A, solid curve). Another sharp increase in levels of p-SMAD1/5/8 activity at 50 ng BMP-4 was observed that then also flattened between 50 – 75 ng BMP-4. On the other hand, the BMP-7 dose response curve showed similar sharp increase in levels of

p-SMAD1/5/8 activity from 0 - 10 ng BMP-4, and remained at this latter level up to 75 ng BMP-7. These shapes in pattern of both dose response curves were consistent over several repeat experiments. Despite not observing satisfactory grading of the dose response curves over increasing doses of both BMPs, the marked difference between the background in the absence of the BMPs and BMPs -4/-7-induced levels of p-SMAD1/5/8 activity observed, was consistent. This implied that a functional assay for assessing BMP activity had been successfully established in line with findings reported by Kuo *et al.* (2010). A graded dose response curve is prerequisite for inhibition studies which are needed to assay BMP antagonist activity. Although not the case in these results, the marked difference between the background and BMPs -4/-7-induced levels of p-SMAD1/5/8 activity meant that there was scope to attempt inhibition of BMP activity.

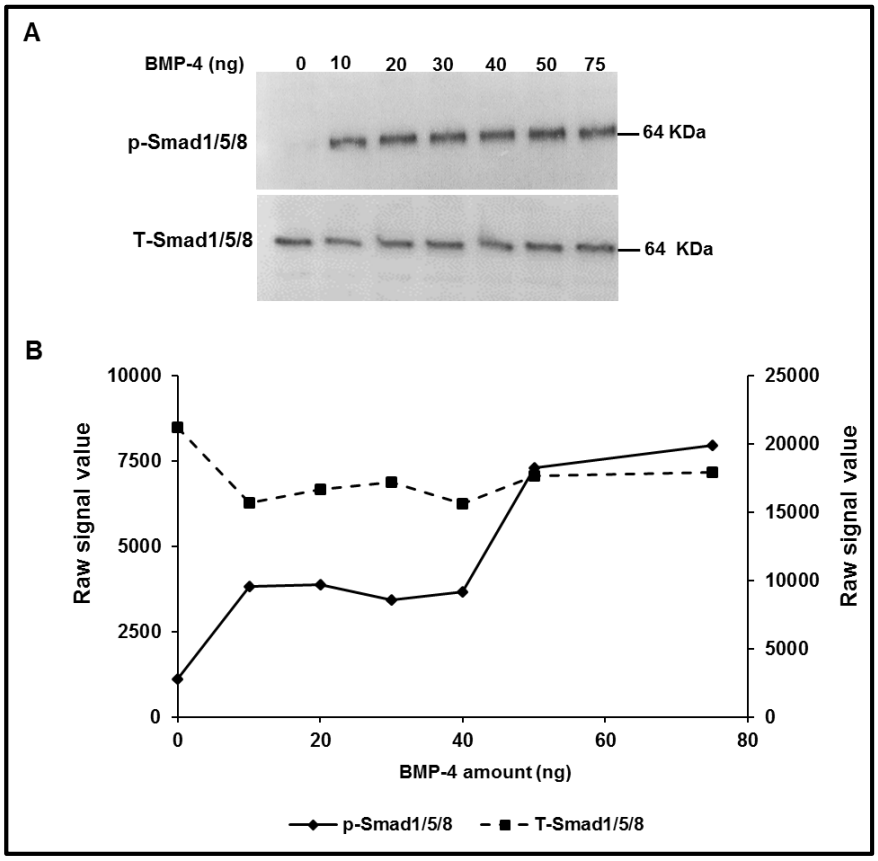

Figure 5.7: BMP-4 dose response curve in the SMAD1/5/8 phosphorylation assay. Undifferentiated C2C12 cell cultures were treated for 45 min at 37 °C with increasing doses of purified BMP-4 protein. A) Western blot detection of p-SMAD1/5/8 at 64 kDa was achieved using a polyclonal p-SMAD1/5/8 primary antibody. T-SMAD1/5/8 activity served as control to p-SMAD1/5/8 activity and was detected in parallel using a polyclonal T-SMAD1/5/8 primary antibody. B) Densitometric quantitation of 64 kDa bands detected in panel A, achieved using the IMAGE Studio Lite software. Results are representative of two independent repeat experiments.

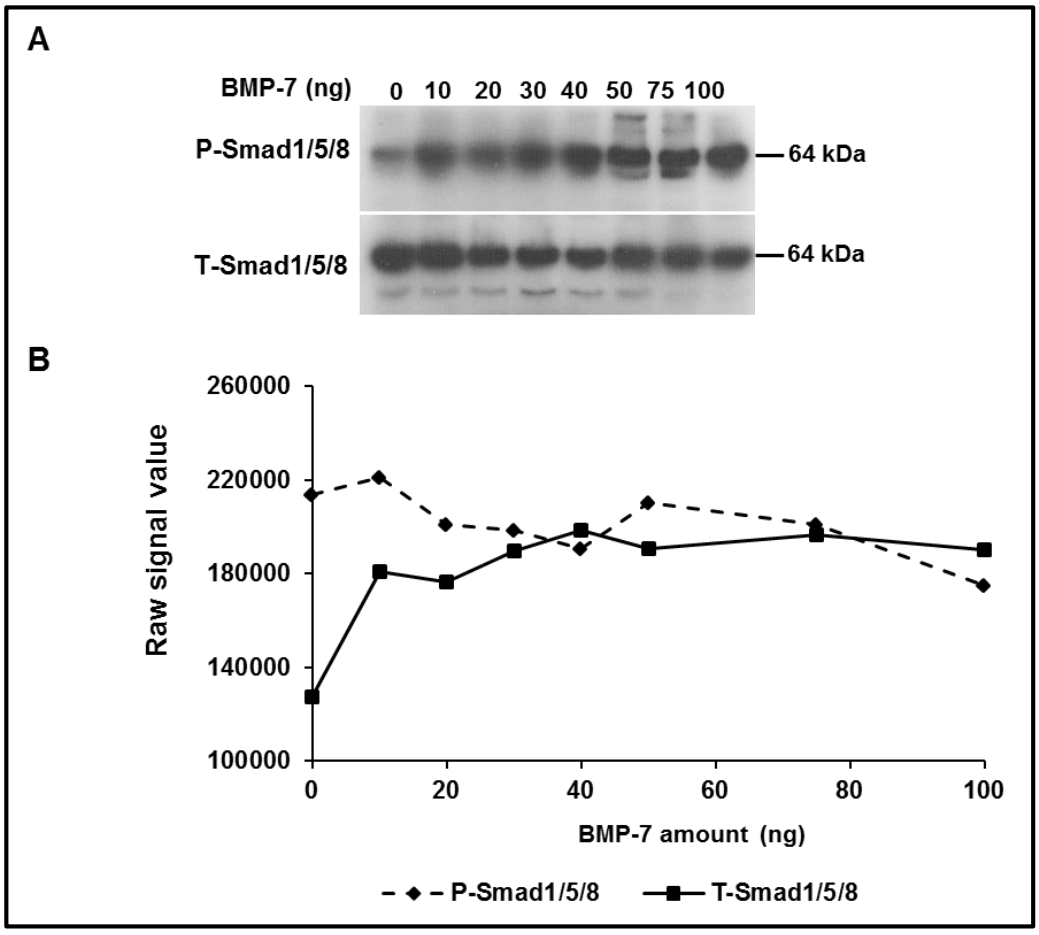

Figure 5.8: BMP-7 induced dose response curve in the SMAD1/5/8 phosphorylation assay.

The BMP-7 dose response curve was generated as described for BMP-4 in the previous figure legend. Results are representative of two independent repeat experiments.

5.4.2. Effect of gremlin-His treatment on SMAD1/5/8 phosphorylation

Next, in order to assess the effect of gremlin in the established SMAD1/5/8 phosphorylation assay, it was important to show that gremlin alone does not induce p-SMAD1/5/8 activity. As such, undifferentiated C2C12 cell cultures were treated initially with commercially purified gremlin-His at high doses of 0.2 µg and 1 µg.

Detection of the 64 kDa p-SMAD1/5/8 protein bands was very faint at both doses of purified gremlin-His (Figure 5.9A, top panel). The p-SMAD1/5/8 levels of activity at 0.2 and 1 µg gremlin-His were not significantly different from the background activity (Figure 5.9B, black columns). Strong detection of T-SMAD1/5/8 protein, 64 kDa, was also observed in the same experimental samples, as shown in Figure 5.9A, bottom gel. Altogether, these results demonstrated that gremlin-His treatment of undifferentiated C2C12 cell cultures does not initiate SMAD1/5/8 phosphorylation, a result in line with

the existing paradigm on its mechanism of action. Therefore, this enabled the investigation of its functional activity by significant inhibition of BMPs -4 and -7-induced cellular signalling activity.

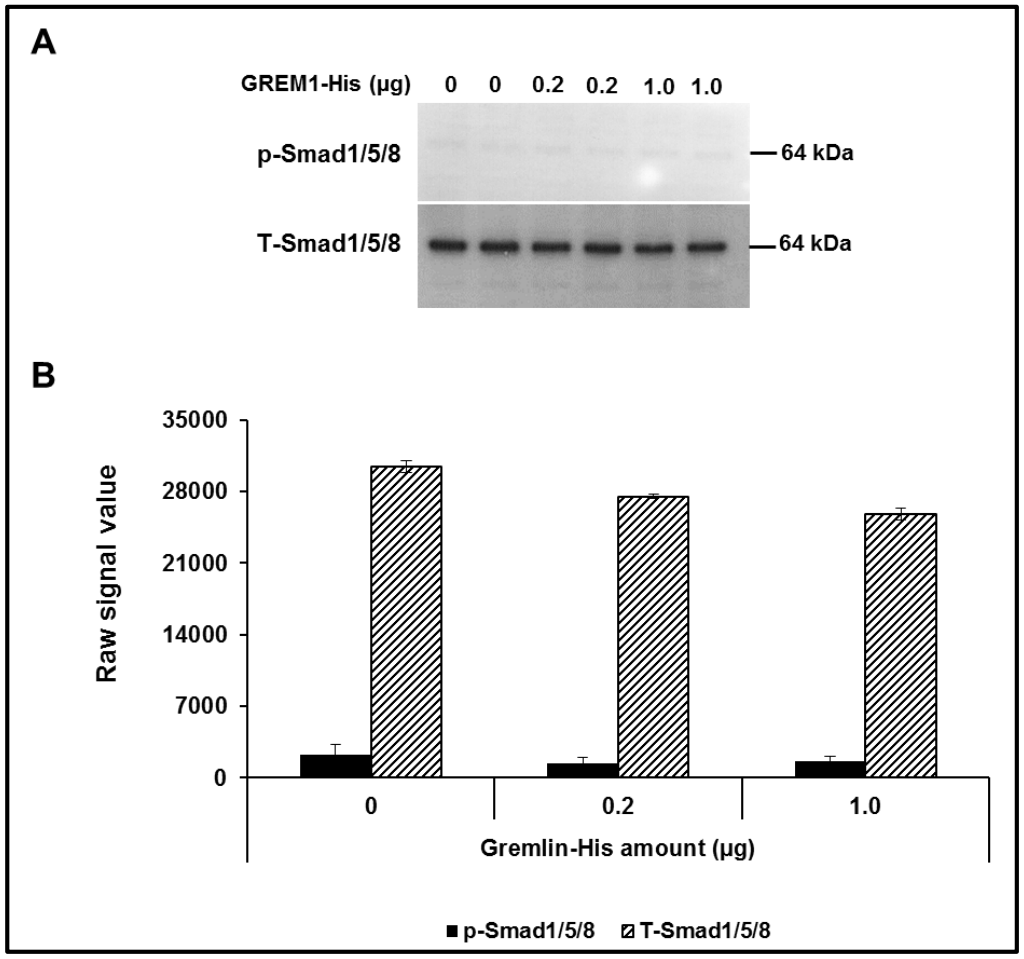

Figure 5.9: Effect of wildtype gremlin-His treatment alone on SMAD1/5/8 phosphorylation.

The BMP-independent effect of gremlin-His was assessed in the SMAD1/5/8 phosphorylation assay. Undifferentiated C2C12 cells were treated with either 0, 0.2 or 1 µg of purified wildtype gremlin-His alone. Western blot detection of p- and T-SMAD1/5/8 at 64 kDa (Panel A), and densitometric quantitation of 64 kDa bands (Panel B) were achieved as described in the legend of Figure 5.7. Error bars represent the SEM of duplicate readings from paired treatment groups (n=2).

5.4.3 The effect of gremlin-His in the BMP-7-induced SMAD1/5/8 phosphorylation

Initial attempts at demonstrating functional activity of gremlin-His were carried out by the investigation of its effect on BMP-7-induced SMAD1/5/8 phosphorylation established previously (Figure 5.8). From the BMP-7 dose response curve, 30 ng BMP-7 was chosen from the flattening portion of the curve. Reiterating, the aim in these

inhibition studies was to significantly inhibit BMP-induced p-SMAD1/5/8 levels of activity hence restoring activity levels equivalent to the background activity in untreated cells. Because is it not known whether gremlin exists as a monomer or a dimer, for complete inhibition, the experiment was conducted using 15 ng and 30 ng gremlin-His so as to match the theoretical stoichiometric ratios of 1:1 or 2:1 for one gremlin dimer or two gremlin monomers complexed to one BMP-7 dimer, respectively. In these experiments, gremlin-His was pre-incubated with BMP-7 at room temperature for 45 min with gentle rotation prior to addition to undifferentiated C2C12 cell cultures.

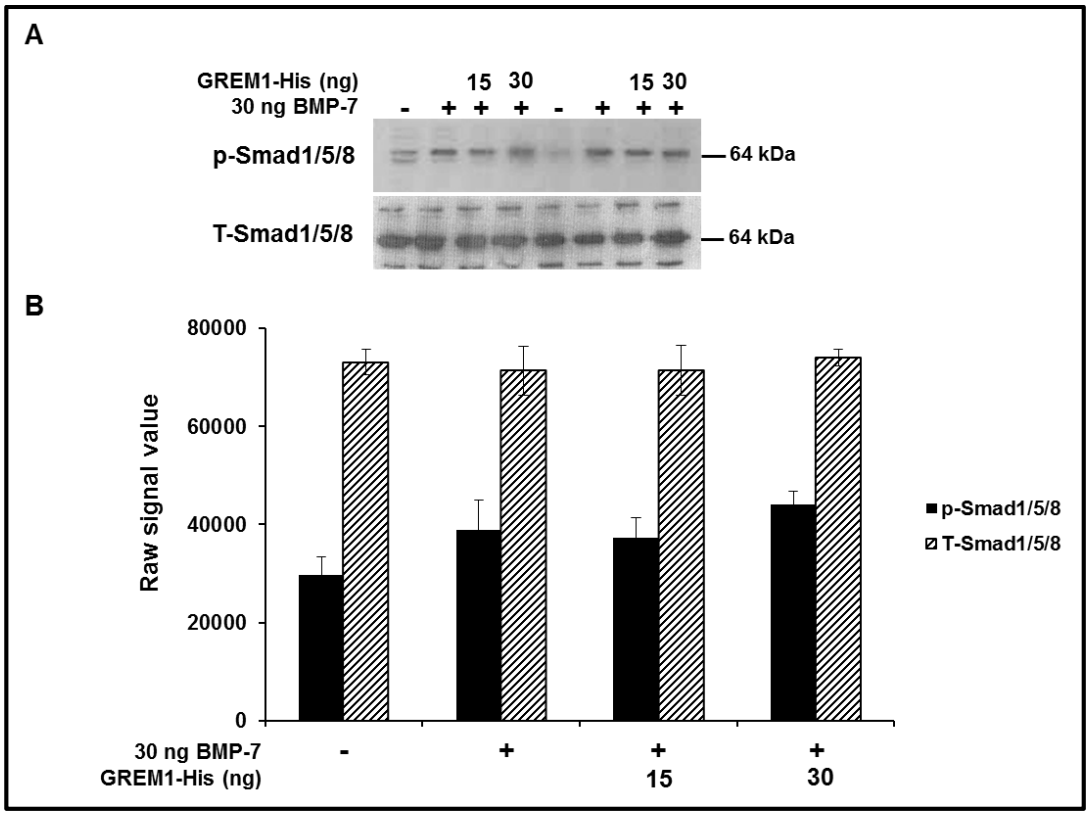

Figure 5.10: Effect of purified gremlin-His on BMP-7-induced SMAD1/5/8 phosphorylation.

The SMAD1/5/8 phosphorylation assay was carried out in undifferentiated C2C12 cells by addition of different amounts of purified gremlin-His pre-incubated with 30 ng purified BMP-7. Western blot detection of p- and T-SMAD1/5/8 at 64 kDa (Panel A) and densitometric quantitation of 64 kDa bands (Panel B) were carried out as described in the legend of Figure 5.7. Error bars represent the SEM of duplicate readings from paired treatment groups (n=2).

As demonstrated in Figure 5.10, inhibition of BMP-7-induced p-SMAD1/5/8 activity was not achieved at either 15 or 30 ng gremlin-His. In Figure 5.10A, top panel,

this was indicated by the persistent strong detection of p-SMAD1/5/8 protein bands, 64 kDa, in the presence of both 15 and 30 ng gremlin-His. These band intensities were comparable to that generated by treating the cell cultures with 30 ng BMP-7 alone. Also, in untreated cell cultures, p-SMAD1/5/8 was detected but appeared less intense compared to those generated in treated cell cultures. In both treated and untreated cell cultures, the T-SMAD1/5/8 protein bands showed comparable band intensities (Figure 5.10B, bottom panel). In terms of p-SMAD1/5/8 levels of activity, no decrease in this activity was observed in cell cultures treated with BMP-7 in the presence of gremlin-His (Figure 5.10B, black columns). The higher than expected background activity observed in untreated cells probed for p-SMAD1/5/8 detection, may have been due to contamination of these lysates. This contamination did not seem to affect the levels of T-SMAD1/5/8 levels of activity in these samples which was very consistent across all samples altogether (Figure 5.10B, shaded columns).

Given that these doses of gremlin-His did not affect BMP-7 activity, higher doses were then applied. This time, the same amount of BMP-7 was pre-incubated with gremlin-His at 30 ng, 60 ng and 150 ng prior to treating the undifferentiated cell cultures (Figure 5.11).

In this case, the p-SMAD1/5/8 detection was by inspection, relatively weaker at both 60 and 150 ng gremlin-His compared to that generated in cell cultures treated with 30 ng BMP-7 only (Figure 5.11A). A decrease in BMP-7-induced p-SMAD1/5/8 levels of activity at both 60 and 150 ng gremlin-His was confirmed by densitometric analyses, however this was not statistically significant (Figure 5.11B). Moreover, the background detection in the untreated cell cultures was very faint, as would normally be expected (Figure 5.11A). The BMP-7-induced p-SMAD1/5/8 levels of activity in gremlin-treated cells remained significantly higher than the background activity in untreated cell cultures. The fact that similar levels of BMP-7 inhibition were achieved at 60 ng gremlin-His and at 150 ng gremlin-His, more than double the lower dose, strongly demonstrated the poor quantitative power of this functional assay.

According to the existing dogma, gremlin is a natural antagonistic of the BMPs -2, -4 and -7, as introduced earlier in this thesis (Chapter 1, Section 1.15). However, strong experimental evidence has been obtained to demonstrate that this is true for the BMPs -2 and -4 but scarcely for BMP-7. For instance, Sudo *et al.* (2004) demonstrated the functional activity of PRDC alongside gremlin-His by their antagonism of these BMPs-mediated signalling using a luciferase-secreted reporter assay. Here, gremlin

antagonism of BMPs -2/-4-SMAD1/5/8-induced luciferase expression was much stronger than that observed for BMP-7-induced signalling. Therefore BMP-4 was used in further studies of inhibition of SMAD1/5/8 signalling.

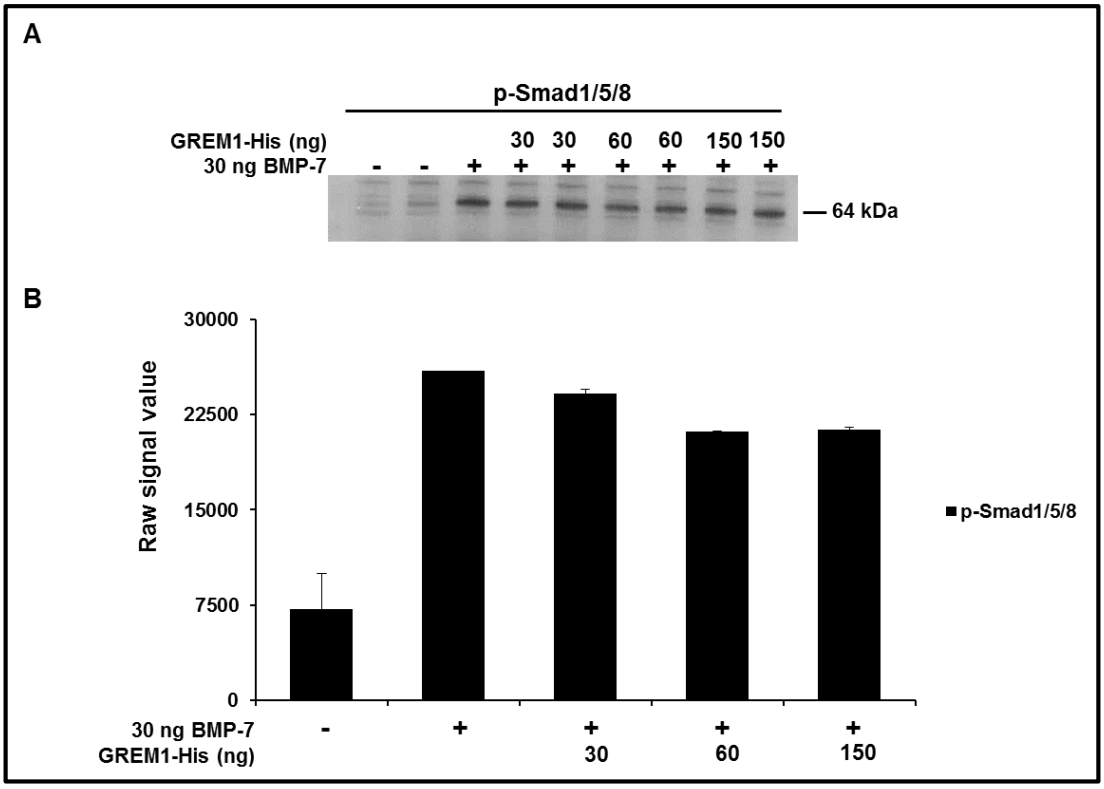

Figure 5.11: Effect of higher doses of purified gremlin-His on BMP-7-induced SMAD1/5/8 phosphorylation.

This experiment was carried out as described in the previous figure legend except that the doses of purified gremlin-His applied were increased as indicated. A) Western blot of p- SMAD1/5/8 (64 kDa). B) Densitometric quantitation of 64 kDa bands as detected in panel A. Error bars represent the SEM of duplicate readings from paired treatment groups (n=2).

5.4.4. Effect of gremlin-His in the BMP-4-induced SMAD1/5/8 phosphorylation

When purified BMP-7 was substituted with purified BMP-4 and pre-incubated with gremlin-His, the same results were achieved; no significant inhibition of BMP-4 induced p-SMAD1/5/8 activity was observed (Figure 5.12). In this case, 25 ng and 50 ng BMP-4 doses were chosen from its dose response curve established previously (Figure 5.7). Inhibition was achieved by pre-incubating purified BMP-4 with purified gremlin-His at 50, 100 and 200 ng, prior to treating the undifferentiated C2C12 cell cultures.

The p-SMAD1/5/8 protein bands, 64 kDa, detected in BMP-4/gremlin-His-treated cell lysates remained as strongly intense as that detected in BMP-4 only-treated cell lysates (Figure 5.12A). This was also observed in densitometric analyses of this band which showed no significant difference between both groups (Figure 5.12B). The fact that the levels of p-SMAD1/5/8 activity in gremlin only-treated cell lysates were similar to the background activity in untreated cells, confirmed observations made earlier in Section 5.4.2. This experiment also demonstrated that gremlin-His on its own does not induce SMAD1/5/8 phosphorylation in undifferentiated C2C12 cell cultures.

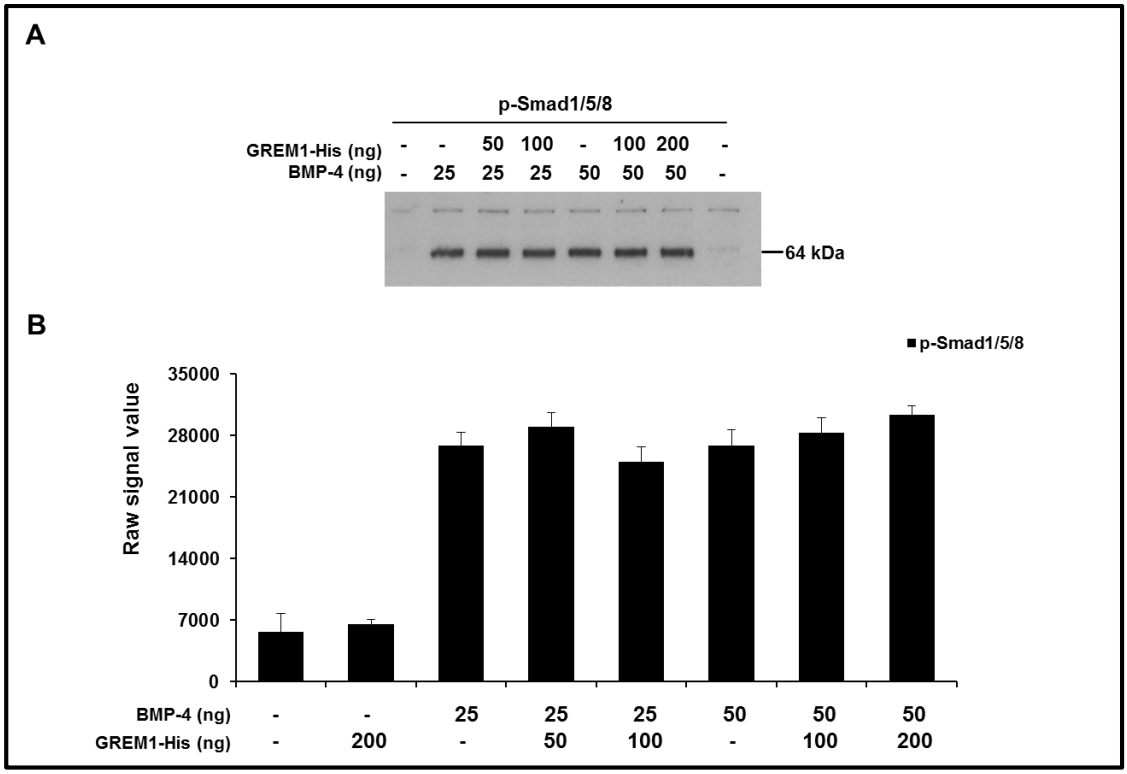

Figure 5.12: Effect of purified gremlin-His on BMP-4-induced SMAD1/5/8 phosphorylation.

This experiment was carried out as described in the legend of Figure 5.10 except that gremlin-His was pre-incubated with either 25 or 50 ng purified BMP-4 instead. A) Western blot of p-SMAD1/5/8 (64 kDa). B) Densitometric quantitation of 64 kDa bands as detected in panel A. Error bars represent the SEM of duplicate readings from paired treatment groups (n=2).

The continued failure to demonstrate significant gremlin-His antagonism of BMP-4-induced p-SMAD1/5/8 levels of activity meant that further work on this SMAD1/5/8 phosphorylation assay was aborted. Such demonstration would have confirmed whether purified gremlin-His was functionally active providing quantitative insight into the effective dose of gremlin necessary for significant inhibition of both BMPs. This

information would have served as a useful reference for subsequent work of similar kind using the expressed gremlin-Myc proteins instead. Nevertheless, unsuccessful results despite using high amounts of gremlin-His of up 200 ng implied that expressed wildtype gremlin-Myc amounts greater than 200 ng would be required. With relatively low levels of its transient expression, it is likely that the expressed gremlin-Myc proteins would be insufficient in this functional assay. Thus the establishment of a more reliable quantitative and responsive functional assay was necessary. The lack of graded BMPs -4 and -7 dose response curves is believed to have been a fundamental problem in this assay and, therefore, must be avoided in the next functional assay. As such no attempts were made at testing our expressed gremlin-Myc proteins since these observations rather suggested that measuring the levels of p-SMAD1/5/8 activity in the BMP signalling pathway, does not yield a satisfactorily quantitative functional assay under the conditions used here; one requiring quite large amounts of gremlin to elicit a small response in p-SMAD1/5/8 activity. This remains a fundamentally limiting problem that must be taken into account when developing any robust functional assay.

5.5. Investigating the functional activity of wildtype gremlin-Myc and its low heparin-binding mutants using a luciferase-secreted reporter assay

5.5.1. Establishment of a luciferase-secreted reporter assay

The BMP-SMAD1/5/8 specific luciferase-secreted reporter assay was one of three methods discussed earlier (Section 5.4.1), which can be applied to assess BMP-induced signalling along this axiomatic pathway. This reporter assay requires at least 16 – 24 h of incubation time period post-BMP treatment of cells before a strong measurable activity in SMAD1/5/8-induced luciferase expression can be detected. As such, this method is not especially suitable for investigating processes associated with fast recycling such as heparitinase treatment of cells in order to strip them of their cell surface HS. On the other hand, this method remains to date as the most sensitive, reliable and cost effective method to demonstrate functional activity in many proteins.

In this study, the establishment of a BMP-4-SMAD1/5/8-specific luciferase-secreted reporter assay was achieved using the 12XSBE-Oc-Luc^{+}-pGL3 reporter gene construct. This reporter gene construct possesses a 12 repeat SMAD binding element (12XSBE) concatemer enhancer region that promotes high affinity binding of p-SMAD1/5/8-SMAD4 complex. The reporter construct was cloned initially by Zhao *et al.* (2003) and was used in this study in order to mirror the approach by Sudo *et al.*

(2004), who used this reporter assay to demonstrate functional activity of BMPs -2, -4 and -7 in P19 embryonic carcinoma cell cultures and their subsequent inhibition using both purified wildtype PRDC and gremlin-His. This current study aimed at establishing the same functional assay in undifferentiated C2C12 myoblastic cell cultures. By adding a suitable volume of luciferin-containing substrate to up-regulated luciferase-containing lysates, the luciferase activity can be quantified, as a direct measure of BMP-induced SMAD1/5/8 activity upstream.

As shown in Figure 5.13, a graded increase in luciferase activity was observed at BMP-4 concentrations ranging between 0 – 10 nM. The same smooth shape in pattern was consistently generated following two different transfection protocols; Lipofectamine 2000- and Fugene 6-based transfection protocols (Figures 5.13 A and B, respectively). Typically, transient transfection of undifferentiated C2C12 cell cultures was carried out in a single tissue culture flask in order to achieve the same transfection efficiency. The transfected cell cultures were then split into 24-well tissue culture plates and allowed to adhere prior to treating them with purified BMP-4 protein. When using the Lipofectamine 2000 protocol, a more than 90% confluency in the cell cultures was required prior to transfection, whereas only 70% confluency was required using the Fugene 6 protocol. Therefore, the Fugene 6 protocol offered a higher throughput experimental route than the Lipofectamine 2000 protocol and also, minimised the risk of achieving 100% cell confluency post-transfection. It is well established that at 100% confluency, undifferentiated cells undergo terminal differentiation which results to changes in intracellular signalling activities (Yoshida *et al.,* 1998).

As shown in Figure 5.13A, the BMP-4 dose response curve generated using the Lipofectamine 2000-based transfection protocol yielded higher luciferase activity compared to that generated using the Fugene 6-based transfection protocol (Figure 5.13B). This observation may be due to the difference in transfection periods although differences in the mechanism of operation of both transfection reagents cannot be ruled out. Nonetheless, the signal-to-background signal ratio in both methods was highly satisfactory. In both cases, a linear responsive range was observed between 0 – 4 nM BMP-4 in the former and 0 – 5 nM BMP-4 in the latter (refer to Figures 5.13 A and B, respectively). Altogether, this is an important result as it overcomes the issue on consistent lack of graded BMPs -4/-7 dose response curves encountered in the SMAD1/5/8 phosphorylation assay discussed previously (refer to Section 5.4.1, Figures 5.7B and 5.8B). Establishing consistent and graded BMP-4 dose response curves using

the luciferase reporter assay was a fundamental prerequisite to carrying out inhibition studies for assay of gremlin activity.

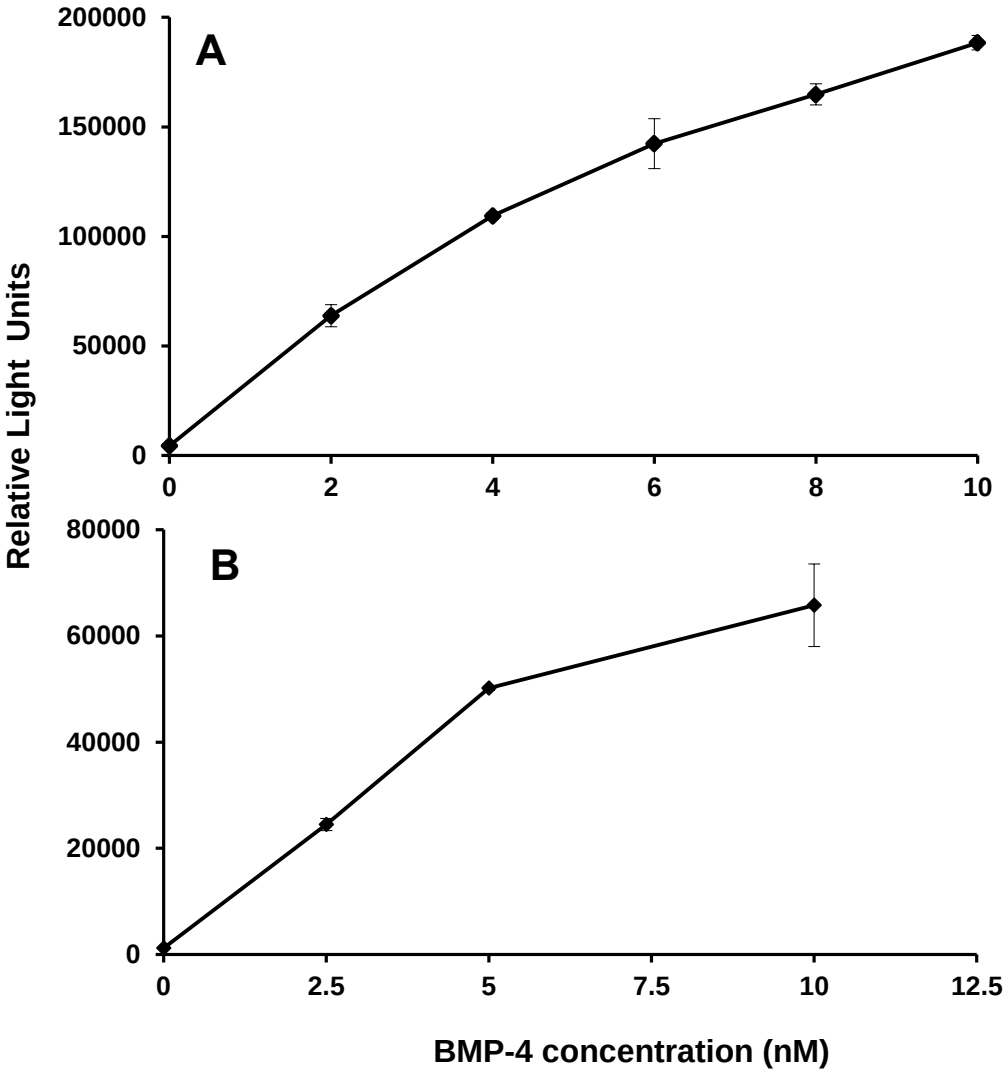

Figure 5.13: BMP-4 dose response curves in the secreted-luciferase reporter assay. Undifferentiated C2C12 cell cultures were transiently transfected with 6 – 9 µg 12XSBE-Oc-luc^{+}-pGL3 reporter construct using the Lipofectamine 2000 (A) and Fugene 6 (B) transfection reagents. Cell cultures were subsequently treated with increasing concentrations of purified BMP-4, added exogenously. Luciferase activity was measured using the GloMax luminometer by addition of 100 µl substrate to 30 µl cell lysate. Error bars represent the SEM of duplicate relative light unit (RLU) values from paired treatment groups (n=2). Results are representative of two independent repeat experiments.

5.5.2. Investigating the functional activity of wildtype gremlin-Myc and its mutants

Having established graded BMP-4 dose response curves (refer to Figure 5.13), the functional activity of concentrated wildtype gremlin-Myc and its low-heparin binding mutant proteins were investigated. This was carried out using both Lipofectamine 2000- and Fugene 6-based transfection protocols, as described in the previous section. The commercially-purified wildtype gremlin-His protein was also used in order to verify the findings by Sudo *et al.* (2004).

The results as shown in Figure 5.14, demonstrated that concentrated expressed wildtype gremlin-Myc together with MGRs 5 and 6 mutant proteins, were functionally active. This was indicated by significant inhibition of 3.6 and 5 nM BMP-4 induced luciferase activity (Figures 5.14 A and B, respectively). Significant inhibition of BMP-4 activity was also observed at 25 nM purified gremlin-His protein in line with the findings by Sudo *et al.* (2004), (Figure 5.14B). Greater gremlin-His-mediated inhibition of BMP-4-induced luciferase activity was observed at 50 nM, demonstrating a concentration-dependent gremlin-mediated antagonism of BMP-4 activity. No significant inhibition of BMP-4 activity was achieved with concentrated MGR3 (Figure 4B).

Previously in this current study, the concentration of the expressed wildtype gremlin-Myc protein in crude culture supernatant was semi-quantified against purified gremlin-His using Western blotting at 50 ng/ml which approximates to about 2 nM (data not shown). Equally, by comparing the wildtype gremlin-Myc dose response curve to those of MGRs 3, 5 and 6 generated previously using the Myc-capture gremlin ELISA, their concentrations were estimated (refer to Figure 4.2, Chapter 4). These data had previously indicated that the slope of MGR5 immunoreactivity in crude culture supernatant was greater than or equalled that of wildtype gremlin-Myc, [MGR5] $\geq$ 2 nM, whereas the slope of MGR6 immunoreactivity was approximately half that of the wildtype, [MGR6] $\cong$ 1 nM. That of MGR3 was at least 40-fold less than wildtype, [MGR3] $\leq$ 0.05.

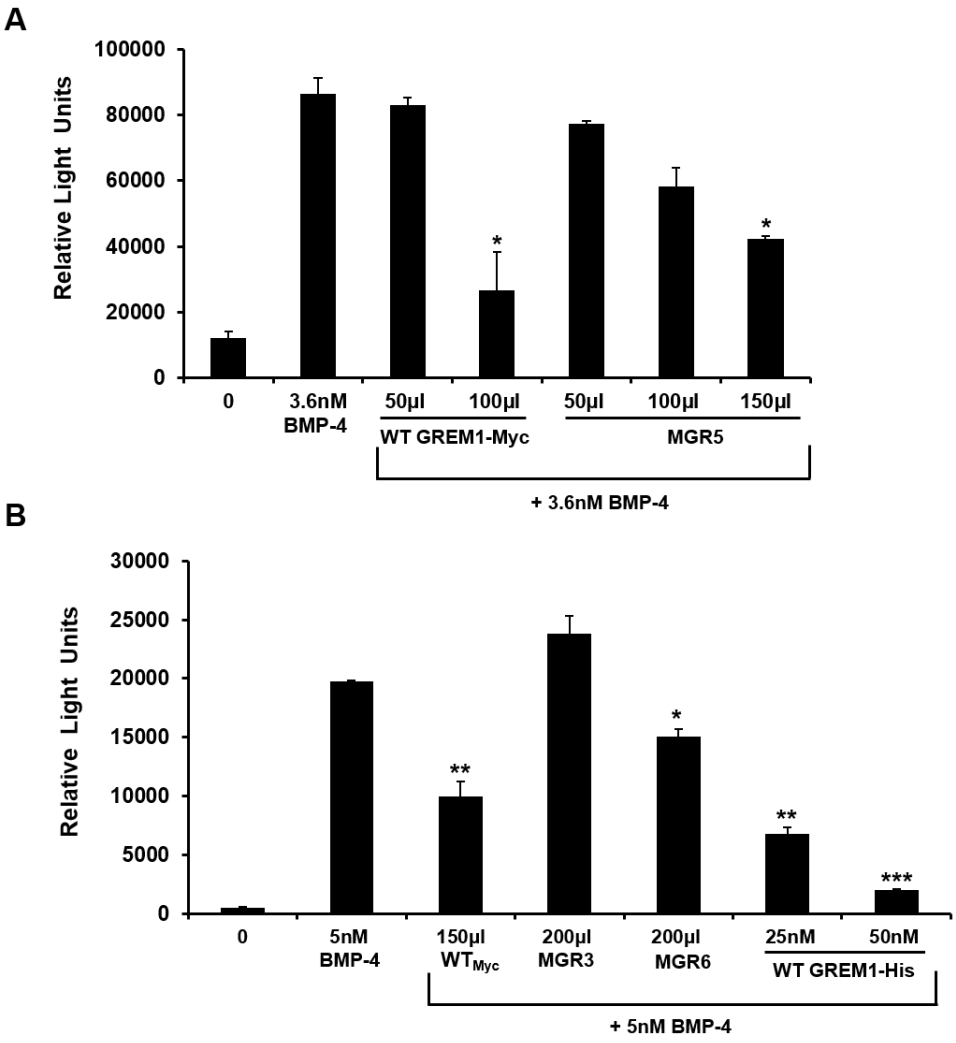

Figure 5.14: Investigating the functional activities of expressed gremlin-Myc proteins.

The experiments were conducted as described in the legend of Figure 5.14. Transfection of C2C12 myoblastic cell cultures were conducted using either (A) Lipofectamine 2000 or (B) Fugene 6 transfection reagents. Fixed BMP-4 doses of 3.6 nM and 5 nM were chosen from BMP-4 dose response curves generated using the respective protocols (refer to Figure 5.13). The commercially-purified wildtype GREM1-His protein in panel B served as positive control. In this case, n = 3. Statistical analyses: Post hoc LSD followed Kruskal-Wallis non-parametric one-way ANOVA. Comparisons made against RLU value at 3.6 and 5 nM BMP-4. * indicates $p<0.05$; **indicates $p< 0.01$; *** indicates $P<0.0001$. Results are representative of at least two independent repeat experiments.

In the results shown in Figures 5.14 A and B, significant BMP-4 inhibition at 100 µl and 150 µl concentrated wildtype gremlin-Myc corresponded to functional activity at concentrations of 8 nM and 12 nM, respectively. Likewise, significant BMP-4 inhibition at 150 µl concentrated MGR5 and 200 µl concentrated MGR6 corresponded to functional activity at concentrations $\geq$ 12 nM and $\cong$ 8 nM,

respectively. Also concentrated MGR5-mediated inhibition of 3.6 nM BMP-4 activity was not significant at 8 nM (100 µl), the same concentration at which concentrated MGR6 showed significant inhibition of 5 nM BMP-4 activity (Figures 5.14 A and B). On this basis, MGR5 may be considered less functionally active than MGR6. In the case of MGR3, 200 µl concentrated MGR3 corresponded to only 0.4 nM which may have explained its functional inactivity (Figure 5.14B).

The purified wildtype gremlin-His protein appeared to show stronger functional activity than the concentrated expressed wildtype gremlin-Myc protein (Figure 5.14B). This can be explained by the difference in the doses that were applied as it has been established that gremlin-mediated antagonism of BMP-4 varies in a concentration-dependent manner.

5.6. Discussion

The work described in this chapter was aimed at investigating BMP binding capability of expressed wildtype gremlin-Myc and its low-heparin binding mutants, MGRs 3, 5 and 6, and also at assessing their functional activity *in vitro.*

Immunoprecipitation of BMP-4 on gremlin-Myc complexes of agarose anti-C-Myc beads indicated that wildtype gremlin-Myc together with MGRs 3, 5 and 6, were able to bind BMP-4. In this experiment, a marked difference in BMP-4 band intensity was observed in boiled bead complex supernatants of all gremlin-Myc proteins compared to that of the EGFP negative control. However in subsequent repeat experiments, this marked difference was less pronounced with even strong BMP-4 detection in EGFP boiled bead supernatants at times. The likely explanation is that purified BMP-4 protein is highly 'sticky' binding non-specifically to the beads. Reducing the loading amount of BMP-4 and introducing Tween20 detergent in washes did not reduce this non-specific binding. This greatly limited interpretation on the specific interaction between these gremlin-Myc proteins and BMP-4. The strong recovery of gremlin in boiled bead complex supernatants following loading of the anti-C-Myc beads with wildtype and mutant crude gremlin-Myc supernatants, demonstrates that gremlin-Myc proteins can be concentrated using anti-C-Myc beads. For example, MGR3 is not detectable by Western blotting of its crude culture supernatant whereas strong detection is achieved in the boiled bead complex supernatant following its immunoprecipitation on anti-C-Myc beads.

In a novel Myc-capture GREM1/BMP-4 double sandwich ELISA, BMP-4 binding of wildtype gremlin-Myc and MGR5 mutant was reproducibly demonstrated using crude culture supernatants. In this assay, both MGRs 3 and 6 failed to capture significant BMP-4 immunoreactivity. Previously in this study, the amount of wildtype gremlin-Myc expressed in its crude culture supernatant was estimated by using both Western blotting and Myc-capture gremlin ELISA. Given that loadings of 0.125 ng/well MGR3 and 2.5 ng/well MGR6 did not generate significant BMP-4 immunoreactivity, it is possible that the limit of detection of the double sandwich ELISA was higher than 2.5 ng thus explaining the trend in results. On this basis, the BMP-4 binding activity of these mutants cannot be ruled out. On another hand, it is also possible that these observations may have genuinely reflected on the true BMP-4 binding capabilities of both MGRs 3 and 6. Perhaps the specific mutations they each incorporate may have damaged a major BMP-binding epitope in them. Both mutants

share the same arginine and lysine substitutions in their basic cluster II, but differ in that MGR3 possesses combined substitutions in its entire basic cluster IIIa whereas MGR6 possesses combined substitutions in its basic cluster I. MGR5 which demonstrates BMP-4 binding, possesses combined substitutions in its basic clusters II and IIIb. Therefore, although all possess the basic cluster II substitutions, the different additional substitutions in both MGRs 3 and 6, may have caused modifications in the folding of the proteins.

Using the same double sandwich ELISA, addition of both unfractionated heparin and the low molecular weight heparin, tinzaparin, both neither promoted nor inhibited the binding interaction of wildtype gremlin-Myc with BMP-4. The important information here was that addition of intact heparin did not result in the inhibition of wildtype gremlin-Myc-induced BMP-4 immunoreactivity. Therefore overall, this strongly supported an initial hypothesis of this study, for the existence of two physically isolated and independent heparin/HS and BMP binding sites on gremlin. These observations go further to reveal the type of subtle structural differences that can lead to different mechanisms of action between even closely related BMP antagonists, such as gremlin and PRDC. Previously, Nolan *et al.* (2013) demonstrated competitive binding between both binding sites to their ligands. This was believed to be the case because of the regional overlap between the binding sites that are both located on convex binding surface of the cystine-knot domain on a PRDC dimer.

A Western blot detection of SMAD1/5/8 phosphorylation assay was established using both BMPs -4 and -7 in order to assess the functional activity of the expressed wildtype gremlin-Myc and its mutants, MGRs 3, 5 and 6. In this semi-quantitative assay, the levels of BMP-induced p-SMAD1/5/8 activity were measured at an early step of the canonical BMP-SMAD1/5/8 signalling pathway. Therefore, a rapid response was observed following treatment of undifferentiated C2C12 myoblastic cell cultures with different doses of these BMPs.

This functional assay was consistently responsive to both BMPs -4 and -7 treatments, but, however, it failed to produce BMPs -4 and -7 dose response curves. This was not ideal, as establishing a dose response curve is a prerequisite in inhibition studies to assay BMP antagonist activity. Irrespectively, the low background activity in untreated cell cultures was a consistent feature of the assay. This meant that only near complete inhibitions of BMP activity could be detected in this functional assay. This was attempted using high doses of purified gremlin-His protein at fixed doses of both

BMPs -4 and -7 chosen from their dose response curves. Unfortunately, such significant inhibition was not achieved. It is possible that the fixed BMPs -4 and -7 doses chosen fell on non-responsive regions of the dose response curves where much higher doses of gremlin-His than those tested would be required. Nonetheless, given that the aim here was to assess the functional activity of gremlin-Myc proteins, present at low amounts in crude culture supernatants, it is clear that this assay was not suitable.

It was demonstrated that gremlin-His treatment of undifferentiated C2C12 cell cultures alone did not induce SMAD1/5/8 phosphorylation in the SMAD1/5/8 phosphorylation assay. This was in line with findings reported by Sudo *et al.* (2004) using a luciferase-secreted reporter assay in P19 embryonal carcinoma cell cultures in which the levels of gremlin-induced luciferase expression were comparable to the background activity in untreated cell cultures.

Instead, attention was turned towards the same SMAD1/5/8-specific luciferase-secreted reporter assay established by Sudo *et al.* (2004) to demonstrate functional activity of the BMPs -2, -4 and -7 and also that of purified PRDC and purified gremlin-His proteins. In this current study, this was established by transfecting undifferentiated C2C12 myoblastic cell cultures with the same 12XSBE-Oc-luc^{+}-pGL3 construct employed by Sudo *et al.* (2004). This functional assay is more quantitative than the potential functional assays considered so far in this study. In the assay, these BMPs induce SMAD1/5/8-mediated transcriptional activation and up-regulation of luciferase expression whereas both Myc- and His-tagged gremlin antagonist proteins, down-regulate BMP-induced response thus is suitable to help assess the functional activity of expressed wildtype gremlin-Myc and its low-heparin binding mutant proteins, MGRs 3, 5 and 6. Given their low expressions in crude CHO-S culture supernatants, these gremlin-Myc proteins were concentrated 20-fold prior to use in this functional assay. This work would also aim at comparing the functional activity of purified gremlin-His protein versus that of the expressed wildtype gremlin-Myc.

Initially, graded BMP-4 dose response curves were established on a consistent basis. Such responses were observed using two different transfection reagents, Lipofectamine 2000 and Fugene 6. A high signal-to-background signal ratio was generated following both experimental protocols.

Next, the functional activity of concentrated wildtype gremlin-Myc and two out of three low-heparin binding mutants, MGRs 5 and 6, were demonstrated. Concentrated wildtype gremlin-Myc protein was more functionally active than both MGRs 5 and 6.

The functional activity of concentrated MGR6 is inconsistent with previous observations on its BMP-4 binding capability in the Myc-capture GREM1/BMP4 double sandwich ELISA. In contrast, ELISA of crude MGR6 culture supernatants did not generate significant BMP-4 immunoreactivity which had previously indicated that MGR6 lacks BMP-4 binding activity.

The lack of any functional activity of MGR3 in both double sandwich ELISA and luciferase reporter assay may have been as a result of its very low expression in the crude CHO-S cell culture supernatant. Even after a 20-fold concentration, the MGR3 concentration remained at least 20 – 40-fold lower than that of concentrated wildtype gremlin-Myc and MGRs 5 and 6. Until MGR3 concentrations can be increased significantly, conclusive observations cannot be made on the functional activity of this mutant.

In the luciferase reporter assay, commercially purified wildtype gremlin-His was shown to be functionally active, in line with findings by Sudo *et al.* (2004). Moreover, its antagonism of BMP-4 activity occurred in a dose-dependent manner. A direct comparison of the functional activity of wildtype gremlin-His versus concentrated expressed wildtype gremlin-Myc was made. The former appeared to be more functionally active than the latter. This difference was likely caused by the discrepancy in concentrations tested. As the aim of this study was to establish whether wildtype gremlin-Myc and its mutants, MGRs 3, 5 and 6 are functionally active, investigating further this difference between His- and Myc-tagged wildtype gremlin was not essential to this study.

CHAPTER 6: General discussion and conclusion

6.1 Mapping of the heparin binding site on gremlin

The primary aim of this study was to map experimentally the heparin/HS binding site on gremlin. Because gremlin has no experimentally determined structure, this study was based on knowledge from its predicted three-dimensional structure. Before this study was underway, within the CAN family, only the NMR structure of sclerostin had been resolved (refer to Figure 1.7), (Veverka *et al.,* 2009). On this resolved sclerostin structure, a heparin binding site was also mapped experimentally; the only one within the CAN family. As discussed fully in Chapter 1, Section 1.8.2, the experimental mapping of the heparin binding site on sclerostin was achieved by NMR spectral analyses which monitored backbone changes in amide signals on sclerostin on addition of heparin oligosaccharides. In parallel, docking calculations of heparin binding were also performed (Veverka *et al.,* 2009). The heparin binding site on sclerostin was mapped as a linear positively charged patch of largely arginine and lysine residues side chains, with eight of the residues located on the β-finger loop 2 (f2 loop) and four in the disoriented loop of the wrist region (refer to Figures 1.7B and 6.1), (Veverka *et al.,* 2009).

It follows that the initial homology modeling upon which this current study was based, employed the NMR structure of sclerostin to generate predicted models of all CAN family members (Rider and Mulloy, 2010). Their docking calculations predicted that all CAN family members except for DAN and Cerberus, but including gremlin, would possess heparin binding capabilities. It is these predictions which led to the hypothesis that gremlin possesses a specific heparin binding site, which would be constituted largely of positively charged arginine and lysine residues. As revealed in this study, these were present within the primary sequence of the gremlin precursor as three main basic clusters, basic clusters I (86 – 91), II (145 – 148) and III (166 – 177). Also notable is the analysis that two out of three basic clusters (basic clusters II and III) are located on the f2 loop (refer to Figure 3.4) within the cystine-knot domain which spans amino acid residues 94 – 184 (Pearce *et al.,* 1999). Interestingly, these three basic clusters are absent in both DAN and Cerberus (refer to Figure 3.4). On this basis, strategic site-directed mutagenesis was targeted on these basic clusters of wildtype gremlin which involved substituting predicted contact arginine and lysine residues with

mostly polar and nonpolar residues possessing neutral side chains, taken from the homologous sequence clusters on either DAN or Cerberus.

As was discussed earlier in Chapter 3, Section 3.3, a standard strategy to site-directed mutagenesis is alanine-scanning mutagenesis which in this context introduces clusters of alanine residues possessing relatively smaller side chains in place of the targeted basic clusters on gremlin (Morrison and Weiss, 2001). The substitution with alanine residues in tandem is not ideal in this case particularly, as it introduces fairly hydrophobic residues at the surface of the gremlin protein and may allow for much flexibility in the β-finger loops because of the small size of the alanine side chains. Therefore this might lead to misfolded gremlin mutants with incorrect cysteine-cysteine pairing. On the other hand, it seems the approach of homologous substitution is ideal as it allows for better chances to retain the conserved cysteine partners within the cystine-knot motif in appropriate orientations and spacing so that the correct disulfide bridges are also retained in the expressed mutants.

The use of such strategic site-directed mutagenesis within the cystine-knot domain of gremlin has a precedent which also argues in favour of the likelihood of correct folding of the gremlin-Myc mutants expressed in this current study. Sun *et al.* (2006) when mapping the BMP-4 binding site on wildtype gremlin-His, cloned and expressed eight different gremlin mutants by substituting sequence clusters along the β-finger loops bonded by cysteine residues. These substitutions were done with sequence clusters from homologous regions of the Mucin-2 cystine-knot domain. Mucin-2 is a distant homologue to CAN family members possessing a similar eight-membered cystine-knot ring, although it is not a BMP antagonist (Forstner *et al.*, 1979). Importantly, in spite of substituting sequences up to 74 amino acid long that spanned across both β-finger loops and which represents approximately 40% of gremlin, an active gremlin chimera capable of BMP-4 binding was still generated. This implied that despite substituting such large sequence cluster on gremlin, its overall tertiary fold was not perturbed (Sun *et al.*, 2006). Moreover, the same results was achieved even by deletion of a sequence cluster of 60 amino acids (32% of the entire structure) in the N-terminal region outside its cystine-knot domain thus yielding a truncated gremlin protein but with a correctly folded cystine-knot motif (Sun *et al.*, 2006). Comparatively, in this current study, the largest combined substitutions encompassed a total six amino acid residues, which represents only approximately 3% of the entire

structure. Therefore, it is highly unlikely that the mutations carried out in this study changed the overall tertiary structure of the gremlin-Myc mutants expressed.

Markedly reduced binding to heparin was demonstrated in six C-Myc-tagged gremlin mutants, MGRs 1 – 6, possessing different mutations of the basic clusters I – III compared to the wildtype gremlin-Myc (refer to Table 3.2 and Figures 4.11 and 4.16). This was observed using both the heparin-binding ELISA, and analytical heparin affinity chromatography. In the latter, the wildtype peak immunoreactivity eluted on average at 0.8 M NaCl which was in line with the previously reported high NaCl molarity required for its elution (Stabile *et al.,* 2007). In their work the major peak of activity of gremlin eluted at 1 M NaCl from a preparative column of heparin-Sepharose. It is highly probable that this discrepancy in gremlin elution peaks might have been due to the column loadings; 2 ml wildtype gremlin-Myc CHO-S culture supernatant in the current study versus 21 L conditioned medium of FGF2-T-MAE cells. Moreover, the difference in column sizes might have equally contributed to the discrepancy; 200 µl AF heparin HC650M bead column used in this current study versus 10 ml heparin-Sepharose column used by Stabile *et al.* (2007). A similar elution peak ranging from 0.8 – 1 M NaCl was reported previously for the NaCl elution of the wildtype BMP antagonist Noggin from an analytical heparin-Sepharose column (Paine-Saunders *et al.,* 2002). Because Noggin has an established physiological relevant interaction with HS *in vivo* in restricting diffusion of BMP morphogens, this strongly suggests that wildtype gremlin-Myc may also bind to HS on cell surfaces to yield a relevant physiological response (Paine-Saunders *et al.,* 2002).

In contrast to wildtype gremlin-Myc, the elution peaks for all the gremlin-Myc mutants was between 0.32 – 0.42 M NaCl which represented approximately 47.5 – 60% reduction in heparin binding of the wildtype. Paine-Saunders *et al.* (2002) demonstrated that a functionally active low-heparin binding Noggin deletion mutant, hNogΔB2, that showed no detectable binding to HS on cell surfaces, eluted between 0.2 – 0.4 M NaCl from a heparin-Sepharose column. This represented approximately 50 – 80% reduction in heparin binding of wildtype Noggin, thus demonstrating that complete abrogation of heparin binding in the gremlin mutants is not a prerequisite for further investigation of their interaction with HS. By markedly affecting the heparin binding of wildtype gremlin using targeted site-directed mutagenesis, these results demonstrated that all of its three contact basic clusters, I – III, contribute to the putative heparin binding site.

As shown in Figures 6.1 and 6.2A, these key arginine and lysine residues within the heparin binding site on gremlin are located mostly on both its β-strands 3 (basic clusters II) and 4 (basic cluster III) that form the f2 loop. The two contact residues of basic cluster I, which constitute the few, are located just outside the β-strand 1 on the disordered N-terminal tail loop (refer to Figures 6.1 and 6.2A).

6.2 Mapping of the heparin binding site on the predicted gremlin model based on the crystal structure of PRDC

Whilst this study was underway, the crystallographic structure of a second CAN family member, PRDC, the closest homologue to gremlin, was elucidated (refer to Figure 1.8), (Nolan *et al.*, 2013). On this structure, those workers were able to map experimentally the BMP binding site on PRDC and also predict its heparin binding site (refer to Chapter 1, Section 1.8.3). The heparin binding site was predicted by scanning its electrostatic surface during which positively charged patches constituted of similarly charged basic amino acid residues were mostly located on the f2 loop with a few residues in the α1 N-terminal helical tail region (refer to Figures 1.8 and 1.9), (Nolan *et al.*, 2013).These recent findings necessitated the remodelling of the gremlin structure based on this new PRDC template with fresh docking calculations. These were then compared against the sclerostin-based mapping predictions upon which this current study was based.

Shown in Figures 6.2 A and B are the predicted monomeric gremlin structures as based on either sclerostin or PRDC, respectively. Noticeably, the PRDC-based gremlin monomer (Figure 6.2B) possesses more extended β-finger loops and a shortened disordered loop in the wrist region compared to the sclerostin-based model (Figure 6.2A). Also present in the former predicted structure, is a flexible and disordered N-terminal tail possessing an α1 helical coil. Importantly, it can be seen that both predicted structures agree on the location of the putative heparin binding site on gremlin in that it is located mostly on both its β-strands 3 and 4 that form the f2 loop with a the few located just outside the β-strand 1 on the disordered N-terminal tail loop (refer to Figures 6.1 and 6.2A).

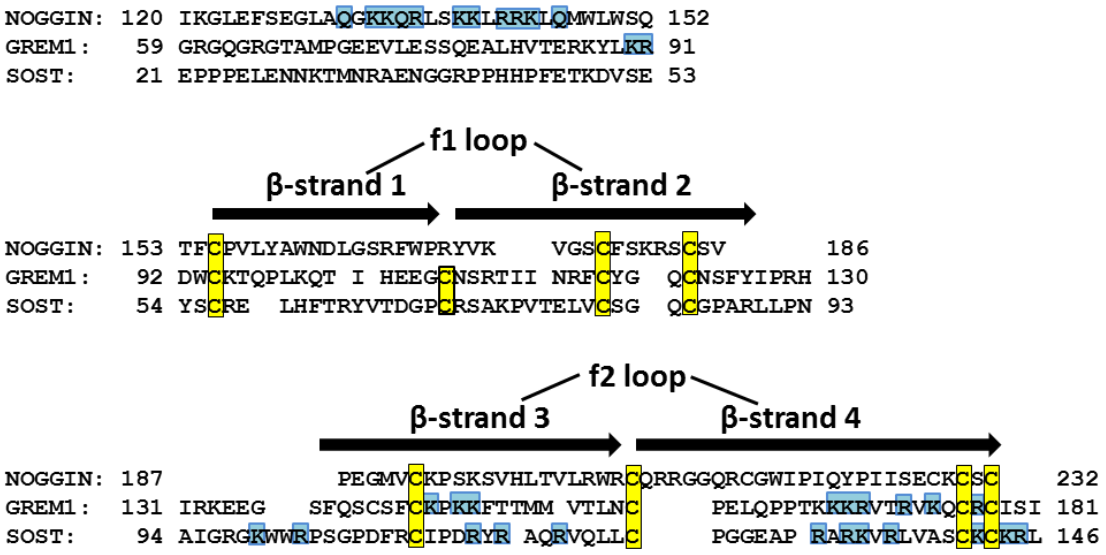

Figure 6.1: Polypeptide sequence alignment of the experimentally mapped heparin binding site on Noggin, gremlin and sclerostin.

Highlighted in light blue are the amino acid residues that form their putative heparin binding sites. Highlighted in yellow are the conserved cysteine residues.

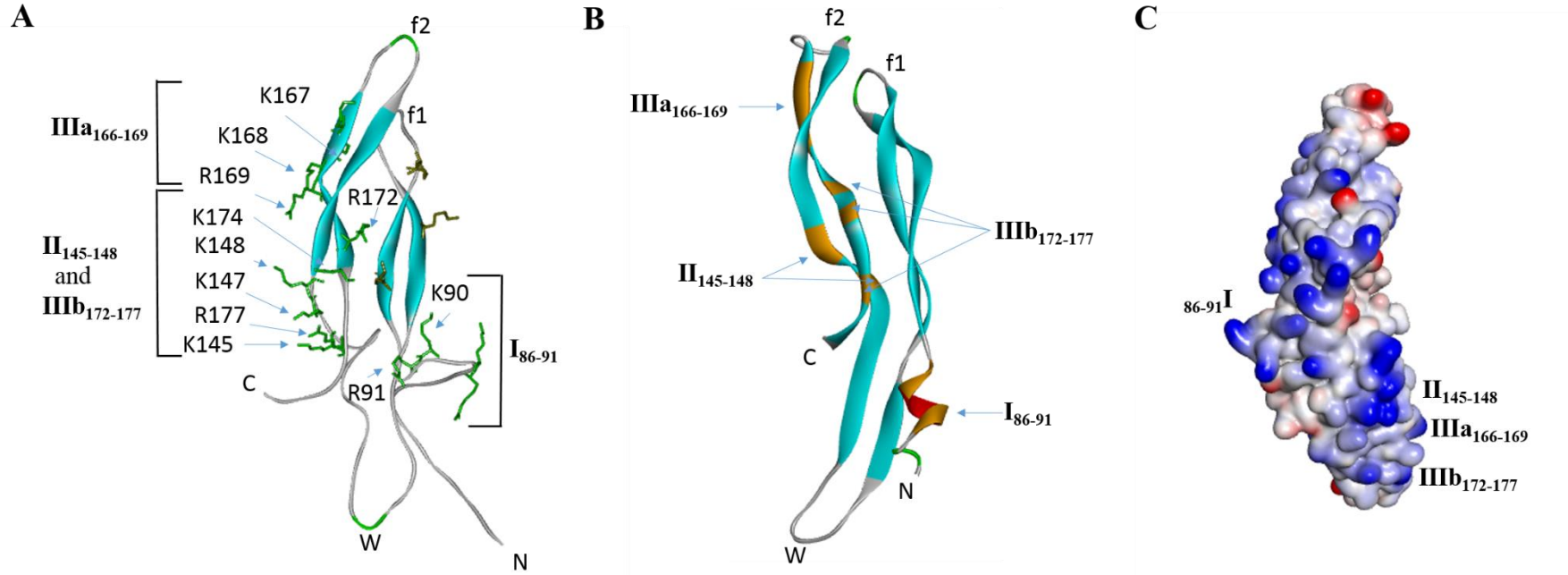

Figure 6.2: Mapping the heparin binding site on predicted wildtype gremlin models.

The experimentally mapped heparin binding site on wildtype gremlin which constitutes of three main basic clusters, basic clusters I – III, shown here on: A) monomeric wildtype gremlin model based on the NMR structure of sclerostin (PDB file: 2K8P). B) Monomeric wildtype gremlin model based on the crystal structure of PRDC (PDB file: 4JPH). C) The electrostatic surface of a dimeric wildtype gremlin model based on PRDC showing one of two heparin binding sites present on the same gremlin molecule. The surface coloured according to their electrostatic potentials: In blue colour are the basic amino acid residue side chains and in red colour are the acidic amino acid residue side chains. Models shown are in the same orientation with fingers pointing upwards. f1 and f2 both denote a paired β-finger loop. W denotes the wrist region. Homology modeling was conducted on the SWISS-MODEL server by our collaborator Professor Barbara Mulloy, Royal Holloway, University of London.

6.3 Comparison of experimentally mapped heparin binding sites within the BMP antagonist family

Altogether, this work establishes gremlin as the second CAN family member after sclerostin and third BMP antagonist including Noggin, to possess an experimentally mapped heparin binding site. A sequence alignment highlighting the experimentally mapped contact amino acid residues forming the heparin binding site on Noggin, gremlin and sclerostin is shown in Figure 6.1. Despite exhibiting high structural similarity, some differences are observed in the location and distribution of the heparin binding site on these BMP antagonists. In Noggin, all contact residues are located outside its cystine-knot domain and based on the three-dimensional structure of its dimer, are clustered exclusively in the wrist region at the tip of the associating α-helical loops where the two monomer heads join thus forming a single heparin binding site (Groppe *et al.,* 2002). By contrast the CAN family members, sclerostin and gremlin share much closer resemblance in the location of their heparin binding sites with the majority of the key contact residues located on the f2 loop (Figure 6.1). However in addition to observing subtle differences in the distribution of the basic contact residues within the f2 loop, the N-terminal tail loop on gremlin is also involved in heparin binding (Figure 6.2B) whereas in sclerostin, its disordered loop in the wrist region is involved instead (Veverka *et al.,* 2009). These findings indicate that the heparin binding site on BMP antagonists has not remained conserved through evolution unlike their structural tertiary folds. This may perhaps explain the diverse roles of HS observed in its interactions with BMP antagonists and other cytokines.

6.4 Nature of the binding interaction between gremlin and heparin

As a highly acidic biomolecule, HS binds to a diverse spectrum of growth factors, cytokines and morphogens such as FGFs, epidermal growth factors (EGFs), interleukins -2, -6 and -12, IFNγ, TGFβ-1, and some neurotrophic factors, BMPs and BMP antagonists (Rapraeger *et al.,* 1991; Lortat-Jacob, 1996; Hsu *et al.,* 1998; Mummery and Rider, 2000; Alfano *et al.,* 2007; Kuo *et al.,* 2010). It is widely believed such binding interaction is stabilised mainly via purely electrostatic interactions between the exposed positively charged residues on protein surfaces and the side chain carboxylate and sulfate acidic groups on HS polysaccharides. However, some findings strongly indicate that these heparin binding proteins may exhibit a strong element of specificity with particular heparin/HS centered on a specific sequence context. A

classic example of this is the unique pentasaccharide recognition sequence on heparin that is required for binding to and full activation of antithrombin III which is centered on a rare 3-*O*-sulfated glucosamine (Rosenberg and Lam, 1979; Lindahl *et al.*, 1980). Considering heparin is highly heterogeneous, the discovery of such specific sequence was evidence that the sequence of heparin/HS can contain biochemical information. This recognition sequence on heparin for antithrombin III, remains to date uniquely specific of the interaction of heparin-binding proteins with heparin. Despite extensive studies on other heparin-binding proteins, particularly the FGFs, a consensus sequence counterpart to the antithrombin III pentasaccharide recognition sequence on heparin has yet to be defined.

On the other hand, the mapping of a specific heparin binding site on the heparin-binding proteins themselves, has contributed considerably to the argument in favour of specific binding of heparin/HS to these proteins. These have been well documented elsewhere (Hileman *et al.*, 1996; Xu and Esko, 2014). Together, these share the notion that the heparin binding site is constituted largely of basic arginine and lysine residues and that its binding interface with heparin is stabilised mainly by specific ionic interactions. This forms the basis for surrogate measurements of binding affinity and specificity of gremlin to heparin in this current study by varying the ionic strength at constant pH.

This study further showed that elution peaks of both the wildtype and its mutants, ranged between 0.2 – 0.42 M NaCl on columns of the simple cationic exchanger SP-Sepharose. These demonstrated weaker binding of gremlin-Myc proteins to SP-Sepharose columns compared to heparin. A similar study was conducted by Proudfoot *et al.* (2001), in which the elution of the chemokine RANTES (regulated on activation normal T cell expressed and secreted) and its various mutants possessing mutations in the predicted heparin binding site was compared on heparin columns and Mono S cation-exchanger columns. Here too, higher elution peaks on the heparin column hence stronger binding to heparin compared to binding onto the Mono S column was observed in the wildtype and most of its mutants. By subtracting each elution peak value on the Mono S column from the corresponding elution peak value on the heparin column, a positive difference was indicative that mutated residues incorporated by the mutants played a role in specific interaction with heparin (Proudfoot *et al.*, 2001). Interestingly, applying similar analyses to this current study would demonstrate a positive difference between the elution peaks of all gremlin

mutants on the heparin and SP-Sepharose columns (refer to Table 4.1, Chapter 4). Therefore, this strongly indicates that the three targeted basic clusters present on wildtype gremlin-Myc favour its specific ionic binding to heparin.

Furthermore, the findings that increasing the ionic strength inhibited binding of wildtype gremlin-Myc to the heparin-BSA capture layer in heparin-binding ELISA were a further strong demonstration that their binding interaction is mainly coulombic. This is consistent with previous findings in which a similar nature of interaction has been demonstrated between heparin and several heparin-binding proteins such as Noggin, sclerostin, RANTES, betacellulin, IL-12 and GDNF (Mummery and Rider, 2000; Proudfoot *et al.,* 2001; Paine-Saunders *et al.,* 2002; Alfano *et al.,* 2007; Veverka *et al.,* 2009). These argue in favour of electrostatic interactions as the main stabilising bonds being specific between sulfate groups on heparin and positively charged arginine and lysine side chains on the proteins. Therefore, by validating the hypothesis that there is a specific heparin binding site on gremlin, which is constituted largely of arginine and lysine residues, mapping of the heparin/HS binding site on gremlin has been achieved successfully in this study.

There is however a potential weakness in studies, such as this current study, that rely on changes in ionic strength at constant pH as a surrogate measure of heparin binding affinity. These assume that the contribution of nonionic interactions towards heparin binding, is not significant. This point is well argued in the findings of Thompson *et al.* (1994) using a combination of site-directed mutagenesis, heparin affinity chromatography and isothermal titrating calorimetry to analyse the contribution of individual bFGF amino acid residues at the binding interface of a bFGF-heparin pentasaccharide co-crystal. Although 7 out of 11 contact amino acids were positively charged, the pure electrostatic interactions with sulfated groups on heparin contributed to only 30% of the free binding energy. As mentioned earlier in Chapter 1, Section 1.13, this unexpectedly low free binding energy contribution by electrostatic interactions alone may be explained. It may have reflected changes to the bFGF structure following its electrostatic attraction to heparin thus leading to a more rigid protein structure as new bonds are formed. As such, specific nonionic interactions such as Van der Waals and hydrogen bonding at this interface contributed the majority thus demonstrating the significant contribution of nonionic interactions in heparin binding. Therefore, by assessing only the ionic interactions of gremlin and heparin, our analysis of this interaction is limited. However, overall the experimental mapping of the heparin

binding site on gremlin also validated the mapping predictions made by Rider and Mulloy, (2010) with respect to gremlin. This achievement indicates that the molecular dynamic simulation on which the prediction was based, is a powerful tool for predicting the heparin/HS binding sites on heparin-binding proteins.

6.5 Effects of Myc and His tags on gremlin binding to heparin/HS

Since the commercially purified 10X polyHis-tagged wildtype gremlin and the expressed wildtype C-Myc-tagged gremlin showed a similar IC_{50} value of 10 µg/ml, this study suggests that neither Myc nor polyHis tags on wildtype gremlin are likely to affect its heparin binding. This was shown by immunoassay of both proteins using the heparin-binding ELISA in its competitive format with soluble unfractionated heparin. Because a K_d value of 20 nM has previously been reported by Chiodelli *et al.* (2011) for high affinity binding of gremlin to immobilised heparin on SPR biosensor chips, it can be assumed that the wildtype gremlin-Myc protein will share similar binding affinity. The potential risk of using the polybasic 10X His-tagged wildtype gremlin in this heparin binding study has been discussed fully in Chapter 4, Section 4.10. In short, reports by Lacy and Sanderson (2002) and by Alfano *et al.* (2007) both demonstrated that the presence of a polyHis tag on heparin-binding proteins can generate an artefactual heparin/HS binding site. Although these reported results represent a novel finding, they are not generalizable to all heparin-binding proteins emphasising need for similar investigations on an individual basis. Nonetheless, it was deemed important in the current study to avoid the use of the polyHis tag in the investigations of the heparin binding properties of gremlin.

6.6 Effects of soluble heparin on gremlin interaction and its BMP ligands

Binding of Noggin to HS on cell surfaces of CHO-K1 cells has been observed *in vitro* (Paine-Saunders *et al.*, 2002). This binding was argued to restrict the diffusion of Noggin hence HS forms a local depot for circulation cytokines. Using pulse-chase experiments, addition of soluble intact heparin to cells rapidly displaced Noggin from the plasma membrane thus accumulating in the medium. This implied that HS is required for the cellular uptake of Noggin. When using the low-heparin binding hNogΔB2 mutant, its accumulation in the medium in the absence of soluble intact heparin was indicative of its lack of HS binding activity. Since hNogΔB2 remained functionally active as a BMP antagonist, this demonstrated that the heparin binding

domain on the wildtype is independent of its BMP antagonist activity (Paine-Saunders *et al.,* 2002). Based on these findings, a model may be proposed in which formation of a trimeric BMP:Noggin:HS complex favours the HS- and Noggin-mediated restricted diffusion of BMP activity gradients. In this current study, the same question was posed as to whether a trimeric BMP:gremlin:heparin/HS complex was also possible, and whether this either promotes or inhibits the interaction of gremlin and its BMP ligands.

In this study, it was revealed that addition of soluble unfractionated heparin in the Myc-capture GREM1/BMP-4 double sandwich ELISA neither promoted nor inhibited the binding interaction of wildtype gremlin-Myc and BMP-4. These findings allow for the formation of a trimeric BMP:gremlin:heparin/HS complex but does not answer the question on its effect on the interaction of gremlin and its BMP ligands. However, the fact that these experiments were conducted on an immobilised heparin-BSA capture layer, which is different from the dynamic binding interactions on cells may limit these observations. Our findings contrast with those of Nolan *et al.* (2013) on PRDC. They demonstrated in SPR experiments that pre-incubation of PRDC with increasing concentrations of both soluble unfractionated heparin and tinzaparin (5.5 – 7.5 kDa) inhibited its binding to immobilised BMP-2 ligands. On the PRDC crystal structure, the experimentally mapped BMP binding site and predicted heparin binding site are located in close proximity on its cystine-knot domain. To explain these findings, a regulatory mechanism was suggested in which heparin ligand binding to its binding site on PRDC triggered allosteric modifications of the nearby BMP binding site thus inhibiting its binding to BMP-2 ligands (Nolan *et al.,* 2013). Therefore, the current findings that heparin neither inhibited nor promoted the binding interaction of wildtype gremlin-Myc and BMP-4 using the double sandwich ELISA strongly indicated at least that its BMP-4 and mapped heparin binding sites do not compete with each other for their ligands. Equivalent BMP-4 immunoreactivities using wildtype and MGR5 on this double sandwich ELISA, strongly demonstrated that their BMP binding activity is not affected by changes to the heparin binding domain; the same heparin binding property observed in Noggin (Paine-Saunders *et al.,* 2002). Overall, this current study demonstrates that both BMP and heparin binding sites exist on gremlin and are physically distinct and may be independently regulated.

6.7 Refining the location of the BMP binding site on gremlin

The crystal structure of the Noggin-BMP-7 complex was discussed in Chapter 1, Section 1.6. In this complex, binding of the BMP dimer to the Noggin dimer occurs at the convex interface of the β-finger loops projecting on opposite sides of its head-to-head oriented homodimer (refer to Figure 1.6). This binding interaction is stabilised mainly by hydrophobic interactions involving the insertion of a hydrophobic side chain from a flexible backbone segment on Noggin into a hydrophobic pocket on BMP-7 (Groppe *et al.*, 2002). In contrast, Sun *et al.* (2006) in their experimental mapping of the BMP binding site on gremlin, claimed that it is constituted largely of positively charged arginine and lysine residues and that the binding interaction between gremlin and BMPs is mainly electrostatic. The experimental mapping of the heparin binding site on wildtype gremlin in this current study using site-directed mutagenesis enabled partial verification into the claims made by Sun *et al.* (2006). Within the primary sequence of gremlin, Sun *et al.* (2006) identified a 30 amino acid region as the putative BMP-4 binding site that ranged between amino acids 146 – 175 within the cystine-knot domain. According to Figure 3.4, Chapter 3, this represents the full β-strand 3 and almost half of β-strand 4 of the f2 loop on gremlin which seems an impressively large region to serve as a legitimate binding site on any protein. Also, it can be seen from the same figure and Figure 6.1, as well, that this region largely incorporated both basic clusters II (145 – 148) and III (172 – 177) on gremlin, which had been substituted in MGRs 3 – 5. Tests using both IP and the double sandwich ELISA indicated that MGR5 and arguably MGR3, both possessed BMP-4 binding capabilities in spite incorporating substitutions within this same 30 amino acid region. The added fact that these substitutions here were of arginine and lysine residues which Sun *et al.* (2006) claimed mediated charge type interactions between gremlin and its BMP ligands, eliminated them as potential contact residues for BMP binding. These refinements would, therefore, confine their mapped BMP-binding site to an 18-amino acid region, spanning amino acids 149 – 166, which is largely constituted of a hydrophobic cluster instead; FTTMMVTLNCPELQPPTK. In addition to concurring with findings from the Noggin-BMP-7 complex discussed earlier, these novel refinements also concurs with experimental mappings by Nolan *et al.* (2013) on the nature of BMP binding site on PRDC whose structure was fully discussed in Chapter 1, Section 1.8.3. The BMP binding site on the PRDC dimer is constituted of Trp-93, Tyr-119, Phe-125, Tyr-126 and Phe-138 that form a hydrophobic patch on the convex binding surface of its

cystine-knot domain thus strongly indicating binding to its BMP ligands via mainly hydrophobic interaction (refer to Figure 1.9, Chapter 1). Interestingly, as all of these residues are conserved in the primary sequence of gremlin, it is possible that these together with those in the refined BMP binding site above, may form the putative BMP binding site on gremlin. Eitherway, the claim by Sun *et al.* (2006) that a sequence of 30 amino acids forms the putative BMP binding site on gremlin through ionic interactions with BMP ligands is doubtful. The experimental mappings of the BMP binding site on the PRDC crystal structure (Nolan *et al.,* 2013) and now of the heparin binding site on gremlin achieved in this current study, have both demonstrated otherwise.

Interestingly, according to the Nolan *et al.* (2013) mapping, the BMP binding site on the PRDC-based gremlin structure appears to be located mainly on the concave surface of the f1 loop (refer to Figure 1.14). This differs from its experimentally mapped heparin binding site which is more confined to the f2 loop and N-terminal tail loop (refer to Figures 6.1 and 6.2 A and B) thus supporting the physically distinct nature of both binding sites on gremlin, as argued previously.

6.8 Significance of the BMP antagonist activity of wildtype gremlin-Myc versus mutants

In the current study, it was established that concentrated wildtype gremlin-Myc and MGRs 5 and 6 mutants were all functionally active, as shown by their antagonism of BMP-4-SMAD1/5/8-induced signalling, *in vitro*, using the secreted luciferase reporter assay established in C2C12 myoblastic cells. A major caveat in these analyses was the difficulty to measure accurately the concentration of these gremlin-Myc proteins present in their culture supernatants. However from best estimates, it seems the concentrated wildtype gremlin-Myc possessing an intact heparin/HS binding site is more functionally active than both mutants which both possess a mutagenized heparin binding site. This indicates that the heparin/HS binding domain on the wildtype may play some role in the BMP antagonist activity of gremlin. Thus, it would be interesting to re-investigate in this functional reporter assay, the effect of soluble heparin on the BMP antagonist activity of gremlin. All in all, the results demonstrate that cloning of gremlin-Myc mutants possessing reduced heparin binding capabilities but yet remaining functionally active has been achieved successfully in this study.

6.9 Gremlin binds to heparan sulfate on cell surfaces

In this study, binding of wildtype gremlin-Myc to heparin at physiological ionic strength (0.18 M NaCl) and pH (pH 7.4) was demonstrated, but its binding to HS was not investigated. Nonetheless, there is convincing evidence that gremlin does bind HS. Chiodelli *et al.* (2011) demonstrated wildtype gremlin bound to the cell surface of CHO-K1 cells and that this binding was inhibited by soluble heparin and HS. Moreover, binding of gremlin to bovine aortic endothelial cells was prevented by pretreatment with either heparitinase II or chlorate thus demonstrating that HS is essential for gremlin binding to cell surfaces (Chiodelli *et al.,* 2011). More recently, this was also demonstrated by a fellow postgraduate in our laboratory investigating binding of the wildtype and mutant gremlin-Myc proteins expressed in this current study to the cell surfaces of C2C12 cells and mouse kidney tissue sections using immunohistochemistry. At equalised gremlin-Myc immunoreactivities on the basis of the Myc-capture gremlin ELISA, 9E10 anti-Myc immuno-fluorescence generated by MGRs 3, 5 and 6 on the cells was considerably weaker than that of wildtype gremlin-Myc at physiological conditions (Askew, unpublished observations). Furthermore, their binding to both C2C12 cells and kidney tissue sections was abolish by pre-incubation with intact heparin. Therefore, our laboratory has demonstrated a marked decrease in the binding of these gremlin-Myc mutants to cell surface HS as a direct consequence of the strategic site-directed mutagenesis conducted herein. Unless the individual domain specificity along heparin and HS chains are not known, it will be misleading to attribute differences in protein binding affinities to their overall sulfation patterns as HS can be more or less sulfated.

6.10 Does gremlin forms a dimer?

As earlier introduced, Noggin and CV2 (refer to Chapter 1, Section 1.6), and including most BMPs themselves (refer to Figure 1.3), form covalently-linked dimers via their unpaired cysteine residue located just outside the cysteine-knot motif. As stated by Veverka *et al.* (2009), sclerostin is an atypical member of the cystine-knot family as it showed no evidence suggesting it dimerizes unlike several of its experimentally resolved cystine-knot homologues that form typically, homo- and hetero-dimeric structures via an interchain unpaired Cys:unpaired Cys bridge (Rider and Mulloy, 2010). More recently, it is now known that PRDC forms a homodimer in its crystal (PDB file: 4JPH; Nolan *et al.,* 2013). However, the PRDC dimer in itself is

not without peculiarity; it forms a head-to-tail oriented dimer that oddly, is stabilised by noncovalent interactions not via the unpaired cysteine residue (Nolan *et al.*, 2013). It is interesting that in spite of possessing the same unpaired cysteine residue (refer to Figure 1.9), PRDC does not follow the common mechanism of dimerization. This as well may help explain how the family of closely related BMP antagonists have evolved structurally to exhibit diverse biological activities. Since PRDC is the closest homologue to gremlin, which also possesses the unpaired cysteine residue (refer to Figure 1.9), this raises the important question as to whether gremlin also exists as a dimer based on the novel mode of dimerization.

As was introduced earlier in Chapter 1, Section 1.16, the gremlin model based on PRDC forms a homodimer (refer Figure 1.14 and 6.2C). Notably, the contact amino acid residues at the binding interface joining both monomers in PRDC (F96 – I106) are conserved in gremlin (F117 – I127), (refer to Figure 1.9). This is a further argument in favour of the PRDC-based gremlin model over the sclerostin-based gremlin model, the first on basis of structural homology. This brings into question whether there is a single or two separate heparin binding sites on gremlin, if a dimer. According to the dimeric gremlin model, two separate heparin binding sites are present which are located on opposite sides of the dimer (refer to Figure 1.14; not shown in Figure 6.2C). This is relevant, as it indicates that heparin/HS may not play a role in promoting gremlin oligomerization unlike observations with most chemokines as a classic example. At physiological concentrations, these chemokines exist in dynamic equilibrium shifting between the monomeric and dimeric conformations. However their interactions with HS have been shown to drive the equilibrium toward the formation of dimers or high-order oligomers (Hoogewerf *et al.,* 1997; Proudfoot *et al.,* 2003; Lortat-Jacob, 2009; Salanga and Handel, 2011).

A simple approach to testing whether a protein dimerizes is by carrying out SDS-PAGE under both non-reducing and reducing conditions. In this current study on gremlin and that of Kattamuri *et al.* (2012) on PRDC, ambiguous results were produced on such tests; it was difficult to assess accurately the difference in migration of both proteins in both non-reducing and reducing polyacrylamide gels. Further work investigating whether gremlin forms a dimer is currently underway in our laboratory. Essentially, this work employs the experimental approach published by Kattamuri *et al.* (2012) of cross-linking 3 µg PRDC protein samples with 0.01% (v/v) glutaraldehyde. Attempts to cross-linking wildtype gremlin-Myc with glutaraldehyde have used varying

concentrations (0.01 – 0.05% (v/v)), neutralizing with 1 M Tris pH 8. The samples were then separated by SDS-PAGE under non-reducing conditions followed by Western blotting using a polyclonal gremlin primary antibody as were described earlier in Chapter 2, Sections 2.23 and 2.25, respectively. By using this approach, the crude wildtype gremlin-Myc culture supernatants pose two difficulties: firstly, the low amounts of wildtype gremlin-Myc protein present in crude culture supernatants may be limiting to this work. This may be resolved by using concentrated material instead. Secondly, the presence of an unknown 50 kDa protein in the cell culture supernatants may confound these tests as its molecular weight matches that expected of the gremlin dimer. Thus far, it has been demonstrated that this unknown protein does not bind to SP-Sepharose matrices (refer to Chapter 4, Section 4.4). Thus the issue of dimerization may be resolved by running a large volume of the crude culture supernatant on an SP-Sepharose column and eluting at an NaCl concentration just above the known elution peak of the wildtype, as was determined in this current study (refer to Chapter 4, Section 4.9). The cross-linking work could then be performed on the dialysed eluate containing the partially-purified wildtype gremlin-Myc protein.

Preliminary results support dimerization of wildtype gremlin-Myc. In cross-linked samples, the disappearance of the gremlin immunoreactive band at 25 kDa is consistent with a loss of the monomer however detection of the expected gremlin dimer immunoreactive band at 50 kDa has yet to be achieved. It is plausible that the cross-linking may occur in a way that blocks access of the gremlin antibody to its epitopes on the gremlin dimer. Nonetheless, more work is needed to resolve this issue.

6.11 Limitations of this study

A major limitation in this study was the relatively low levels of expression of gremlin-Myc proteins in crude CHO-S cell culture supernatants. This was persistent throughout the study and therefore, limiting to its findings. It is generally known that cysteine-rich proteins are difficult to express in both bacterial and mammalian expression systems (Sermadiras *et al.,* 2013). The fact that proteins such as wildtype gremlin and its mutants possess a cystine-knot motif, which forms a complicated tertiary structure makes their recombinant expressions even more challenging (Schmoldt *et al.,* 2005). Correct folding requires that three disulfide bonds form between the six cysteine residues that form the native cystine-knot motif. Therefore, this limitation in gremlin-Myc levels of expression is a problem for all cysteine knot

proteins, not affecting this study alone. Moreover, given that bacterial expression systems are not suitable for proteins that undergo extensive post-translational modifications including disulfide bridge formation, the expression of gremlin-Myc proteins in their native glycosylated and phosphorylated forms was achievable only in mammalian expression systems (Topol *et al.*, 2000a; de Marco, 2009). The total volume of crude gremlin-Myc culture supernatants harvested following transient transfections was limited by the scaling up of the transient transfection cultures. The alternative of stable transfections could have been considered except that this is not practicable for protein expressions intended for use on analytical basis. Transient transfections provided a rapid and cost effective method of expressing several different gremlin-Myc proteins for comparison of their heparin binding capabilities following site-directed mutagenesis.

Furthermore, a loss in wildtype gremlin-Myc immunoreactivity is observed upon long term storage of the partially-purified form over two weeks at -20 °C without multiple freeze-thawing. This suggests that recombinant gremlin-Myc proteins may be prone to proteolytic degradation and may be unstable in the absence of protease inhibitors and carrier protein when in crude or partially-purified forms, respectively. These findings together with the use of only transient transfections, limited the work in this study using purified gremlin-Myc proteins instead.

6.12 Future work

The successful expression of functionally active wildtype gremlin-Myc and its mutants, MGRs 5 and 6 both possessing reduced binding to HS, raised the issue into future experiments investigating the role of HS in the interaction of gremlin and its BMP ligands. Such tests can be conducted using the same C2C12-luciferase reporter assay that was successfully established in this study. The role of HS can then be tested by treating cells with heparitinase and chlorate that will strip them off their cell surface HS and block sulfation in general, including that in nascent HS chains, respectively. It should be interesting to compare side-by-side the wildtype to both MGRs 5 and 6, which will demonstrate further whether HS is essential for gremlin antagonism of BMP signalling activities *in vitro.* When using the double sandwich ELISA, it was demonstrated that heparin neither inhibited nor promoted the binding interaction of wildtype gremlin-Myc and BMP-4. It would be interesting to test whether this remains the case in the dynamic setting of the cell surface that this functional assay offers as

well. In previous findings by Kuo *et al.* (2010), a catalytic coreceptor role of HS was suggested in promoting heteromeric types I and II receptor complexes, but not remaining stably associated with the BMP-receptor signalling complex. In their study, reduced BMPs -2 and -4-induced SMAD1/5/8 phosphorylation was observed in both heparitinase- and chlorate-treated C2C12 and PC12 cells. Interestingly, a non-heparin binding BMP-2 mutant, EMBMP2, was resistant to the same treatments, which rather indicated that BMP-2 binding to HS is not essential for BMP-2 signalling (Kuo *et al.*, 2010). However, the fact that this BMP-2 mutant was expressed in bacteria that are unable to incorporate the post-translational modifications present in the native BMP-2 protein itself, makes the findings uncertain. The comparative use of wildtype and low heparin-binding gremlin-Myc mutants incorporating similar post-translational modifications makes this an insightful investigation.

6.13 Conclusion

Overall it can be said that the findings in this study herein have advanced our understanding on the heparin binding properties of gremlin. Gremlin can now be included alongside sclerostin and Noggin in the repertoire of BMP antagonists with an experimentally mapped heparin binding site. In these BMP antagonists, the heparin binding site is constituted largely of interspersed basic clusters of arginine and lysine residues which drive their specific ionic interactions with acidic sulfate groups on heparin and HS chains. Although the structural folds of these BMP antagonists have remained conserved through evolution, it is now apparent that the location of the heparin binding site on these structures has not remained so. This may be reflective of the diverse biological roles of HS within this family of closely related BMP antagonists. In gremlin, the heparin binding site has been mapped on its predicted f2 β-stranded paired loop and α1 helix in the flexible and disordered N-terminal loop; differing from that of the predicted BMP binding site situated mainly on the concave binding surface of its f1 β-stranded paired loop. This shows that heparin and BMP binding sites on gremlin are physically distinct.

Biochemically, it appears heparin is not essential in the binding interaction of wildtype gremlin and its BMP ligands, as it neither promoted nor inhibited their interaction. However, functional cell signalling studies offering dynamic binding interactions on cell surfaces may yet indicate otherwise.

There is strong evidence that the physically distinct BMP and heparin/HS binding site on wildtype gremlin-Myc are independent of each other. Two functionally active C-Myc-tagged gremlin mutants, MGRs 5 and 6 possessing markedly reduced binding to heparin retained their BMP-4 antagonist activity comparable to the wildtype. Also, evidence from another *in vitro* study in our laboratory (Askew, unpublished work), indicates that the mutants show markedly reduced binding affinities to some HS under physiological conditions. Therefore, the wildtype and both these gremlin-Myc mutants will serve as powerful tools in future investigations of the biological role of HS in gremlin-mediated activities.

Acknowledgements

I would like to start by remembering all those I have lost during the course of this project and prior to it, my grandmother, my uncle who was also a second dad to me and my dearest mother, Bekono Therese. May they rest in peace.

I would like to thank my father, Michel Tatsinkam for his active presence in all my endeavours. Herein, I particularly thank him for his sponsorship towards my studies including this doctorate degree. I would also like to thank the School of Biological Science, Royal Holloway, University of London for the three-year college research scholarship.

To my supervisor, Dr Chris Rider, it has been six truly special years we have journeyed together and as my mentor, guardian, and most importantly, my friend, I thank you for everything; 'The big picture.'

I am grateful for all the advice and guidance of my tutor, Pr George Dickson and also thank him and all members of the Dickson group for putting me in a position of trust, with access to their laboratory equipment.

I would like to thank our collaborator Pr Barbara Mulloy, for help with homology modeling and docking calculations and also for her trust in my work, and Dr Philip Chen, for help with molecular cloning particularly site-directed mutagenesis and for his feedback on this chapter. Particular thanks also to David McClarence for all his advice and strong support and to Joy Askew for her contributions via the MSc program.

Many thanks to all other members of my family particularly, my stepmother, Chantal Tatsinkam and my second uncle, Albert Kemgla, including all my brothers and sisters. Also, I would like to thank all friends particularly, Priyavudh Herabutya, Pradeep Harish and Paul De Saram.

And finally, to my best friend, Amanda Milani Noakes, thank you for the relentless motivation and emotional support during the past three years.

References

Aikawa, J., Grobe, K., Tsujimoto, M. and Esko, J. D. 2001. Multiple isozymes of h3eparan sulfate/heparin GlcNAc N-deacetylase/GlcN N-sulfotransferase. Structure and activity of the fourth member, NDST4. *J Biol Chem,* 276**,** 5876-82.

Alborzinia, H., Schmidt-Glenewinkel, H., Ilkavets, I., Breitkopf-Heinlein, K., Cheng, X., Hortschansky, P., Dooley, S. and Wolfl, S. 2013. Quantitative kinetics analysis of BMP2 uptake into cells and its modulation by BMP antagonists. *J Cell Sci,* 126**,** 117-27.

Alfano, I., Vora, P., Mummery, R. S., Mulloy, B. and Rider, C. C. 2007. The major determinant of the heparin binding of glial cell-line-derived neurotrophic factor is near the N-terminus and is dispensable for receptor binding. *Biochem J,* 404**,** 131-40.

Ali, I. H. and Brazil, D. P. 2014. Bone morphogenetic proteins and their antagonists: current and emerging clinical uses. *Br J Pharmacol,* 171**,** 3620-32.

Avsian-Kretchmer, O. and Hsueh, A. J. 2004. Comparative genomic analysis of the eight-membered ring cystine knot-containing bone morphogenetic protein antagonists. *Mol Endocrinol,* 18**,** 1-12.

Babitt, J. L., Huang, F. W., Wrighting, D. M., Xia, Y., Sidis, Y., Samad, T. A., Campagna, J. A., Chung, R. T., Schneyer, A. L., Woolf, C. J., Andrews, N. C. and Lin, H. Y. 2006. Bone morphogenetic protein signaling by hemojuvelin regulates hepcidin expression. *Nat Genet,* 38**,** 531-9.

Baeuerle, P. A. and Huttner, W. B. 1986. Chlorate--a potent inhibitor of protein sulfation in intact cells. *Biochem Biophys Res Commun,* 141**,** 870-7.

Balemans, W. and Van Hul, W. 2002. Extracellular regulation of BMP signaling in vertebrates: a cocktail of modulators. *Dev Biol,* 250**,** 231-50.

Berninsone, P. M. and Hirschberg, C. B. 2000. Nucleotide sugar transporters of the Golgi apparatus. *Curr Opin Struct Biol,* 10**,** 542-7.

Bitomsky W. and Wade R.C. 1999. Docking of glycosaminoglycans to heparin-binding proteins: validation for aFGF, bFGF, and antithrombin and application to IL-8. *J Am Chem Soc,* 121, 3004-13.

Bourin, M. C. and Lindahl, U. 1993. Glycosaminoglycans and the regulation of blood coagulation. *Biochem J,* 289 (Pt 2)**,** 313-30.

Brandan, E. and Hirschberg, C. B. 1988. Purification of rat liver N-heparan-sulfate sulfotransferase. *J Biol Chem,* 263**,** 2417-22.

Brown, M. A., Zhao, Q., Baker, K. A., Naik, C., Chen, C., Pukac, L., Singh, M., Tsareva, T., Parice, Y., Mahoney, A., Roschke, V., Sanyal, I. and Choe, S. 2005. Crystal structure of BMP-9 and functional interactions with pro-region and receptors. *J Biol Chem,* 280**,** 25111-8.

Campbell, P., Hannesson, H. H., Sandback, D., Roden, L., Lindahl, U. and Li, J. P. 1994. Biosynthesis of heparin/heparan sulfate. Purification of the D-glucuronyl C-5 epimerase from bovine liver. *J Biol Chem,* 269**,** 26953-8.

Camus, L. M. and Lambert, L. A. 2007. Molecular evolution of hemojuvelin and the repulsive guidance molecule family. *J Mol Evol,* 65**,** 68-81.

Chen, B., Blair, D. G., Plisov, S., Vasiliev, G., Perantoni, A. O., Chen, Q., Athanasiou, M., Wu, J. Y., Oppenheim, J. J. and Yang, D. 2004a. Cutting edge: bone morphogenetic protein antagonists Drm/Gremlin and Dan interact with Slits and act as negative regulators of monocyte chemotaxis. *J Immunol,* 173**,** 5914-7.

Chen, D., Zhao, M. and Mundy, G. R. 2004b. Bone morphogenetic proteins. *Growth Factors,* 22**,** 233-41.

Chen, H. B., Shen, J., Ip, Y. T. and Xu, L. 2006. Identification of phosphatases for Smad in the BMP/DPP pathway. *Genes Dev,* 20**,** 648-53.

Chen, Y. G. and Massague, J. 1999. Smad1 recognition and activation by the ALK1 group of transforming growth factor-beta family receptors. *J Biol Chem,* 274**,** 3672-7.

Chien, A., Edgar, D. B. and Trela, J. M. 1976. Deoxyribonucleic acid polymerase from the extreme thermophile Thermus aquaticus. *J Bacteriol,* 127**,** 1550-7.

Chiodelli, P., Mitola, S., Ravelli, C., Oreste, P., Rusnati, M. and Presta, M. 2011. Heparan sulfate proteoglycans mediate the angiogenic activity of the vascular endothelial growth factor receptor-2 agonist gremlin. *Arterioscler Thromb Vasc Biol,* 31**,** e116-27.

Choay, J., Petitou, M., Lormeau, J. C., Sinay, P., Casu, B. and Gatti, G. 1983. Structure-activity relationship in heparin: a synthetic pentasaccharide with high affinity for antithrombin III and eliciting high anti-factor Xa activity. *Biochem Biophys Res Commun,* 116**,** 492-9.

Chuang, Y. J., Swanson, R., Raja, S. M. and Olson, S. T. 2001. Heparin enhances the specificity of antithrombin for thrombin and factor Xa independent of the reactive center loop sequence. Evidence for an exosite determinant of factor Xa specificity in heparin-activated antithrombin. *J Biol Chem,* 276**,** 14961-71.

Cline, J., Braman, J. C. and Hogrefe, H. H. 1996. PCR fidelity of pfu DNA polymerase and other thermostable DNA polymerases. *Nucleic Acids Res,* 24**,** 3546-51.

Damon, D. H., Halegoua, S., D'amore, P. and Wagner, J. A. 1992. Rapid fibroblast growth factor-induced increases in protein phosphorylation and ornithine decarboxylase activity: regulation by heparin and comparison to nerve growth factor-induced increases. *Exp Cell Res,* 201**,** 154-9.

David, L., Mallet, C., Mazerbourg, S., Feige, J. J. and Bailly, S. 2007. Identification of BMP9 and BMP10 as functional activators of the orphan activin receptor-like kinase 1 (ALK1) in endothelial cells. *Blood,* 109**,** 1953-61.

de Backer, M., Mcsweeney, S., Rasmussen, H. B., Riise, B. W., Lindley, P. and Hough, E. 2002. The 1.9 A crystal structure of heat-labile shrimp alkaline phosphatase. *J Mol Biol,* 318**,** 1265-74.

de Marco, A. 2009. Strategies for successful recombinant expression of disulfide bond-dependent proteins in Escherichia coli. *Microb Cell Fact,* 8**,** 26.

Dente, L., Cesareni, G. and Cortese, R. 1983. pEMBL: a new family of single stranded plasmids. *Nucleic Acids Res,* 11**,** 1645-55.

Derynck, R. and Zhang, Y. 1996. Intracellular signalling: the mad way to do it. *Curr Biol,* 6**,** 1226-9.

Dietrich, C. P., Silva, M. E. and Michelacci, Y. M. 1973. Sequential degradation of heparin in Flavobacterium heparinum. Purification and properties of five enzymes involved in heparin degradation. *J Biol Chem,* 248**,** 6408-15.

Dotto, G. P., Enea, V. and Zinder, N. D. 1981. Functional analysis of bacteriophage f1 intergenic region. *Virology,* 114**,** 463-73.

Dotto, G. P. and Horiuchi, K. 1981. Replication of a plasmid containing two origins of bacteriophage. *J Mol Biol,* 153**,** 169-76.

Ducy, P. and Karsenty, G. 2000. The family of bone morphogenetic proteins. *Kidney Int,* 57**,** 2207-14.

Esko, J. D. and Lindahl, U. 2001. Molecular diversity of heparan sulfate. *J Clin Invest,* 108**,** 169-73.

Esko, J. D. and Selleck, S. B. 2002. Order out of chaos: assembly of ligand binding sites in heparan sulfate. *Annu Rev Biochem,* 71**,** 435-71.

Esko, J. D. and Zhang, L. 1996. Influence of core protein sequence on glycosaminoglycan assembly. *Curr Opin Struct Biol,* 6**,** 663-70.

Faham, S., Hileman, R. E., Fromm, J. R., Linhardt, R. J. and Rees, D. C. 1996. Heparin structure and interactions with basic fibroblast growth factor. *Science,* 271**,** 1116-20.

Ferro, D. R., Provasoli, A., Ragazzi, M., Casu, B., Torri, G., Bossennec, V., Perly, B., Sinay, P., Petitou, M. and Choay, J. 1990. Conformer populations of L-iduronic acid residues in glycosaminoglycan sequences. *Carbohydr Res,* 195**,** 157-67.

Forster, M. and Mulloy, B. 2006. Computational approaches to the identification of heparin-binding sites on the surfaces of proteins. *Biochem Soc Trans,* 34**,** 431-4.

Forstner, J. F., Jabbal, I., Qureshi, R., Kells, D. I. and Forstner, G. G. 1979. The role of disulphide bonds in human intestinal mucin. *Biochem J,* 181**,** 725-32.

Fraga, H., Fernandes, D., Fontes, R. and Esteves Da Silva, J. C. 2005. Coenzyme A affects firefly luciferase luminescence because it acts as a substrate and not as an allosteric effector. *FEBS J,* 272**,** 5206-16.

Gallagher, J. T. 2001. Heparan sulfate: growth control with a restricted sequence menu. *J Clin Invest,* 108**,** 357-61.

Gallagher, J. T. and Walker, A. 1985. Molecular distinctions between heparan sulphate and heparin. Analysis of sulphation patterns indicates that heparan sulphate and heparin are separate families of N-sulphated polysaccharides. *Biochem J,* 230**,** 665-74.

Gazdar, A. F., Butel, J. S. and Carbone, M. 2002. SV40 and human tumours: myth, association or causality? *Nat Rev Cancer,* 2**,** 957-64.

Gettins, P. G., Fan, B., Crews, B. C., Turko, I. V., Olson, S. T. and Streusand, V. J. 1993. Transmission of conformational change from the heparin binding site to the reactive center of antithrombin. *Biochemistry,* 32**,** 8385-9.

Goyard, S. and Beverley, S. M. 2000. Blasticidin resistance: a new independent marker for stable transfection of Leishmania. *Mol Biochem Parasitol,* 108**,** 249-52.

Greenwald, J., Groppe, J., Gray, P., Wiater, E., Kwiatkowski, W., Vale, W. and Choe, S. 2003. The BMP7/ActRII extracellular domain complex provides new insights into the cooperative nature of receptor assembly. *Mol Cell,* 11**,** 605-17.

Griffith, D. L., Keck, P. C., Sampath, T. K., Rueger, D. C. and Carlson, W. D. 1996. Three-dimensional structure of recombinant human osteogenic protein 1: structural paradigm for the transforming growth factor beta superfamily. *Proc Natl Acad Sci U S A,* 93**,** 878-83.

Groppe, J., Greenwald, J., Wiater, E., Rodriguez-Leon, J., Economides, A. N., Kwiatkowski, W., Affolter, M., Vale, W. W., Izpisua Belmonte, J. C. and Choe, S. 2002. Structural basis of BMP signalling inhibition by the cystine knot protein Noggin. *Nature,* 420**,** 636-42.

Guillot, N., Kollins, D., Gilbert, V., Xavier, S., Chen, J., Gentle, M., Reddy, A., Bottinger, E., Jiang, R., Rastaldi, M. P., Corbelli, A. and Schlondorff, D. 2012.

BAMBI regulates angiogenesis and endothelial homeostasis through modulation of alternative TGFbeta signaling. *PLoS One,* 7**,** e39406.

Harmer, N. J., Robinson, C. J., Adam, L. E., Ilag, L. L., Robinson, C. V., Gallagher, J. T. and Blundell, T. L. 2006. Multimers of the fibroblast growth factor (FGF)-FGF receptor-saccharide complex are formed on long oligomers of heparin. *Biochem J,* 393**,** 741-8.

Hasan, M., Najjam, S., Gordon, M. Y., Gibbs, R. V. and Rider, C. C. 1999. IL-12 is a heparin-binding cytokine. *J Immunol,* 162**,** 1064-70.

Hata, A., Lagna, G., Massague, J. and Hemmati-Brivanlou, A. 1998. Smad6 inhibits BMP/Smad1 signaling by specifically competing with the Smad4 tumor suppressor. *Genes Dev,* 12**,** 186-97.

Higuchi, R., Krummel, B. and Saiki, R. K. 1988. A general method of in vitro preparation and specific mutagenesis of DNA fragments: study of protein and DNA interactions. *Nucleic Acids Res,* 16**,** 7351-67.

Hileman, R. E., Fromm, J. R., Weiler, J. M. and Linhardt, R. J. 1998. Glycosaminoglycan-protein interactions: definition of consensus sites in glycosaminoglycan binding proteins. *Bioessays,* 20**,** 156-67.

Hinck, A. P. 2012. Structural studies of the TGF-betas and their receptors - insights into evolution of the TGF-beta superfamily. *FEBS Lett,* 586**,** 1860-70.

Hirschberg, C. B., Robbins, P. W. and Abeijon, C. 1998. Transporters of nucleotide sugars, ATP, and nucleotide sulfate in the endoplasmic reticulum and Golgi apparatus. *Annu Rev Biochem,* 67**,** 49-69.

Ho, S. N., Hunt, H. D., Horton, R. M., Pullen, J. K. and Pease, L. R. 1989. Site-directed mutagenesis by overlap extension using the polymerase chain reaction. *Gene,* 77**,** 51-9.

Hogan, B. L. 1996. Bmps: multifunctional regulators of mammalian embryonic development. *Harvey Lect,* 92**,** 83-98.

Hoodless, P. A., Tsukazaki, T., Nishimatsu, S., Attisano, L., Wrana, J. L. and Thomsen, G. H. 1999. Dominant-negative Smad2 mutants inhibit activin/Vg1 signaling and disrupt axis formation in Xenopus. *Dev Biol,* 207**,** 364-79.

Hoogewerf, A. J., Kuschert, G. S., Proudfoot, A. E., Borlat, F., Clark-Lewis, I., Power, C. A. and Wells, T. N. 1997. Glycosaminoglycans mediate cell surface oligomerization of chemokines. *Biochemistry,* 36**,** 13570-8.

Hricovini, M., Guerrini, M., Torri, G. and Casu, B. 1997. Motional properties of E. coli polysaccharide K5 in aqueous solution analyzed by NMR relaxation measurements. *Carbohydr Res,* 300**,** 69-76.

Hsu, D. R., Economides, A. N., Wang, X., Eimon, P. M. and Harland, R. M. 1998. The Xenopus dorsalizing factor Gremlin identifies a novel family of secreted proteins that antagonize BMP activities. *Mol Cell,* 1**,** 673-83.

Huang, F. and Workman, J. L. 2013. Directing transcription to the right way. *Cell Res,* 23**,** 1153-4.

Humphries, D. E. and Silbert, J. E. 1988. Chlorate: a reversible inhibitor of proteoglycan sulfation. *Biochem Biophys Res Commun,* 154**,** 365-71.

Irie, A., Habuchi, H., Kimata, K. and Sanai, Y. 2003. Heparan sulfate is required for bone morphogenetic protein-7 signaling. *Biochem Biophys Res Commun,* 308**,** 858-65.

Iwano, M., Plieth, D., Danoff, T. M., Xue, C., Okada, H. and Neilson, E. G. 2002. Evidence that fibroblasts derive from epithelium during tissue fibrosis. *J Clin Invest,* 110**,** 341-50.

Jiao, X., Billings, P. C., O'connell, M. P., Kaplan, F. S., Shore, E. M. and Glaser, D. L. 2007. Heparan sulfate proteoglycans (HSPGs) modulate BMP2 osteogenic bioactivity in C2C12 cells. *J Biol Chem,* 282**,** 1080-6.

Kane, R., Stevenson, L., Godson, C., Stitt, A. W. and O'brien, C. 2005. Gremlin gene expression in bovine retinal pericytes exposed to elevated glucose. *Br J Ophthalmol,* 89**,** 1638-42.

Karagiannis, G. S., Musrap, N., Saraon, P., Treacy, A., Schaeffer, D. F., Kirsch, R., Riddell, R. H. and Diamandis, E. P. 2014. Bone morphogenetic protein antagonist gremlin-1 regulates colon cancer progression. *Biol Chem*.

Karsenty, G. 2003. The complexities of skeletal biology. *Nature,* 423**,** 316-318.

Katagiri, T., Yamaguchi, A., Komaki, M., Abe, E., Takahashi, N., Ikeda, T., Rosen, V., Wozney, J. M., Fujisawa-Sehara, A. and Suda, T. 1994. Bone morphogenetic protein-2 converts the differentiation pathway of C2C12 myoblasts into the osteoblast lineage. *J Cell Biol,* 127**,** 1755-66.

Katoh, M. 2004. Identification and characterization of human CKTSF1B2 and CKTSF1B3 genes in silico. *Oncol Rep,* 12**,** 423-7.

Kattamuri, C., Luedeke, D. M., Nolan, K., Rankin, S. A., Greis, K. D., Zorn, A. M. and Thompson, T. B. 2012. Members of the DAN family are BMP antagonists that form highly stable noncovalent dimers. *J Mol Biol,* 424**,** 313-27.

Kavsak, P., Rasmussen, R. K., Causing, C. G., Bonni, S., Zhu, H., Thomsen, G. H. and Wrana, J. L. 2000. Smad7 binds to Smurf2 to form an E3 ubiquitin ligase that targets the TGF beta receptor for degradation. *Mol Cell,* 6**,** 1365-75.

Ke, S. H. and Madison, E. L. 1997. Rapid and efficient site-directed mutagenesis by single-tube 'megaprimer' PCR method. *Nucleic Acids Res,* 25**,** 3371-2.

Khan, S., Fung, K. W., Rodriguez, E., Patel, R., Gor, J., Mulloy, B. and Perkins, S. J. 2013. The solution structure of heparan sulfate differs from that of heparin: implications for function. *J Biol Chem,* 288**,** 27737-51.

Khokha, M. K., Hsu, D., Brunet, L. J., Dionne, M. S. and Harland, R. M. 2003. Gremlin is the BMP antagonist required for maintenance of Shh and Fgf signals during limb patterning. *Nat Genet,* 34**,** 303-7.

Khorramian, B. A. and Stivala, S. S. 1986. Small-angle x-ray scattering of high- and low-affinity heparin. *Arch Biochem Biophys,* 247**,** 384-92.

Kim, B. T., Kitagawa, H., Tamura, J., Saito, T., Kusche-Gullberg, M., Lindahl, U. and Sugahara, K. 2001. Human tumor suppressor EXT gene family members EXTL1 and EXTL3 encode alpha 1,4- N-acetylglucosaminyltransferases that likely are involved in heparan sulfate/ heparin biosynthesis. *Proc Natl Acad Sci U S A,* 98**,** 7176-81.

Kimura, K., Toyooka, S., Tsukuda, K., Yamamoto, H., Suehisa, H., Soh, J., Otani, H., Kubo, T., Aoe, K., Fujimoto, N., Kishimoto, T., Sano, Y., Pass, H. I. and Date, H. 2008. The aberrant promoter methylation of BMP3b and BMP6 in malignant pleural mesotheliomas. *Oncol Rep,* 20**,** 1265-8.

Kimura, M., Takatsuki, A. and Yamaguchi, I. 1994. Blasticidin S deaminase gene from Aspergillus terreus (BSD): a new drug resistance gene for transfection of mammalian cells. *Biochim Biophys Acta,* 1219**,** 653-9.

Kingsley, D. M. 1994. The TGF-beta superfamily: new members, new receptors, and new genetic tests of function in different organisms. *Genes Dev,* 8**,** 133-46.

Kirsch, T., Nickel, J. and Sebald, W. 2000a. BMP-2 antagonists emerge from alterations in the low-affinity binding epitope for receptor BMPR-II. *EMBO J,* 19**,** 3314-24.

Kirsch, T., Sebald, W. and Dreyer, M. K. 2000b. Crystal structure of the BMP-2-BRIA ectodomain complex. *Nat Struct Biol,* 7**,** 492-6.

Kitagawa, H., Shimakawa, H. and Sugahara, K. 1999. The tumor suppressor EXT-like gene EXTL2 encodes an alpha1, 4-N-acetylhexosaminyltransferase that transfers N-acetylgalactosamine and N-acetylglucosamine to the common glycosaminoglycan-protein linkage region. The key enzyme for the chain initiation of heparan sulfate. *J Biol Chem,* 274**,** 13933-7.

Kjellen, L. and Lindahl, U. 1991. Proteoglycans: structures and interactions. *Annu Rev Biochem,* 60**,** 443-75.

Kobayashi, M., Habuchi, H., Habuchi, O., Saito, M. and Kimata, K. 1996. Purification and characterization of heparan sulfate 2-sulfotransferase from cultured Chinese hamster ovary cells. *J Biol Chem,* 271**,** 7645-53.

Korchynskyi, O. and ten Dijke, P. 2002. Identification and functional characterization of distinct critically important bone morphogenetic protein-specific response elements in the Id1 promoter. *J Biol Chem,* 277**,** 4883-91.

Kozak, M. 1980. Influence of mRNA secondary structure on binding and migration of 40S ribosomal subunits. *Cell,* 19**,** 79-90.

Kozak, M. 1984. Point mutations close to the AUG initiator codon affect the efficiency of translation of rat preproinsulin in vivo. *Nature,* 308**,** 241-6.

Kozak, M. 1986. Point mutations define a sequence flanking the AUG initiator codon that modulates translation by eukaryotic ribosomes. *Cell,* 44**,** 283-92.

Kozak, M. 1987. An analysis of 5'-noncoding sequences from 699 vertebrate messenger RNAs. *Nucleic Acids Res,* 15**,** 8125-48.

Kozak, M. 2002. Pushing the limits of the scanning mechanism for initiation of translation. *Gene,* 299**,** 1-34.

Kozak, M. and Shatkin, A. J. 1978. Identification of features in 5' terminal fragments from reovirus mRNA which are important for ribosome binding. *Cell,* 13**,** 201-12.

Kuo, W. J., Digman, M. A. and Lander, A. D. 2010. Heparan sulfate acts as a bone morphogenetic protein coreceptor by facilitating ligand-induced receptor hetero-oligomerization. *Mol Biol Cell,* 21**,** 4028-41.

Lacy, H. M. and Sanderson, R. D. 2002. 6xHis promotes binding of a recombinant protein to heparan sulfate. *Biotechniques,* 32**,** 254, 256, 258.

Larrain, J., Carey, D. J. and Brandan, E. 1998. Syndecan-1 expression inhibits myoblast differentiation through a basic fibroblast growth factor-dependent mechanism. *J Biol Chem,* 273**,** 32288-96.

Lebleu, V. S., Taduri, G., O'connell, J., Teng, Y., Cooke, V. G., Woda, C., Sugimoto, H. and Kalluri, R. 2013. Origin and function of myofibroblasts in kidney fibrosis. *Nat Med,* 19**,** 1047-53.

Lin, X., Duan, X., Liang, Y. Y., Su, Y., Wrighton, K. H., Long, J., Hu, M., Davis, C. M., Wang, J., Brunicardi, F. C., Shi, Y., Chen, Y. G., Meng, A. and Feng, X. H. 2006. PPM1A functions as a Smad phosphatase to terminate TGFbeta signaling. *Cell,* 125**,** 915-28.

Lind, T., Tufaro, F., Mccormick, C., Lindahl, U. and Lidholt, K. 1998. The putative tumor suppressors EXT1 and EXT2 are glycosyltransferases required for the biosynthesis of heparan sulfate. *J Biol Chem,* 273**,** 26265-8.

Lindahl, U., Backstrom, G., Thunberg, L. and Leder, I. G. 1980. Evidence for a 3-O-sulfated D-glucosamine residue in the antithrombin-binding sequence of heparin. *Proc Natl Acad Sci U S A,* 77**,** 6551-5.

Lindahl, U., Kusche-Gullberg, M. and Kjellen, L. 1998. Regulated diversity of heparan sulfate. *J Biol Chem,* 273**,** 24979-82.

Lindahl, U., Kusche, M., Lidholt, K. and Oscarsson, L. G. 1989. Biosynthesis of heparin and heparan sulfate. *Ann N Y Acad Sci,* 556**,** 36-50.

Little, S. C. and Mullins, M. C. 2006. Extracellular modulation of BMP activity in patterning the dorsoventral axis. *Birth Defects Res C Embryo Today,* 78**,** 224-42.

Liu, A. and Niswander, L. A. 2005. Bone morphogenetic protein signalling and vertebrate nervous system development. *Nat Rev Neurosci,* 6**,** 945-54.

Liu, F., Pouponnot, C. and Massague, J. 1997. Dual role of the Smad4/DPC4 tumor suppressor in TGFbeta-inducible transcriptional complexes. *Genes Dev,* 11**,** 3157-67.

Liu, Q., Yin, Y., Wang, B. and Zhou, H. 2013. The activity of SV40 promoter can be inhibited by overexpression of heme oxygenase-1 in tumor cells. *Cell Biochem Biophys,* 65**,** 287-95.

Lortat-Jacob, H. 2009. The molecular basis and functional implications of chemokine interactions with heparan sulphate. *Curr Opin Struct Biol,* 19**,** 543-8.

Lortat-Jacob, H., Baltzer, F. and Grimaud, J. A. 1996. Heparin decreases the blood clearance of interferon-gamma and increases its activity by limiting the processing of its carboxyl-terminal sequence. *J Biol Chem,* 271**,** 16139-43.

Lortat-Jacob, H., Esterre, P. and Grimaud, J. A. 1994. Interferon-gamma, an anti-fibrogenic cytokine which binds to heparan sulfate. *Pathol Res Pract,* 190**,** 920-2.

Lux, A., Attisano, L. and Marchuk, D. A. 1999. Assignment of transforming growth factor beta1 and beta3 and a third new ligand to the type I receptor ALK-1. *J Biol Chem,* 274**,** 9984-92.

Luyten, F. P., Cunningham, N. S., Ma, S., Muthukumaran, N., Hammonds, R. G., Nevins, W. B., Woods, W. I. and Reddi, A. H. 1989. Purification and partial amino acid sequence of osteogenin, a protein initiating bone differentiation. *J Biol Chem,* 264**,** 13377-80.

Macdonald, C. C. and Mcmahon, K. W. 2010. Tissue-specific mechanisms of alternative polyadenylation: testis, brain, and beyond. *Wiley Interdiscip Rev RNA,* 1**,** 494-501.

Machovich, R. and Aranyi, P. 1977. Effect of calcium ion on the interaction between thrombin and heparin. Thermal denaturation. *Thromb Haemost,* 38**,** 677-84.

Macias-Silva, M., Abdollah, S., Hoodless, P. A., Pirone, R., Attisano, L. and Wrana, J. L. 1996. MADR2 is a substrate of the TGFbeta receptor and its phosphorylation is required for nuclear accumulation and signaling. *Cell,* 87**,** 1215-24.

Macias, D., Ganan, Y., Sampath, T. K., Piedra, M. E., Ros, M. A. and Hurle, J. M. 1997. Role of BMP-2 and OP-1 (BMP-7) in programmed cell death and skeletogenesis during chick limb development. *Development,* 124**,** 1109-17.

Maciel, T. T., Melo, R. S., Schor, N. and Campos, A. H. 2008. Gremlin promotes vascular smooth muscle cell proliferation and migration. *J Mol Cell Cardiol,* 44**,** 370-9.

Mamoun, C. B., Gluzman, I. Y., Goyard, S., Beverley, S. M. and Goldberg, D. E. 1999. A set of independent selectable markers for transfection of the human malaria parasite Plasmodium falciparum. *Proc Natl Acad Sci U S A,* 96**,** 8716-20.

Manning, G., Whyte, D. B., Martinez, R., Hunter, T. and Sudarsanam, S. 2002. The protein kinase complement of the human genome. *Science,* 298**,** 1912-34.

Margalit, H., Fischer, N. and Ben-Sasson, S. A. 1993. Comparative analysis of structurally defined heparin binding sequences reveals a distinct spatial distribution of basic residues. *J Biol Chem,* 268**,** 19228-31.

Massague, J., Seoane, J. and Wotton, D. 2005. Smad transcription factors. *Genes Dev,* 19**,** 2783-810.

McCormick, C., Duncan, G., Goutsos, K. T. and Tufaro, F. 2000. The putative tumor suppressors EXT1 and EXT2 form a stable complex that accumulates in the Golgi apparatus and catalyzes the synthesis of heparan sulfate. *Proc Natl Acad Sci U S A,* 97**,** 668-73.

McCormick, C., Duncan, G. and Tufaro, F. 1999. New perspectives on the molecular basis of hereditary bone tumours. *Mol Med Today,* 5**,** 481-6.

McDonald, N. Q. and Hendrickson, W. A. 1993. A structural superfamily of growth factors containing a cystine knot motif. *Cell,* 73**,** 421-4.

McLean, S. and Di Guglielmo, G. M. 2010. TGF beta (transforming growth factor beta) receptor type III directs clathrin-mediated endocytosis of TGF beta receptor types I and II. *Biochem J,* 429**,** 137-45.

McLellan, J. S., Yao, S., Zheng, X., Geisbrecht, B. V., Ghirlando, R., Beachy, P. A. and Leahy, D. J. 2006. Structure of a heparin-dependent complex of Hedgehog and Ihog. *Proc Natl Acad Sci U S A,* 103**,** 17208-13.

McMahon, R., Murphy, M., Clarkson, M., Taal, M., Mackenzie, H. S., Godson, C., Martin, F. and Brady, H. R. 2000. IHG-2, a mesangial cell gene induced by high glucose, is human gremlin. Regulation by extracellular glucose concentration, cyclic mechanical strain, and transforming growth factor-beta1. *J Biol Chem,* 275**,** 9901-4.

Michos, O., Goncalves, A., Lopez-Rios, J., Tiecke, E., Naillat, F., Beier, K., Galli, A., Vainio, S. and Zeller, R. 2007. Reduction of BMP4 activity by gremlin 1 enables ureteric bud outgrowth and GDNF/WNT11 feedback signalling during kidney branching morphogenesis. *Development,* 134**,** 2397-405.

Michos, O., Panman, L., Vintersten, K., Beier, K., Zeller, R. and Zuniga, A. 2004. Gremlin-mediated BMP antagonism induces the epithelial-mesenchymal feedback signaling controlling metanephric kidney and limb organogenesis. *Development,* 131**,** 3401-10.

Mitola, S., Ravelli, C., Moroni, E., Salvi, V., Leali, D., Ballmer-Hofer, K., Zammataro, L. and Presta, M. 2010. Gremlin is a novel agonist of the major proangiogenic receptor VEGFR2. *Blood,* 116**,** 3677-80.

Miyazono, K., Kamiya, Y. and Morikawa, M. 2010. Bone morphogenetic protein receptors and signal transduction. *J Biochem,* 147**,** 35-51.

Morrison, K. L. and Weiss, G. A. 2001. Combinatorial alanine-scanning. *Curr Opin Chem Biol,* 5**,** 302-7.

Mullis, K., Faloona, F., Scharf, S., Saiki, R., Horn, G. and Erlich, H. 1986. Specific enzymatic amplification of DNA in vitro: the polymerase chain reaction. *Cold Spring Harb Symp Quant Biol,* 51 Pt 1**,** 263-73.

Mulloy, B. and Forster, M. J. 2000. Conformation and dynamics of heparin and heparan sulfate. *Glycobiology,* 10**,** 1147-56.

Mulloy, B., Forster, M. J., Jones, C. and Davies, D. B. 1993. N.m.r. and molecular-modelling studies of the solution conformation of heparin. *Biochem J,* 293 (Pt 3)**,** 849-58.

Mulloy, B., Heath, A. and Behr-Gross, M. E. 2007. Establishment of replacement batches for heparin low-molecular-mass for calibration CRS, and the International Standard Low Molecular Weight Heparin for Calibration. *Pharmeuropa Bio,* 2007**,** 29-48.

Mummery, R. S. and Rider, C. C. 2000. Characterization of the heparin-binding properties of IL-6. *J Immunol,* 165**,** 5671-9.

Murakami, G., Watabe, T., Takaoka, K., Miyazono, K. and Imamura, T. 2003. Cooperative inhibition of bone morphogenetic protein signaling by Smurf1 and inhibitory Smads. *Mol Biol Cell,* 14**,** 2809-17.

Murphy, K. J., Merry, C. L., Lyon, M., Thompson, J. E., Roberts, I. S. and Gallagher, J. T. 2004. A new model for the domain structure of heparan sulfate based on the novel specificity of K5 lyase. *J Biol Chem,* 279**,** 27239-45.

Najjam, S., Gibbs, R. V., Gordon, M. Y. and Rider, C. C. 1997. The binding of interleukin 2 to heparin revealed by a novel ELISA method. *Biochem Soc Trans,* 25**,** 3S.

Nakamura, J. and Yanagita, M. 2012. Bmp modulators in kidney disease. *Discov Med,* 13**,** 57-63.

Namkoong, H., Shin, S. M., Kim, H. K., Ha, S. A., Cho, G. W., Hur, S. Y., Kim, T. E. and Kim, J. W. 2006. The bone morphogenetic protein antagonist gremlin 1 is overexpressed in human cancers and interacts with YWHAH protein. *BMC Cancer,* 6**,** 74.

Nelsen, S. M. and Christian, J. L. 2009. Site-specific cleavage of BMP4 by furin, PC6, and PC7. *J Biol Chem,* 284**,** 27157-66.

Newfeld, S. J., Wisotzkey, R. G. and Kumar, S. 1999. Molecular evolution of a developmental pathway: phylogenetic analyses of transforming growth factor-beta family ligands, receptors and Smad signal transducers. *Genetics,* 152**,** 783-95.

Nilsen, I. W., Overbo, K. and Olsen, R. L. 2001. Thermolabile alkaline phosphatase from Northern shrimp (Pandalus borealis): protein and cDNA sequence analyses. *Comp Biochem Physiol B Biochem Mol Biol,* 129**,** 853-61.

Nishimura, R., Hata, K., Matsubara, T., Wakabayashi, M. and Yoneda, T. 2012. Regulation of bone and cartilage development by network between BMP signalling and transcription factors. *Journal of Biochemistry,* 151**,** 247-254.

Nishinakamura, R. and Sakaguchi, M. 2014. BMP signaling and its modifiers in kidney development. *Pediatr Nephrol,* 29**,** 681-6.

Nohe, A., Keating, E., Knaus, P. and Petersen, N. O. 2004. Signal transduction of bone morphogenetic protein receptors. *Cell Signal,* 16**,** 291-9.

Nolan, K., Kattamuri, C., Luedeke, D. M., Deng, X., Jagpal, A., Zhang, F., Linhardt, R. J., Kenny, A. P., Zorn, A. M. and Thompson, T. B. 2013. Structure of protein related to Dan and Cerberus: insights into the mechanism of bone morphogenetic protein antagonism. *Structure,* 21**,** 1417-29.

Onichtchouk, D., Chen, Y. G., Dosch, R., Gawantka, V., Delius, H., Massague, J. and Niehrs, C. 1999. Silencing of TGF-beta signalling by the pseudoreceptor BAMBI. *Nature,* 401**,** 480-5.

Paine-Saunders, S., Viviano, B. L., Economides, A. N. and Saunders, S. 2002. Heparan sulfate proteoglycans retain Noggin at the cell surface: a potential mechanism for shaping bone morphogenetic protein gradients. *J Biol Chem,* 277**,** 2089-96.

Pavlov, G., Finet, S., Tatarenko, K., Korneeva, E. and Ebel, C. 2003. Conformation of heparin studied with macromolecular hydrodynamic methods and X-ray scattering. *Eur Biophys J,* 32**,** 437-49.

Pearce, J. J., Penny, G. and Rossant, J. 1999. A mouse cerberus/Dan-related gene family. *Dev Biol,* 209**,** 98-110.

Pellegrini, L., Burke, D. F., Von Delft, F., Mulloy, B. and Blundell, T. L. 2000. Crystal structure of fibroblast growth factor receptor ectodomain bound to ligand and heparin. *Nature,* 407**,** 1029-34.

Perk, J., Iavarone, A. and Benezra, R. 2005. Id family of helix-loop-helix proteins in cancer. *Nat Rev Cancer,* 5**,** 603-14.

Proudfoot, A. E., Fritchley, S., Borlat, F., Shaw, J. P., Vilbois, F., Zwahlen, C., Trkola, A., Marchant, D., Clapham, P. R. and Wells, T. N. 2001. The BBXB motif of RANTES is the principal site for heparin binding and controls receptor selectivity. *J Biol Chem,* 276**,** 10620-6.

Proudfoot, A. E., Handel, T. M., Johnson, Z., Lau, E. K., Liwang, P., Clark-Lewis, I., Borlat, F., Wells, T. N. and Kosco-Vilbois, M. H. 2003. Glycosaminoglycan binding and oligomerization are essential for the in vivo activity of certain chemokines. *Proc Natl Acad Sci U S A,* 100**,** 1885-90.

Rapraeger, A. C., Krufka, A. and Olwin, B. B. 1991. Requirement of heparan sulfate for bFGF-mediated fibroblast growth and myoblast differentiation. *Science,* 252**,** 1705-8.

Rider, C. C. and Mulloy, B. 2010. Bone morphogenetic protein and growth differentiation factor cytokine families and their protein antagonists. *Biochem J,* 429**,** 1-12.

Riggins, G. J., Thiagalingam, S., Rozenblum, E., Weinstein, C. L., Kern, S. E., Hamilton, S. R., Willson, J. K., Markowitz, S. D., Kinzler, K. W. and Vogelstein, B. 1996. Mad-related genes in the human. *Nat Genet,* 13**,** 347-9.

Rodrigues-Diez, R., Rodrigues-Diez, R. R., Lavoz, C., Carvajal, G., Droguett, A., Garcia-Redondo, A. B., Rodriguez, I., Ortiz, A., Egido, J., Mezzano, S. and Ruiz-Ortega, M. 2014. Gremlin activates the Smad pathway linked to epithelial

mesenchymal transdifferentiation in cultured tubular epithelial cells. *Biomed Res Int,* 2014**,** 802841.

Rosenberg, R. D. and Lam, L. 1979. Correlation between structure and function of heparin. *Proc Natl Acad Sci U S A,* 76**,** 1218-22.

Rosengart, T. K., Johnson, W. V., Friesel, R., Clark, R. and Maciag, T. 1988. Heparin protects heparin-binding growth factor-I from proteolytic inactivation in vitro. *Biochem Biophys Res Commun,* 152**,** 432-40.

Roxburgh, S. A., Kattla, J. J., Curran, S. P., O'meara, Y. M., Pollock, C. A., Goldschmeding, R., Godson, C., Martin, F. and Brazil, D. P. 2009. Allelic depletion of grem1 attenuates diabetic kidney disease. *Diabetes,* 58**,** 1641-50.

Ruppert, R., Hoffmann, E. and Sebald, W. 1996. Human bone morphogenetic protein 2 contains a heparin-binding site which modifies its biological activity. *Eur J Biochem,* 237**,** 295-302.

Salanga, C. L. and Handel, T. M. 2011. Chemokine oligomerization and interactions with receptors and glycosaminoglycans: the role of structural dynamics in function. *Exp Cell Res,* 317**,** 590-601.

Sambrook, J., Fritsch, E.F. and Maniatis, T. 1989. Molecular Cloning: A laboratory Manual. 2nd edn. Cold Spring Harbor, USA: Cold Spring Harbor Laboratory Press.

Sampath, T. K., Muthukumaran, N. and Reddi, A. H. 1987. Isolation of osteogenin, an extracellular matrix-associated, bone-inductive protein, by heparin affinity chromatography. *Proc Natl Acad Sci U S A,* 84**,** 7109-13.

Sanderson, P. N., Huckerby, T. N. and Nieduszynski, I. A. 1987. Conformational equilibria of alpha-L-iduronate residues in disaccharides derived from heparin. *Biochem J,* 243**,** 175-81.

Scheufler, C., Sebald, W. and Hulsmeyer, M. 1999. Crystal structure of human bone morphogenetic protein-2 at 2.7 A resolution. *J Mol Biol,* 287**,** 103-15.

Schlessinger, J., Plotnikov, A. N., Ibrahimi, O. A., Eliseenkova, A. V., Yeh, B. K., Yayon, A., Linhardt, R. J. and Mohammadi, M. 2000. Crystal structure of a ternary FGF-FGFR-heparin complex reveals a dual role for heparin in FGFR binding and dimerization. *Mol Cell,* 6**,** 743-50.

Schmoldt, H. U., Wentzel, A., Becker, S. and Kolmar, H. 2005. A fusion protein system for the recombinant production of short disulfide bond rich cystine knot peptides using barnase as a purification handle. *Protein Expr Purif,* 39**,** 82-9.

Sekelsky, J. J., Newfeld, S. J., Raftery, L. A., Chartoff, E. H. and Gelbart, W. M. 1995. Genetic characterization and cloning of mothers against dpp, a gene required for decapentaplegic function in Drosophila melanogaster. *Genetics,* 139**,** 1347-58.

Sermadiras, I., Revell, J., Linley, J. E., Sandercock, A. and Ravn, P. 2013. Recombinant expression and in vitro characterisation of active Huwentoxin-IV. *PLoS One,* 8**,** e83202.

Shi, W., Chang, C., Nie, S., Xie, S., Wan, M. and Cao, X. 2007. Endofin acts as a Smad anchor for receptor activation in BMP signaling. *J Cell Sci,* 120**,** 1216-24.

Shi, Y. and Massague, J. 2003. Mechanisms of TGF-beta signaling from cell membrane to the nucleus. *Cell,* 113**,** 685-700.

Shi, Y., Wang, Y. F., Jayaraman, L., Yang, H., Massague, J. and Pavletich, N. P. 1998. Crystal structure of a Smad MH1 domain bound to DNA: insights on DNA binding in TGF-beta signaling. *Cell,* 94**,** 585-94.

Solomon, L. 1963. Hereditary multiple exostosis. *J. Bone Joint Surg,* 45B, 292-304.

Stabile, H., Mitola, S., Moroni, E., Belleri, M., Nicoli, S., Coltrini, D., Peri, F., Pessi, A., Orsatti, L., Talamo, F., Castronovo, V., Waltregny, D., Cotelli, F., Ribatti, D. and Presta, M. 2007. Bone morphogenic protein antagonist Drm/gremlin is a novel proangiogenic factor. *Blood,* 109**,** 1834-40.

Stinski, M. F. and Isomura, H. 2008. Role of the cytomegalovirus major immediate early enhancer in acute infection and reactivation from latency. *Med Microbiol Immunol,* 197**,** 223-31.

Stringer, S. E., Forster, M. J., Mulloy, B., Bishop, C. R., Graham, G. J. and Gallagher, J. T. 2002. Characterization of the binding site on heparan sulfate for macrophage inflammatory protein 1alpha. *Blood,* 100**,** 1543-50.

Stringer, S. E. and Gallagher, J. T. 1997. Specific binding of the chemokine platelet factor 4 to heparan sulfate. *J Biol Chem,* 272**,** 20508-14.

Sudo, S., Avsian-Kretchmer, O., Wang, L. S. and Hsueh, A. J. 2004. Protein related to DAN and cerberus is a bone morphogenetic protein antagonist that participates in ovarian paracrine regulation. *J Biol Chem,* 279**,** 23134-41.

Sugahara, K. and Kitagawa, H. 2000. Recent advances in the study of the biosynthesis and functions of sulfated glycosaminoglycans. *Curr Opin Struct Biol,* 10**,** 518-27.

Sugahara, K. and Kitagawa, H. 2002. Heparin and heparan sulfate biosynthesis. *IUBMB Life,* 54**,** 163-75.

Sun, J., Zhuang, F. F., Mullersman, J. E., Chen, H., Robertson, E. J., Warburton, D., Liu, Y. H. and Shi, W. 2006. BMP4 activation and secretion are negatively regulated by an intracellular gremlin-BMP4 interaction. *J Biol Chem,* 281**,** 29349-56.

Suzuki, C., Murakami, G., Fukuchi, M., Shimanuki, T., Shikauchi, Y., Imamura, T. and Miyazono, K. 2002. Smurf1 regulates the inhibitory activity of Smad7 by targeting Smad7 to the plasma membrane. *J Biol Chem,* 277**,** 39919-25.

Takada, T., Katagiri, T., Ifuku, M., Morimura, N., Kobayashi, M., Hasegawa, K., Ogamo, A. and Kamijo, R. 2003. Sulfated polysaccharides enhance the biological activities of bone morphogenetic proteins. *Journal of Biological Chemistry,* 278**,** 43229-43235.

Takeda, M., Mizuide, M., Oka, M., Watabe, T., Inoue, H., Suzuki, H., Fujita, T., Imamura, T., Miyazono, K. and Miyazawa, K. 2004. Interaction with Smad4 is indispensable for suppression of BMP signaling by c-Ski. *Mol Biol Cell,* 15**,** 963-72.

ten Dijke, P. and Hill, C. S. 2004. New insights into TGF-beta-Smad signalling. *Trends Biochem Sci,* 29**,** 265-73.

Thompson, L. D., Pantoliano, M. W. and Springer, B. A. 1994. Energetic characterization of the basic fibroblast growth factor-heparin interaction: identification of the heparin binding domain. *Biochemistry,* 33**,** 3831-40.

Topol, L. Z., Bardot, B., Zhang, Q., Resau, J., Huillard, E., Marx, M., Calothy, G. and Blair, D. G. 2000a. Biosynthesis, post-translation modification, and functional characterization of Drm/Gremlin. *J Biol Chem,* 275**,** 8785-93.

Topol, L. Z., Marx, M., Laugier, D., Bogdanova, N. N., Boubnov, N. V., Clausen, P. A., Calothy, G. and Blair, D. G. 1997. Identification of drm, a novel gene whose expression is suppressed in transformed cells and which can inhibit growth of normal but not transformed cells in culture. *Mol Cell Biol,* 17**,** 4801-10.

Topol, L. Z., Modi, W. S., Koochekpour, S. and Blair, D. G. 2000b. DRM/GREMLIN (CKTSF1B1) maps to human chromosome 15 and is highly expressed in adult and fetal brain. *Cytogenet Cell Genet,* 89**,** 79-84.

Urban, A., Neukirchen, S. and Jaeger, K. E. 1997. A rapid and efficient method for site-directed mutagenesis using one-step overlap extension PCR. *Nucleic Acids Res,* 25**,** 2227-8.

Urist, M. R. 1965. Bone: formation by autoinduction. *Science,* 150**,** 893-9.

Urist, M. R. and Strates, B. S. 1971. Bone morphogenetic protein. *J Dent Res,* 50**,** 1392-406.

Vainio, S. and Lin, Y. 2002. Coordinating early kidney development: lessons from gene targeting. *Nat Rev Genet,* 3**,** 533-43.

Veverka, V., Henry, A. J., Slocombe, P. M., Ventom, A., Mulloy, B., Muskett, F. W., Muzylak, M., Greenslade, K., Moore, A., Zhang, L., Gong, J., Qian, X., Paszty, C., Taylor, R. J., Robinson, M. K. and Carr, M. D. 2009. Characterization of the structural features and interactions of sclerostin: molecular insight into a key regulator of Wnt-mediated bone formation. *J Biol Chem,* 284**,** 10890-900.

Volkin, D. B., Tsai, P. K., Dabora, J. M., Gress, J. O., Burke, C. J., Linhardt, R. J. and Middaugh, C. R. 1993. Physical stabilization of acidic fibroblast growth factor by polyanions. *Arch Biochem Biophys,* 300**,** 30-41.

Walsh, D. W., Godson, C., Brazil, D. P. and Martin, F. 2010. Extracellular BMP-antagonist regulation in development and disease: tied up in knots. *Trends Cell Biol,* 20**,** 244-56.

Wang, E. A., Rosen, V., Cordes, P., Hewick, R. M., Kriz, M. J., Luxenberg, D. P., Sibley, B. S. and Wozney, J. M. 1988. Purification and characterization of other distinct bone-inducing factors. *Proc Natl Acad Sci U S A,* 85**,** 9484-8.

Wang, S. N., Lapage, J. and Hirschberg, R. 2001. Loss of tubular bone morphogenetic protein-7 in diabetic nephropathy. *J Am Soc Nephrol,* 12**,** 2392-9.

Watanabe, M., Masuyama, N., Fukuda, M. and Nishida, E. 2000. Regulation of intracellular dynamics of Smad4 by its leucine-rich nuclear export signal. *EMBO Rep,* 1**,** 176-82.

Waterston, R. H., Lindblad-Toh, K., Birney, E., Rogers, J., Abril, J. F., Agarwal, P., Agarwala, R., Ainscough, R., Alexandersson, M., An, P., Antonarakis, S. E., Attwood, J., Baertsch, R., Bailey, J., Barlow, K., Beck, S., Berry, E., Birren, B., Bloom, T., Bork, P., Botcherby, M., Bray, N., Brent, M. R., Brown, D. G., Brown, S. D., Bult, C., Burton, J., Butler, J., Campbell, R. D., Carninci, P., Cawley, S., Chiaromonte, F., Chinwalla, A. T., Church, D. M., Clamp, M., Clee, C., Collins, F. S., Cook, L. L., Copley, R. R., Coulson, A., Couronne, O., Cuff, J., Curwen, V., Cutts, T., Daly, M., David, R., Davies, J., Delehaunty, K. D., Deri, J., Dermitzakis, E. T., Dewey, C., Dickens, N. J., Diekhans, M., Dodge, S., Dubchak, I., Dunn, D. M., Eddy, S. R., Elnitski, L., Emes, R. D., Eswara, P., Eyras, E., Felsenfeld, A., Fewell, G. A., Flicek, P., Foley, K., Frankel, W. N., Fulton, L. A., Fulton, R. S., Furey, T. S., Gage, D., Gibbs, R. A., Glusman, G., Gnerre, S., Goldman, N., Goodstadt, L., Grafham, D., Graves, T. A., Green, E. D., Gregory, S., Guigo, R., Guyer, M., Hardison, R. C., Haussler, D., Hayashizaki, Y., Hillier, L. W., Hinrichs, A., Hlavina, W., Holzer, T., Hsu, F., Hua, A., Hubbard, T., Hunt, A., Jackson, I., Jaffe, D. B., Johnson, L. S., Jones, M., Jones, T. A., Joy, A., Kamal, M., Karlsson, E. K., *et al.* 2002. Initial sequencing and comparative analysis of the mouse genome. *Nature,* 420**,** 520-62.

Weiskirchen, R. and Meurer, S. K. 2013. BMP-7 counteracting TGF-beta1 activities in organ fibrosis. *Front Biosci (Landmark Ed),* 18**,** 1407-34.

Wen, X. Z., Akiyama, Y., Baylin, S. B. and Yuasa, Y. 2006. Frequent epigenetic silencing of the bone morphogenetic protein 2 gene through methylation in gastric carcinomas. *Oncogene,* 25**,** 2666-73.

Wordinger, R. J., Zode, G. and Clark, A. F. 2008. Focus on molecules: gremlin. *Exp Eye Res,* 87**,** 78-9.

Wosnick, M. A., Barnett, R. W., Vicentini, A. M., Erfle, H., Elliott, R., Sumner-Smith, M., Mantei, N. and Davies, R. W. 1987. Rapid construction of large synthetic genes: total chemical synthesis of two different versions of the bovine prochymosin gene. *Gene,* 60**,** 115-27.

Wozney, J. M., Rosen, V., Celeste, A. J., Mitsock, L. M., Whitters, M. J., Kriz, R. W., Hewick, R. M. and Wang, E. A. 1988. Novel regulators of bone formation: molecular clones and activities. *Science,* 242**,** 1528-34.

Xiao, Y. T., Xiang, L. X. and Shao, J. Z. 2007. Bone morphogenetic protein. *Biochem Biophys Res Commun,* 362**,** 550-3.

Xu, D. and Esko, J. D. 2014. Demystifying heparan sulfate-protein interactions. *Annu Rev Biochem,* 83**,** 129-57.

Xu, L., Chen, Y. G. and Massague, J. 2000. The nuclear import function of Smad2 is masked by SARA and unmasked by TGFbeta-dependent phosphorylation. *Nat Cell Biol,* 2**,** 559-62.

Yamashita, H., ten Dijke, P., Heldin, C. H. and Miyazono, K. 1996. Bone morphogenetic protein receptors. *Bone,* 19**,** 569-74.

Yayon, A., Klagsbrun, M., Esko, J. D., Leder, P. and Ornitz, D. M. 1991. Cell surface, heparin-like molecules are required for binding of basic fibroblast growth factor to its high affinity receptor. *Cell,* 64**,** 841-8.

Yoshida, N., Yoshida, S., Koishi, K., Masuda, K. and Nabeshima, Y. 1998. Cell heterogeneity upon myogenic differentiation: down-regulation of MyoD and Myf-5 generates 'reserve cells'. *J Cell Sci,* 111 (Pt 6)**,** 769-79.

Zanotti, S., Smerdel-Ramoya, A., Stadmeyer, L. and Canalis, E. 2008. Activation of the ERK pathway in osteoblastic cells, role of gremlin and BMP-2. *J Cell Biochem,* 104**,** 1421-6.

Zawel, L., Dai, J. L., Buckhaults, P., Zhou, S., Kinzler, K. W., Vogelstein, B. and Kern, S. E. 1998. Human Smad3 and Smad4 are sequence-specific transcription activators. *Mol Cell,* 1**,** 611-7.

Zhang, J. L., Qiu, L. Y., Kotzsch, A., Weidauer, S., Patterson, L., Hammerschmidt, M., Sebald, W. and Mueller, T. D. 2008. Crystal structure analysis reveals how the

Chordin family member crossveinless 2 blocks BMP-2 receptor binding. *Dev Cell,* 14**,** 739-50.

Zhang, Q., Shi, Y., Wada, J., Malakauskas, S. M., Liu, M., Ren, Y., Du, C., Duan, H., Li, Y. and Zhang, Y. 2010. In vivo delivery of Gremlin siRNA plasmid reveals therapeutic potential against diabetic nephropathy by recovering bone morphogenetic protein-7. *PLoS One,* 5**,** e11709.

Zhao, B., Katagiri, T., Toyoda, H., Takada, T., Yanai, T., Fukuda, T., Chung, U. I., Koike, T., Takaoka, K. and Kamijo, R. 2006. Heparin potentiates the in vivo ectopic bone formation induced by bone morphogenetic protein-2. *J Biol Chem,* 281**,** 23246-53.

Zhao, M., Qiao, M., Harris, S. E., Oyajobi, B. O., Mundy, G. R. and Chen, D. 2004. Smurf1 inhibits osteoblast differentiation and bone formation in vitro and in vivo. *J Biol Chem,* 279**,** 12854-9.

Zhao, M., Qiao, M., Oyajobi, B. O., Mundy, G. R. and Chen, D. 2003. E3 ubiquitin ligase Smurf1 mediates core-binding factor alpha1/Runx2 degradation and plays a specific role in osteoblast differentiation. *J Biol Chem,* 278**,** 27939-44.

Zhong, X., Desilva, T., Lin, L., Bodine, P., Bhat, R. A., Presman, E., Pocas, J., Stahl, M. and Kriz, R. 2007. Regulation of secreted Frizzled-related protein-1 by heparin. *J Biol Chem,* 282**,** 20523-33.

Zimmerman, L. B., De Jesus-Escobar, J. M. and Harland, R. M. 1996. The Spemann organizer signal noggin binds and inactivates bone morphogenetic protein 4. *Cell,* 86**,** 599-606.